Synthesis and Cardioprotective Activities of Green Tea Polyphenols and their Analogues

Olubukunola Pickard

A thesis submitted for the award of the degree of

Doctor of Philosophy

at the

University of Southampton

Faculty of Natural and Environmental Science

School of Chemistry

September 2013

Abstract

Synthesis and Cardioprotective Activities of Green Tea Polyphenols and their Analogues

Olubukunola Pickard, University of Southampton

Faculty of Natural and Environmental Sciences

School of Chemistry

PhD. Thesis, September 2013

Cardiovascular disease is a major killer worldwide and it is becoming clear the significance of our diet in curbing the disease. Green tea is one of the most widely consumed beverages in the world and has recently attracted significant attention in the scientific community for its health benefits. Its consumption has been associated with lower incidences of coronary artery diseases in the Japanese population. This is mainly attributed to its polyphenolic constituents that include epicatechin, epicatechin gallate, epigallocatechin and epigallocatechin gallate.

The aim of this research was to synthesise the four major polyphenols present in green as well as analogues. These compounds would then be tested on H9C2 cardiac myoblast cells and neonatal rat cardiomyocytes in order to further understand the structure-activity

relationship as well as potentially improve the cardioprotective function of these polyphenols following oxidative stress and ischaemia/reperfusion injury focusing on the expression of STAT-1 and ERK-1/2 proteins.

In H9C2 cardiac myoblast cells following the induction of oxidative stress using H_2O_2, EGCG, EGC and to a minor extent ECG inhibited STAT-1 activation but not ERK-1/2 phosphorylation suggesting that although the ERK-1/2 pathway gets activated, its downstream activation of STAT-1 is inhibited by the above polyphenols. EC, on the other hand, inhibited ERK-1/2 activation which in turn cannot activate STAT-1. Quantitative assessment of viable cells showed that pretreatment with EGCG resulted in the lowest amount of non-viable cells reducing cell death by 30%. With neonatal rat cardiomyocytes following ischaemia/reperfusion injury, pretreatment with EGCG reduced the amount of non-viable cells by 5% but pretreatment with acetylated EGCG at half the concentration of EGCG reduced non-viable cells by 8%.

Structure-activity relationships of the green tea polyphenol analogues identified some key aspects in the structures of the polyphenols important in their cardioprotective function. Results indicated that ABD ring system is required for cardioprotective function but the presence of a third OH group in the ring may not be necessary. Substitution of ring C with benzoic and naphthoic rings improved the potency by more than 13-fold compared to EGCG with EC_{50} values of 1.60 and 0.77 μM respectively. Further research into these analogues could realise their potential and contribute to the understanding of the cardioprotective activities of green tea.

A review on the previous synthesis approaches, isolation and biosynthesis of the green tea polyphenols is presented in Chapter 1 and also the different signalling pathways of interest in this work. An evaluation of the biological activities of the four major polyphenols is provided in Chapter 3. Experimental procedure and characterisation data are in Chapter 5.

Contents

List of Figures

List of Tables

Abbreviations

The following abbreviations are used during this thesis.

$\mathbf{{}^{\cdot}O_2^-}$	Superoxide anion radicals
$\mathbf{{}^{\cdot}OH}$	Hydroxyl radicals
$\boldsymbol{\alpha}_D$	optical rotation
Ang II	Angiotensin II
APC	Apoptosis repressor with caspase recruitment domain
Aq.	Aqueous
ATP	Adenosine-5'-triphosphate
Bcl-2	B-cell lymphoma/leukaemia 2 gene/protein
Bn	Benzyl
BSA	Bovine serum albumin
°C	degrees centigrade
c-Jun	c-Jun NH_2-terminal kinases
CHD	Coronary heart disease
$\mathbf{cm^{-1}}$	wavenumber
CRM1	Chromosome region maintenance 1
d	doublet
DAPI	4',6 diamidino-2-phenylindole (DNA binding dye)
DCC	Dicyclohexylcarbodiimide
DCM	Dichloromethane
DEAD	Diethylazodicarboxylate
DEPT	Distortionless enhancement by polarisation transfer

DIABLO	Direct IAP binding protein with low PI
DIBAL	Diisobutylaluminium hydride
DISC	Death inducing signalling complex
DME	Dimethyl ether
DMEM	Dulbecco's modified eagles medium
DMSO	Dimethyl sulfoxide
DNA	Deoxyribonucleic acid
DOC	Sodium deoxycholate
DSPs	dual-specificity protein phosphatases
DTT	Dithiothreitol
EC	Epicatechin
ECG	Epicatechin gallate
e.e.	enantiomeric excess
EGC	Epigallocatechin
EGCG	Epigallocatechin gallate
ESI	Electrospray ionisation
ERK-1/2	Extracellular signal-regulated kinases
ETC	Election transport chain
FADD	FAS associated death domain
FBS	Fetal bovine serum
FLIP	FLICE inhibitory protein
g	gram(s)
GAS	Interferon-γ activated sequence
GTP	Green tea polyphenol
H_2O_2	Hydrogen peroxide
HPLC	High-performance liquid chromatography
Hz	hertz
I/R	Ischamia/Reperfusion
IAPS	Inhibitors of apoptosis

IFN	Interferon
IL-6	Interleukin-6
IL-10	Interleukin-10
IS	Ionspray interface
ISRE	Interferon-stimulated response element
J	coupling constant
JAK	Janus activated kinase
Kg	Kilogram(s)
LAH	Lithium aluminium hydride
LC	Liquid chromatography
LC-MS	Liquid chromatography mass spectrometry
LIF	Leukemia inhibition factor
LRMS	Low resolution mass spectrometry
m	medium / multiplet
mRNA	messenger RNA
MAPK	Mitogen-activated protein kinases
Me	Methyl
MEK/MKK	MAPK or ERK kinase/MAPK kinase
MEKK/MKKK	MEK kinase/MAPK kinase kinase
MI	Myocardial infarction
min	Minute(s)
mL	Millilitre(s)
mM	Millimolar
mmol	Millimole(s)
mol	Mol(s)
MOM	methoxymethyl ether
MS	Mass specroscopy
MPTP	Mitochondrial permeability transition pore
m/z	mass / charge ratio

NF-κB	Nuclear factor-κB
NRCM	Neonatal rat cardiomyocytes
o	ortho
p	para
p53	Tumour suppressor gene
ppm	parts per million
PAGE	Polyacrylamide Gel Electrophoresis
PBS	Phosphate buffer saline
PBST	PBS-tween®
PDC	Pyridinium dichromate
pH	Symbol used to express the acidity or alkalinity of a solution (from 0-14) which is associated with the activity of dissolved hydrogen ions (H^+). Calculation: pH = -log [H^+]
PIAS	Protein inhibitors of activated STATs
PPh_3	Triphenylphosphine
PPTS	Pyridinium *p*-toluene-sulfonate
PTPs	Protein tyrosine phosphatases
PVDF	Polyvinyl difluoride
pyr.	Pyridine
q	Quartet
RIPA	Radioimmunoprecipitation assay
ROS	Reactive oxygen species
RNA	Ribonucleic acid
s	singlet/strong
SDS	Sodium dodecyl sulphate
SH2	Src homology 2
Smac	Second mitochondria-derived activator of caspase
SOCS	Suppressors of cytokine signalling
SOD	Superoxide dismutase

STAT	Signal transducers and activators of transcription
t	triplet
t	tertiary
tert	tertiary
TBAF	Tert-*n*butylammonium flouride
TBDMSCl	*tert*-Butyldimethylsilyl chloride
TBDMS-triflate	*tert*-Butyldimethylsilyl trifluoromethanesulfonate
TEMED	Tetramethylethylenediamine
TES	Triethylsilyl
THF	Tetrahydrofuran
TFA	Triflouroacetic acid
TLC	Thin layer chromatography
TNF-α	Tumor necrosis factor α
UPLC	Ultra high performance liquid chromatography
uv	Ultraviolet
VCAM-1	Vascular cell adhesion molecule-1
VSMC	Vascular smooth muscle cells
w	weak
XIAP	X chromoshome-linked inhibitors of apoptosis

Acknowledgements

Firstly, I would like to thank my supervisors Prof Paul A. Townsend and Prof David Harrowven for the opportunity to work on this project. Thank you Paul for your support, patience and encouragement through some difficult times that kept me going to the end. I'm very grateful to you David for letting me be a part of your group, without your support and guidance the synthesis part of my project wouldn't have been finished and for proof reading because this thesis wouldn't not have been written without you. Special thanks to the EPSRC and the Gerald Kerkut Charitable Trust for funding my work.

I'd very much like to thank all the support staff in the School of Chemistry, Dr. Neil Wells for keeping the NMR facilities up and running, Dr. John Langley and Ms. Julie Herniman in the Mass Spectrometry department and last but definitely not least, Karl and Keith for making my Stores visits always interesting. I'd also like to thank members of the School of Medicine, Julie for being the best P. A. ever, Dr. David Johnston in the biomedical imaging unit for the amazing confocal images in this study, Dr. Sonya James the microscopy officer in Tenovus, and of course Mel and Kelly for fixing everything in Duthie and ensuring everything ran smoothly. Thanks also go to the BRF staff for training me in animal work and making sure I had pups for my work.

I must of course thank the Townsend group and Karus Therapeutics, the Pips, both past and present, whose members are too numerous to mention individually, for making my time in the School of Medicine so fantastic and the lab such a great place to work in. I'm going miss the endless cake supplies, our ice-cream breaks on the steps of the hospital and endless chats about everything and nothing.

I'd like to extend a huge thank you to the Harrowven group for making me a part of their team. Thanks Majdouline and Mubina for making my transition into the lab that much easier and for endless support in finishing my last set of experiments. Thanks to Karen, Ian, Guillaume, Pia, Elena, Sharon and Franciane for making the first year of my PhD that much more interesting and keeping my spirits up throughout.

There are a few people in need of a special mention:

Becky, for sharing my love of Lego and movies and bringing the kid inside me a little closer to the surface!

Sam, for always making sure the lab ran smoothly, endless gossip, my large collection of shoes and her special antics!

Sarah, not only for her diligent proof reading but also being there for the highs and lows, willingness to help me out when I needed it and knowing when I desperately needed a coffee break!

Tom, for not only leaving the lab in a mess but providing support when I needed it, endless Minion videos and understanding Latex so I don't have to!

Lastly, I would like to thank my family, the Adeosuns and Pickards. Thank you Mum for your endless support throughout my undergraduate and postgraduate degrees. I could not have done any of this without you. My siblings and their families, for not really understanding what I do, but being as supportive as ever. My in-laws, for their love and support, being there through some hard times and providing a home for Andy and I. And finally, my husband Andy. You have supported me in more ways than I can imagine and without you I would not have made it through to the end. You're my best friend and I love you so much and our little Jelly Bean, whose made the writing up that much more memorable. We can't wait to meet you!

Declaration

The research described in this thesis was carried out under the supervision of Prof. D. C. Harrowven and Prof. Paul A. Townsend at the University of Southampton between October 2009 and September 2013. No part of this thesis has previously been submitted for a degree.

The work described is entirely my own, except where I have *either* acknowledged help from a named person *or* given a reference to a published source or a thesis. Text taken from another source is enclosed in quotation marks and a reference given. Pictures taken from another source are clearly indicated in the caption.

Signature:

Date:

Chapter 1

Introduction

Coronary heart disease (CHD) is one of the biggest killers in the world, causing more than 82,000 deaths in the UK each year.[2] CHD is caused by the narrowing or blocking of the coronary arteries by a build-up of fatty deposits called plaques, in a condition called atherosclerosis which restricts blood flow to the heart. This can cause chest pains (angina) and if the restriction is to a section of the heart muscle, a myocardial infarction (MI) can occur.

1.0.1 Atherosclerotic plaque

Atherosclerosis is one of the leading causes of death in developed countries. The term implies a mature plaque comprising of two parts: the "atheromatus" which is a soft lipid-rich "gruel"; and the "sclerotic" which is a hard collagen-rich tissue and makes up more than 70% of the average coronary sclerotic plaque. The narrowing of the lumen is determined by the plaque mass as well as the local remodelling of the vessel size. The plaque in the arterial system is made up of inflammatory cells, extracellular matrix, smooth muscle cells, intracellular and extracellular lipids.[3]

The progression from a stable, thrombus-resistent plaque to an unstable, vulnerable, plaque involves a number of factors such as proliferation of smooth muscle cells, lipid

deposition, thrombosis, inflammation and endothelial dysfunction.[3] Vulnerable plaques are characterised by having a thin inflamed fibrous cap covering a large lipid-rich core and is dependent on three factors: the size and consistence of the atherosclerotic core; thickness of the fibrous cap over the core; and the inflammation and repair in the core.[4] The disruption of vulnerable plaques is triggered by a number of factors such as blood pressure, heart contraction and vasospasm.[5] The rupture tends to occur at the thinnest part of the plaque cap where there are large of amounts of weak and vulnerable lipid-filled macrophages. According to Richardson *et al.* more than 63% of plaques ruptured at the junction of the plaque cap, suggesting that the shoulder might be more susceptible to rupture.[6] Plaque disruption leads to a thrombotic response with an initial blood flow obstruction caused by platelet aggregation, which further complicates the problem causing unstable angina, MI and potentially death (Figure 1.1).[7]

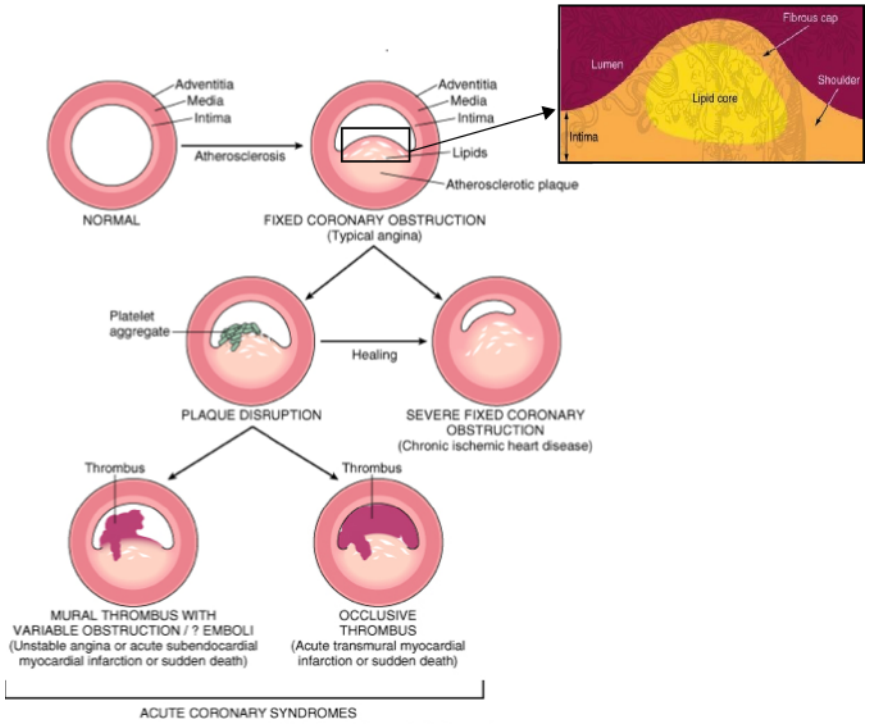

Figure 1.1 Atherosclerotic plaque. The rupture of an unstable atherosclerotic plaque that triggers platelet aggregation and formation of a thrombus that may not be occulsive. An acute plaque disruption that leads to a complete thrombotic occulsion can lead to severe MI or sudden death. (Taken from Kumar *et al.*[7])

1.0.2 Ischaemia-Reperfusion injury

Following a plaque rupture, the initial thrombotic response leads to platelet aggregation which further restricts blood flow to the heart, depriving it of oxygen and nutrients in a process is called *ischaemia*. Surgical intervention and antithrombotic drugs allow the restoration of blood flow. However in a paradoxical reaction, restoration of blood and oxygen, which is essential for restoring cardiac function, also results in exacerbated levels of myocardial damage and a larger infarct size. The phenomenon is called *ischaemia-reperfusion injury (I/R injury)*. This injury culminates in the death of viable cardiac myocytes and partly explains why, despite optimal reperfusion, the rate of human death after an acute MI is close to 10% and the rate of cardiac failure after an acute MI is nearly 25%.[8]

The term myocardial reperfusion injury was first defined by Jennings *et al.*[9] on the structural and electrophysiological changes of the ischaemic canine heart subjected to reperfusion. There are four types of cardiac dysfunction caused by myocardial reperfusion injury: myocardial stunning, reperfusion arrhythmias, no-reflow phenomenon, and lethal reperfusion injury.[8] Myocardial stunning is a mechanical impairment to the myocardial contractile function that occurs after reperfusion and continues despite the restoration of blood flow and lack of irreversible damage.[10] The clinical problems associated with this are dependent upon the size of the affected myocardium and the heart usually recovers after a few weeks. Reperfusion arrhythmias are a disruption of the heart's normal rhythm that occur within 6 h of reperfusion and can be potentially fatal. Ventricular arrhythmias are caused by an increased Ca^{2+} overload during ischaemia, which leads to a depolarisation and results in cellular electric instability.[11] The third type of cardiac function is the no-reflow phenomenon; this refers to the inability to restore blood flow to an ischaemic area of the myocardium due to microvascular obstruction.[12] Microscopic examination reported by Flores *et al.* showed that cellular oedema compressing the capillaries in the ischaemic zone may also contribute to the blood flow restoration.[13,14]

Lethal reperfusion injury is the most detrimental of the cardiac dysfunctions discussed here. Its existence as an independent mediator of myocardial death is still controversial due to an inability to measure the progression of necrosis *in situ* from ischaemia to reperfusion.[15,16] There is some evidence to suggest that its existence has been shown by the reduction in myocardial necrosis following treatment at the beginning of reperfusion.[17] Reperfusion injury involves an inflammatory cascade with major mediators including oxygen radicals, calcium loading, and neutrophils.[18] The decrease in the release of basal nitric oxide initiates a series of events, including neutrophil adhesion to the coronary endothelial cell surface within 20 mins after the onset of reperfusion and neutrophil accumulation in the myocardium 3 h after reperfusion. These events lead to enhanced myocardial cell injury and increased myocardial necrosis.

1.1 Myocardial Cell Death in Ischaemia - Reperfusion Injury

There are three morphologically distinct forms of cell death that occur in the heart: necrosis, apoptosis and autophagy. Necrosis is uncontrolled cell death that occurs when cells are exposed to extreme physiological conditions such as respiratory poisoning and hypoxia, resulting in damage to the plasma membrane. There is a rapid loss of cellular homeostasis, accumulation of water and electrolytes causing rapid swelling and cell membrane rupture. This leads to an outflow of cellular material and extensive damage to surrounding cells; inducing an inflammatory response.[19] Prolonged ischaemia has been associated with an increased level of necrotic cardiomyocytes. Extensive ischaemia alone can kill myocytes by necrosis but is it debatable whether the reperfusion process can activate this cell death pathway.[20]

In the heart autophagy occurs at low levels under normal conditions and is important in maintaining homeostasis. The process is an important survival mechanism that is rapidly activated in response to starvation, when recycling of fatty acids and amino acids from

long-lived proteins, organelles and lipids that are necessary for survival. Autophagy involves the sequestration of large double-membrane vesicles called autophagosomes, which then fuse with the lysosome and combines the internal vesicle with the interior of this organelle where it is degraded by hydrolases and reused.[21,22] The response of autophagy in the heart during MI is quite complex. Enhanced levels of autophagy have been observed in cardiomyocytes after I/R injury both in a pro-survival and pro-death manner. It promotes survival under mild stress conditions with low levels of oxidative stress by removing and recycling damaged organelles in order to maintain energy levels and protein synthesis.[23,24]In contrast, under severe ischaemia and reperfusion conditions there is a prolonged upregulation of autophagy leading to excessive self-digestion of essential organelles and proteins, further enhancing cell death.[25]

Apoptosis is a highly regulated, programmed form of cell death, requiring energy to remove damaged cells without an inflammatory response.[26] This process of cell death is also a biologically important process involved in cell proliferation and differentiation to control tissue and organ homeostasis during development. Apoptosis is characterised by condensation of the nucleus, cell shrinkage due to reduction of the cytoplasm and membrane blebbing. Extensions form around the membrane eventually forming a membrane-enclosed vesicle, apoptotic bodies, containing processed organelles and nuclear fragments. This process ensures that the cell destroys itself from within and avoids leakage of its contents into the extracellular space. These vesicles are rapidly recognised and phagocytised by adjacent cells or macrophages.[19]

Apoptosis is activated in cardiac myocytes by multiple stressors found in cardiovascular disease such as cytokine production, increased oxidative stress and DNA damage. Apoptosis represents a potentially preventable form of cell death owing to its active nature and as such has important therapeutic implications for new cardioprotective treatment. Apoptosis has been observed in cardiac myocytes in atherosclerosis, MI, I/R injury and chronic heart failure.

Studies undertaken using cardiomyocytes from patients that die of acute MI showed that in addition to overt necrosis, a subset of myocytes undergo apoptosis during I/R injury. Apoptotic cardiomyocytes were observed particularly in the border zones of histologically infarcted myocardium, whereas very few apoptotic cells were present in the non-infarcted myocardium.[27] Questions have been raised on the importance of apoptosis in cardiac cells as they undergo active apoptosis (<1% TUNEL positive cells).[28,29] Transgenic mice generated with conditionally active caspase 8 showed very low levels of myocyte apoptosis, significantly lower than those observed in failing human hearts, resulted in lethal dilated cardiomyopathy.[30] This finding inferred that even a low level of cell death over a period of time could be detrimental to the heart because of the inability of heart muscle cells to divide and reproduce.

Apoptosis is mediated by two distinct pathways: the extrinsic death receptor pathway and the intrinsic mitochondrial death pathway, both of which result in caspase activation, involving different initiator caspases but converge on the same effector caspases.[26] Caspases are members of the cysteine protease enzymes, they exist as inactive precursors called pro-caspases and are activated by cleavage into their active form after induction of apoptosis via any of the pathways listed above. The activated caspases undergo proteolytic cleavage as well as activate other protease enzymes and other proapoptotic proteins in the cell. This caspase activation in apoptosis is an all or nothing process i.e. once activated it is self-amplifying and irreversible, as such the apoptotic program is tightly controlled.

The extrinsic pathway, also known as the death receptor pathway, involves the binding of extracellular death signal proteins such as tumor necrosis factor α (TNF-α)[31] or Fas ligand (FasL also called APO-1 or CD95L) to their associated cell surface receptors TNF-α receptor and Fas (CD95) respectively.[32] This leads to the homotrimerisation of the receptor and enlistment of adaptor proteins such as Fas-associated death domain (FADD). The Fas/FADD complex binds to pro-caspase 8 leading to its cleavage to the active caspase 8 and other effector caspases.[32,33] Both Fas and TNF-α are expressed in the heart and contribute to CHD. Elevated levels of TNF-α are present in patients with

end-stage heart failure[34] and following I/R injury there is an increase in TNF-α levels both locally in the heart and in the blood (Figure 1.2).

The intrinsic pathway is also known as the mitochondria cell death pathway. The mitochondria provide energy in the form of ATP to the cells via oxidative phosphorylation to the constantly contracting myocytes. In cardiac myocytes mitochondria make up about 30% of the cell volume and are located below the sarcolemma.[33] The mitochondria is also responsible for cell death in response to intracellular stress including oxidative stress, and DNA damage. Apoptosis results from the release of cytochrome C, endonuclease G (Endo G) and apoptosis-inducing factor (AIF), which can lead to the activation of the initiator caspase 9 and eventual activation of effector caspases (Figure 1.2).

When cytochrome C is released into the cytosol, it binds with Apaf-1 initiating a conformational change and recruitment and activation of caspase 9. Activated caspase 9 cleaves pro-caspase 3 to produce the effector caspase 3, initiating a cascade of events that culminates in cell death.[33] Endo G is localised in the mitochondrial intermembrane space and plays a part in I/R cell death by translocating to the nucleus and causing DNA cleavage.[36] Active caspase 3 has been reported to cleave DNA repair enzyme poly (ADP-ribose) polymerase (PARP) and activate endonucleases that cleave DNA.[37,38] AIF is located in the mitochondria inner membrane oriented towards the intermembrane space and is necessary for oxidative phosphorylation. During apoptosis AIF is cleaved and released into the cytosol then translocates to the nucleus and regulates chromatin condensation and DNA fragmentation.[39]

This intrinsic pathway is modulated by the Bcl-2 family of proteins, which is made up of anti-apoptotic proteins (Bcl-2 and Bcl-xL) and pro-apoptotic proteins (Bad, Bak, and Bax).[40,41] Pro-apoptotic proteins/Bcl-2 family members induce cell death by permeabilising the outer mitochondria membrane leading to the release of cytochrome C and AIF from the outer membrane space.[33] In the heart, Bax and Bad[42] has been shown to be active during oxidative stress[43] and simulated I/R injury.[44] Anti-apoptotic proteins such as Bcl-2 have been shown to prevent p53-mediated apoptosis in cardiac myocytes[45] and

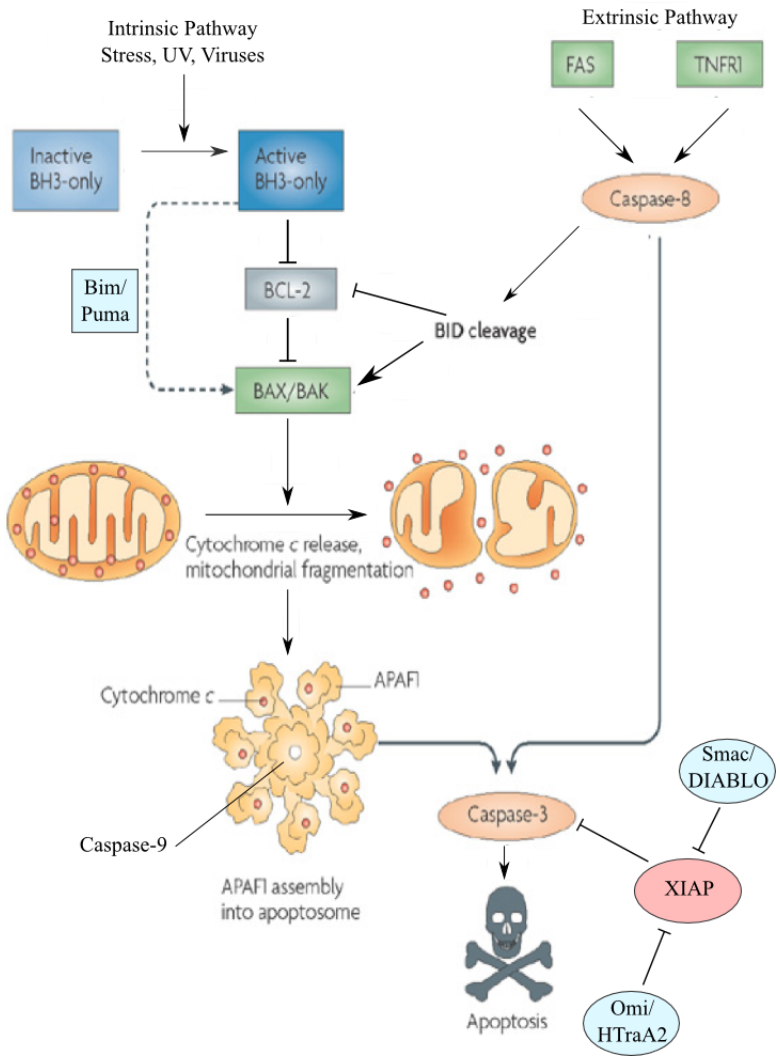

Figure 1.2 Intrinsic and extrinsic pathways of apoptosis. The intrinsic pathway begins with the activation of BH3-only proteins which prevents the activation of some Bcl-2 proteins family members. This results in the activation of Bax and Bak, which can also be activated by some BH3-only proteins such as Bim and Puma can also activate Bax and/or Bak. Once activated, Bax and Bak promote the release of cytochrome c into the cytosol and mitochondria fission, which in turn results in the activation of APAF1into an apoptosome. Active caspase-9 proteolytically cleaves and activates caspase-3. The extrinsic pathway invovles direct activation of caspase-8, which leads to caspase-3 activation and cell death. The process is also regulated by XIAP protein, which inhibit the activities of caspses-9 and -3 (Figure taken from,[35] modified)

prevented the permeabilisation of the outer mitochondria membrane by inhibiting the activation of Bax and Bak thus preserving the integrity of the mitochondria.[46]

The intrinsic pathway is also modulated by the inhibitors of apoptosis (IAPs) including IAP1, IAP2, and XIAP (X chromoshome-linked IAP). These are the most potent caspase inhibitors and act by targeting caspases 9, 3 and 7.[47] IAPS are regulated by smac (second mitochondria-derived activator of caspase)/DIABLO and OMI/HRTA2. During apoptosis smac/DIABLO is released from the mitochondria and binds to IAPs preventing their binding to caspases and promoting cell death.[48] Inhibiton of OMI/HRTAR have been reported to reduce apoptosis and infarct size in rats after I/R injury.[49] Regulatory proteins such as ARC (apoptosis repressor with caspase recruitment domain) and FLIP (FLICE inhibitory protein) are also known to regulate both the extrinsic and intrinsic pathways. ARC inhibit the extrinsic pathway by binding to caspase 8[50] and the intrinsic pathway by inhibiting BAX activation and translocation.[51] FLIP also prevents the FADD-mediated recruitment of caspase 8.[52]

1.2 Oxidative Stress in Myocardial Cell Death During Ischaemia-Reperfusion Injury

Oxidative stress is a condition that increases the formation of reactive oxygen species (ROS) both intra- and extracellularly which causes deleterious effects on the heart during heart failure. ROS are paramagnetic with one or more unpaired electrons making them very unstable and highly reactive. The best known species are generated from the reduction of O_2 to obtain superoxide anion radicals ($\cdot O_2^-$), hydroxyl radicals ($\cdot OH$) and hydrogen peroxide (H_2O_2). Under normal physiological conditions 95% of O_2 is reduced to H_2O and the remaining 5% is reduced via a univalent pathway resulting in the formation of radicals.[53] These radicals are capable of damaging vascular cells and cardiac myocytes and their increase is associated with the pathogenesis of atherosclerosis and cardiomyopathy.[54]

Under normoxic conditions where neutral pH is observed, the superoxide $\cdot O_2^-$ is relatively unreactive and in equilibrium with its protonated form $\cdot HO_2^-$ when in an aqueous environment whereas during acidic conditions such as ischaemia it favours it's protonated form. The superoxide anion is relatively short-lived (2-4 μs) and readily diffused and can cause lipid peroxidation and weakening of the cell membrane.

The most harmful form of ROS is the hydroxyl radical ($\cdot$OH), which are produced from the Haber-Weiss and Fenton reactions. Hydroxyl radicals are highly reactive and unstable, they interact with a large number of compounds and the cell membrane in a diffusion-controlled manner.[53] Hydrogen peroxide H_2O_2 is the most stable ROS form, with a relaitvely long lifespan. it can also enter ther cell by diffusion across the cell membrane and is able to oxidise to generate hydroxyl radicals as a result. Excess H_2O_2 leads to the degradation of heme rings of haemoglobin leading to the release of Fe which stimulate $\cdot$OH production and lipid peroxidation. In the absence of metal catalysts (Cu and Fe), H_2O_2 and $\cdot$OH are readily removed (Figure 1.3).

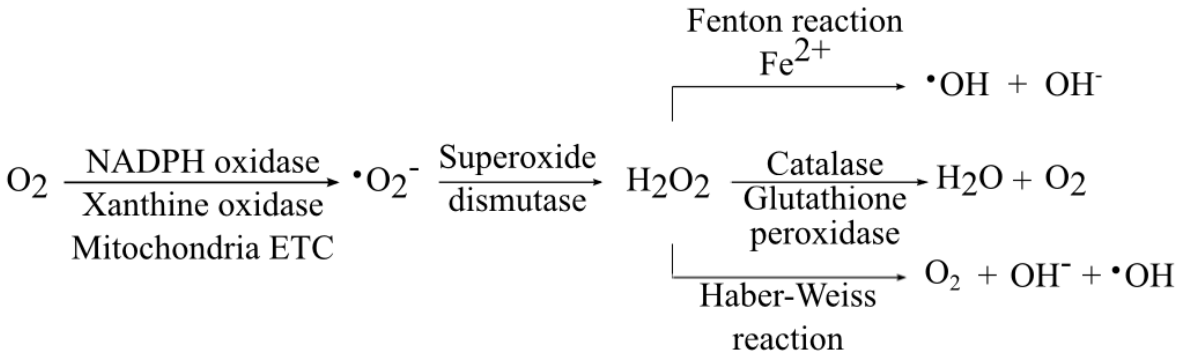

Figure 1.3 Sources of ROS. Under normal conditions these species are converted to H_2O. During I/R injury, the balance is lost producing excess ROS that results in cellular injury.

The levels of ROS are regulated by free radical scavenging enzymes superoxide dismutase (SOD), catalase, and glutathione peroxidase (GPx). SOD is involved in the removal of the superoxide anion by catalysing their disproportionation to H_2O_2 and oxygen. Catalase in combination with GPx removes H_2O_2. Carotenoids and flavonoids also have the ability to scavenge ROS which protect the cell by improving the cell's defence mechanism. (Figure 1.3).[55]

In the heart ROS are formed within the mitochondria via a number of pathways: election transport chain (ETC), xanthine oxidase and NAPDH oxidase, cytochrome P450, to mention a few. The reduction of O_2 by the mitochondrial ETC is essential for the production of biological energy occurring at complexes I (NADH coenzyme Q reductase) and III (ubiquinol cytochrome c reductase). Sollott *et al.* reported that ROS trigger the opening of the mitochondrial permeability transition pore (MPTP) in cardiac myocytes which caused a burst of additional mitochondrial ROS generation in what they termed "ROS-induced ROS release."[56]

During I/R injury endogenous scavengers are unable to cope with the elevated production of ROS. The increased levels of ROS during ischaemia and reperfusion have been demonstrated using electron paramagnetic resonance (EPR) methods.[57] Zweier *et al.* demonstrated that oxygen radicals were generated during ischaemia and a burst of oxygen radical generation occurred at the start of reperfusion when using perfused rat hearts. The generation of ROS significantly increased within the first few minutes of reperfusion, more than ninety times higher than during ischameia, as reported by Bolli *et al.*[58] Ischaemia and the early stages of reperfusion are marked by acidosis and the strong reducing state favours the release of ferric and ferrous ions from metalloproteins. These processes facilitate iron-catalysed Fenton reactions which tips towards conversion of superoxide anion and hydrogen peroxide to the highly reactive hydroxide radicals.[59,60]

A brief exposure to ischaemia leads to an inherent preservation of energy levels to prevent further injury by switching to anaerobic glycolysis, therefore increasing glucose uptake and decreasing contractility. Extensive ischaemia leads to severe ATP deficiency, irreversible injury and ultimately cell death. During ischaemia complexes I, II, and III of ETC are impaired, which is considered a major site of ROS production.[61] ROS can also be produced by endothelial cells and phagocytes in the circulation. The impaired function of the scavengers also leads to a build up of H_2O_2 which becomes increasingly capable of generating the damaging hydroxyl radical.

Reperfusion, in addition to enabling cell survival, leads to the further generation of ROS and in combination with the reintroduction of ATP and the induction of MPT can result in hypercontraction and further cell death.[62] ROS also affects a number of signalling pathways involved in cardiac function such as the activation of G protein-coupled receptors (GPCR), which control apoptotic cell death and cell proliferation of developing cardiomyocytes.

Taken together, ischaemia induces ROS production and reperfusion leads to ROS overproduction to a toxic level that impairs mitochondrial function, impairs recovery and induces cell death. Addition of antioxidants to cultured myocytes has been shown to reduce myocyte death following simulated I/R injury. Furthermore, long-term treatment has been reported to attenuate apoptosis following MI in rats[63,64] A novel scavenger, edaravone, has been shown to possess preventive effects by improving myocardial cell survival in patients with acute MI following ischaemia and reperfusion by quenching reactive oxygen.[55] Despite the many studies on the use of antioxidants in the treatment of patients undergoing MI, clinical studies results are yet to be compelling. Flaherty *et al.* found no benefit in administering human SOD to patients with acute MI.[65] Some experts suggest that more than one antioxidant may be required and others believe that the introduction of these new agents could lead to further toxicity.[66]

1.3 Signalling Pathways in Myocardial Cell Death

In the treatment of MI, several targets for therapeutic intervention are being studied involving the signalling pathway that control cell death or survival. In particular, mitogen-activated protein kinases (MAPK) pathways, which are involved in myocardial cell death during MI, have attracted attention for their potential therapeutic intervention and are described in detail in the section below.

1.3.1 MAPK Signalling Pathways in Myocardial Cell Death

Mitogen-activated protein kinases (MAPK) are evolutionarily conserved enzymes that regulate a vast number of processes including cell differentiation, proliferation and apoptosis by connecting cell-surface receptors to regulatory targets within cells. The MAPK pathway is activated by a variety of stimuli in response to physical and chemical stresses, resulting in phosphorylation-dependent activation. These in turn phosphorylate target proteins including transcription factors, kinases and other enzymes. As a result they play a role in controlling gene expression, metabolism, cell survival and morphology. MAPK are made up of four subfamilies including extracellular signal-regulated kinases (ERK-1/2); c-Jun NH_2-terminal kinases (JNK1,-2, -3); p38 kinases ($\alpha, \beta, \gamma, \delta$); and big MAPK (BMK or ERK5).[67,68] Their activation is controlled by a dual phosphorylation of a Thr-X-Tyr motif (X is either a Gly, Pro, or Glu), which is further controlled by a three-tiered cascade where MAPK kinase kinase (MAPKKK, MAP3K, MEKK or MKKK) activates MAPK kinase (MAPKK, MAP2K, MEK, or MKK) and this in turn activates MAP kinase (Figure 1.4).[68] This cascade of activation enables specific responses to different stimuli and also signal amplification.[69]

Once activated MAPK phosphorylate serine or threonine residues in a proline directed (Pro-X-Thr/Ser-Pro) motif on their target proteins.[71] The specificity and efficiency of the signalling pathway is determined by proline residue and by specific docking sites; MAPK binding substrates and scaffold proteins can insulate components and prevent cross-talk.[72,73] The degree and duration of MAPK signalling is modulated by protein phosphatases (protein tyrosine phosphatases (PTPs), serine/threonine protein phosphatases and dual-specificity protein phosphatases (DSPs)) that can downregulate MAPK activity by dephosphorylation of either the threonine or tyrosine residues.[71]

1.3.1.1 p38 MAPK

p38 kinases were first identified in a drug screen in involving a drug that inhibited TNF-α-mediated inflammatory response.[74] This regulated the expression of a number of cy-

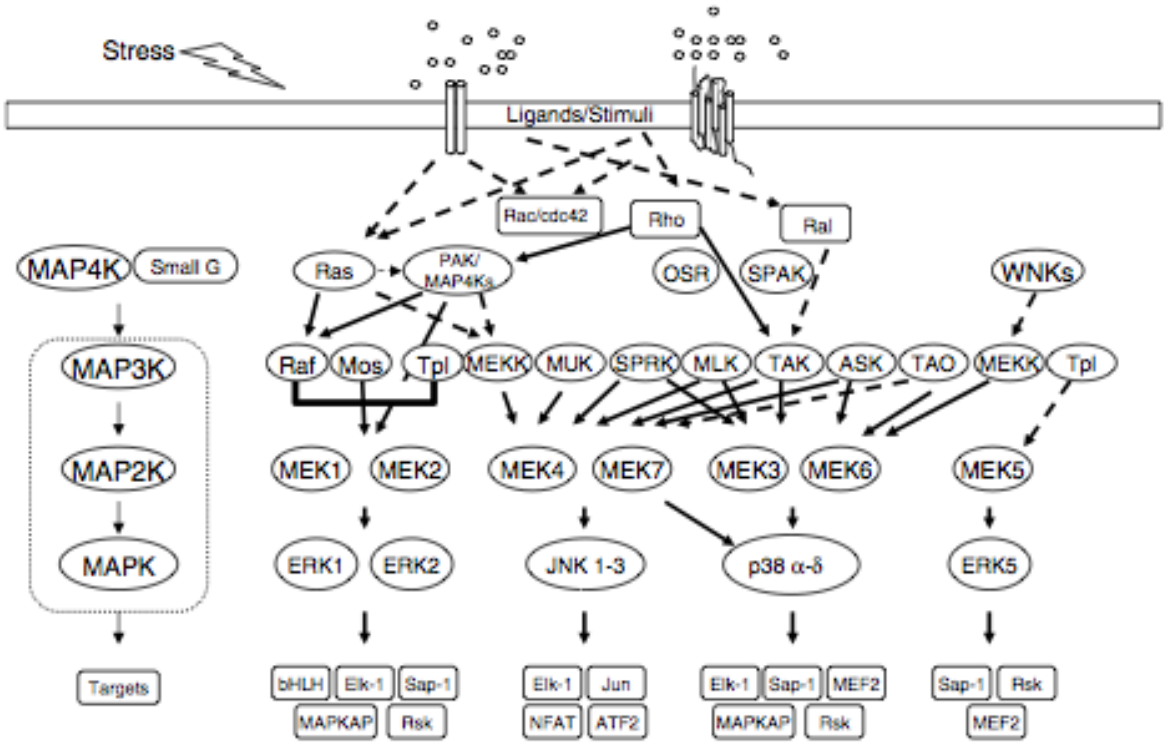

Figure 1.4 MAPK cascades. Illustration of the three-tiered MAPK cascades for MAPK family members. Their activation is controlled by a dual phosphorylation of a Thr-X-Tyr motif (X is either a Gly, Pro, or Glu) further controlled by a three-tiered cascade where MAPK kinase kinase (MAPKKK, MAP3K, MEKK or MKKK) activates MAPK kinase (MAPKK, MAP2K, MEK, or MKK) and this in turn activates MAP kinase. Dotted lines indicated moderate activation by growth factors, serum and ligands for heterotrimeric G protein-coupled receptors, cytokine transforming growth factors, osmotic and other cell stresses. Taken from Cobb *et al.*[70]

tokines including interleukin (IL)-1β, TNF-α, vascular cell adhesion molecule-1 (VCAM-1), a cell adhesion molecule and other proinflammatory-related molecules.[73]

The role of p38 in I/R injury is very well documented with some evidence to suggest its involvement in myocardial cell death and others implying it has cardioprotective effects. p38 is reported to be activated by ischaemia in a perfused rat heart model and leading to an increase in injury.[75] Both p38α and p38β are present in the heart with p38α being the predominant isoform with the two isoforms exerting different physiological responses.[76] Studies using neonatal rat cardiomyocytes showed that overexpression of the α isoform produced pro-apoptotic effects and the β caused hypertrophy.[76] Marber *et al.* demonstrated, using adenoviral-mediated overexpression, the activity of p38α increased during ischaemia while p38β decreased implying that the β isoform was protective in a preconditioning manner.[77]

A cardioprotective function of p38 during ischaemia specifically after ischaemic preconditioning has been well studied.[78,79] Following multiple cycles of ischaemia and reperfusion, there was a decrease in p38 activation during sustained periods of ischaemia. Dhingra *et al.* demonstrated a role for p38 in TNF-α-mediated apoptosis via ROS production. Their observations showed an increase in p38 phosphorylation and a decrease in ERK-1/2 phosphorylation.[80] Inhibition of p38 was shown to prevent ROS production by the mitochondria and mitochondrial Ca^{2+} overload during I/R injury.[81] The cardioprotective effect of p38 was demonstrated by altering glucose utilisation[82] and by inhibiting endogenous p38. This was achieved by inducing the activity of dual-specific phosphatase (MKP-1) thereby reducing p38 phosphorylation.[83] The complex role of p38 in cardioprotection of myocardial cell death is dependent on number of factors and remains unclear.

1.3.1.2 JNK MAPK

JNK members play an important role in various stress conditions such as inflammation, neural development and apoptosis. Of the three main kinases, JNK1 and -2 are ubiquitously expressed, however JNK3 is expressed in the brain and heart exclusively. All

JNK are alternatively spliced producing ten different protein sequences with more than 80% homology.[84] They are involved in a number of biological processes including cysteine production, cell survival, cell death and differentiation and therefore are involved in diabetes, atherosclerosis, neurological disorders and cancer.[68] They respond strongly to cellular stressors such as heat shock, I/R injury, oxidative stress and UV radiation.[68]

The role of JNK in I/R injury is less well defined; numerous studies have shown that it is activated during the reperfusion phase but fewer studies have established its presence during ischaemia.[85,86] As a stress-induced signalling pathway JNK has been shown to have both pro- and anti-apoptotic functions. *In vivo* I/R experiments have shown that JNK1 and not JNK2 was proapototic.[87] JNK has been shown to enhance apoptosis during I/R through atrogin-1, an E3 ubiquity ligase that functions by degrading MAPK phosphatase-1 thereby sustaining the activation of JNK. This resulted in increased levels of apoptosis by increasing the amount of cleaved caspases-3 and -9, Bax and decrease the levels of Bcl-2.[88] JNK have also been shown to mediate the translocation of AIF from the mitochondria to the nucleus, further enhancing apoptosis.[89] Selective inhibitors of JNK have been shown to reduce infarct size and apoptosis after I/R injury.[90]

In contrast, the activity of JNK has also been reported to promote cardiac myocyte survival following I/R injury in response to nitric oxide.[91] In another study, the activation of caspase-9 had been curbed by its interaction with Apaf-1 and therefore delaying caspase-9 activation by the apoptosome.[92]Its activation of Akt, a pro-survival protein, in post-ischaemic cardiomyocytes has been considered to a the cardioprotective pathway.[93] The role of JNK in I/R injury remains controversial possibly due to the complexity of the signalling pathways.

1.3.1.3 ERK MAPK

The ERK signalling pathway has been well-studied in cell biology; ERK-1 and ERK-2 are 83% identical and share similar signalling activities. ERK-1/2 are involved in a number of biological processes including transcription, cell cycle control, cell death

and migration. Due to their diverse functions they play a significant role in cancer, cardiovascular diseases and have the ability to influence the immune system.[68] They are not functionally redundant as demonstrated by gene knockout experiments where ERK1 null mice generally had a normal phenotype but ERK2 null mice were embryonically fatal[94,95]

ERK-mediated cell death has been reported in a numerous studies; it was first reported by Bhat and Zhang[96] where they discovered that inhibition of ERK with a MEK1 inhibitor PD98059 reduced H_2O_2-induced cell death in oligodendrocytes. Its association with ROS-induced cell death has also been reported by a number of groups such as a report that showed ERK-1/2 and p53 were found to be responsible for doxorubicin-induced apoptotic cell death in H9C2 cells and neonatal cardiomyocytes.[97,98]

A number of studies have hypothesised about the cardioprotective signalling of MEK1-ERK-1/2 route in the MAPK pathway. In a report by Molkentin *et al.* using gene-targeted mice, $ERK1^{-/-}$, $ERK2^{+/-}$ and transgenic mice heart were subjected to I/R injury to induce MI and cell death. They reported that the MEK1 transgenic mice were protected from I/R injury, $ERK2^{+/-}$ heterozygous mice showed an increase in infarct size and cell death and $ERK1^{-/-}$ did not show an elevated susceptibility to cell death. These results suggested that loss of 1 allele of ERK2 altered ERK-1/2 activity; demonstrating the importance of this signalling pathway.[99]

ERK-1/2 exert their cardioprotective effects via a downstream mechanism. They can activate p90rsk, which in turn phopshorylates and activates pro-apoptotic Bad in the mitochondria.[100] Activation of ERK-1/2 by IL-10 has been shown to inhibit TNF-α-induced-apoptosis by blocking IKK phsophorylation and eventual NF-κB activation.[101] In response to I/R injury in neonatal cardiomyocytes ERK-1/2 activated the transcription factor GATA4, which resulted in an elevated expression of anti-apoptotic protein Bcl-xL.[102] Yazaki *et al.*[103] demonstrated in cardiomyocytes that ERK was activated transiently in a concentration-dependent manner by H_2O_2. Suppression of this activity with the MEK inhibitor, PD98059 resulted in an increase in apoptotic cell death of

cardiomyocytes.[100]

1.3.2 JAK-STAT Signalling Pathways in Myocardial Cell Death

The janus kinase-signal transducers and activators of transcription (JAK-STAT) pathway is a major signalling pathway for a variety of cytokines and growth factors. It is involved in the transmission of information received from extracellular signals through transmembrane receptors which result in activation of target promoters in the nucleus, thus providing a way of transcriptional regulation. Extracellular signalling polypeptides such as growth factors or cytokines play crucial role in immune response, inflammation and tumorigenesis. Cytokines mediate their response through activation of the JAK/STAT pathway and are recognised by specific transmembrane receptors of receptor complexes on target cells. This can result in alteration of gene expression in the target cells. This intercellular signalling plays a significant role in growth control, developmental regulation and homeostasis in multicellular organisms.[104,105]

STAT factors are a family of transcription factors that facilitate intracellular signalling such as proliferation, differentiation, cell survival and apoptosis initiated at the cell surface. The STAT family is made up of seven members (STAT-1, STAT-2, STAT-3, STAT-4, STAT-5a, STAT-5b, STAT-6), all of which contain a transactivation domain in the C-terminus as well as phosphorylation sites for the kinase activation. There is enough diversity in the amino acid sequences of family members to allow differential activation by groups of cytokines.[104] They possess a series of conserved structural domains; the N-terminus, involved in reciprocal STAT interactions and is loosely bound to the rest of the STAT protein; the coiled domain for nuclear transport dimerisation; the DNA binding domain, which binds to conserved regulatory sequences in the promoters of target genes; the src homology 2 (SH2) domain, which controls receptor binding; and the C-terminus, which contains the phosphorylation sites necessary for STAT activation.[106] The STAT-1 protein was the first to be discovered in this family and is essential for interferon (IFN) signalling and important in cell growth and death. It is composed of 750

amino acids and is 91 kDa in size (Figure 1.5).[107,108] STAT proteins are inactive in the cytoplasm and are activated by phosphorylation at specific tyrosine and serine residues by the JAK and MAP kinase families respectively; this causes the STAT proteins to homo- or heterodimerise, translocate to the nucleus and regulate gene expression.

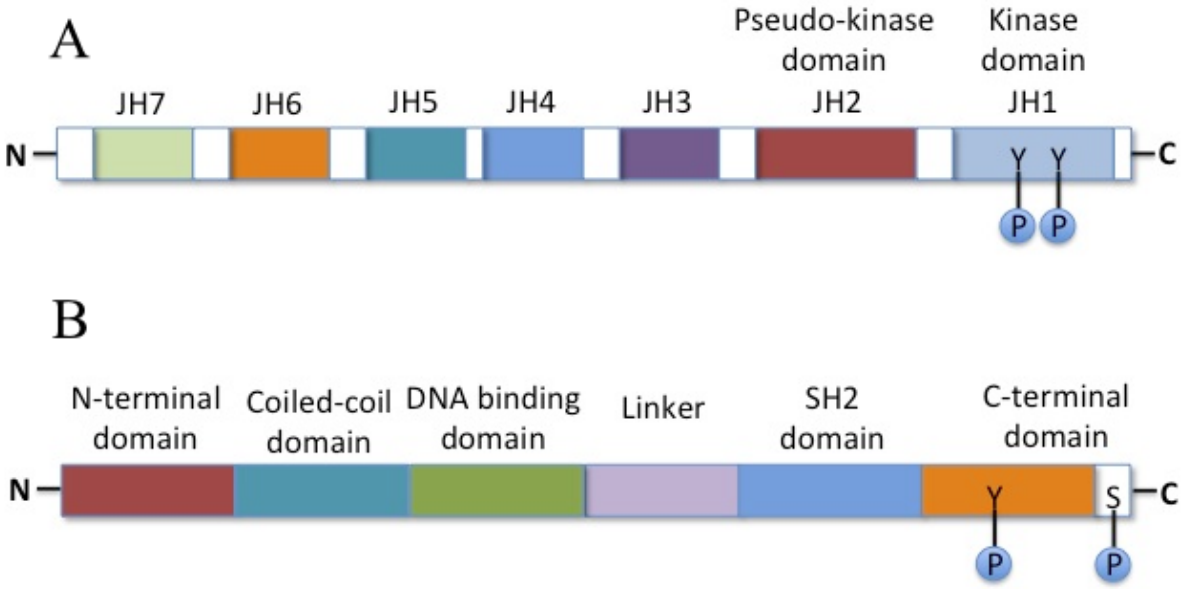

Figure 1.5 Diagram of JAK (A) and STAT (B) structure. JAKs share seven regions of high homology, JH1 - JH7. JH1 has been shown to encode the kinase. JH2 represents a pseudokinase domain, which appears to regulate JH1 catalytic activity. JH3 - JH7 have been implicated in receptor association. STATs also share several conserved domains, including an N-terminal domain (NH_2), a coiled-coil domain, the DNA binding domain (DBD), a linker domain, an SH2 domain, and a C-terminal domain containing the phosphorylation sites (circled P).

Receptor-associated proteins from the JAK family initiate STAT activation in response to cytokine stimulation. The JAK family is made up of four proteins, JAK1, JAK2, JAK3 and TYK2, all of which have an affinity for different receptors. JAKs are important in transmitting signals from the cell surface to the nucleus.[109] JAKs include the JH1 domain (the kinase domain) and the JH2 domain (the pseudokinase domain). The JH1 domain is responsible for the catalytic activity of JAKs, while the JH2 domain has been postulated to be a docking site for STATs[109] (Figure 1.5). They bind specifically to intracellular domains of cytokine receptor signalling chains and catalyse ligand-induced self- phosphorylation as well as phosphorylation of intracellular tyrosine residues on the receptor creating STAT-docking sites.[104]

1.3.2.1 STAT-1 Activation

Cytokines are molecules including proteins and peptides released by macrophages that bring about intercellular signalling.[110] Their participation in signalling pathways results in the transduction of signals to the nucleus from the cell surface. STAT-1 activation is initiated by interferon-γ (IFN-γ) signalling which is upregulated in response to inflammatory and immuno responses. The IFN-γ receptor is made of two subunits: α subunit which are responsible for IFN-γ binding and associates with JAK1 and β subunit associates with JAK2 and is responsible for signal transduction. The IFN-γ ligand binding induces the dimerisation of the subunits and also the activation and trans-phosphorylation of JAK. JAK phosphorylates the tyrosine residues at the cytoplasmic receptor domain creating a docking site for the SH2 domain in STAT-1 (Figure 1.6). The importance of STAT-1/IFN-γ has been established in many studies including one that showed STAT-1 knockout mice were highly susceptible to microbial infection and tumour formation due to the inability to induce IFN-inducible genes.[111]

STAT-1 binds to activated tyrosine residues where they are phosphorylated leading to STAT-1 homo- and heterodimerisation.[104] This dimer is further phosphorylated at the conserved serine 727 (S727) by p38 MAPK making it an active transcription factor.[112] Mutational analyses have indicated that serine phosphorylation of STAT-1 is required for maximal transcription.[113] The STAT-1 dimer translocates across the nuclear pore complex in an active bidirectional process that is energy dependent.[114] This process is facilitated by the association between the STAT-1 dimer and importin α5.[115,116] Once in the nucleus it binds to the GAS sequence (gamma-activated sites, an IFN-γ activation site) in the promoter region of of target genes and regulates gene expression.[107,117] The activation and nuclear export of STAT-1 is controlled by steady levels of transcriptionally active dimers and is maintained by STAT-1 being constantly shuttled in and out of the nucleus with reactivation from the cell membrane.[118] Studies have reported that dephosphorylation of the Y701 by nuclear tyrosine phosphates is required in order for it to be exported back to the cytoplasm.[119,120] Once dephosphorylated STAT-1 dissociates

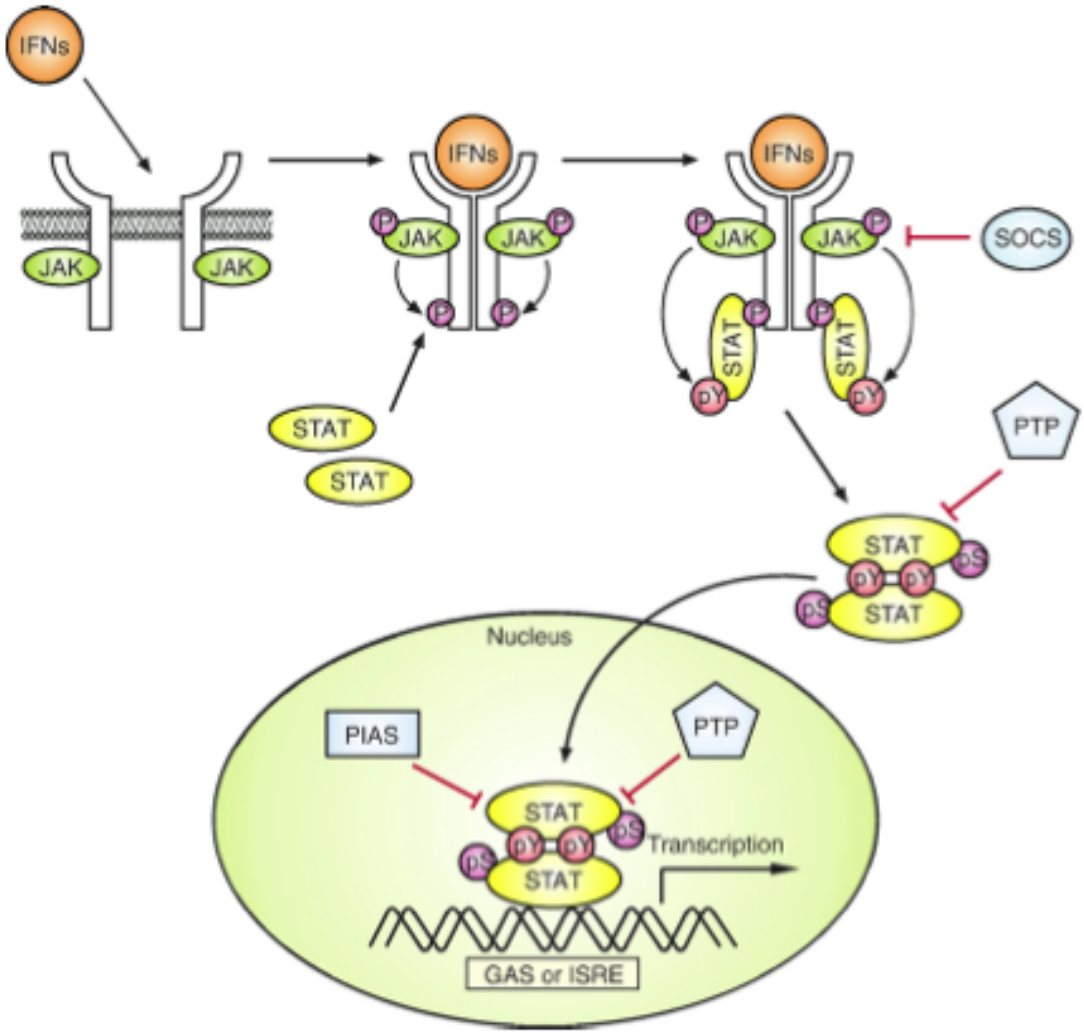

Figure 1.6 Mechanism of negative regulation of the JAK/STAT pathway. Cytokines bind to the receptors leading to a conformational change and activation of JAK by phosphorylation. STAT binds to the phosphorylated docking sites where they are phosphorylated and dimerise before translocating to the nucleus where they bind to DNA regulate gene expression. STAT-1 is negatively regulated by members of the protein inhibitors of activated STATs (PIAS) family that act in the nucleus; the protein tyrosine phosphatase (PTPs) family that act in the nucleus and cytoplasm; and suppressors of cytokine signalling (SOCS) family that are negative regulators of IFN-γ signalling.

from the DNA in the nucleus where specific amino acid sequences in the DNA-binding domain of STAT-1 are recognised by the chromosome region maintenance 1 (CRM1) and is exported back to the cytoplasm.[119]

The phosphorylation of STAT-1 at both the tyrosine and the serine residues has been considered necessary for STAT-1 function. Studies involving a point mutation of STAT-1 (Y701F) prevented it from forming homodimers involving SH2 interactions however they also showed that it could still bind to DNA and regulate gene expression of Hsp70 and Bcl-x.[121] This suggested that STAT-1 could function as a monomer or part of a complex with non-STAT partners but the mechanism is remains unknown, possibly by sequestering other transcription factors. The activation and nuclear translocation of STAT-1 in human fibroblasts, following IFN-γ treatment, occured within 15 min and remained for 2-2.5 h before they are actively deactivated after 4 h.[122,123]

STAT-1 activity can be modulated by its association with a number of regulatory proteins. These proteins include members of the protein inhibitors of activated STATs (PIAS) family that act in the nucleus; the protein tyrosine phosphatase (PTPs) family that act in the nucleus and cytoplasm; and suppressors of cytokine signalling (SOCS) family that are negative regulators of IFN-γ signalling.

SOCS1 and SOCS3 are potent inhibitors of the JAK-STAT pathway. Studies have shown the importance of the negative regulation of SOCS1 in JAK/STAT signalling pathway. For instance, SOCS1 null mice were found to die between the age of 2 and 3 weeks of a disease involving fatty degeneration, liver necrosis and macrophage infiltration of several organs brought on by a chronically unregulated IFN-γ/STAT-1 and IL-6/STAT6 activity. This study suggested the importance of SOCS1 in the regulation of IFN-γ and minimising the risk of pathological responses.[124,125] SOCS directly antagonise STAT-1 specific SOCS activation in a negative feedback loop.[126] Activated STAT-1 initiates the transcription of SOCS gene and the resulting proteins bind to the phosphorylated JAKS. SOCS negatively regulates STAT-1 in one of three ways; directly binding to the IFN-γ receptors and preventing the phosphorylation and recruitment of STAT-1; directly

binding to JAKs or the receptors and inhibiting JAK kinase activity; or interacting with the elongin BC complex, an activator of RNA polymerase II,[127] resulting in the ubiquination of JAKs.[128] The SH2 domain of SOCS1 and SOCS3 enables their binding to the active site of JAK1, JAK2 and Tyk2, inhibiting their function.[129]

Protein tyrosine phosphatases are tyrosine phosphatases that negatively regulate the activity of JAK/STAT pathway specifically SHP2 which dephosphorylated the Y701 and S727 residues of STAT-1 following IFN-γ induction.[130] One study of the SHP1 phosphatase which has a mutation on the SH2 domain[131] is thought to inhibit the JAK/STAT pathway either by binding to the tyrosine phosphorylated receptor thereby dephosphorylating and deactivating JAK2; or by directly binding to JAK2 in an SH2-independent manner.[131] Studies have confirmed that SHP2 plays a role in control of IFN-γ signalling pathway and has a role in STAT-1 tyrosine phosphorylation. In SHP2$^{-/-}$ cells, there is an elevation of caspase-1 an IFN-γ induced STAT-1 target gene.[121] CD45, another membrane-bound phosphatase has also being shown *in vitro* to directly dephosphorylate JAK2 however the mechanism remains unclear.[132]

Another class of negative regulators are PIAS proteins, made up of PIAS1, PIAS3, PIASx, and PIASy. They inhibit by binding to activated STAT dimers preventing them from binding to DNA. *In vivo* immunoprecipitation studies on U3A and human lypmhoblastoid cells treated with IFN-γ and IL-6 indicated that PIAS1 and PIAS3 interact with STAT-1 and STAT-3 respectively and inhibit STAT-mediated gene expression.[133–135]

1.3.2.2 STAT-1 signalling in the heart during I/R injury

Previous studies have demonstrated a significant role for the JAK/STAT signalling pathway in I/R injury, apoptosis and cardiac hypertrophy.[136] The JAK/STAT pathway was first demonstrated to be activated in rat cardiomyocytes following exposure to leukemia inhibition factor (LIF), Pan *et al.* determined that STAT-1 and STAT-3 were activated after pressure overloaded-induced hypertrophy produced by constricting the abdominal aorta. Immunoprecipitation and western blot analysis showed that JAK1 and JAK2 were

activated within 5 min of pressure overload with the phosphorylation of STAT-1 peaking within 5 to 15 min and STAT-3 peaking at 60 min[137]

Recent work has shown that STAT-1 and STAT-3 were activated in the isolated intact heart following I/R.[138–140] Ng *et al.*'s study observed an increase in the phosphorylation of high molecular weight proteins corresponding to the size of cytokine receptors in the ischaemic hearts compared to control hearts.[138] Left anterior descending (LAD) ligation in a rat model showed phosphorylation of JAK2, STAT-1, STAT-3, STAT-5a and STAT-6 within 5 min of MI, these remained active for 5 days.[141] Activated STATs bind to the promoter of the angiotensinogen gene resulting in an increase in the mRNA level of angiotensin II that regulates cardiac contractility and cell communication.[141,142]

There is evidence to suggest that STAT-3 may be cardioprotective in the heart following I/R injury. Pretreatment with JAK inhibitor AG-490 reduced STAT-3 phosphorylation, increased caspase-3 activity, increased Bax expression[143] and thus enhanced apoptosis. Treatment of cultured cardiac myocytes with cardiotropin-1 (CT-1), an activator of the STAT-3 pathway, enhanced cell survival following simulated I/R injury and therefore lower levels of apoptosis was observed.[144] STAT-3 deficient mice were also more susceptible to MI with a higher proportion of apoptotic cardiac myocytes following I/R injury in addition to a larger infarct size Figure 1.7).[145]

STAT-1 also plays a role in enhancing apoptotic cell death in cardiac myocytes following simulated I/R injury, via the induction of the Fas and FasL genes as well as caspase-1 activation.[146] Stephanou *et al.* reported that following simulated I/R injury, there was an increase in the phosphorylation of STAT-1 but not STAT-3, possibly due to the upregulation of caspase-1.[147] A previous study demonstrated that exposure of cardiac myocytes to ischaemia *in vitro* and in intact heart exposed to IFN-γ, a cytokine known to trigger cell cycle arrest and death in non-cardiac cells, results in rapid induction and activation of STAT-1 compared to the control lacking STAT-1.[148]

Over-expression of STAT-1 enhanced apoptotic cell death following simulated I/R injury, conversely, over-expression of STAT-3 triggered a pro-survival mechanism resulting in a

reduction of STAT-1 induced apoptotic cell death.[140] STAT-1 also inhibited the expression of anti-apototic proteins Bcl-2 and Bcl-x. Therefore the activity of STAT-1 seems to induce apoptotic cell death through up regulating pro-apoptotic proteins and repressing anti-apoptotic ones.[149] Cardiac myocytes with defective STAT-1 are shown to be resistant to apoptosis by I/R injury and surprisingly the influence of STAT-1 on cell death required only the phosphorylation of the serine residue but not the tyrosine residue.[139] Serine phosphorylation was activated by p38 MAPK during I/R injury and this pathway can be blocked by the addition on SB203580, a known p38 MAPK inhibitor.[139,150] Overall, the up regulation of STAT-1 plays a significant role in apoptotic cell death during MI in cardiomyocytes.

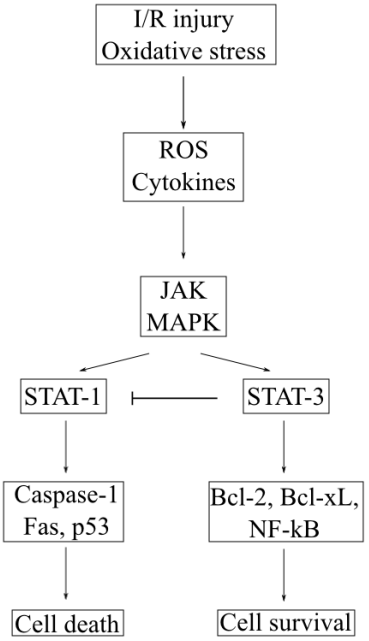

Figure 1.7 Pathway outlining the roles of STAT-1 and STAT-3 in the heart. During I/R injury and oxidative stress, there is an activation of JAK and MAPK that facilitate the activation and phosphorylation of STAT-1 and STAT-3. The relative levels of the STAT genes determine the activation of either the pro-apoptotic or anti-apoptotic genes.

It has been suggested that STAT-3 might counteract the apoptotic activities of STAT-1 in fibroblasts and possibly in cardiac myocytes after I/R. Increasing amounts of STAT-3 with STAT-1 in cardiomyocytes led to a dose-dependent reduction in STAT-1 induced apoptosis after I/R.[140] Studies in mice monitored the levels of STAT-1 and STAT-3 during ischaemia and reperfusion demonstrated that the levels of STAT-1 Y701 was induced within 15 min after reperfusion in the risk area compared to the control. STAT-1 Y701

phosphorylation levels peaked at 30 min and decreased to a plateau at 60 min. The levels of STAT-1 S727 phosphorylation surprisingly were enhanced only after ischaemia and not during reperfusion.[122,151] These increase phosphorylation levels of STAT-1 confirmed the pro-apoptotic role of STAT-1 during I/R injury. In contrast both STAT-3 Y705 and STAT3 S727 phosphorylation were both observed during the ischaemia and the reperfusion with STAT-3 Y705 peaking at 30 min. Knockdown by siRNA of STAT-1 prevented the induction of caspase-1, Fas, and FasL mRNA following simulated I/R injury thereby protecting the cells from I/R induced cell death.[139] Pretreatment with JAK inhibitor AG-490 reduced STAT-3 phosphorylation; increase caspase-3 activity and Bax expression and thus enhanced apoptosis.,[152] whereas treatment of cultured cardiac myocytes with CT-1 enhanced cell survival following simulated I/R injury, leading to lower levels of apoptosis.[144] STAT-3 deficient mice were also more susceptible to MI with higher apoptotic cardiac myocytes following I/R injury as well as larger infarct size.[145] These data suggest that both STAT-1 and STAT-3 both play a role in modulating the effects of I/R injury to cardiomyocytes.

Due to the role of STAT-1 in apoptotic cell death during I/R injury its inhibition may be a potential therapeutic target in order to minimise the occurrence of cell death in the myocardium. Townsend *et al.* demonstrated the role of STAT proteins in I/R-induced apoptosis in the heart and reported that epigallocatechin gallate (EGCG), a major component in green tea reduced STAT-1 phosphorylation and protected cardiac myocytes against I/R-induced apoptotic cell death.[153] They have also shown the protective effects of EGCG and green tea extract infusion on both cultures of cardiac myocytes and isolated rat hearts; ECGC reduced STAT-1 Y701 and S727 phosphorylation and protected the cardiac myocytes against I/R-induced apoptotic cell death. EGCG also reduced the expression of Fas receptor. Furthermore, the oral administration of the green tea extract and EGCG infusion limited the severity of myocyte apoptosis and magnitude of the infarction. Overall the consumption of green tea mediated cardioprotection and enhanced cardiac function during I/R injury suggesting further investigation is warranted.

1.4 Green Tea

Tea, *Camellia sinensis*, is believed to have been consumed in Southeast Asia over for two thousand years and its distinct flavour and associated health benefits have resulted in a rapidly spreading worldwide consumption.[154] The different manufacturing methods alter the chemical composition of tea leaves resulting in three major types of tea: black, oolong and green tea (Figure 1.8). Black tea, which accounts for 78% of the world tea consumption, undergoes a fermentation process where fresh tea leaves are crushed causing an enzyme-catalysed oxidation by polyphenol oxidase and polymerisation of tea catechins leading to a formation of oligomers like theaflavins. Oolong tea, which accounts for 2% of the world tea consumption, is prepared by partial fermentation' where the tea leaves are bruised and as result a higher level of tea catechins are retained and theaflavin oligomers are also formed. Green tea, which accounts for 20% of the world tea consumption, is prepared by pan-frying or steaming fresh tea leaves inactivating the polyphenol oxidase and preserving the characteristic tea catechins.[155] This work focuses on green tea and the polyphenols which are a major component in its chemical composition and their cardioprotective capabilities following I/R injury.

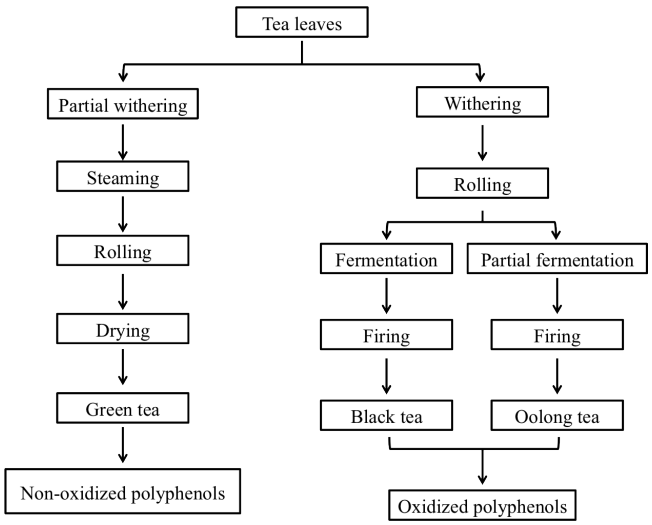

Figure 1.8 Tea manufacturing process.

Polyphenols make up one of the most vast and widely distributed groups of natural products in plants with more than 8000 reported structures, many of which are found in

food.[156] These highly diverse natural products are characterised by the presence of at least one aromatic ring with one or more hydroxyl group present and can contain several sub-groups of phenolic compounds. Studies have shown that the different polyphenol subgroups can differ significantly in terms of stability, bioavailability and physiological function.[157158]

One of the major groups of polyphenols in plants is the flavonoids which have a *C6-C3-C6* structural backbone with two aromatic rings linked by a three carbon bridge (Figure 1.9). Depending on the hydroxylation variation in the carbon bridge, they can be further divided into subclasses of flavonols, flavones, flavan-3-ol, anthocyanidine, flavonones and isoflavone.

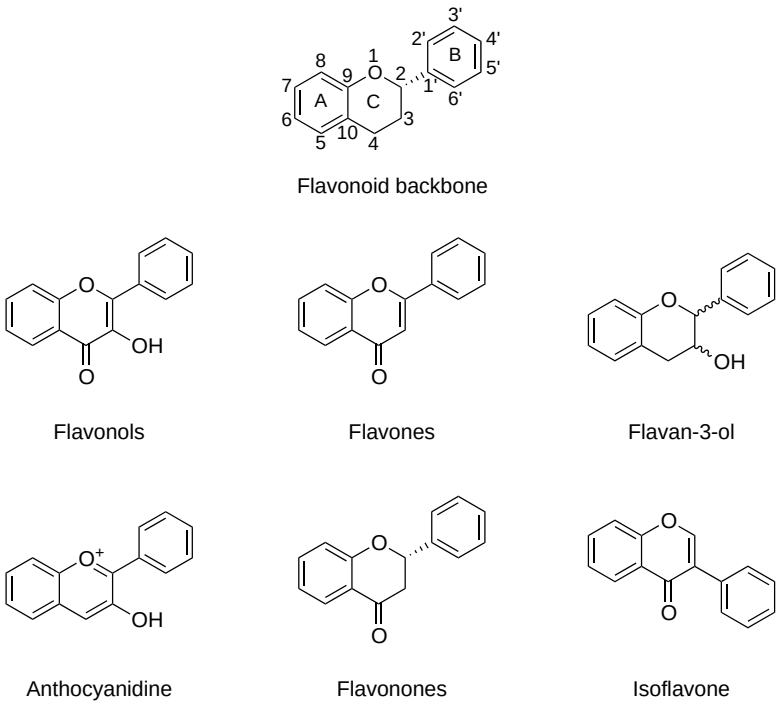

Figure 1.9 Flavonoid skeleton and sub-classes.

Flavan-3-ols are commonly called catechins. They lack the double bond between C2 and C3 and also have no carbonyl group on the C4 carbon. The catechins include the simple monomers (+)-catechin and its isomer (−)-epicatechin. B ring hydroxylation and esterification with gallic acid leads to gallocatechins. The four gallocatechin isomers depicted in Figure 1.10 are the major flavonoids found in tea leaves and chocolate. Flavan-3-ols can also form complex proanthocyanidins polymers, that are commonly known as

condensed tannins.

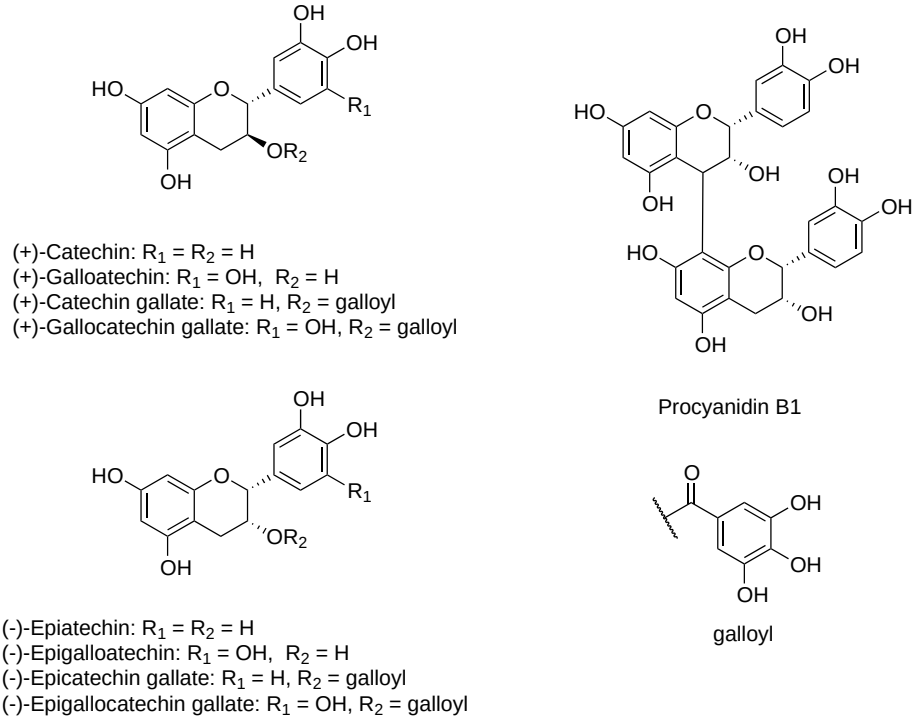

Figure 1.10 Flavan-3-ols and Procyanidin.

The subjects of this thesis, epicatechin **1** (EC), epicatechin gallate **2** (ECG), epigallocatechin **3** (EGC), and epigallocatechin gallate **4** (EGCG) (Figure 1.11) are the major catechins found in green tea leaves. They are characterised by a meta-5,7-dihydroxy substitution in ring A and di- or tri-hydroxy substitution in ring B. Epicatechin gallate and epigallocatechin gallate have an additional galloyl group appended via the C3 carbon.

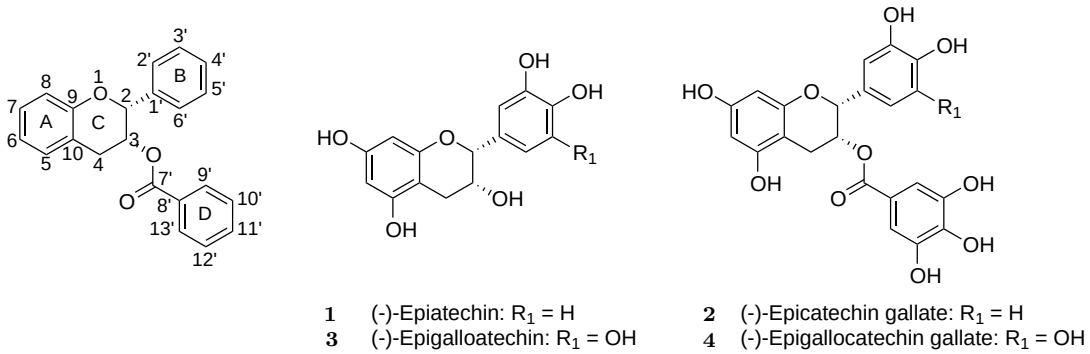

Figure 1.11 Labelling and numbering of the polyphenolic systems in tea leaves.

1.4.1 Green Tea Composition

The chemical composition of green tea is complex. It comprises of proteins derived from amino acids such as glutamic acid, glycine, leucine; lipids; carbohydrates such as cellulose, glucose and fructose; vitamins B, C and E; caffeine; pigments such as chlorophyll and carotenoids; and a number of minerals and trace elements such as Ca, Na, P, Co, K, and Al[1] (Table 1.1).

Table 1.1 Mean % composition (dry weight) of green tea and black tea.[1]

Compound	Green tea	Black tea
Proteins	15	15
Amino acids	4	4
Fibre	26	26
Carbohydrates	7	7
Lipids	7	7
Pigments	2	2
Minerals	5	5
Phenolic compounds (Flavanoids)	30	5
Oxidised phenolic compounds (Theaflavins)	0	25

Flavan-3-ols constitute the most important components in free tea with the four major ones being epicatechin (approximately 6% of the total catechins present), epigallocatechin ($\approx$ 19%), epicatechin gallate ($\approx$ 13%), and epigallocatechin gallate ($\approx$ 59%).[1] Phenolic acids present include gallic acid, caffein acid and also chlorogenic acid and flavonols such as kaempferol, myricetin and quercetin (Figure 1.12). The relative catechin content, however, is dependent on the geographical location of the tea leaves (soil, climate, fertilisers); how the tea leaves are processed before drying (the fermentation stage); the types of green tea (caffeinated or decaffeinated); and the infusion (brew time, preparations and amount of leaves used).[159,160] Several studies[161–163] have reported that decaffeinated and instant tea have less tea catechin contents compared to freshly brewed.

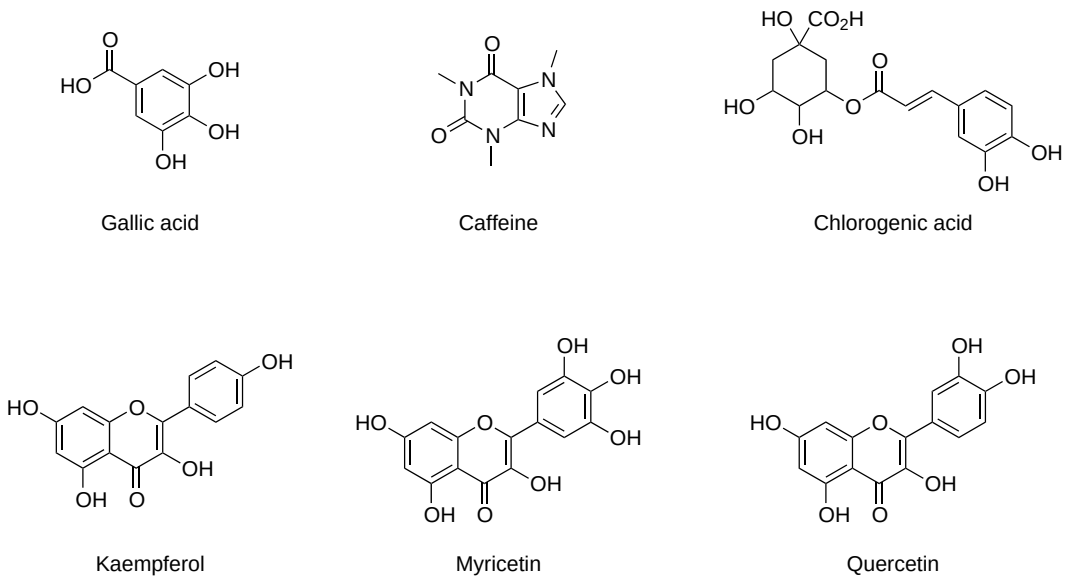

Figure 1.12 Chemical structures of some compounds present in green tea.

A USDA database for the flavonoid content of selected foods indicated that in a 1% infusion (1 g tea leaves/100 mL boiling water) the catechin composition was as follows: EC (8.3 mg), EGC (29.2 mg), ECG (17.9 mg), and EGCG (the highest with 70.2 mg).[164] Wie[161] indicated that a cup of green tea (2.5 g of green tea leaves in 200 mL of boiling water) could contain 90 mg of EGCG. Fernandez *et al.*[165] determined that in 45 tea samples from different geological origins (India, China, Japan, Kenya, to mention a few), the amount of catechins was always higher in green tea with average contents of the major catechins being EGCG and EGC 7.36% and 3.96% respectively. Cabrera *et al.*[166] analysed 45 samples of different types of tea, including black, red, green and oolong, and reported the mean content of the four major catechins. They determined that green tea had a higher content of catechins than the others as well as the highest levels of EGCG (Figure 1.13).

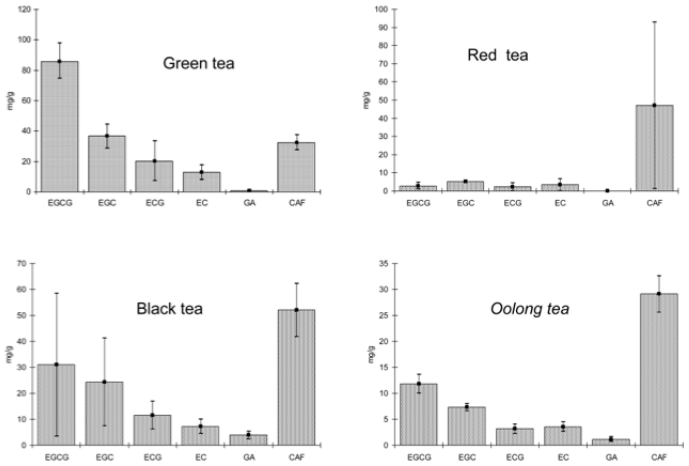

Figure 1.13 Levels of catechins [EGCG, (–)-epigallocatechin gallate; EGC, (–)-epigallocatechin; ECG, (–)-epicatechin gallate; EC, (–)-epicatechin], gallic acid (GA), and caffeine (CAF) in each type of tea. Taken from Carera *et al.*[166]

1.4.2 Isolation and Structural Elucidation of Green Tea Flavonoids

A number of spectrophotometric methods have been used for the estimation of total phenolic and flavonoid content in tea, including as high-performance liquid chromatography (HPLC), gas chromatography[167] and capillary electrophoresis.[168] Although these methods are simple and effective, they lacked specificity for individual compounds. In order to precisely quantify and identify individual polyphenols, the compounds must be separated. Reversed-phase high performance liquid chromatography (HPLC) coupled with a diode array detector and/or mass spectrometric detector (LC-MS) is the most widely use analytical tool for the quantification of polyphenols. Yayabe *et al.*[169] used Sephadex LH-20 column chromatography and preparative HPLC to separate tea catechins from green tea solution. Goto *et al.*[170] developed an HPLC analysis method for eight tea catechins and caffeine using an ODS column and a water-acetonitrile-phosphoric acid mobile phase. Beecher *et al.*[171] discovered that the use of methanol on the mobile phase resulted in a different elution order (EGC, EGCG, EC, ECG) compared to acetonitrile (ECG, EC, EGCG, EGC) and sharper peak shapes were observed by the addition of an aqueous acetate buffer. Spectra of EC, EGC, ECG and EGCG all exhibited maximum absorbance at 210 nm. Quantitative values for catechin levels in the infusions indicated that EGCG was the highest concentration, while epicatechin was the lowest and the order

of concentration in green tea and black tea was EGCG>ECG>EGC>EC. Evaluation of elution methods by Sander *et al.*[172] revealed that the presence of 0.05% of trifluroacetic acid as an acidic modifier in the mobile phase was necessary to achieve good resolution of the catechin peaks and reproducibility in retention times. A more recently developed method in chromatography called ultra high performance liquid chromatography (UPLC) significantly enhanced the separation of polyphenols while improving the efficiency and analysis time compared to a conventional HPLC.[173]

The identity of a polyphenol can be confirmed by matching the retention time collected from the UV/VIS spectra data with that form a diode array detector. When standards are not available, techniques such as tandem mass spectrometry and nuclear magnetic resonance can provide enough information to deduce the identity of the polyphenols present in a sample. Poon *et al.*[174] reported a direct fusion of extracted tea samples into a mass spectrometer fitted with either an electrospray ionisation interface (ESI-MS) or an ionspray interface (IS), with or without liquid chromatography (LC) separation. They observed green tea polyphenols in the mass spectra and achieved best sensitivity in the negative ionisation mode. Further structural characterisation of analogues present was accomplished by tandem mass spectrometry, utilising the product and parent-ion scans of the fragment ions characteristic of catechins and gallic acid. The mass spectrum contained several signals from the polyphenols ($[M - H]^-$) including *m/z* 169 (gallic acid), 289 (EC); 305 (EGC); 441 (ECG); and 457 (EGCG) (Figure 1.12). When the ion at 457 was studied, fragments displayed were *m/z* 125 (dihydroxy phenol moiety), 169 (gallic acid), 287 (loss of water from the EGC moiety) and 305 (EGC moiety), to further confirm the compound EGCG. Similarly, for the ion at 441, the fragment ions at *m/z* 125 (trihydroxy phenol moiety), 169 (gallic acid), 271 (loss of water from the catechin moiety) and 289 (catechin) were observed to confirm the identity of compound ECG.

It is worth noting that although a number of conventional methods have been used to separate tea catechins, with HPLC being the method of choice, very few of the published methods gave satisfactory results. This was due to limited efficiency and long retention times to obtain sufficient resolution of the peaks. What they do provided is a starting

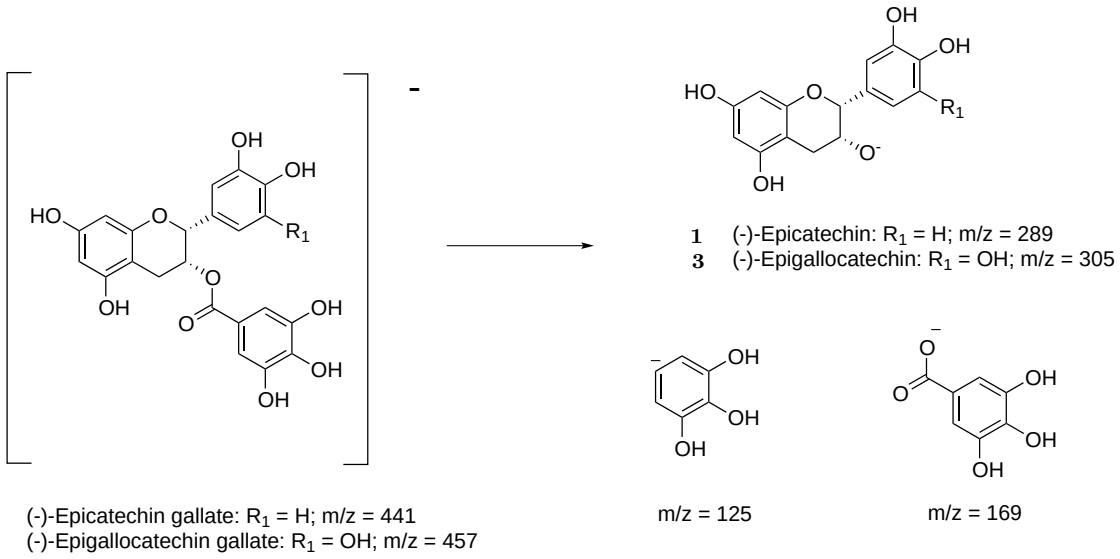

Figure 1.12 Interpretation of Tandem Mass spectra signals of the polyphenolic systems in tea leaves.

point for the purification of individual catechins.

1.4.3 Epidemiological Studies of Green Tea

The intake of green tea has been inversely associated with the risk of cardiovascular disease (CVD). A cohort study in Japan showed that people who consume over 10 cups of green tea a day had a decreased risk of death from CVD.[175] A cohort study in the Netherlands performed a 10-15 year follow-up of cohorts of 550-800 men. It revealed a decrease in coronary heart disease mortality associated with an increase in flavonol intake.[176] Consumption of 8 g of powdered green tea per day for two weeks improved blood vessel dilation in chronic smokers indicating that green tea consumption could potentially help to prevent cardiovascular diseases in smokers.[177]

A cross-sectional study by Sasazuki *et al.*,[178] involving 512 coronary arteriography patients, found that green tea intake was inversely associated with coronary atherosclerosis in men but not women. However, a similar study however by Hirano *et al.*[179] did not find a correlation between green tea consumption and coronary heart disease in Japanese patients who has undergone coronary angiography, although there was a reduction in the risk of MI with the consumption of more than two cups of green tea per day. A cross-

section study showed that consumption of 120-599 mL of green tea per day for at least one year decreased the development of hypertension by 46% and consumption of more that 600 mL per day reduced the risk by 65% compared to subjects that only consumed 120 mL per day.[180]

The cardioprotective effects of green tea has also been demonstrated in a number of animal studies. Green tea catechins were shown to reduce the development of atheroschlerosis and reduce the development of lesions in hypercholesterolemia apolipoprotein E-Deficient mice.[181] Green tea catechins also had an effect on lipid metabolism and prevented the appearance of atherosclerotic plaque by decreasing the absorption of triglycerides and cholesterol.[182] A report by Srinivasulu *et al.*[183] showed that green tea treatment (300 mg/kg body weight) for 4 weeks impeded cardiac dysfunction in diabetic rats by improving oxidative stress and lipid profile.

Although there is some epidemiological evidence suggesting the protective effects of green tea consumption, other studies show no correlation between green tea consumption and a reduction in CVD risk. A cohort study by Rimm *et al.* in the United States on over 30,000 male professionals found a modest but insignificant inverse association between flavonoid intake and coronary heart disease. However, the study revealed an inverse association with mortality from CHD among men with previous CHD history.[184] The Caerphilly study on Welsh male population showed no inverse association between intake of flavonoids and reduction in the risk of ischaemic heart disease.[185] They suggested that the addition of milk removed the antioxidant capabilities of the flavonoids, but this contradicts other reports that suggesting that the addition of milk to tea had no significant effect on the antioxidant properties.[186]

1.4.4 Cardioprotective Effects of Green Tea Flavonoids

Coronary heart disease is multifaceted, involving oxidative stress and damage;[187,188] inflammation;[189] platelet aggregation[190] and lipid peroxidation.[191] Green tea catechins have been reported to be beneficial during I/R injury by acting as an antioxidant and

anti-inflammatory agent, a transition metal chelator[192] and an inhibitor of enzymes that promote oxidative stress.[192] These cardioprotective effects are attributed to their ability to modulate a number of signalling pathways that limit the damaging effects of I/R injury.

1.4.4.1 Antioxidative Effects

As previously described, cells and tissues are constantly being threatened by free radicals produced under normal conditions and several antioxidant defence mechanisms neutralise these species rendering them inactive. During I/R injury, production levels of ROS exceed the capacity of the endogenous scavengers causing oxidative stress, DNA and protein damage and lipid peroxidation. In turn this leads to damage to the cell membrane and organelles membrane and sometimes death.[187]

Flavonoids can prevent the injury caused by ROS in a number of ways including their ability to function as direct radical scavengers; metal chelators and as inhibitors of xanthine oxidase and NADPH oxidase.[192] It is well established that flavonoids are efficient free radical scavengers of superoxide[193] and hydroxyl radicals,[194,195] resulting in the formation of a less reactive and more stable radical species.

Some of the antioxidant effects are through the chelation of metal ions such as iron and copper.[196,197] These transition metals are important cofactors of the Fenton reaction catalysing the production of hydroxyl radicals ($\cdot$OH) from H_2O_2 and $\cdot O_2{}^-$.[198] The hydroxyl and carbonyl groups present in the tea catechins have a high affinity for metal ions and can chelate these metal ions to form inactive complexes, preventing them from catalysing the reaction and thus inhibiting the damaging effects of ROS species. A report by Melidou *et al.* discovered that intracellular chelation of iron by flavonoids in Jurkat cells protected them form DNA damage induced by H_2O_2.[199] Recent findings have also demonstrated that by using flavonoids rutin, taxifolin, epicatechin, luteolin, and their complexes with transition metal Fe^{2+}, Fe^{3+}, and Cu^{2+} the flavonoid-metal complexes demonstrate higher scavenger potencies towards superoxide anion than the

parent flavonoids.[200] Another mechanism proposed involves an electron transfer from the catechins to the ROS-damaged sites on DNA.[201] This reaction resulted in a fast chemical repair of the DNA by reducing the amount of strand breaks and base damage.

The ROS scavenging abilities of the green tea catechins is attributed to their chemical structure particularly due to the presence of the hydroxyl groups.[202] Free radical scavenging studies show that the most potent scavengers were EGCG and ECG due to the presence of the ring C galloyl group, which increased their phospholipid/water partition coefficient and in turn their solubilisation. They also improved the efficiency of hydroxyl radical scavenging. The difference between EGCG and ECG was only slight due to the presence of an extra hydroxyl group on ring B that improved the scavenging capabilities of superoxide anion by electron delocalisation resulting in a more stable semiquinone radical.[194,203] It has been suggested that the more hydroxyl group a catechin possessed, the more efficient it is as a radical scavenger.[204] With EGC and EGCG, the hydroxyl groups present on ring A also play a role in the antioxidant activities by undergoing oxidation and decarboxylation when reacted with H_2O_2.[202] Indirectly, these catechins have also been shown to increase the levels of endogenous scavengers. Rats orally given green tea extract exhibited higher levels of glutathione reductase, superoxide dismutase and catalase, which subsequently reduced oxidative damage and lipid peroxidation.[205]

Despite the body of work on the antioxidant effects of green tea catechins, several human and animal studies do not show an effect on a plasma level. This might be due to their poor bioavailability with an insufficient concentration circulating to exert the expected effect. In addition, a number of studies indicate that these catechins acted more as pro-oxidants and induce oxidative damage by generating ROS. EC and EGCG exhibit pro-oxidant behaviour by generating superoxide anion and hydroxyl radicals in the presence of copper.[206]

1.4.4.2 Anti-Inflammatory Effects

Atherosclerosis is now considered an inflammatory disease that begins with inflammation of the arterial wall which in turn activates the vascular endothelial cells. This leads to an increase in the expression of various leukocyte adhesion molecules, such as vascular cell adhesion molecule-1 (VCAM-1), causing an increased adhesion of monocytes to the injured site and subsequently a penetration into the innermost layer of the arterial wall.[189]

Green tea catechins have been shown to inhibit the leukocyte adhesion and transmigration onto the endothelial space.[207] EGCG and ECG reduced cytokine-induced VCAM-1 expression and monocyte adhesion to the endothelial cells.[208] In cultured human endothelial monolayers, EGCG has also been shown to inhibit the attraction of neutrophils to the inflammation site, inhibit the migration of neutrophils, and also reduce chemokine production.[209] EGCG and ECG also induced apoptosis of monocytes by activation of caspase 8 and 9 in a dose-dependent manner but EC and EGC had no effect possibly due to the lack of the galloyl moiety.[210]

1.4.4.3 Effects on Signalling Pathways

The cardioprotective effects of EGCG on the heart during I/R injury is not just due to its antioxidant capabilities but also due to its inhibitory effects on interferon-γ activation of STAT-1. Surface plasmon resonance analysis on the interaction between immobilized STAT-1 and EGCG or ECG or quercetin, a strong antioxidant flavonoid without anti-STAT-1 activity, showed that only EGCG directly interacted with STAT-1 protein.[211] Computer modeling also indicated that EGCG may strongly interact with STAT-1 at a site near the SH2 domain, which is important in the phosphorylation activation. Townsend *et al.*[153] reported that STAT-1 played a significant role in pro-apoptotic cell death following I/R injury. They found that in neonatal rat cardiac myocytes, EGCG reduced reduced STAT-1 phosphorylation and protected apoptotic cell death. It was also discovered that oral administration of 0.1% green tea extract limited the infarct size and also apoptosis in the isolated rat heart exposed to I/R injury associated with improved

hemodynamic recovery and ventricular function.

MAPK kinases act as signal transducers of cell proliferation activated by external stimuli.[212] Angiotensin II (Ang II) is involved in the proliferation of vascular smooth muscle cells (VSMC) in the parthenogenesis of atherosclerosis.The pretreatment of primary cultured rat aortic VSMC inhibited the Ang II-induced phosphorylation of ERK 1/2, JNK 1/2, and p38 MAPK.[213] This inhibition may result in the reduced risk of coronary heart disease by ingesting green tea.

Another possible mechanism involved the inhibition of the transcription factor Nuclear factor-κB (NF-κB), important in the expression of pro-inflammatory molecules such as cytokines and chemokines. Activation and regulation of NF-κB is controlled by inhibitory protein IκB by sequestering it in the cytoplasm of the immune/inflammatory effector cells. NF-κB is activated by phosphorylation; ubiquination and proteolysis of IκB; and NF-κB is translocated into the nucleus where it binds to specific promoter sites activating gene transcription. This leads to an activation of intracellular and extracellular regulatory events causing an inflammatory cascade. The activation of NF-κB can be inhibited by treatment with antioxidants, protease inhibitors, proteasome inhibitors and corticosteroids.[214] In a study on rats given EGCG (10 mg/kg) intravenously followed by a period of myocardial ischemia reperfusion injury, there was a decrease in IL-6 and neutrophilic infiltration associated with the initial stages of inflammation mediated by the NF-κB pathway during the reperfusion stage.[215] EGCG was shown to inhibit proteosome activity by the accumulation of IκB-β, an inhibitor of the NF-κB signalling pathway.[216] In another report, EGCG inhibited NF-κB activation through the inhibition of IκB phosphorylation in JB6 mouse epidermal cell line by blocking a TPA-induced tumour promoter.[217]

1.4.5 Bioavailability & Biotransformation of Green Tea Flavonoids

The health benefits of green tea catechins are not only dependent on the amount consumed but also on the bioavailability. Understanding the absorption and metabolism is

important in determining their biological activity *in vivo* within target tissues.

After oral dosage of green tea catechins are absorbed in the small intestines with peak absorption between 1-2 h after consumption. Bioavailability is low however due to the acidic conditions during digestion leading to poor absorption, fast metabolism and excretions. As a result only about 5% of administered catechins are present in the plasma. A study on rats given 0.6% GTP in their drinking water showed that over 28 days, significant amounts of EC and EGC were found in the oesophagus, large intestine, kidney, lung and bladder. EC and EGC levels were low in the gut, spleen and thyroid. EGCG levels were higher in the oesophagus and large intestine which was likely to be due to a poor systematic absorption of this compound. These catechins were also metabolised rapidly, with EGCG mainly being excreted through the bile while EGC and EC were excreted though the urine and bile.[218]

The poor bioavailability of EGCG could be explained by Lipinski's Rule of 5,[219] which states that a compound is likely to have poor bioavailability if the molecular weight is more than 500; contain 5 or more hydrogen bonds; has 10 or more hydrogen acceptors and a clogP of more than 5. Due to the number of hydrogen bond donors and acceptors present in EGCG, it would have a larger polar surface area and a large hydration shell as it is capable of interacting with a greater number of water molecules. All this, in combination with its large molecular mass, would make it less likely to pass through the lipid bilayer membrane and so less bioavailable. The poor bioavailability of these catechins could also be due to their large molecular masses. Thus, EGCG (458 Da) has limited bioavailability compared to smaller molecules such as EGC (306 Da) and EC (290 Da).[220]

Lu *et al.*[221] observed that after oral administration of green tea to rats only 14% EGC, 3% EC and less than 1% EGCG appeared in the blood stream. In human volunteers they observed that there was a notable increase in catechin plasma concentration 2-4 h after consumption. However, the plasma concentrations ranged from 0.6 to 1.8 μM.

It is known that green tea catechins undergo extensive biotransformation including methylation, glucuronidation, sulfation and ring-fission metabolism leading to the formation of a number of metabolites (Scheme 1.1).[222] Enzymology studies have shown that EGCG and EGC are readily methylated by the enzyme catechol-*O*-methyltransferase (COMT). EGCG forms 4'-*O*-methyl-(–)-EGC and 4"-*O*-methyl-(–)-EGCG or 4',4"-*O*-dimethyl-(–)-EGCG at high and low concentrations respectively.[223] EGC is metabolised to form 4'-*O*-methyl-EGC.[224] Uridine 5'-diphosphoglucuronosyltransferase (UGT) and sulfotransferase (SULT) bring about the catalytic reaction of the tea catechins leading to the formation of glucuronidated and sulfated conjugates respectively.[225] This can also occur with methylated EGCG to form even more metabolites.[226] EC does not undergo glucuronidation in human liver or small intestinal microsome but the rat liver however efficiently forms glucuronidated EC.[227] Tea catechins do become sulfated in humans, mouse, and rat liver cytosol by the enzyme sulfotransferase with the most efficient being the human liver cytosol as discovered by Walee *et al.* They indicated that sulfation was the major pathway in EC metabolism in the human liver and not glucuronidation.[227] In the gut of human volunteers 2 h after oral ingestion of green tea, ring fission catechin metabolites were formed. They included 5-(3',4',5'-trihydroxyphenyl)-γ-valerolactone (M4), 5-(3',4'-dihydroxyphenyl)-γ-valerolactone (M6) and 5-(3',5'-dihydroxyphenyl)-γ-valerolactone (M6') believed to be derived from microbial metabolism in the colon (Scheme 1.1).[228] These were further broken down to phenylacetic and phenylpropionic acids which may either be absorbed or passed out in the faeces.[224,226] ECG metabolites are yet to be found in human urine or plasma.[229]

Overall these biotransformations of green tea catechins alter their physical and chemical properties which may reduce biological activity. Very little research has been conducted on the biological activity of such metabolites and the cases studied have shown limited activity compared to the parent compound. A study into the radical scavenging activity, for example, and in their ability to inhibit the release of arachidonic acid from HT-29 human colon cancer cells, showed that EGCG metabolites were less effective compared to the parent compound EGCG.[230] Lambert *et al.* showed that valerolactone metabo-

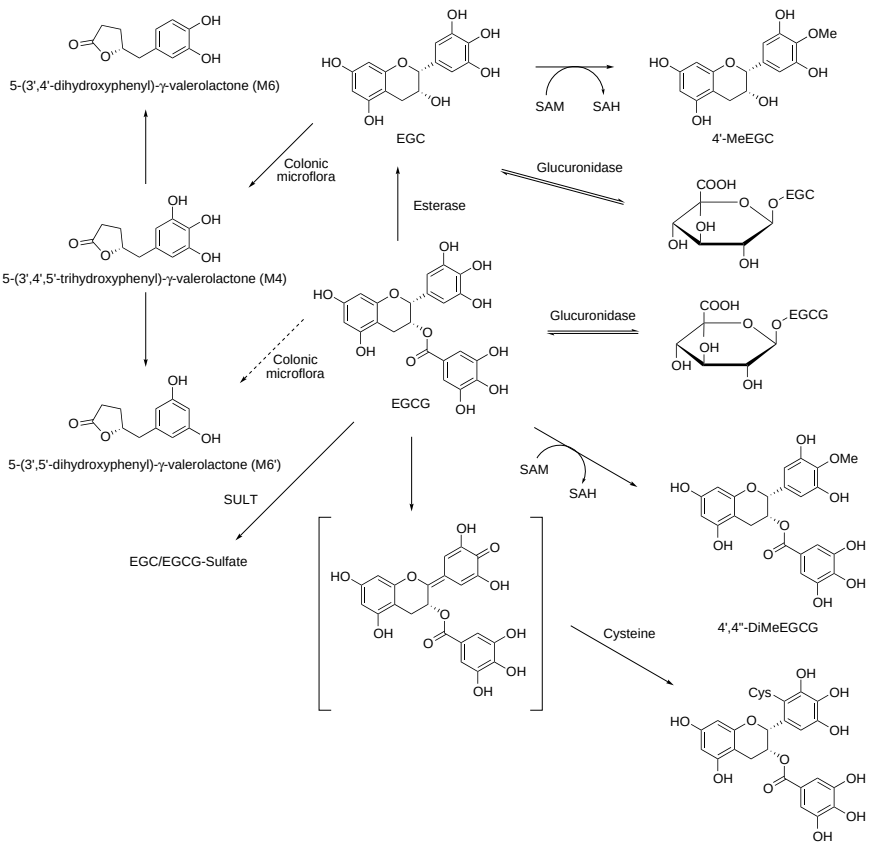

Scheme 1.1 Biotransformation of green tea catechins. Abbreviations: 4'-MeEGC, 4'-*O*-(–)-epigallocatechin; 4',4"-diMeEGCG, 4',4"-di-*O*-(–)-epigallocatechin gallate; COMT, catechol-*O*-methyltransferase; SAH, *S*-adenosylhomocysteine; SAM, *S*-adenosylmethionine; SULT, sulfotransferase; UGT, UGT, UDP-glucuronosyltransferase. Adopted from Lambert *et al.*[222]

lites could have anticancer and anti-inflammatory activity in terms of growth inhibitory activity in human colon cancer cell lines (HT29 and HCT116).[231]

Many of the mechanistic studies of tea catechins have been conducted on numerous cell lines with concentrations ranging from 10-1000 μM. Such high concentrations are not achievable in target tissues other than the skin and GI tract. Hence the poor bioavailability of these polyphenols should be taken into consideration when studying their beneficial effects.

1.4.6 Biosynthesis of Green Tea Flavonoids

The biosynthesis of flavonoids involves a complex network of routes based on the shikimate pathway. It is a seven-step metabolic pathway used by bacteria, fungi and plants leading

to the production of the aromatic amino acids phenylalanine, tyrosine, and tryptophan. The *C6-C3-C6* flavonoid backbone is formed in two biosynthetic pathways. The carbon bridge and ring B are made up of a phenylpropanoid units that are synthesised from *p*-coumaroyl-CoA (synthesised from phenylalanine) via the phenylpropanoid metabolic pathway. Ring A is formed from the condensation of three acetate units in the malonic acid pathway.[157] The first step involves a condensation reaction between malonyl-CoA and *p*-coumaroyl-CoA catalysed by chalcone synthase (CHS) via a sequential decarboxylation condensation reaction (Scheme 1.2).

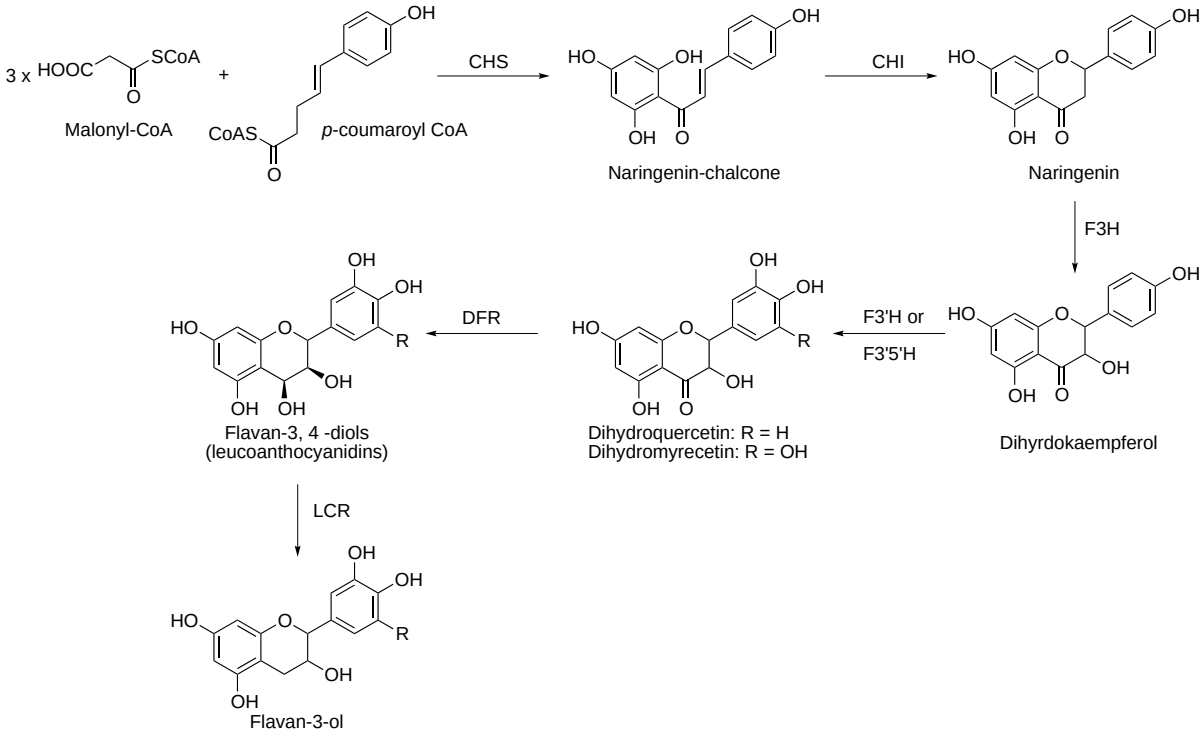

Scheme 1.2 Schematic diagram of the biosynthetic pathway of flavan-3-ols. Enzyme abbreviations: CHS, chalcone synthase; CHI, chalcone isomerase; F3H, flavanone 3-hydroxylase; F3'H, flavonoid-3'-hydroxylase or F3'5'H, flavonoid-3'5'-hydroxylase ; DFR, dihydroflavonol 4-reductase; LCR, leucoanthocyanidin 4-reductase.

An isomerisation retained with the help of chalcone synthase enables a conjugate ring closure leading to the formation off naringenin. This pivotal intermediate enables the synthesis of other polyphenol classes and their sub-group such as flavonols including proanthocyanidin (Scheme 1.2). Subsequent enzymatic modifications lead to the formation of flavan-3,4-diols. Reduction catalysed by the enzyme leucoanthocyanidin 4-reductase then leads to the synthesis of flavan-3-ol.

1.4.7 Previous Syntheses Green Tea Flavonoids

Initial forays into the synthesis of flavan-3-ols were mainly based on simpler catechins. The first total synthesis approach of EGCG **4** was reported by Chan and Li in 2001.[232] Their strategy provided access to the racemate and individual enantiomers of EGCG and was the basis for the syntheses of flavan-3-ols for many years after. Their approach to EGCG **4** involved the assembly of three aromatic fragments and selective formation of the *cis*-disubstituted benzopyran while maintaining stereochemical integrity at the C3 position (Scheme 1.3).

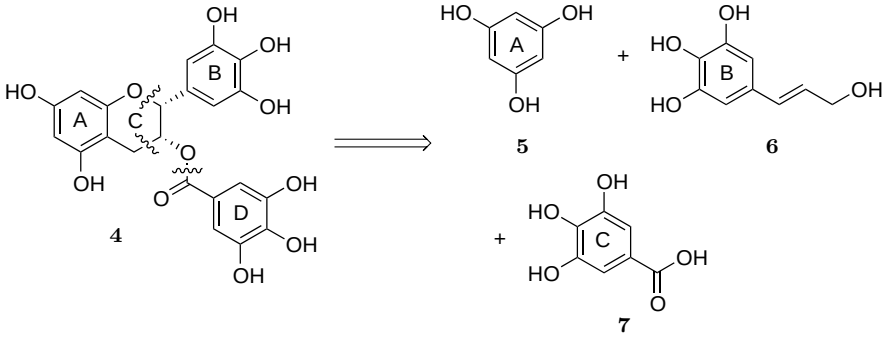

Scheme 1.3 Li and Chan's disconnection approach.

The synthesis began with the Friedel-Crafts type coupling of cinnamyl alcohol **9** and phenol **8** with cat.H_2SO_4/SiO_2 in CS_2/CH_2Cl_2 to give **10** (Scheme 1.4). Dihydroxylation of **10** with catalytic OsO_4 and NMO gave racemic diol **11**, while asymmetric dihydroxylation of **10** with AD-mix α or AD-mix β gave access to the two enantiomers. The *ortho* ester intermediate was achieved by converting **11** using triethyl orthoformate with PPTS in CH_2Cl_2. The resulting crude was treated with K_2CO_3 in acetone to induce the cyclisation resulting in the formation of benzyopyrans **13** after the removal of the formate ester.

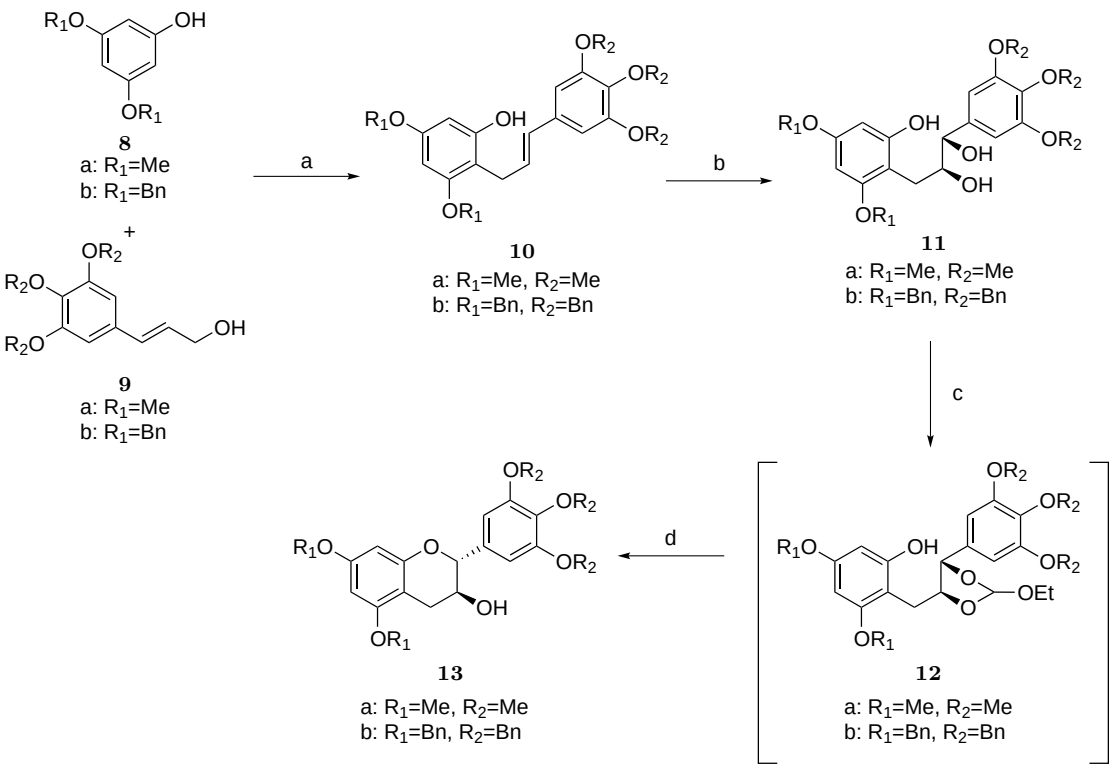

Reagents and conditions. a) H_2SO_4, CH_2Cl_2, CS_2, rt; b) cat. OsO_4, NMO, acetone, H_2O; c) $CH(OEt)_3$, PPTS, CH_2Cl_2, rt; d) K_2CO_3, MeOH, acetone, rt.

Scheme 1.4 Li and Chan's synthesis of the *trans* chroman-3-ol **12**.

Formation of the required *cis* isomer **15** was achieved by a Dess-Martin oxidation of **13** to the ketone **14**, followed by reduction with L-selectride® in THF. (Scheme 1.5). Esterfication of **15a** with 3,4,5-tri-*O*-benzylgalloyl chloride and DMAP in CH_2Cl_2 gave the ester **16**. Finally, catalytic hydrogenation of **16a** with 20% $Pd(OH)_2/C$ afforded EGCG **4**.

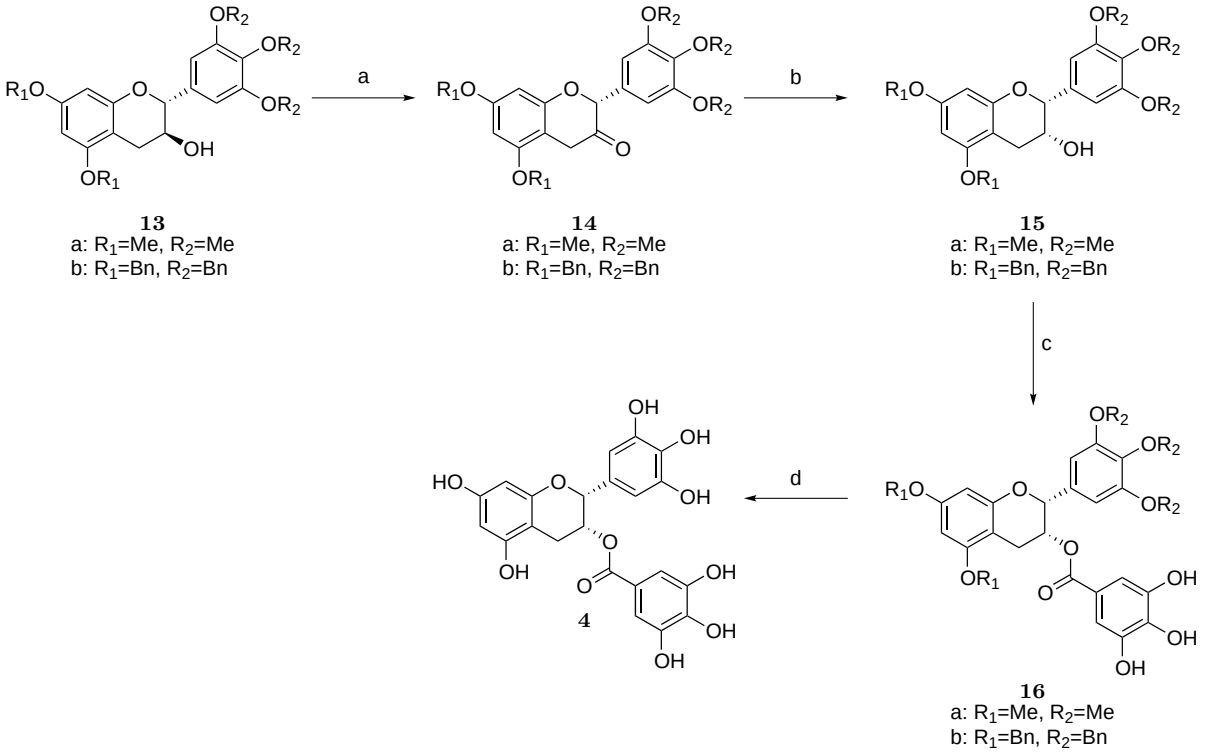

Reagents and conditions. a) Dess-Martin Periodinane, CH_2Cl_2, rt; b) L-Selectride, -78 °C,rt; c) 3,4,5-tri-*O*-benzylgalloyl chloride, DMAP, CH_2Cl_2; d) H_2, $Pd(OH)_2$, MeOH, THF, rt.

Scheme 1.5 Li and Chan's synthesis of epigallocatechin gallate **4**.

Over the last ten years there have been been a number of total syntheses of green tea catechins and their analogues which featured benzylated EGC **15a** as a a key intermediate. The approaches fall into one of four synthetic strategies described below (Scheme 1.6).

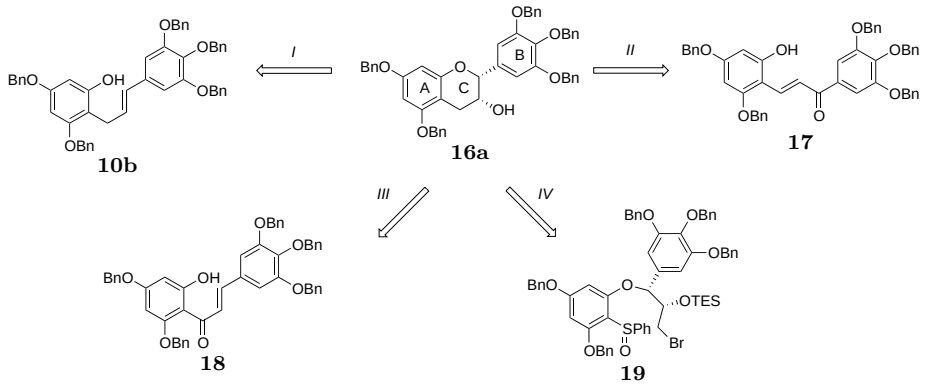

Scheme 1.6 Synthetic strategies to the synthesis of green tea catechins.

The first strategy is based on the synthesis of allylphenol **10b** as described above with the approach by Li and Chan. Strategy *II* uses a crossed aldol reaction to construct the requisite precursor **17**, which was first demonstrated by Taylor *et al.*[233] in a synthesis of epicatechin gallate analogues (Scheme 1.7). Their synthesis began with commercially available 2,4,6-trihydroxybenzaldehyde, which was treated successfully with BnBr and K_2CO_3 then NaH and MOMCl to give **21**. A crossed Aldol condensation between **21** and acetophenone **22** next gave the enone **23** in good yield. Reduction of the enone alkene with catechol borane followed by ketone reduction with $NaBH_4$ produced benzyl alcohol **25**. Its conversion to the corresponding bromide **26** was followed by base induced elimination to achieve precursor **27**.

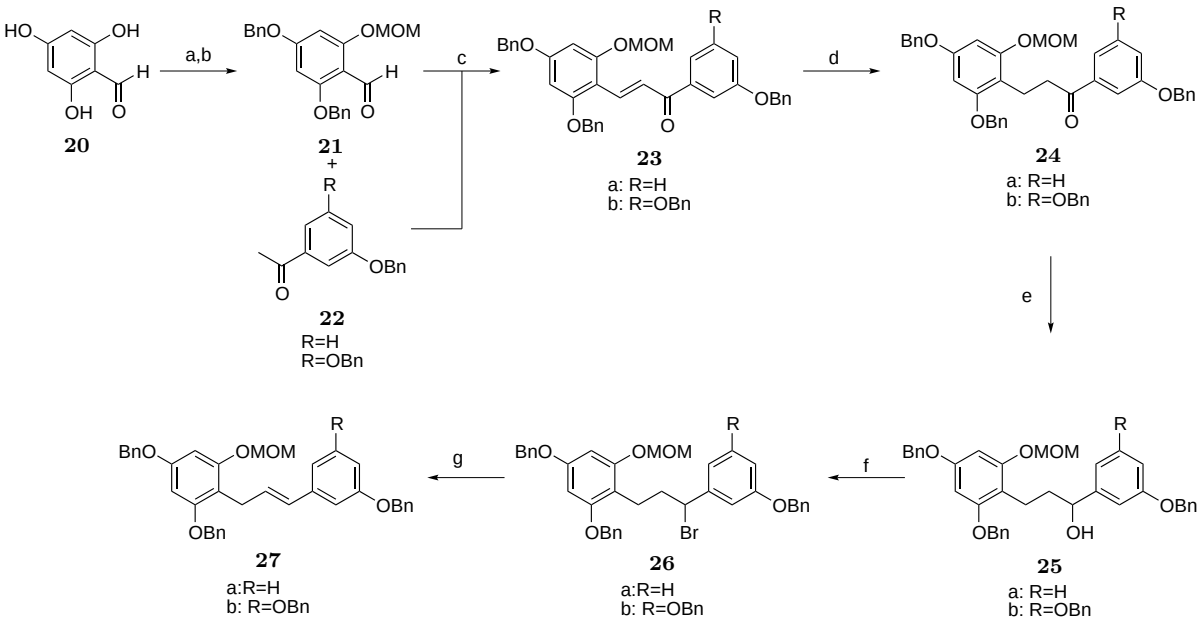

Reagents and conditions. a) K_2CO_3, BnBr, DMF, rt, 69%; b) NaH, MOMCl, THF 0 °C to RT, 88%; c) KOH aq. (50%), EtOH, THF, RT, 16 h, R = H 69%, R = OBn 94%; d) Catechol borane, THF, - 78 °C to RT, R = H 86% crude, R = OBn 86% crude; e) $NaBH_4$, MeOH, RT, R = H 99% crude, R = OBn 99% crude; f) PPh_3, Br_2, Et_3N, CH_2Cl_2, 0 °C to RT, R = H 85%, R = OBn 99%; g) DBU, PhMe, 110 °C, 16 h, R = H 57%, R = OBn 53%.

Scheme 1.7 Taylor *et al.*'s approach to (–)-epicatechin gallate analogues.

Sharpless dihydroxylation of **27** using AD-mix β next gave diol **28** with an e.e. of 75%. Acid-catalysed cyclisation of **28** to **31** proved impossible using 3M HCl which was attributed to the lack of an activating *para*-hydroxyl group in ring B. Rather, cyclisation to

the 2,3-*cis* substituted product was was achieved via Li and Chan orthoformate intermediate **29** which was transformed into a single diasteroisomer of bromide **30** through the action of AcBr in $CHCl_2$. Cyclisation and deformylation was then achieved with K_2CO_3 to give *cis*-2,3 disubstituted benzopyran **31**. The final steps in the synthesis involved a DCC coupling with 3,4,5-tribenzyloxybenzoic acid and global debenzylation by hydrogenolysis with $Pd(OH)_2/C$ to give the enantiomerically pure analogues (Scheme 1.8).

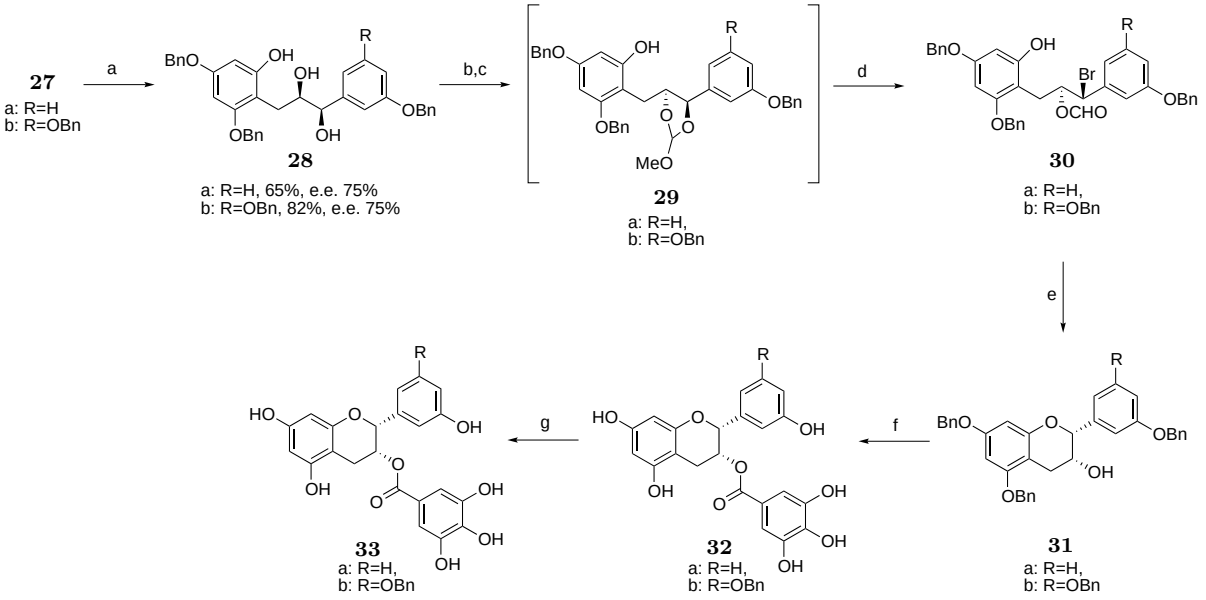

Reagents and conditions. a) AD-mix β, *t*-BuOH, H_2O, $MeSO_2NH_2$, 0 °C, 5 days; b) HCl, MeOH, Et_2O, reflux, 5 h, R = H: 100% crude, R = OBn: 100% crude; c) $HC(OMe)_3$, PPTS cat., CH_2Cl_2, rt; w/up; d) AcBr, CH_2Cl_2, rt, R = H: 81% crude, R = OBn: 91% crude; e) K_2CO_3, acetone, RT, 5 h; w/up then K_2CO_3, MeOH, rt, 16 h, R = H: 61%, R = OBn: 45%; f) DCC, tri-OBn gallic acid, DMAP, CH_2Cl_2, rt, 16 h, R = H: 64%, R = OBn: 67%; g) H_2, 10% $Pd(OH)_2/C$, EtOAc, rt, 12 h, R = H: 94%, R = OBn: 37%.

Scheme 1.8 Taylor *et al.*'s approach to (–)-epicatechin gallate analogues.

Strategy *III* was developed by Zaveri *et al.*[234] and involves the cyclisation of a chalcone to the flav-3-ene (Scheme 1.9). Their *O*-Benzyl-protected 3,4,5-trihydroxybenzaldehyde **30** was condensed with 4',6'-bis(benzyloxy)-2'-hydroxyacetophenone **37** in piperidine/EtOH to afford the chalcone **18**. Using a method reported by Clark-Lewis and Skingle,[235] this compound was treated with $NaBH_4$ in THF/EtOH at reflux to induce the reductive cyclisation to flav-3-ene **38**. A hydroboration/oxidation sequence next gave the *trans*-flavan-3-ol **13b** with < 5% of the *cis*-flavan-3-ol as a contaminant. Esterification with

3,4,5-trimethoxybenzoyl chloride and deprotection by hydrogenation afforded the *trans* analogue **40**. Alternatively, application of the oxidation and reduction sequnces developed by Li and Chan (Dess-Martin Periodinane oxidation followed by a L-Selectide® reduction) gave the *cis* catechin **15a** from which the target compound **39** was readily prepared.

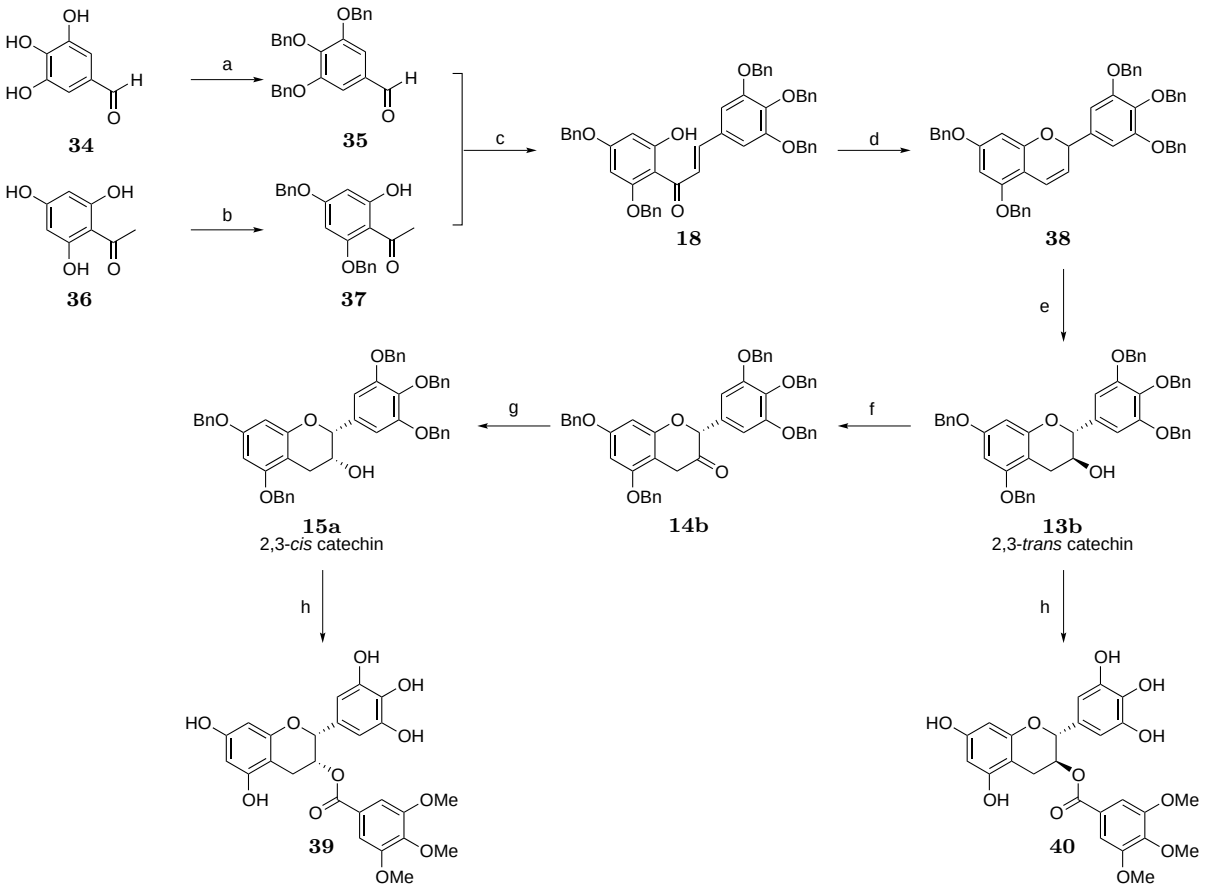

Reagents and conditions. a) i) BnBr, K_2CO_3, DMF, ii) LAH, THF, iii) PCC, CH_2Cl_2, 87%; b) 2 equiv. of BnBr, K_2CO_3, HMPA, 75%; c) Piperidine, EtOH, reflux, 65-75%; d) $NaBH_4$, THF/ EtOH, 55%; e) i) BH_3-THF ii) H_2O_2, NaOH, 60-70%; f) Dess-Martin periodinane, CH_2Cl_2, 50%; g) L-Selectride, THF, 75-80%; h) i) 3,4,5-trimethoxybenzoyl chloride, DMAP, Et_3N, ii) H_2/Pd/C, dioxane, 66%.

Scheme 1.9 Zaveri's approach to (–)-epicatechin gallate analogues.

Strategy *IV* is based on the use of a nucleophilic aromatic substitution to achieve the union of key fragments followed by a sulfinyl-metal exchange reaction to effect a cyclisation. The method was designed by Suzuki *et al.*[236] to enable the stereocontrolled access to various epicatechins and their gallates (Scheme 1.10).

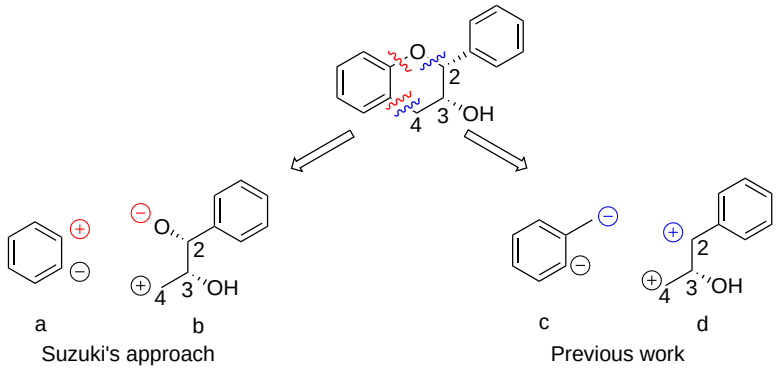

Scheme 1.10 Suzuki *et al.*'s change of the connectivity for reverse polarity strategy.

Thus, the electrophilic flouro-sulfoxide[236] unit **41** and the epoxy alcohol **42**.[237] were first united via a aromatic nucleophilic substitution (S_NAr) reaction. The resulting ether **43** was advanced to bromide **19** using standard procedures. Then transformed into **40** by the addition of PhLi (2.0 equiv in THF, room temp., 1 h). The use of *n*-BuLi resulted in a poorer yield and recovery of starting material (Scheme 1.11).

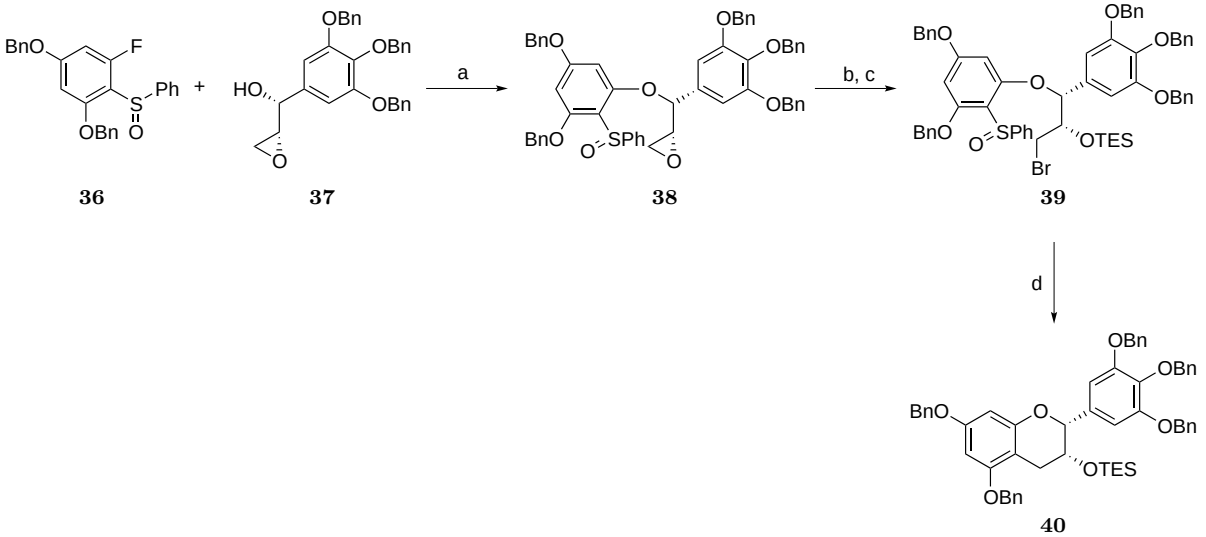

Reagents and conditions. a) NaH, toluene, DMPU, rt, 39%; b) Li_2NiBr_4, THF, 0 °C; c) TESOTf, 2,6- lutidine, CH_2Cl_2, 0 °C, 2 steps, 97%; d) PhLi, THF, RT, 81%.

Scheme 1.11 Suzuki *et al.*'s approach to (–)-epicatechin gallate analogues.

Conversion of **44** to EGC **3** was readily accomplished by removal of the TES group using *n*-Bu_4NF to alcohol **15a** followed by global deprotection of the benzyl groups by hydrogenolysis over 20% $Pd(OH)_2/C$ to (–)-EGC **3**. For (Đ)-EGCG **4**, esterification of **15a** with 3,4,5-tri-*O*-benzylgallic acid followed by hydrogenolysis of all benzyl groups proved higher yielding (Scheme 1.12).

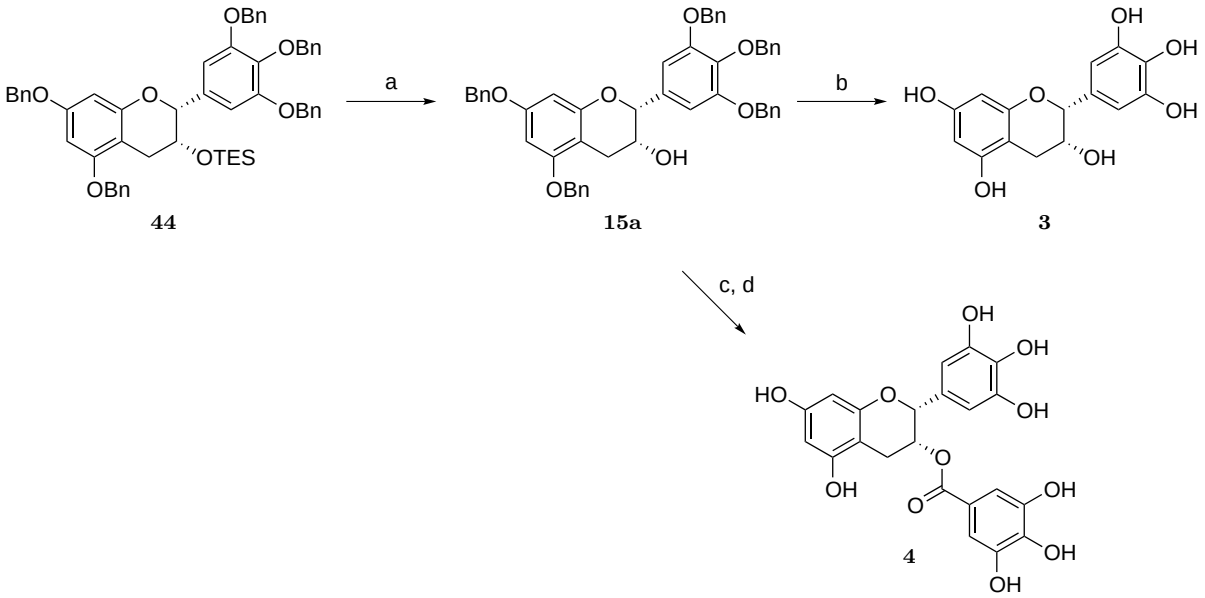

Reagents and conditions. a) *n*-Bu_4NF, THF, 0 °C, 99%; b) H_2, $Pd(OH)_2$, THF, MeOH, H_2O (4:4:1), RT, 71%; c) 3,4,5-tri-*O*-benzylgallic acid, EDCI · HCl, DMAP, Et_3N, CH_2Cl_2, RT; d) H_2 , H_2/Pd/C, THF, MeOH, H_2O (4:4:1), RT, 68% 2 steps).

Scheme 1.12 Suzuki *et al.*'s approach to (–)-epicatechin gallate analogues.

1.5 Objectives

Previous work in the Townsend group has demonstrated the protective effects of green tea catechins and their ability to enhance cardiac function during I/R injury. The purpose of this work is to generate a library of analogues for cardiac testing in order to gain an insight into the components that influence cardiac function following I/R injury and oxidative stress. The catechins are made up of two or three phenol rings, which are modifiable to analogues via the total synthesis of EGCG.

The objectives for this project are:

1. Synthesis of green tea polyphenols and analogues
    i The total synthesis of ECG and EGCG
    ii The synthesis of novel analogues to elucidate structure activity relationships with a view to improve both efficacy and potency
2. Evaluate the cardioprotective effects of green tea polyphenols and analogues during oxidative stress using H_2O_2
    i Establish an *in vitro* model to induce cell death in H9C2 cells cardiac myoblasts
    ii Assess the effects of GTP and analogues on H9C2 cells and their ability to protect against oxidative stress leading to cell death
3. Evaluate the cardioprotective effects of green tea polyphenols and analogues during I/R injury in H9C2 cells
    i Establish an *in vitro* model to induce cell death
    ii Assess the effects of GTP and analogues on H9C2 cells and their ability to protect against simulated I/R injury leading to cell death
4. Evaluate the cardioprotective effects of green tea polyphenols and synthesised analogues during I/R injury in neonatal rat cardiomyocytes (NRCM)
    i Establish an *in vitro* model to induce cell death
    ii Assess the effects of GTP and analogues on NRCM and ability to protect against simulated I/R injury leading cell death

Chapter 2

Synthesis of Green Tea Polyphenols and Analogues

2.1 Synthetic Strategies

Our proposed retrosynthesis for epigallocatechin gallate (EGCG) in Scheme 2.1 was chosen because it offered the flexibility needed to prepare analogue compounds. Critically, it involved the formation of the core ABD ring system via key intermediate **13b** and allowed access to the target compounds, their enantiomers and potential analogues. *trans*-catechin **13b** can be submitted to a published sterochemical inversion of the C-3 hydroxyl by sequential Dess-Martin oxidation and L-Selectride ® reduction to **15a**. Deprotection of the resulting 2,3-*cis*-catechin would produce epigallocatechin **3**. An EDC coupling of the 2,3-*cis*-catechin with 3,4,5-*tris*-(benzyloxy)benzoic acid followed by global deprotection would furnish the target compound epigallocatechin gallate **4**.

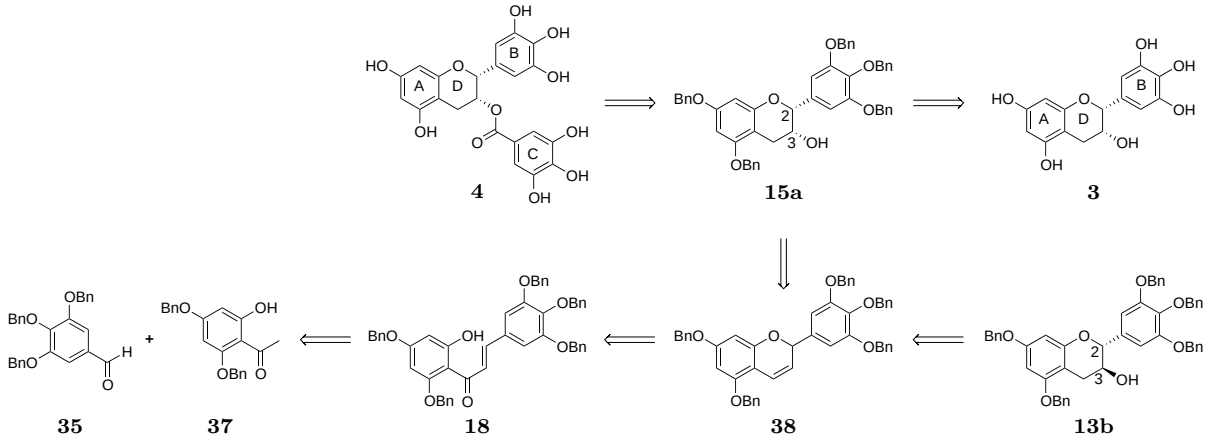

Scheme 2.1 Retrosynthesis of EGCG **4** and EGC **3**.

2.2 Forming the core ABD ring system

Our initial approach to *trans*-catechin **13b** was based on a route developed by Taylor *et al.*[238] (Scheme 2.1). It involved a condensation between acetophenone **37** and benzaldehyde **35** to afford the prop-2-en-1-one **18**.

Our first task was to synthesise the starting materials **35** and **37** (Scheme 2.2). 1-(2,4-*Bis*-(benzyloxy)-6-hydroxyphenyl)ethanone **37** was synthesised in reasonable yield from 1-(2,4,6-trihydroxyphenyl)ethanone **36** by selective 2,4-benzylation using two molar equivalents each of benzyl bromide and potassium carbonate. Benzyl protecting groups were chosen due to their stability towards acidic and basic conditions. 3,4,5-*tris*-(benzyloxy) benzaldehyde **35** was synthesised in threes streps from commercially available 3,4,5-trihydroxybenzoic acid **45**. First, protection of the benzoic acid as its methyl ester **46** was achieved in 95% yield by an esterification with methanol.

Initial attempts to effect the global protection of the free phenolic groups in **46** employed 3 molar equivalents each of benzyl bromide and potassium carbonate. However, this resulted in a complex product mixture comprised of mono-, di-, and tribenzoylated methyl 3,4,5-trihydroxybenzoate, and recovered starting material. By using 6 molar equivalents each of benzyl bromide and potassium carbonate the desired methyl 3,4,5-trihydroxybenzoate **47** was given in 75% yield. The next step involved re-

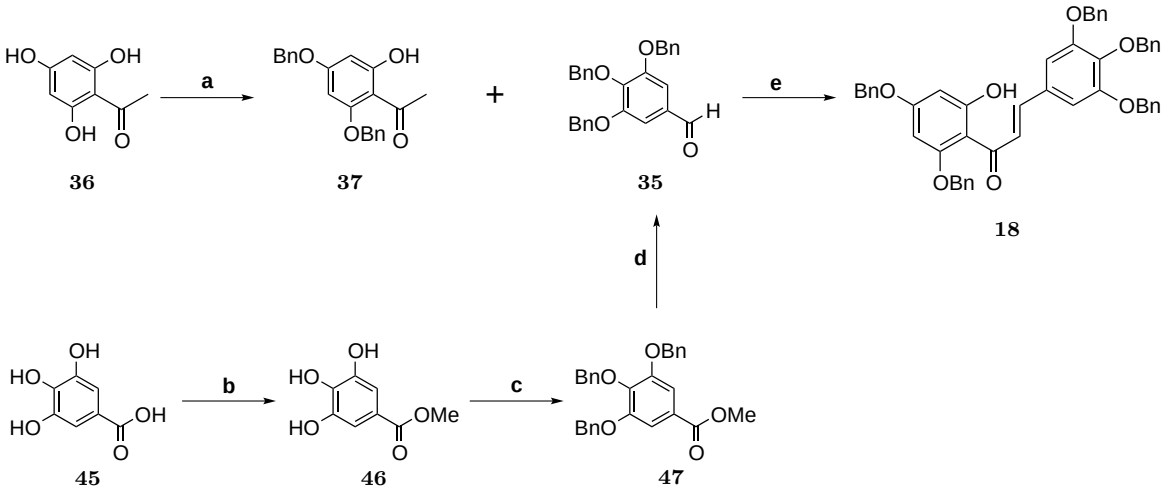

36 **37** **35** **18** **45** **46** **47**

Scheme 2.2 Reagents and conditions. a) BnBr, K_2CO_3, DMF, 45%; b) MeOH, cat. H_2SO_4, reflux, 93%; c) BnBr, K_2CO_3, DMF, 75%; d) i) LAH, THF, 95%; ii) PDC, DCM, 4Å molecular sieves, rt, 82%; e) 40% aq. KOH, EtOH, THF, rt, 33%.

duction of the methyl ester to the corresponding alcohol with lithium aluminium hydride (LAH) reduction followed by oxidation of the crude alcohol with pyridinium dichromate (PDC) oxidation in the presence of 4Å molecular sieves. Once the reaction had gone to completion, it was quenched with diethyl ether and filtered through a layer of silica gel to obtain 3,4,5-*tris*-(benzyloxy)benzaldehyde **35** in good yield (Scheme 2.2). The condensation reaction to form *(E)*-1-(2,4-*bis*-(benzyloxy)-6-hydroxyphenyl)-3-(3,4,5-*tris*-(benzyloxy)phenyl)prop-2-en-1-one **18** was completed using 40% potassium hydroxide in ethanol and tetrahydrofuran (THF) with a yield of 45%.

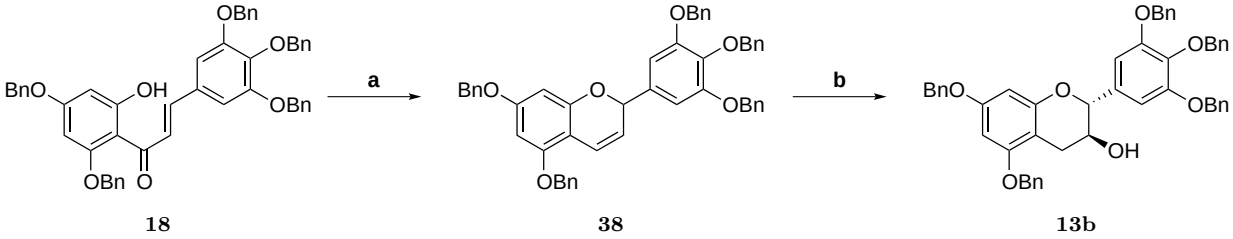

18 **38** **13b**

Scheme 2.3 Reagents and conditions. a) i) $NaBH_4$, THF/EtOH; b) i) BH_3-THF, THF; ii) H_2O_2/EtOH.

Our attempts to effect the reduction of **18** and subsequent cyclisation to **38** using sodium borohydride[234] failed (Scheme 2.3). The reaction was monitored via TLC and did show the formation of a product but upon its isolation by column chromatography failed. Several other methods reported in the literature by Romeo *et al.* ($NaBH_4$ in EtOH/THF, reflux)[239] and Nadia *et al.* ($NaBH_4$, DME, 85 °C followed by $BF_3.OEt_2$)[240] were also tried

without success as the compound degraded rapidly in silica gel. Attempts to perform the hydroboration-oxidation sequence on crude **38** also failed to deliver **13b**. This lack of success may be due to the sensitivity of **38** to acid and oxygen, and the possible formation of a highly reactive *ortho*-quinone **48** (Scheme 2.4). This finding led us to abandon attempts to use **38** as an intermediate in the synthesis of the green tea polyphenols.

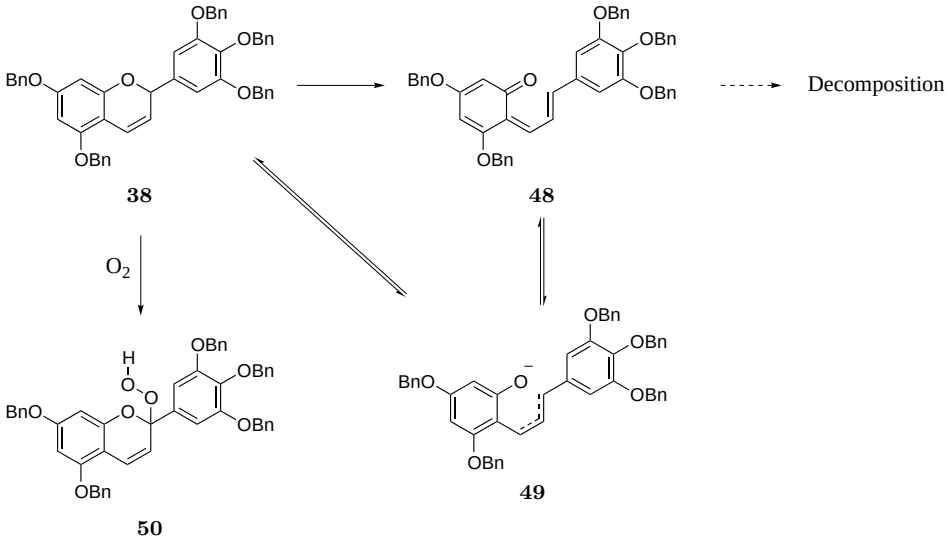

Scheme 2.4 Proposed mechanism of decomposition of flavane **38**.

We next considered using the allyl phenol **10b** as a precursor to the *trans*-catechin **13b** via a Sharpless asymmetric dihyroxylation to form the diol **11b**. The diol could then be submitted to an acid-mediated cyclisation to give the 2,3-*trans*-catechin **13b**. The allyl phenol **10b** would be synthesised via a Grubb's cross metathesis involving **50** and **51** (Scheme 2.5).

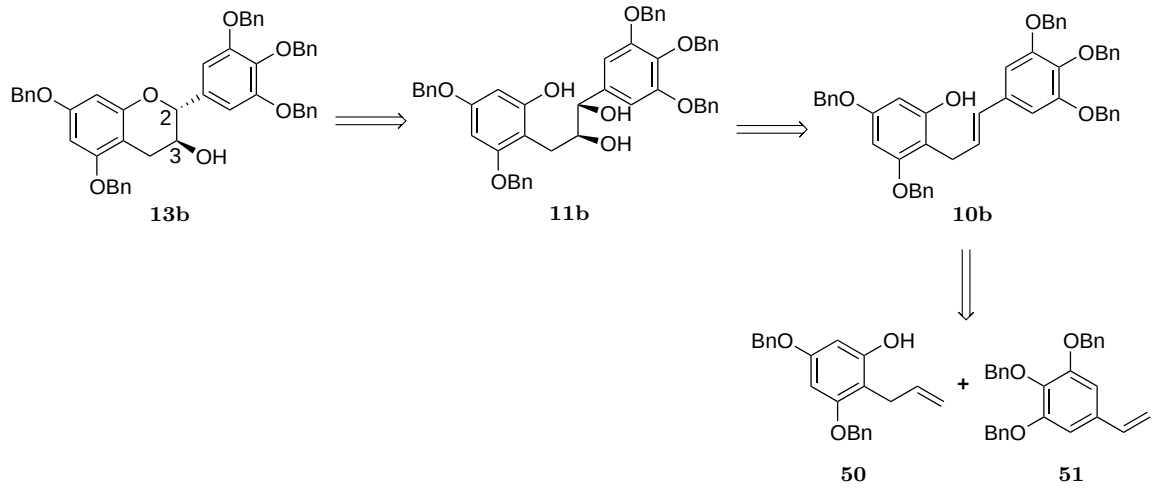

Scheme 2.5 Retrosynthesis of *trans* intermediate **13b** via cross-metathesis.

Before attempting the cross metathesis we decided to examine the reduction of enone **18** to **10b** using a two-step deoxygenation reaction employing ethyl chloroformate and sodium borohydyride as designed by Krohn *et al.*[241] (Scheme 2.5). Unfortunately this only resulted in the transformation of the ketone to the ester **52**. Selective reduction of the ketone **33** with $NaBH_4$ in the presence of cerium chloride at low temperature (0-5 °C) resulted in the formation of the alcohol **53** but not the desired **10b**.

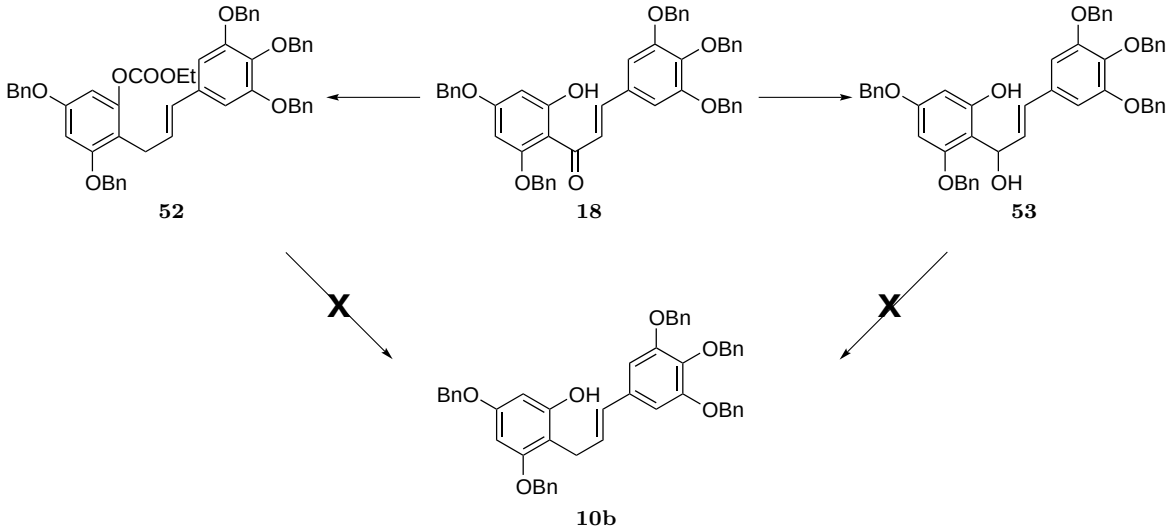

Scheme 2.6 Deoxygenation/reduction reaction to obtain **10b**.

Entry	Reagents and conditions
1	i) Et_3N, ClCOOEt, THF ii) $NaBH_4$, EtOH-H_2O
2	$NaBH_4$, $CeCl_3.7\,H_2O$, THF, EtOH[242]

The cross metathesis strategy began with the synthesis of the two starting materials **50** and **51** as described in Scheme 2.7 below. Previously synthesised 3,4,5-*tris*-(benzyloxy) benzaldehyde **35** was submitted to a Horner-Wadsworth-Emmons reaction with methyltriphenylphosphonium bromide to produce vinyl tribenzene **51** in good yield. (2,4-*bis*-(benzyloxy)-6-hydroxyphenyl)boronic acid **56** was made from commercially available phloroglucinol **5**. Direct benzylation with 3 molar equivalents of benzyl bromide and potassium carbonate resulted in a mixture of the expected *O*-benzylated and undesired *C*-benzylated products that were difficult to separate using column chromatography. Similar results were obtained with BnCl, NaH in DMF. The yield was improved using the method of Kawamoto *et al.*[243] This involved the introduction of electron-withdrawing acetyl groups to all the phenolic hydroxyls **54** thereby reducing the electron density in the arene leading to regiospecific formation of 1,3,5-*tris*-(benzyloxy)benzene **55**.

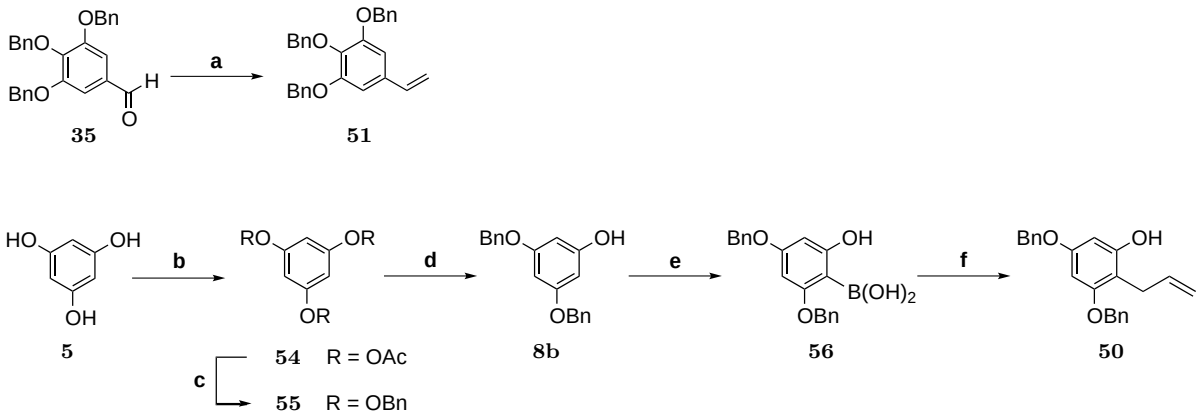

Scheme 2.7 Reagents and conditions. a) Methyltriphenylphosphonium bromide, NaH, THF, 82%; b) Ac_2O, pyridine, CH_2Cl_2, 97%; c) BnCl, NaH, H_2O, DMF, 60%; d) BuSH, NaH, DMF, 60%; e) *n*-BuLi, TMEDA, $B(OMe)_3$, THF, 68%; f) Suzuki cross-coupling.

The next step involved the selective debenzylation to produce **8b**. Hydrogenolysis of **55** using palladium on carbon at 0 °C cleaved one benzyl protecting group to produce **8b** with a yield of 32%. However, the experiment was not reproducible so other avenues were explored. A procedure reported by Wan *et al.*[244] involved the selective cleavage of one benzyl group using *n*-butanethiol. In our hands this resulted in an improved yield of 3,5-*bis*-(benzyloxy)phenol **8b** to 60%. In this case, cleavage of the second and third benzyl group was slowed by the formation of the anion of **8b** making the phenol a worse leaving group. **8b** was reacted with two equivalents of *n*-butyllithium (BuLi) then

trimethylborate to form a boronic acid ester which was hydrolyzed with 2 M HCl to give the corresponding boronic acid intermediate **56**.

The Suzuki coupling between boronic acid **56** and allybromide **57** to form **8** was attempted with a variety of palladium catalysts but failed to yield the desired compound. What was observed was a competitive hydrolytic deboronation of **56** leading back to the phenol **8b** (Scheme 2.8). As there was the possibility that the size of the benzyl protecting groups could hinder formation of the aryl palladium intermediate, a commercially available 3,5-dimethoxyphenol was used to synthesise a less bulky boronic acid intermediate. This too resulted in a deboronation under palladium catalysts. An *ortho*-lithiation of **8a** and **8b** followed by quenching with allylbromide also failed to produce the respective intermediates. (Entry 7, Scheme 2.8).

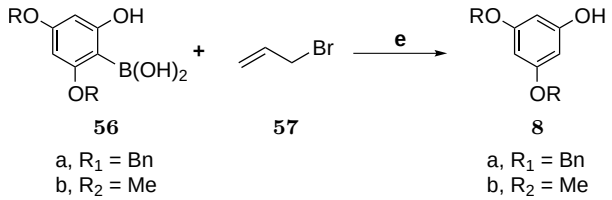

Scheme 2.8 Suzuki cross coupling reactions to obtain starting material **50**.

Entry	Reagents and conditions
1	$Pd(dba)_4$, K_2CO_3, Toluene, reflux
2	$Pd(dba)_4$, Na_2CO_3, Toluene, reflux
3	$Pd(PPh_3)_4$,Toluene, reflux
4	$Pd(PPh_3)_4$, 2 M $NaHCO_3$, dioxane, microwave
5	$Pd(PPh_3)_4$, $Ba(OH)_2$, 1,2-dimethoxyethane (DME), reflux
6	$Pd(PPh_3)_4$, $Ba(OH)_2$, DME:H_2O (6:1), reflux
7	*n*-BuLi, TMEDA,THF, -78 °C

Suzuki *et al.* suggested that aqueous conditions and *ortho* substituents may accelerate the hydrolytic deborontation but this could be mitigated by the use of boronic esters and $Ba(OH)_2$ as the base.[245] 2-Bromo-3,5-dimethoxyphenol **58** was successfully synthesised from **8a** and this was reacted with a variety of boron coupling agents. Unfortunately these reactions did not produce the desired intermediate **63** either (Scheme 2.9).

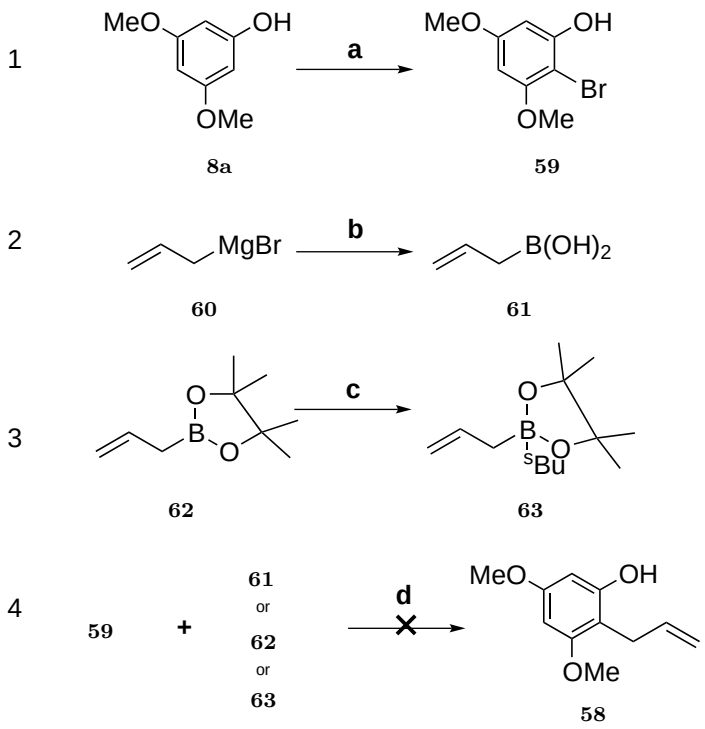

Scheme 2.9 Reagents and conditions. a) NBS, DCM, -78 °C, 75%; b) $B(OMe)_3$, $B(OMe)_3$, Et_2O, -78 °C to rt, 3 M HCl 58%; c) *s*-BuLi, THF, -78 °C to rt; d) See table below.

Entry	Reagents and conditions
1	$Pd(PPh_3)_4$, $Ba(OH)_2$, 1,2-dimethoxyethane (DME), reflux
2	$Pd(PPh_3)_4$, $Ba(OH)_2$, DME:H_2O(6:1), reflux
3	$PdCl_2$(dppf), NaOAc, THF, reflux

An *ortho*-Claisen rearangement as described by Reddy *et al.*,[246] was also attempted (Scheme 2.10) involving the *O*-allylation of the dimethoxyphenol followed by thermolysis of the allyl ether **64**. The allyl ether **64** was successfully prepared in 87% yield. When submitted to the *ortho*-Claisen rearrangement the resulting product **63** proved difficult to isolate and analyse due to decomposing. As a result, the Grubb's cross-metathesis strategy was abandoned as a potential route to the *trans*-alkene **13b**.

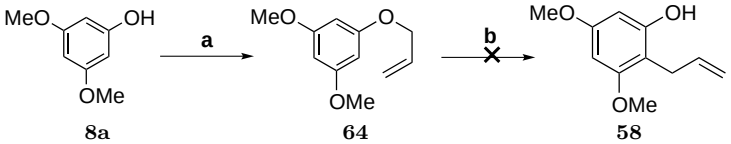

Scheme 2.10 Reagents and conditions. a) K_2CO_3, allylbromide, acetone, reflux, 87%; b) *N, N*-dimethylaniline, 210 °C, 58%.

The next strategy considered involved a Friedel-Craft type reaction similar to that described by Li and Chan in Chapter 1. This pathway was considered primarily because previously reported synthesis of epigallocatechin gallate and other catechins have used this method to build the *trans*-alkene intermediate.

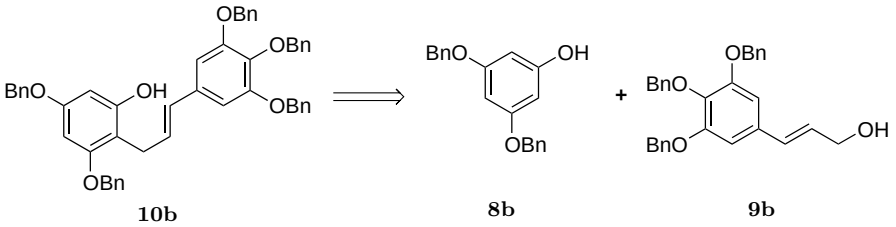

Scheme 2.11 Disconnection approach to *trans*-alkene intermediate via Freidel-Craft alkylation.

3,5-Bis(benzyloxy)phenol **8b** had previously being synthesised as described in Scheme 2.7 above. *(E)*-3-(3,4,5-*tris*-(benzyloxy)phenyl)prop-2-en-1-ol **9b** was prepared from previously synthesized 3,4,5-*tris*-(benzyloxy)benzaldehyde **35** by using a Horner-Wadsworth-Emmons reaction with triethyl phosphonoacetate to produce *(E)*-ethyl 3-(3,4,5-*tris* (benzyloxy)phenyl) acrylate **65**. This was with diisobutylaluminium hydride (DIBAL) then quenched by addition of saturated Rochelle's salt solution and methanol. Purification by column chromatography gave *(E)*-3-(3,4,5-*tris*-(benzyloxy)phenyl)prop-2-en-1-ol **9b** in good yield (Scheme 2.12).

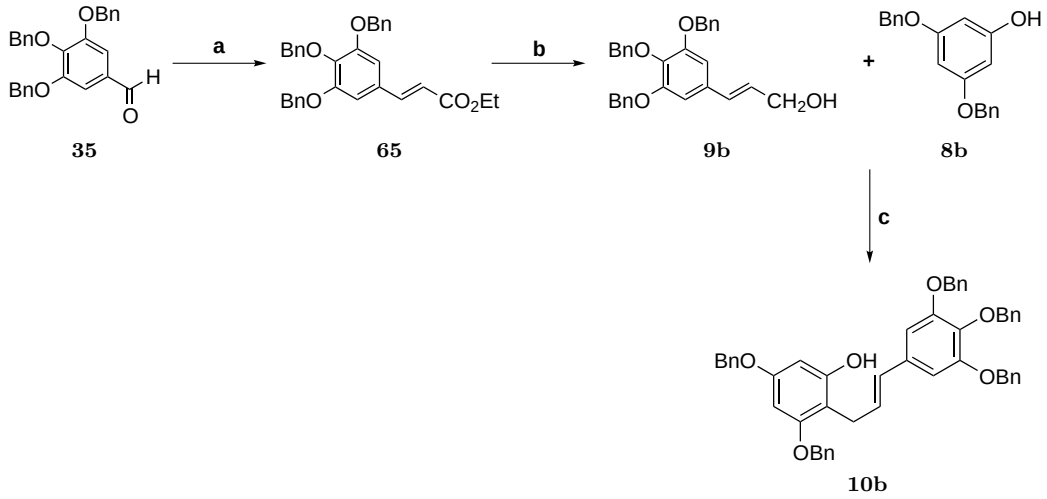

Scheme 2.12 Reagents and conditions. a) triethyl phosphonoacetate, NaH, THF, rt, 96%; b) DIBAL (1 M in toluene), THF, -78 °C, 67%; c) Freidel-Crafts alkylation (see table below).

Entry	Reagents and conditions
1	$MeSO_3H$, CH_2Cl_2, 0 °C[247]
2	DIAD, PPh_3, toluene, -20 °C[244]
3	$AlCl_3$, CH_2Cl_2, 0 °C to rt
4	$BF_3 \cdot Et_2O$, CH_2Cl_2, 0 °C to rt
5	Montmorillonite K-10, CH_2Cl_2, 0 °C to rt

Initial attempts at the Freidel-Crafts alkylation using Bronsted and Lewis acids and a Mitsunobu reaction (entry 2, Scheme 2.12) produced complex product mixtures that included both starting materials and an array of alkylated products that was difficult to separate by column chromatography. However, ESI^+ mass spectroscopy of the crude product showed a peak corresponding to the desired product **10b**. Pleasingly, when the Friedel-Crafts alkylation was attempted with montmorillonite K-10, a solid acid catalyst, the reaction proceeded successfully. The yield was improved by using 3,5-*bis*-(benzyloxy)phenol in excess and by the drop-wise addition of prop-2-en-1-ol **9b** to a solution of phenol **8b** at before stirring at room temperature until the reaction completion. In this way **10b** could be formed in acceptable yield.

TLC showed the presence of phenol **8b** and *trans*-alkene *(E)*-3,5-*bis*-(benzyloxy)-2-(3-(3,4,5-*tris*-(benzyloxy)phenyl)allyl)phenol **10b**. The reaction mixture was filtered through a layer of celite and concentration *in vacuo*, then the crude mixture was subjected to silylation with *tert*-butylchlorodimethylsilane (TBDMSCl) to afford **66** in an overall yield of 60% from **8b** (Scheme 2.13). The yield was further improved to 76% when the TBS protection was performed using TBDMS-triflate and 2,6,lutidine rather than with catalytic DIPEA and triethylamine. The benefit of this pathway was that it allowed us to achieve purification by column chromatography.

Stereoselective Sharpless asymmetric dihydroxylation of **66** using AD-mix-α afforded the TBS-protected diol **67** which was used in the next step without further purification. Desilylation of this compound using *n*-tetrabutylammonium fluoride gave the optically active triol **11b** in 45% yield (Scheme 2.13). Conversion of the 1, 2-diol moiety to an *ortho*

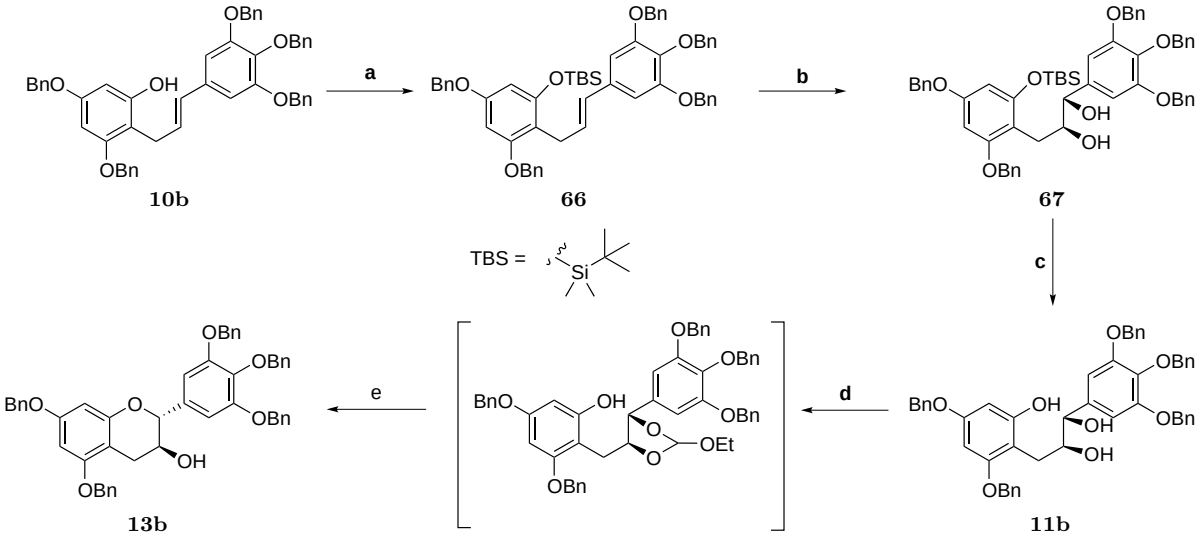

Scheme 2.13 Reagents and conditions. a) TBDMS-triflate, 2,6-lutidine, DMF, RT, 76% (two steps); b) AD-mix α, *t*-BuOH:H_2O, CH_2Cl_2, $MeSO_2NH_2$ (1:1:1), 0 °C, CH_2Cl_2; c) TBAF, THF, rt, 45% (two steps) 99% *ee*; d) $CH_3(OEt)_3$, PPTS, CH_2Cl_2; e) K_2CO_3, MeOH: $C_2H_4Cl_2$ (1:1), 65% 98% *ee*.

ester with triethyl orthoformate then enabled a stereoselective cyclisation with K_2CO_3 to construct the *trans*-catechin **13b** and establish the C-2 stereogenic centre. The *trans* stereochemistry confirmed by the ^{1}H NMR matched literature values.[232] The isomer was also confirmed by the optical rotation which compared to one reported by Krohn *et al.* ($[\alpha]_D$ = - 8.1 (c = 1.38, $CHCl_3$ [Lit.[241] - 8.96 (c = 1.11, $CHCl_3$).

2.3 Enantioselective synthesis of EGC and EGCG

Dess-Martin oxidation[248] of the hydroxyl group in **13b** gave the corresponding ketone **14b** which was used in the next step without further purification. Reduction of the ketone with L-Selectride® at -78 °C produced selectively the 2,3-*cis*-catechin **15a** in a modest yield of 60% yield (Scheme 2.14).

It was noted that the remaining mass balance was largely comprised of unreacted **13b**, yet no further enhancement in yield was observed after addition of further L-Selectride®. Romanczyk *et al.* suggested that the starting material may be partially enolized which is hydrolysed back to the ketone on work-up.[249] The *cis* stereochemistry confirmed by

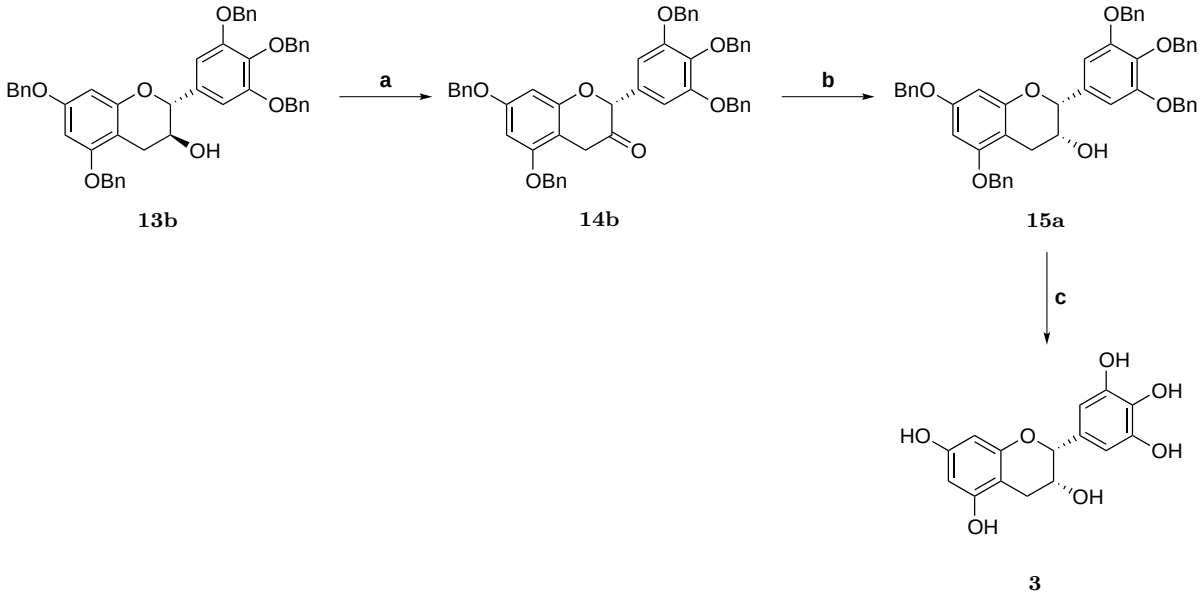

Scheme 2.14 Reagents and conditions. a) Dess-Martin Periodinane, CH_2Cl_2, rt, 67%; b) L-Selectride®, LiBr, THF, -78 °C, 74%, 95% *ee*; c) H_2, $Pd(OH)_2$, MeOH/EtOAc , rt, 26%.

the ^{1}H NMR matched literature values.[232] Catalytic hydrogenation with $Pd(OH)_2$ gave the target compound epigallocatechin **3** in 26% yield after purification by HPLC.

We were now in a position to prepare our target compound EGCG **4**. To that end, methyl 3,4,5-*tris*-(benzyloxy)benzoate **47** was hydrolysed to form 3,4,5-*tris*-(benzyloxy)benzoic acid **68**. This was coupled with *cis*-catechin **14b** using carbodiimide coupling methodology to afford the benzylated EGCG **41**. Catalytic hydrogenation produced the target compound, epigallocatechin gallate **4**, which was purified by HPLC (Scheme 2.15).

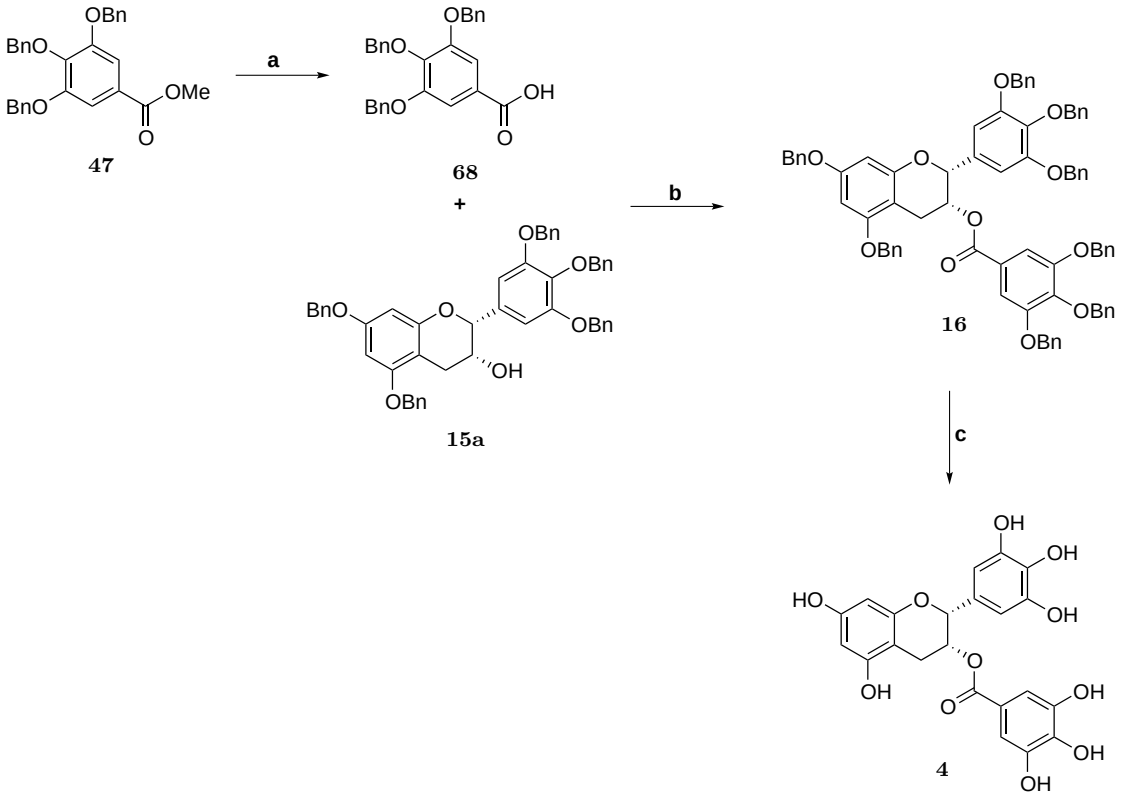

Scheme 2.15 Reagents and conditions. a) KOH, MeOH, dioxane, reflux, 93%; b) EDC.HCl, DMAP, Et_3N, HOBt, DCM, 0 °C to rt 88%; c) H_2, 20% $Pd(OH)_2$, MeOH/EtOAc, rt, 26%.

2.4 Enantioselective synthesis of EC and ECG

Having successfully synthesised epigallocatechin **3** and epigallocatechin gallate **4**, the same pathway was used to synthesise epicatechin and epicatechin gallate. Prop-2-en-1-ol **74** was first synthesised from commercial available 3,4-*bis*(benzyloxy)benzoic acid **69** (Scheme 2.16). Thus, benzoic acid **69** was converted to its methyl ester **69** using acid catalysis. The free hydroxyl groups in **70** were next protected by reacting with excess benzyl bromide and potassium carbonate to give **71**. Reduction with $LiAlH_4$ followed by PCC oxidation next gave 3,4-*bis*-(benzyloxy)benzaldehyde **72**, which underwent a Horner-Wadsworth-Emmons reaction with triethyl phosphonoacetate to give the α,β-unsaturated ester **73**. A DIBAL reduction then gave the key intermediate *(E)*-3-(3,4-*bis*-

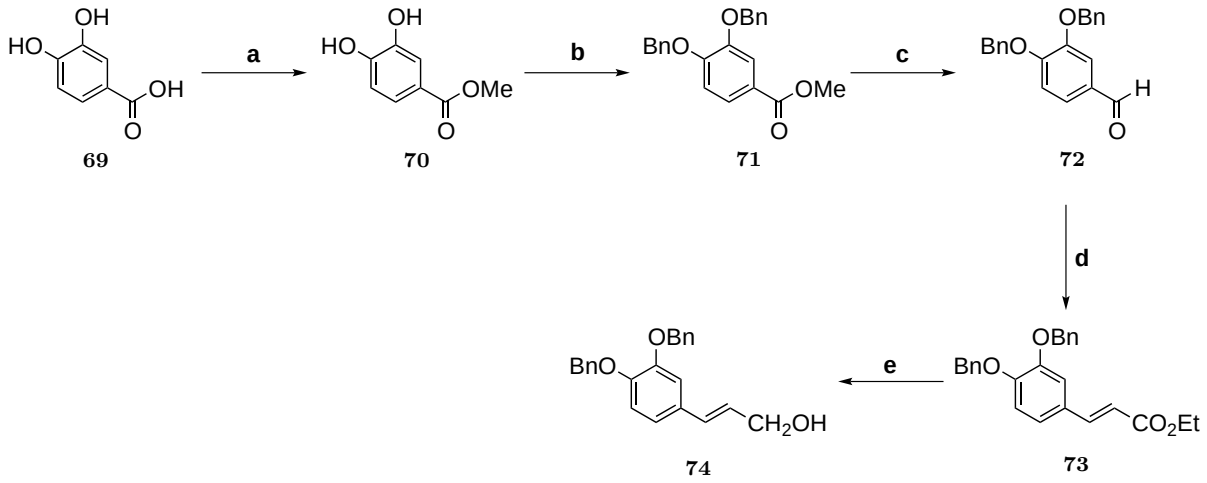

Scheme 2.16 Reagents and conditions. a) MeOH, cat. H_2SO_4, reflux, 70%; b) BnBr, K_2CO_3, DMF, 64%; c) i) LAH, THF, 73%; ii) PDC, DCM, 4Å molecular sieves, rt, 70%; d) triethyl phosphonoacetate, NaH, THF, RT, 67%; e) DIBAL (1M in toluene), THF, -78 °C, 49%.

(benzyloxy)phenyl)prop-2-en-1-ol **74** in 49% yield.

A Friedel-Crafts alkylation reaction between phenol **8b** and cinnamyl alcohol **74** was successfully achieved using Montmorillonite k-10 as the acid catalyst to give allyl phenol which was protected with TBDMSCl to form **75**. As before, a sequence involving asymmetric dihydroxylation, phenol deprotection (to **77**), *ortho* ester formation and base-induced cyclisation successfully produced the desired optically active chroman-3-ol **78**.

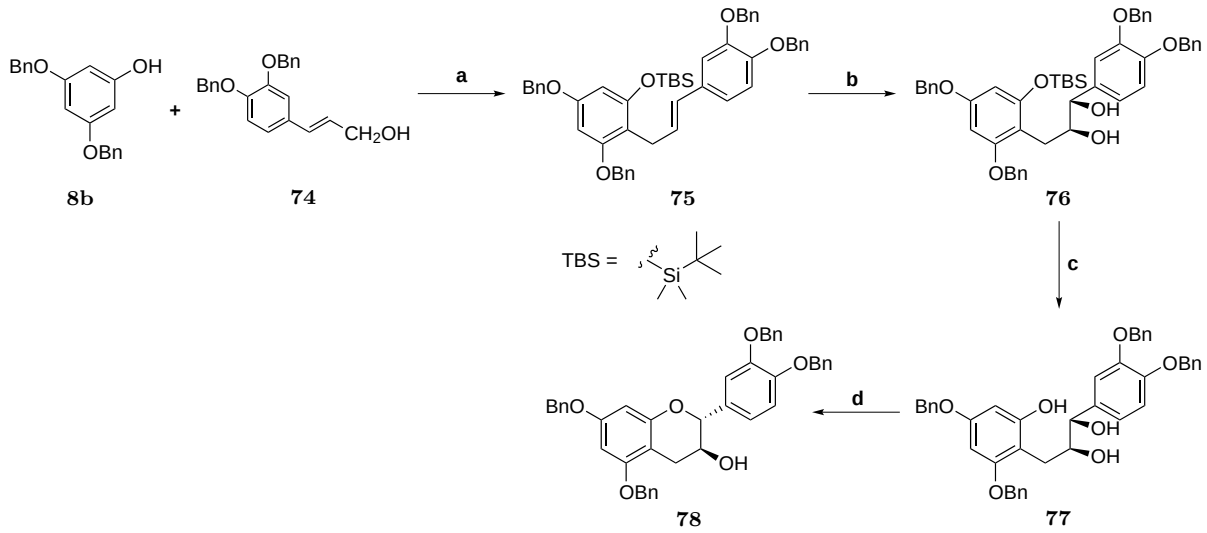

Scheme 2.17 Reagents and conditions. a) i) Montmorillonite k-10,DCM, 0 °C to rt; ii) TBDMSCl, imidazole, DMF, RT, 36% (two steps); b) i) AD-mix α, *t*-BuOH:H_2O, CH_2Cl_2, $MeSO_2NH_2$ (1:1:1), 0 °C, CH_2Cl_2; c) TBAF, THF, rt, 43% (two steps) 99% *ee*; d) i) $CH_3(OEt)_3$, PPTS, CH_2Cl_2 ii) K_2CO_3, MeOH: $C_2H_4Cl_2$ (1:1), 34% (2 steps) 99% *ee*.

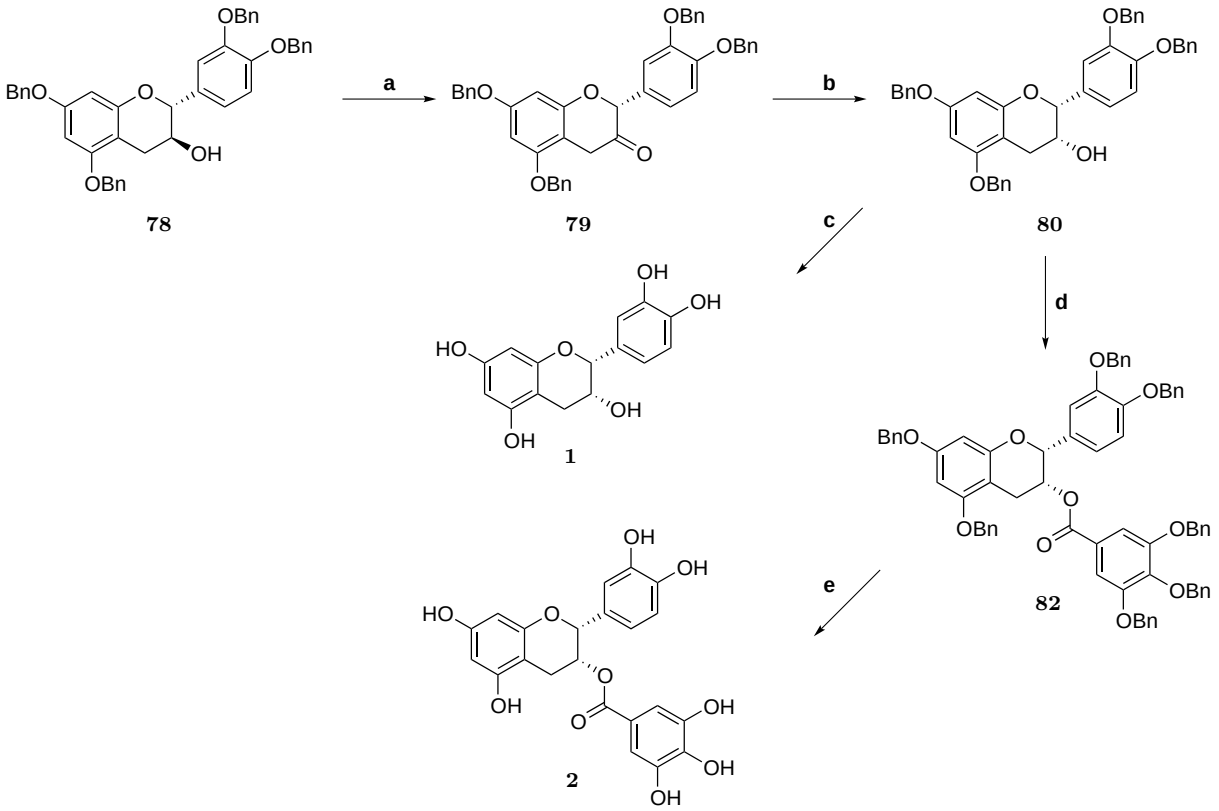

Scheme 2.18 Reagents and conditions. a) Dess-Martin Periodinane, CH_2Cl_2, rt, 87%; b) L-Selectride®, LiBr, THF, -78 °C, 40% 89% *ee*; c) H_2, $Pd(OH)_2$, MeOH/EtOAc , rt, 27%; c) **42**, EDC.HCl, DMAP, Et_3N, HOBt, CH_2Cl_2, 0°Cto rt 79%; d) H_2, $Pd(OH)_2$, MeOH/EtOAc , rt, 43%.

2, 3 *trans*-catechin **78** was now subjected to the same C-3 steroechemistry inversion using the oxidation-reduction sequence previously developed in our synthesis of **15a** (Scheme 2.14) to produce *(2R,3R)*-5,7-*bis*-(benzyloxy)-2-(3,4-*bis*-(benzyloxy)phenyl)chroman-3-ol **80** in modest yield. Hydrogenolysis of **80** using a palladium catalyst produced epicatechin **1** in a disappointing 26% yield after purification by HPLC. EDC coupling of **80** with 3,4,5-*tris*-(benzyloxy)benzoic acid **68** then gave protected epicatechin gallate **80** in good yield. Catalytic hydrogenolysis completed the sequence producing the target compound epicatechin gallate **2** in 42% yield after purifiication by HPLC (Scheme 2.18).

2.5 Enantioselective synthesis of ECG and EGCG analogues

To understand the structure-activity relationship of green tea polyphenols, a number of analogues were synthesised. The poor bioavailability of the polyphenols is mainly due to biotransformation such as methylation and glucoronidation. Consequently, we also prepared the analogues **84** and **85** from epicatechin **1** as described in Scheme 2.19.

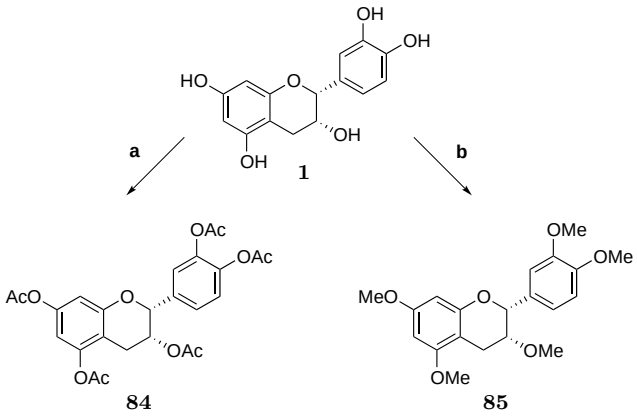

Scheme 2.19 Reagents and conditions. a) Ac_2O, pyridine, CH_2Cl_2, rt, 65%; b) MeI, NaH, 0°C to rt 39%.

It was hoped the addition of acetyl groups would improve absorption, creating a a "pro-drug" that could be delivered to the cells. These would be hydrolysed in within the cell to produce the desired polyphenol. An acetylated EGCG analogue **84** was also synthesised from **4** with good yield in Scheme 2.20.

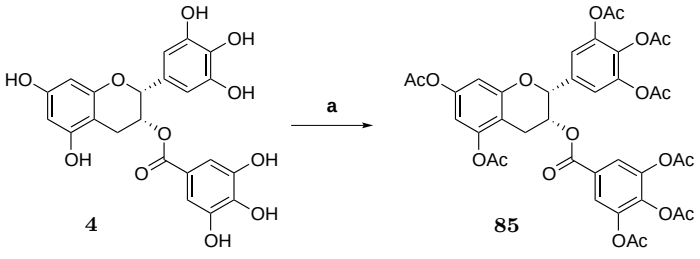

Scheme 2.20 Reagents and conditions. a) Ac_2O, pyridine, CH_2Cl_2, rt, 65%.

Other analogues were made by through the modification of the C-ring subunit in EGC **3** due to the possibility that its function might be improved by the presence of the galloyl group. The commercially available benzoic acids **85**, **87**, **89**, and **91** were coupled

to benzylated EGC **15a** resulting in four further analogues (Scheme 2.21). All of the analogues were purified by HPLC before biological evaluation.

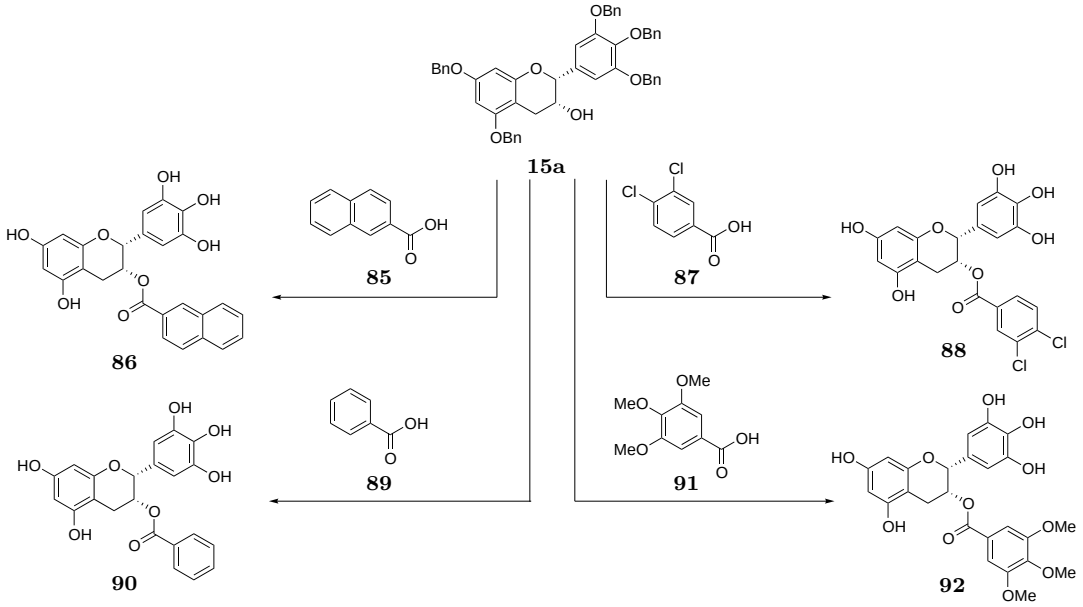

Scheme 2.21 Reagents and conditions. a) **14b**, EDC.HCl, DMAP, Et_3N, HOBt, CH_2Cl_2, 0°Cto rt; b) H_2, $Pd(OH)_2$, MeOH/EtOAc , rt (Yield (two steps) **85** to **86** 5.6%; **88** to **89** 48%; **86** to **87** 12.2%; **90** to **91** 5.6%.

2.6 Conclusion

In summary, we have synthesised the four polyphenols present in green tea as well as a few analogues using a route that is both robust and reproducible. The overall synthetic route is described in Scheme 2.22 below. Although it is a lengthy route it allowed access to the *cis* and *trans* stereoisomers and also a number of analogues through the modification of the ring C. The sequence could potentially be shortened by converting the 2,3-*trans*-catechin to the 2,3-*cis* catechin using a Mitsunobu reaction (diethylazodicarboxylate (DEAD) and PPh_3, THF, rt) rather than the oxidation-reduction route followed in our synthesis.

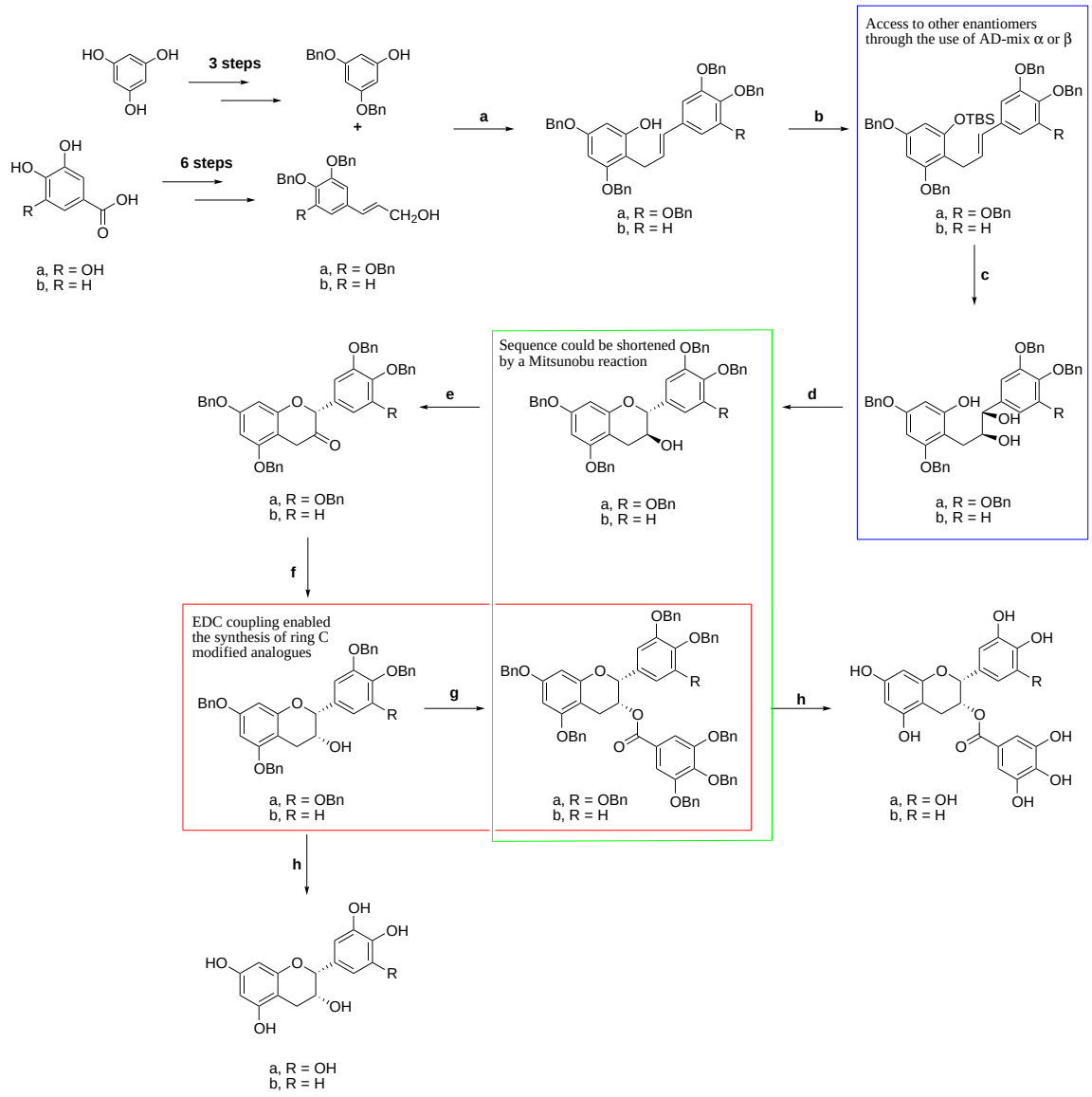

Scheme 2.22 Reagents and conditions. a) Montmorillonite k-10,DCM, 0 °C to rt; b) TBDMS-triflate, 2,6-lutidine, DMF, rt; c) i) AD-mix α, *t*-BuOH:H_2O, CH_2Cl_2, $MeSO_2NH_2$ (1:1:1), 0 °C, CH_2Cl_2; ii) TBAF, THF, rt; d) i) $CH_3(OEt)_3$, PPTS, CH_2Cl_2 ii) K_2CO_3, MeOH: $C_2H_4Cl_2$ (1:1); e) Dess-Martin Periodinane, CH_2Cl_2, rt; f) L-Selectride®, LiBr, THF, -78 °C; g) EDC.HCl, DMAP, Et_3N, HOBt, CH_2Cl_2, 0°Cto rt; h) H_2, $Pd(OH)_2$, MeOH/EtOAc , rt.

In the next step, the structure-activity relationship of the polyphenols and their analogues would be explored in order to understand and potentially improve the cardioprotective activities of green tea polyphenols. This would involve *in vitro* studies of the green tea polyphenols and their analogues on H9C2 myoblast cells and neonatal rat cardiac myocytes to assess their cardioprotective functions following oxidative stress and simulated I/R injury.

Chapter 3

Biological Evaluation of Green Tea Polyphenols and Analogues

3.1 Introduction

Previous work has demonstrated the cardioprotective effects of EGCG in cardiac myocytes against I/R-induced apoptotic cell death.[153] EGCG inhibited STAT-1 activity and in turn reduced the expression of STAT-1 dependent pro-apoptotic gene, Fas. Oral administration of green tea extract limited the infarct size of isolated rat hearts exposed to I/R injury, resulting in improved hemodynamic recovery and ventricular function. Nevertheless, the poor bioavailability of GTPs necessitates the use of very high working concentrations, which may not be feasible in human studies. The aims of this chapter are as follows.

1. Evaluate the cardioprotective effects of GTP during oxidative stress using H_2O_2 in H9C2 cardiac myoblast cells
2. Evaluate the cardioprotective effects of GTP during I/R injury in H9C2 cells
3. Investigate the effects of GTP and their analogues on H9C2 cells
4. Evaluate the cardioprotective effects of GTP and analogues during I/R injury in

neonatal rat cardiomyocytes (NRCM)

3.2 Results

3.2.1 Evaluation of protein level expressions of STAT-1 and ERK/MAPK in H9C2 cells myoblast cells

As discussed in Chapter 1, the extrinsic pathway of apoptosis is initiated by a number of cell surface receptors. STAT-1 is activated by IFN-γ signalling, which is upregulated in response to external stimuli such as stress. The IFN-γ ligand binding to the IFN-γ receptor induces the dimerisation of its subunits causing a conformational change and binding of JAK. JAK-1 and JAK-2 trans-activate one another and phosphorylate the tyrosine residues at the cytoplasmic receptor domain creating a docking site for the SH2 domain present in STAT-1.

Initial experiments were carried out to confirm that STAT-1 and ERK/MAPK were expressed in a H9C2 myoblast cell line. H9C2 cells were plated at a density of $5x10^5$ cells per 10 cm dish and incubated until 70% confluence had been reached. Cells were treated with 50 or 100 ng of IFN-γ for 1 - 24 h and protein expression was assessed by immunoblotting.

IFN-γ induced STAT-1 Y701 phosphorylation, which was detected by the high protein levels of STAT-1 Y701 shown by immunoblot in Figure 3.1. A 1 h incubation with 50 and 100 ng of IFN-γ resulted in an increase in band intensity of STAT-1 Y701, however, STAT-1 S727 remained the same, as did the total STAT-1 and β-actin protein levels. The expression of phosphorylated STAT-1 Y701 decreased over time and returned to the non-teated levels by 4 h of treatment. This suggested that at the longer time-points all the STAT-1 proteins had already been activated at the tyrosine residue and then dephosphorylated. Levels of STAT-1 S727, which is responsible for the transcriptional response, showed no change compared to the non-treated cells cells suggesting that this

may be a background expression being detected. A treatment of 100 ng/mL of IFN-γ for 1 h was determined as optimal to identify STAT-1 induction and was therefore used in future experiments as a positive control.

Total ERK was detected in untreated cells and this basal level remained constant across samples. The levels of phosphorylated ERK-1/2 reduced under the conditions that resulted in elevated levels of STAT-1 Y701 within 1 h of IFN-γ treatment (Figure 3.1).

The protein levels of phosphorylated ERK-1/2 reduced with an increase in the levels of STAT-1 phosphorylation suggesting that ERK may have been activated at the beginning of the treatment time-point and contributed to the activation of STAT-1 before it was dephosphorylated and therefore deactivated. Higher levels of phosphorylated ERK-1/2 were detected at the longer incubation times which corresponded to lower levels of activated STAT-1. This suggests that maximal levels of phosphorylated STAT-1 may have been achieved and so no further action from activated ERK was required.

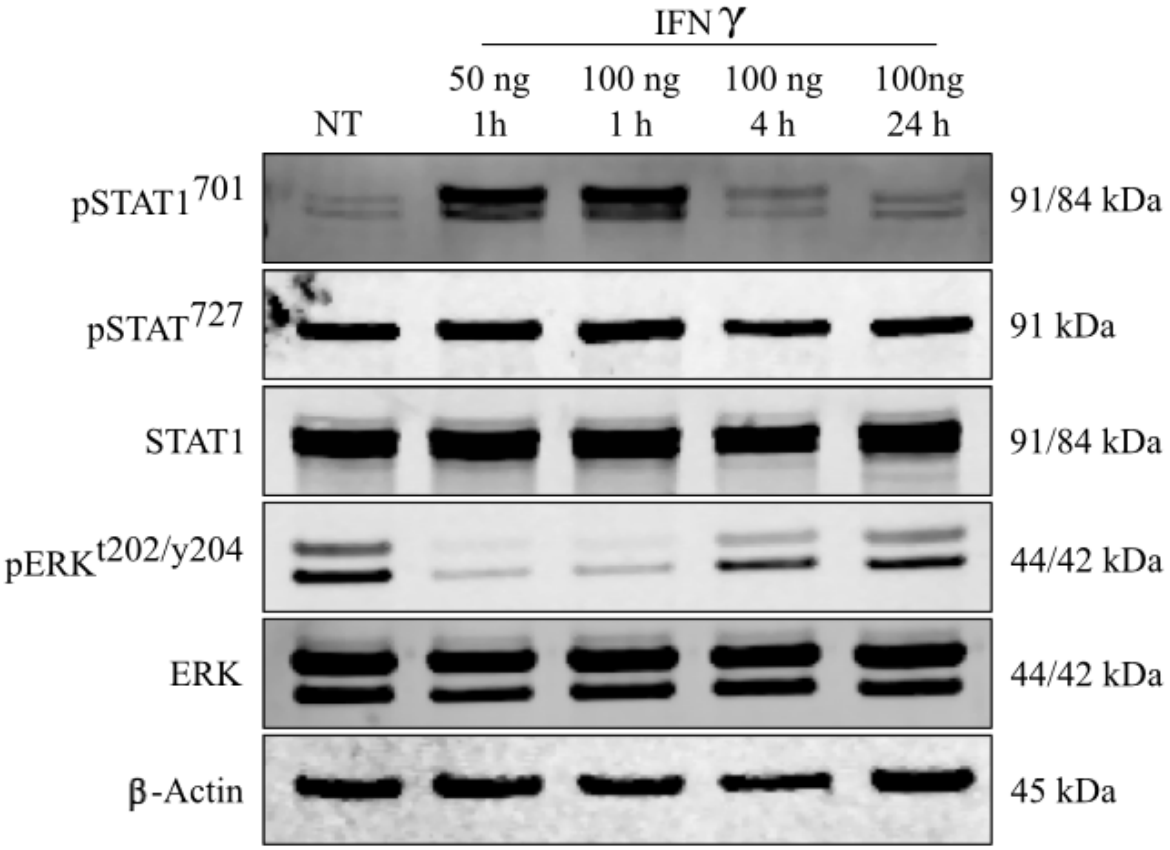

Figure 3.1 STAT-1 is activated by IFN-γ at 1 h treatment but ERK-1/2 is not activated at this time-point. Analysis of protein expression of STAT-1 and ERK/MAPK in H9C2 cells. Cells were treated with 50 or 100 ng of IFN-γ for 1 - 24 h. Cells were harvest at indicated time-points and assessed by immunoblotting using antibodies against STAT-1 Y701, STAT-1 S727, total STAT-1, phosphorylated ERK-1/2, total ERK and β-actin, which was used as the loading control. Levels of STAT-1 Y701 were shown to increase with exposure to 50 and 100 ng IFN-γ for 1 h but levels decreased at longer time-points. The levels of STAT-1 S727, however, increased slightly after 1 h treatment but decreased after 4 h and 24 h. The levels of total STAT-1 also remained constant between condition. The levels of phosphorylated ERK-1/2 decreased with increasing STAT-1 Y701 and the inverse was observed at longer time points. The levels of total ERK remained constant under the different conditions. Representative blot of three different experiments is shown.

3.2.2 Effects of GTP on cell viability of H9C2 cells

The influence of the GTP on cell survival was assessed by CyQUANT^{TM} and CellTiter-Glo assays. The CyQUANT^{TM} assay is a flourescence-based cell proliferation assay that measures density of cells in culture using DNA content, whereas CellTiter-Glo is a luminescent cell viability assay used to determine the amount of viable cells in cultures based on ATP content as this signals metabolically active cells.

The CyQUANT^{TM} assay enabled the calculation of the EC_{50} of each compound, which is the concentration of drug required to give 50% of the maximal response. H9C2 cells were seeded at 5,000 cells per well of a 96-well plate and left overnight to attach. The cells were incubated with the four major GTPs at concentrations ranging from 0 - 1000 μM for 24 h and cell viability was assessed. As shown in Figure 3.2, the lowest EC_{50} calculated, thus the most potent, was with EC at 2.90 ($\pm$ 1.51) μM followed by EGC at 19.01 ($\pm$ 1.07) μM, EGCG at 21.37 ($\pm$ 1.10) μM and the highest determined ECG at 450.5 ($\pm$ 1.35) μM. EC, EGC and EGCG had a similar shape in their dose-response curve suggesting that they were stimulatory drugs on cell proliferation whereas ECG, with the highest EC_{50} concentration had a reverse shaped curve suggesting that it was an inhibitory drug on cell proliferation. The curve could be explained by the lack of OH group which differentiates it from EGCG and could potentially be a significant substituent that prevents it from functioning as a pro-survival scavenger drug.

.

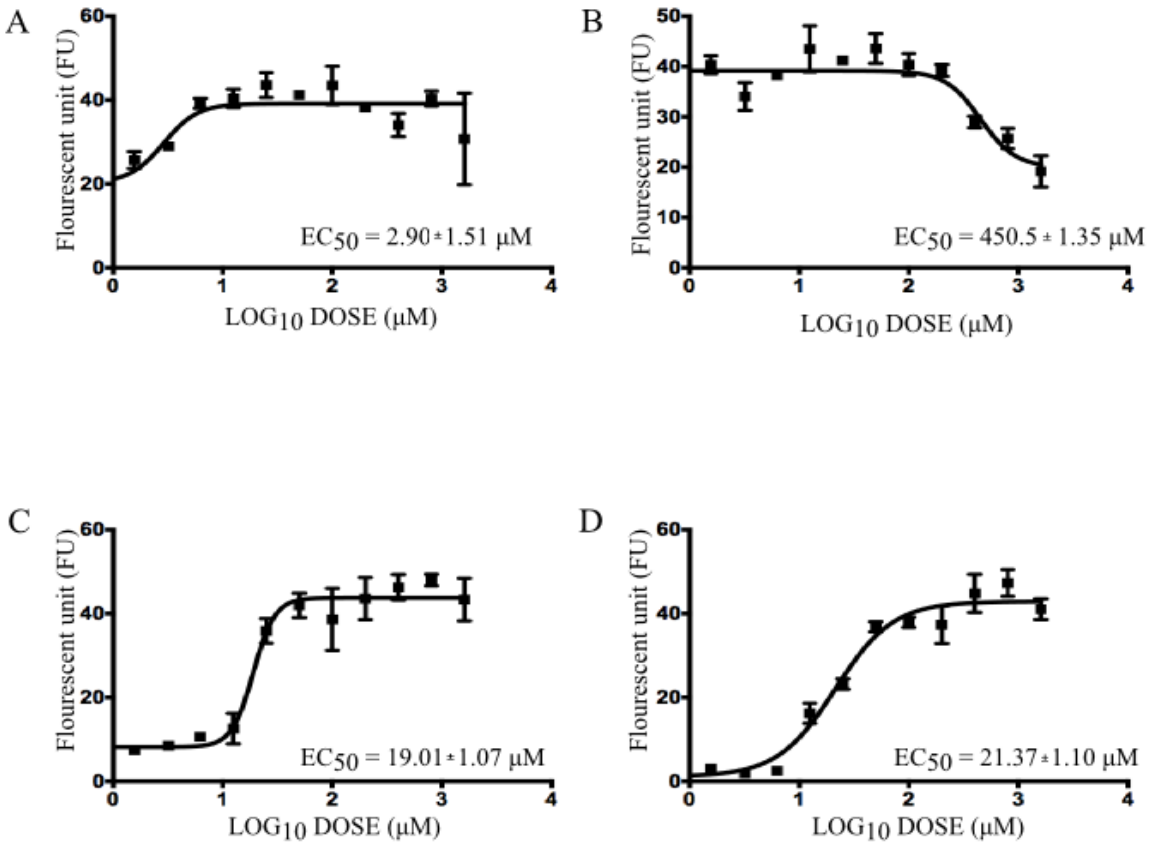

Figure 3.2 GTPs stimulated cell proliferation except ECG, which inhibited cell proliferation. Cell viability assay of H9C2 cells treated with GTP to calculate the EC_{50} concentration. Cells were treated with A) EC B) ECG C) EGC D) EGCG at concentrations ranging from 0 - 1600 μM for 24 h. Cells were stored at -78 °Cfor 24 h and assessed for viability by CyQUANT^{TM} assay. The EC_{50} concentration was calculated by a log dose-response curve using GraphPad Prism. The EC_{50} were calculated 2.90 ($\pm$ 1.51) μM for EC; 450.5 ($\pm$ 1.35) μM for ECG; 19.01 ($\pm$ 1.07) μM for EGC; 21.37 ($\pm$ 1.10) μM for EGCG. Representative graphs of three different experiments.

The CellTiter-Glo activity was normalised to control cells, which were defined as 100% survival. H9C2 cells were seeded at 5,000 cells per well of a 96-well plate and left overnight to attach. The cells were incubated with the four major GTP at concentrations ranging from 0 - 1000 μM for 24 h and cell viability was assessed.

The CellTiter-Glo assay showed a reduction of cell viability in a concentration-dependent manner as shown in Figure 3.3 in all GTPs. The shape of the curve for EC showed it to be the least potent as the gradient over the active concentrations, was less where real change could be seen at 400.5 μM and there is no plateau at the bottom of the curve. The shape of the curve of ECG indicated it to be more potent than EC with real change observed at 50 μM with a curve that does plateau off. EGC and EGCG show similar curves in shapes with greater change in the gradient over the different concentrations with changes observed at 25 and 12.5 μM respectively.

After 24 h of treatment the viability of cells at 100 μM concentration of EC, ECG, EGC, and EGCG was 84.5%, 52.9%, 2.2%, and 5.9% respectively compared to non-treated control cells, indicating that the more toxic effects of EGC were exhibited at this time and concentration. Similar results were obtained after 1hr incubation (data not shown). At 50 μM concentration, the cell viability improved to 90%, 71.6%, 51.66%, and 43.60% for EC, ECG, EGC, and EGCG respectively.

Interestingly, ECG had a similar shaped curve compared to the other three GTPs indicating that its possible anti-survival effects were on cell proliferation rather that metabolism. The results for EGCG were also worth noting as the working concentration for a number of studies involving this catechin were performed at 100 μM. After 3 independent experiments, it was decided that 100 μM would be used mainly because previous work on the cardioprotective effects of EGCG in NRCM, a much more sensitive primary cell culture, was done using 100 μM.

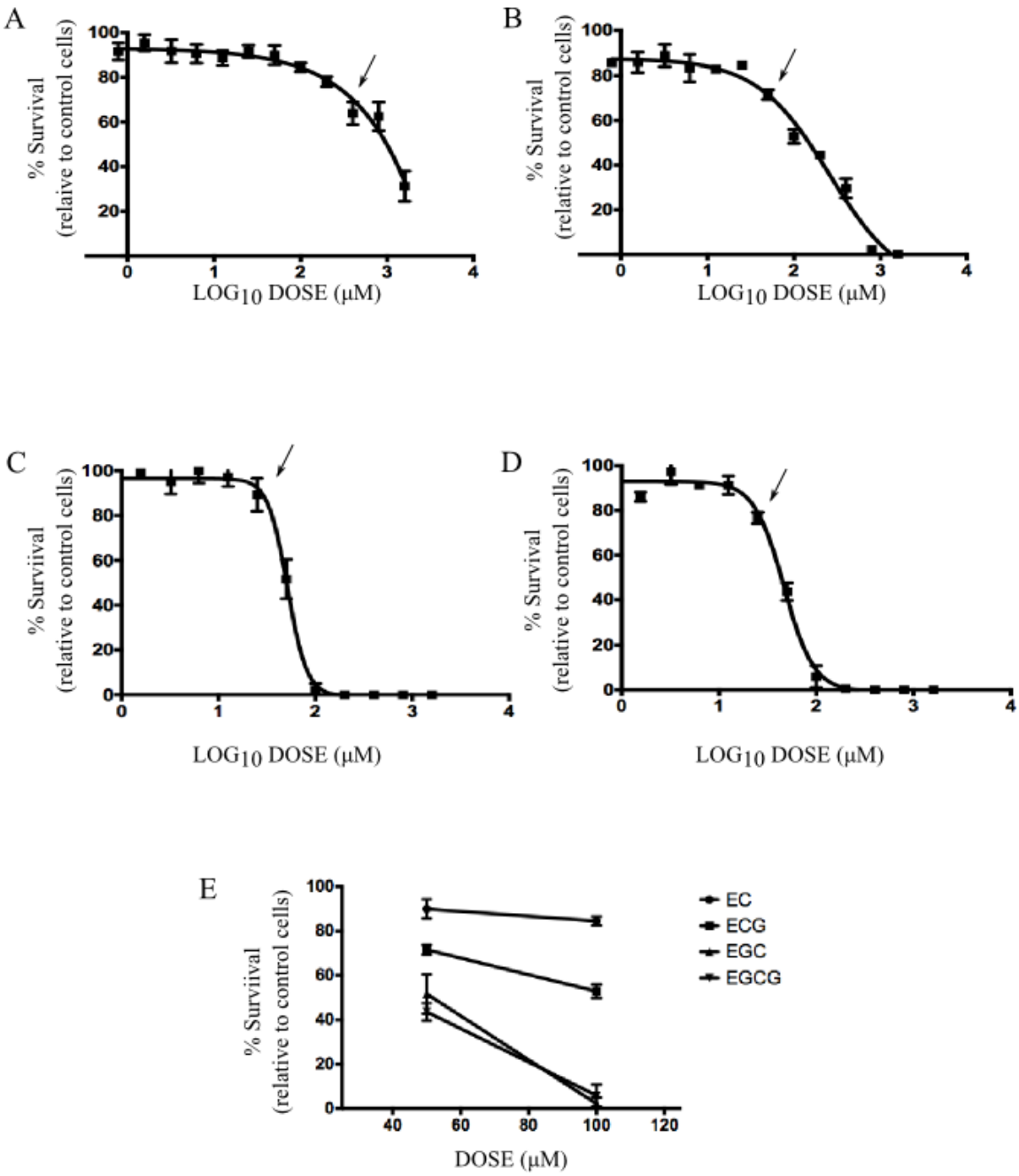

Figure 3.3 Cell viability assay to determine the effects of GTP on H9C2 cells. A) EC B) ECG C) EGC D) EGCG E) Cell viability 50 μM and 100 μM following a 24 h treatment. Data normalised to the activity of the non-treated control cells. Cell viability decreased at 100 μM compared to 50 μM more so with EGC and EGCG. Cells were treated with indicated GTP at concentrations ranging from 0 - 1600 μM for 24 h. Cells were assessed for viability by CellTiter-Glo assay. Cell viability was determined by a log dose-response curve using GraphPad Prism. Representative graphs of three different experiments.

3.2.3 Evaluating the cardioprotective effects of GTP during oxidative stress using H_2O_2

3.2.3.1 Induction of cell death by H_2O_2 in H9C2 cells

Oxidative stress is a condition that increases the formation of ROS generated intra- and extracellularly, which causes deleterious effects on the heart during heart failure, causing cell death. In our system exogenous oxidant, H_2O_2, was used to induce cell death due to its ability to generate intracellular ROS and induce oxidative stress. To determine whether H_2O_2 induced cell death in H9C2 cardiac myoblasts, the cells were treated with varying concentrations of H_2O_2 for up to 1 h analysed by immunoblotting and phase-contrast microscopy. H_2O_2 caused a concentration-dependent increase in cell death in H9C2 cells as determined by immunoblotting.

As shown in Figure 3.4 there was an increase in the phosphorylation levels of STAT- 1 Y701 as the concentration increased particularly after treatment with 400 and 500 μM of H_2O_2 after 1 h but the levels observed were not as intense when compared with IFN-γ treated cells. Similar concentration-dependent increase in phosphorylation levels were observed with STAT-1 S727 with high intensity bands observed following 400 and 500 μM of H_2O_2 1 h treatments. There were also changes observed in phosphorylated ERK-1/2 following H_2O_2 treatment with the highest intensity bands observed at high H_2O_2 concentration treatments.

Surprisingly elevated levels of phosphorylated ERK-1/2 was detected after 100 μM H_2O_2 treatment that was dramatically reduced compared to 200 μM H_2O_2 treatment and the non-treated cells. When compared to the phosphorylation of STAT-1 Y701 and S727, the results suggested that STAT-1 activation may not be dependent on ERK-1/2 activation at lower concentrations but possibly when cells are treated with high H_2O_2 concentrations. The total levels of STAT-1 and ERK-1/2 showed no significant changes over the varying concentrations indicating that the observations were due to increased phosphorylation

rather than an increase in total protein.

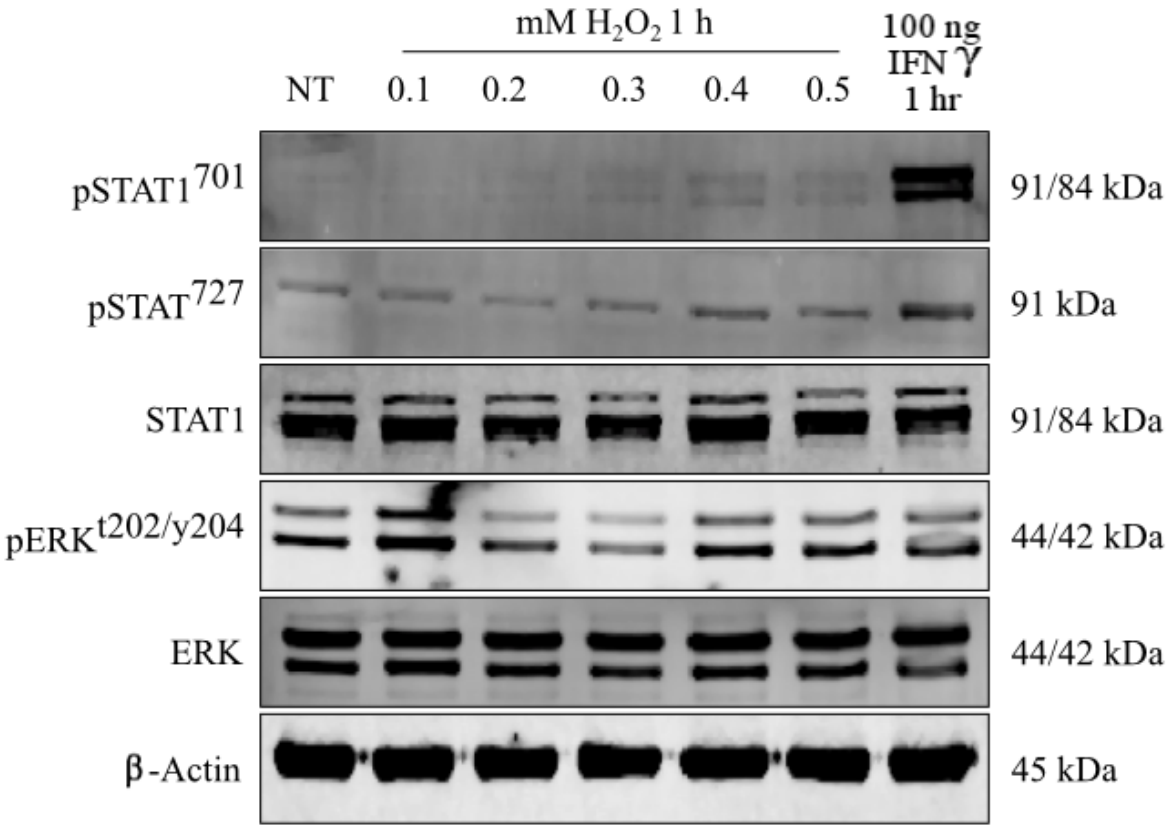

Figure 3.4 H_2O_2 induces cell death in H9C2 cells following 1 h treatment with 100 - 500 μM. Cell were treated with 100 - 500 μM of H_2O_2 for 1 h. Cell lysates were submitted to we tern blot analysis to detected changes in phosphorylated STAT-1, STAT-1, phosphorylated ERK-1/2 and ERK. β-Actin was used as a loading control. Exposure to H_2O_2 resulted in an increase in levels of STAT-1 Y701, STAT-1 S727 and phosphorylated ERK-1/2 in a concentration-dependent manner. The levels of total STAT-1 and ERK remained constant under the different conditions. Representative blot of three different experiments.

When these conditions were analysed by immunoflourescence, the results observed were similar to that of the immunoblotting in Figure 3.4 above. There was an increased phosphorylation of STAT-1 Y701 as the concentration of H_2O_2 increased compared to the non-treated cells but not as elevated as the positive control IFN-γ treated cells (Figure 3.5). As shown in Figure 3.5 the positive control, IFN-γ treated cells, showed an increase in the phosphorylation of STAT-1 Y701 and S727 due to an increase in the intensity of their respective stainings compared to the non-treated cells. STAT-1 Y701 was found to be diffused in the cytoplasm with some localisation in the nucleus while STAT-1 S727 was more localised in the nucleus than in the cytoplasm.

Phosphorylation of STAT1 Y701 and S727 were also indirectly studied by immunoflourescence (Figure 3.6). Treatment with 400 μM of H_2O_2 for 1 h also showed a more cytoplasmic diffused STAT-1 Y701 compared to STAT-1 S727 localised in the nucleus. Incubation with 500 μM of H_2O_2 for 1 h also showed similar staining to the 400 μM treatment but a more punctate foci were observed with the STAT-1 Y701 staining.

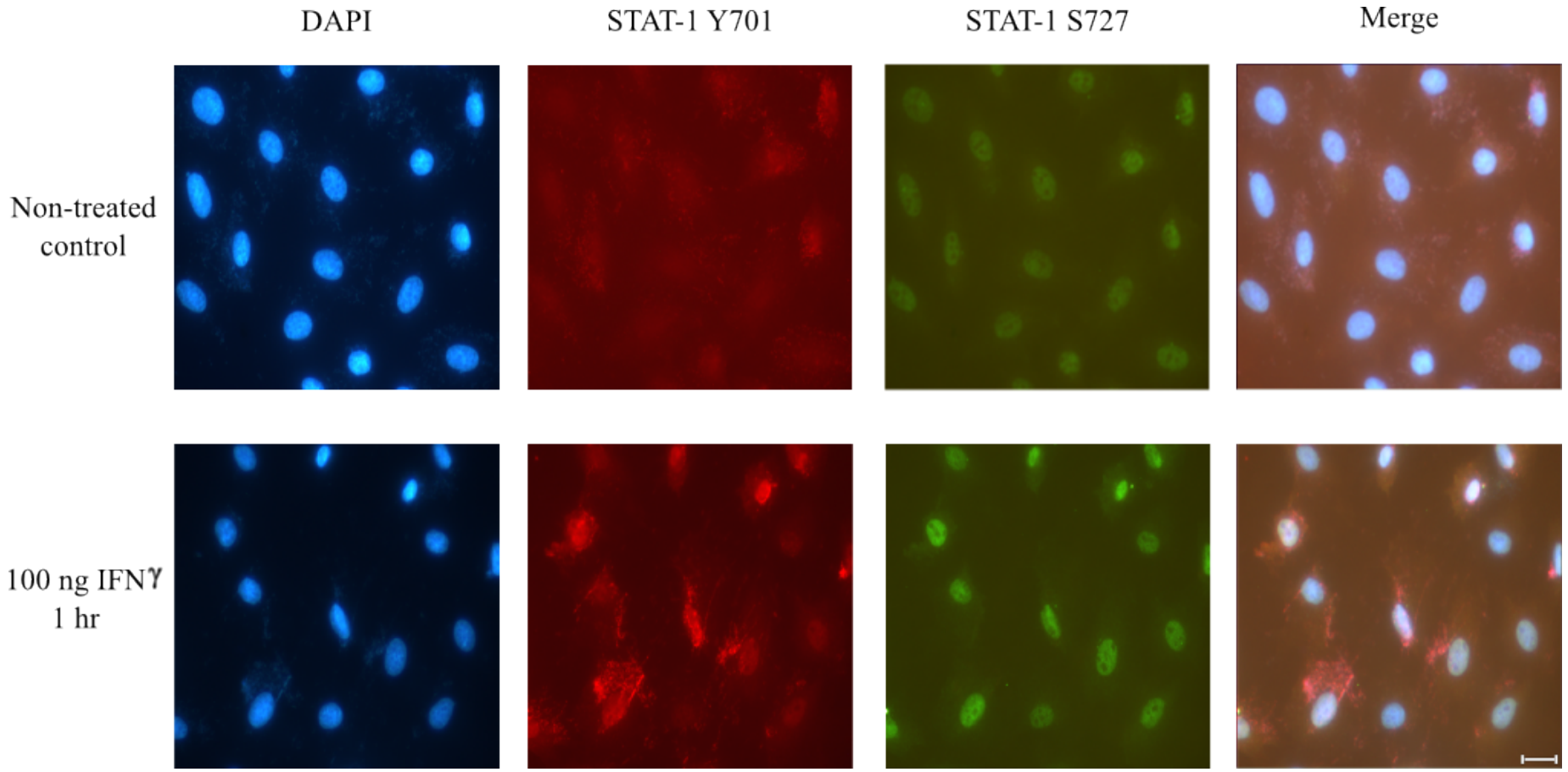

Figure 3.5 Induction of apoptotic cell death of H9C2 cells following an exposure to 100 ng/mL of IFN-γ for 1 h. Cells were seeded on coverslips for 24 h either non-treated cells or exposed to 100 ng/mL of IFN-γ for 1 h. Cells were fixed in 4% paraformaldehyde and protein activation assessed by indirect immunoflourescent staining with flourescein-conjugated antibodies (STAT-1 Y701, red; and STAT-1 S727, green). Cell nuclei was counterstained with DAPI. As expected elevated levels of phosphorylated STAT-1 Y701 and S727 were detected with an IFN-γ treatment compared to the non-treated control cells. Representative images of three different experiments. Scale bar = 20 μM.

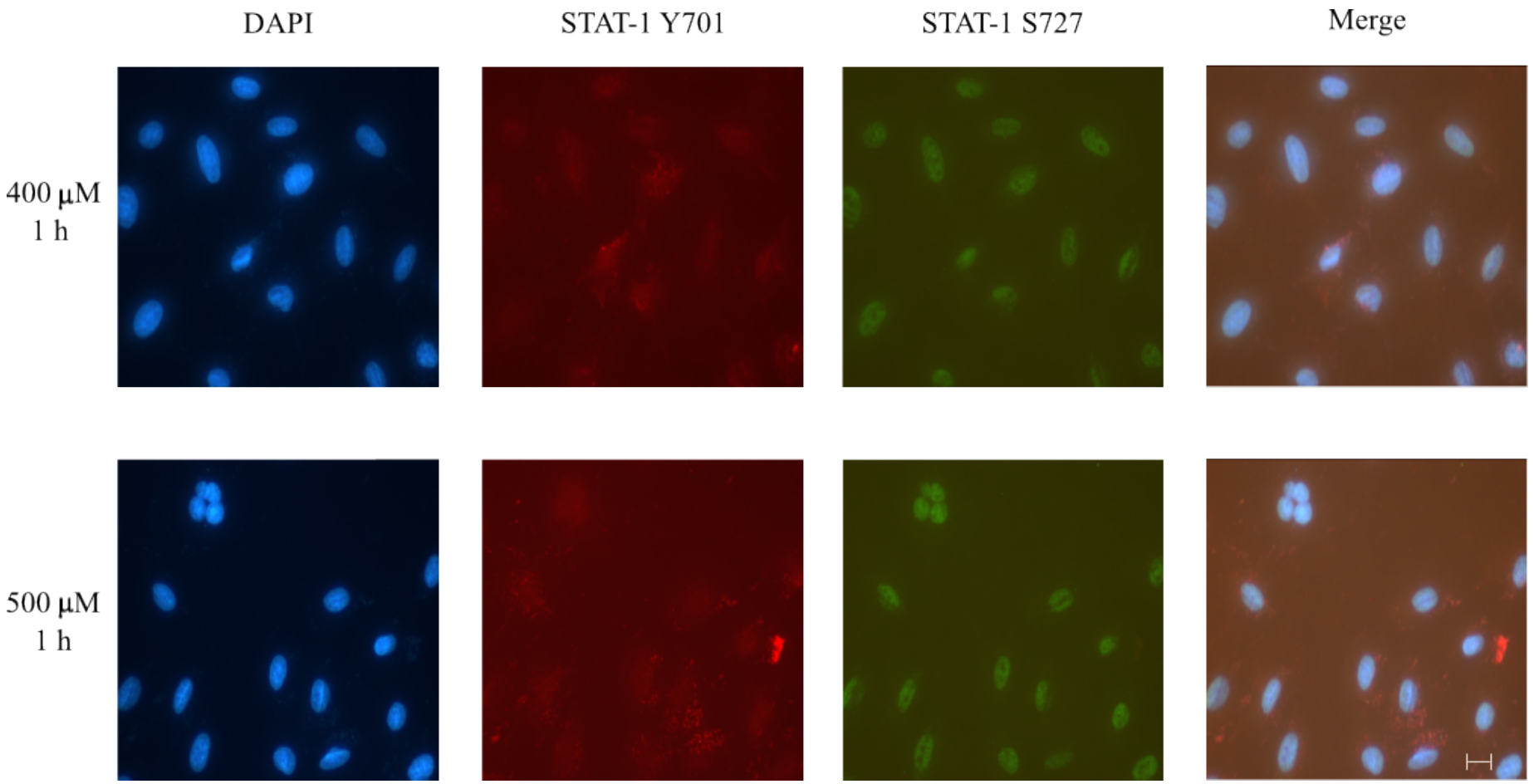

Figure 3.6 Induction of apoptotic cell death of H9C2 cells following an exposure to H_2O_2. Cells were seeded on coverslips for 24 h before exposure to 400 μM (top) and 500 μM (bottom) of H_2O_2 for 1 h of treatment. Cells were fixed in 4% paraformaldehyde and protein activation assessed by indirect immunoflorescent staining with flourescein-conjugated antibodies (STAT-1 Y701, red; and STAT-1 S727, green). Cell nuclei was counterstained with DAPI. There was an increase in levels of phosphorylated STAT-1 Y701 and S727 following an exposure to H_2O_2 for 1 h compared to the non-treated control cells. Representative images of three different experiments. Scale bar = 20 μM.

The H_2O_2-treated cells exhibited morphological changes consistent with apoptosis such as cell shrinkage and membrane blebbing, particularly after 1 h treatment with 400 μM and 500 μM H_2O_2 (Figure 3.7).

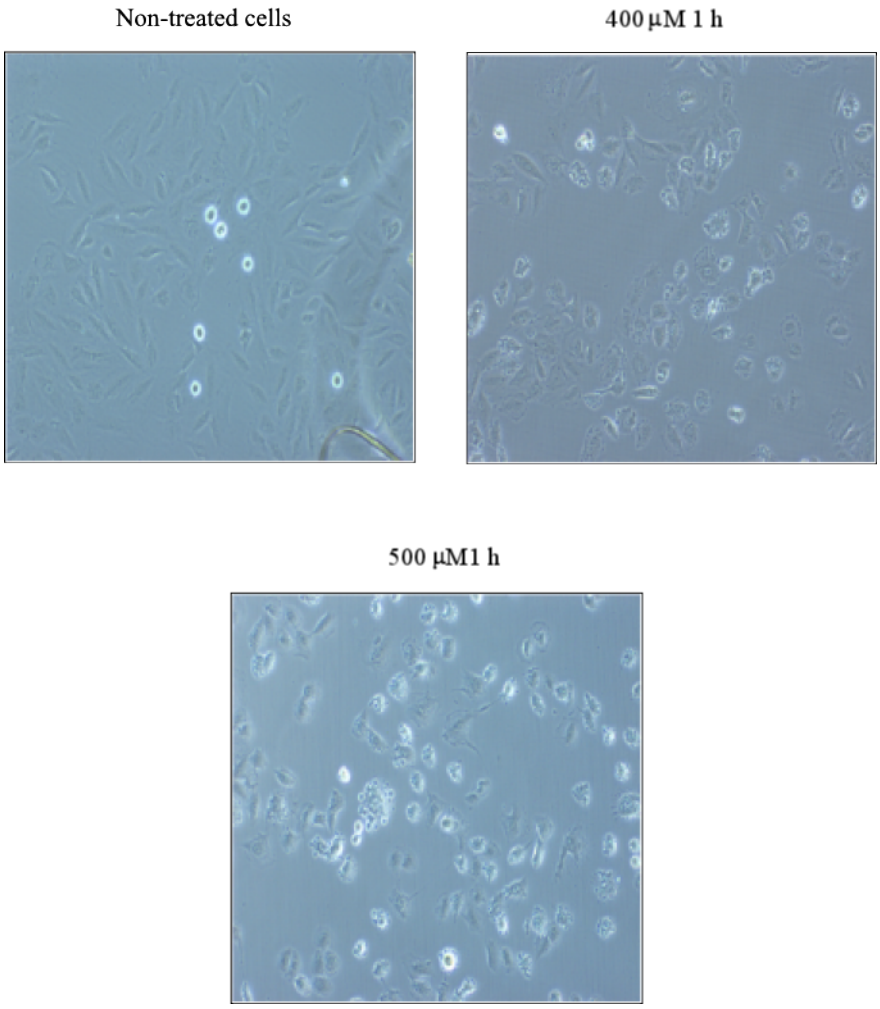

Figure 3.7 Phase-contrast microscope images of H9C2 cells following treatment with 400 μM and 500 μM of H_2O_2 for 1 h. Morphological changes consistent with apoptosis including cells shrinkage, membrane blebbing, and DNA fragmentation were observed with increasing H_2O_2 concentrations. Representative images of three different experiments.

Similarly, H_2O_2 incubation led to an increased phosphorylation of ERK-1/2 after 1 h as the concentration increased in agreement with previous studies.[97] Proteins were measured indirectly by immunoflourescence using flourescein-conjugated secondary antibodies for phosphorylated ERK-1/2. One can observe an elevated level of phosphorylated ERK-1/2 following an exposure to 500 μM H_2O_2 compared to 400 μM after 1 h as shown by the increase in intensity and nuclear translocation of active ERK-1/2 in Figure 3.8. It is noteworthy that extension of the incubation time to 24 h resulted in cells with severe membrane rupture, which was difficult to assess by protein analysis. Regardless, a shorter time-point was more appropriate with conditions during an *in vivo* I/R injury.

Taken together, H_2O_2 induced apoptotic cell death in H9C2 myoblasts. Based this data, the most detrimental conditions were 400 μM and 500 μM of H_2O_2 for 1 h incubation. These conditions were studied further to understand the effects of GTP preconditioning in the protection of the heart against oxidative stress.

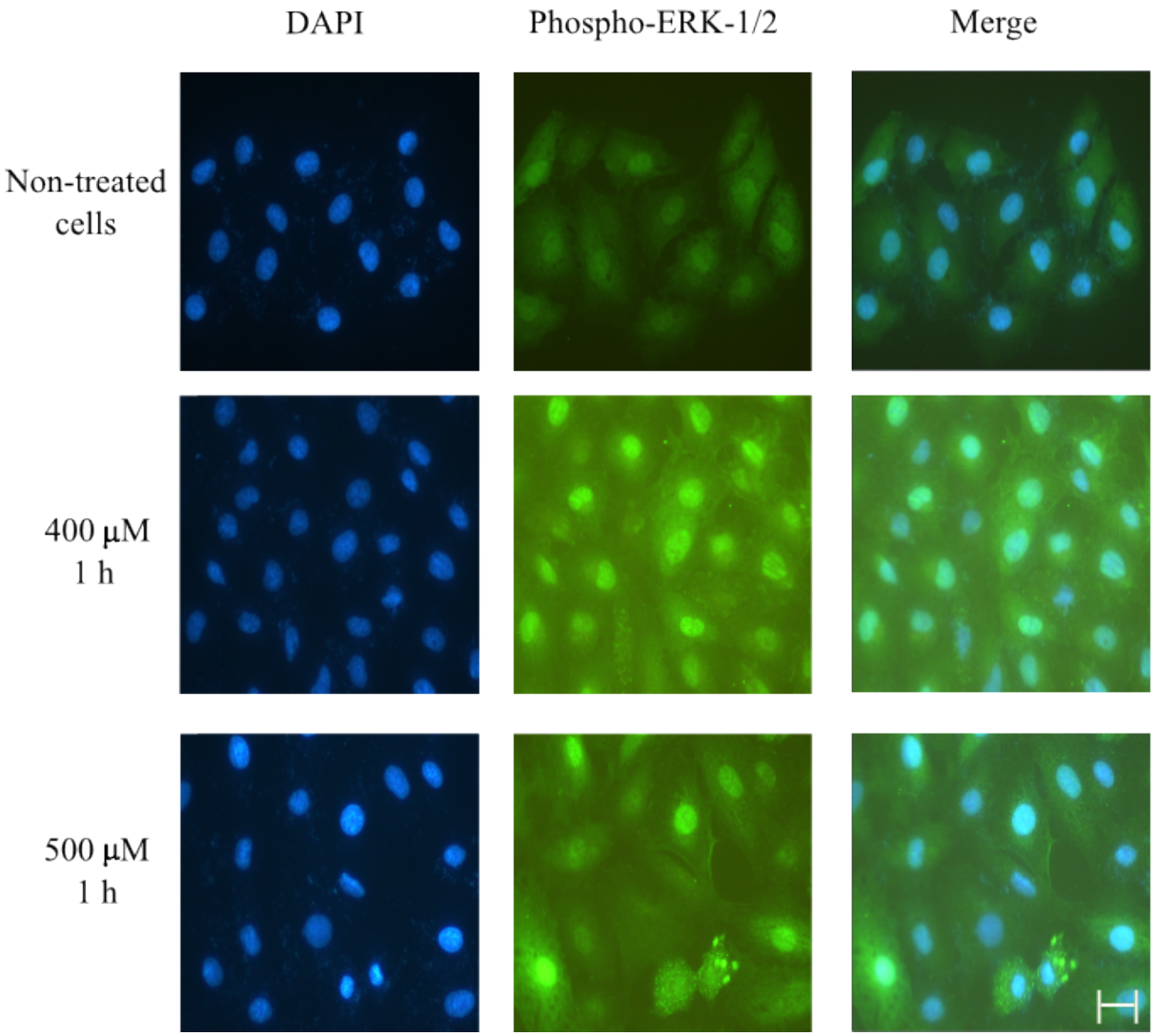

Figure 3.8 Treatment with 400 μM and 500 μM of H_2O_2 for 1 h showed an increased in phosphorylated ERK-1/2. Microscopic images of H9C2 cells following exposure to H_2O_2. A) Phase-contrast images of cells treated with 400 μM and 500 μM of H_2O_2 for 1 h. Phosphorylation and translocation of ERK-1/2. Proteins were measured using immunoflourescence using flourescein-conjugated secondary antibodies. Cell nuclei was stained with DAPI and phosphorylated-ERK in green. The merged images demonstrate the nuclear translocation of ERK-1/2 following an H_2O_2 induction. Representative images of three different experiments. Scale bar = 20 μM.

3.2.3.2 Effects of GTP on H9C2 cells following H_2O_2-induced cell death

To further investigate the effects of GTPs on H9C2 myoblast cells following oxidative stress induction, cells were incubated with the four GTPs for 1 h. The cells were washed with PBS and fresh media was added before the addition of H_2O_2 to induce oxidative stress. The levels of proteins of interest were assessed by immunoblotting and cell viability was quantified using trypan blue exclusion, and CyQUANT^{TM} assays, where non-treated cells were used as a control.

As expected, the protein levels of phosphorylated STAT-1 Y701 increased with the exposure to 400 and 500 μM H_2O_2 (Figure 3.9). When the cells were pre-treated with EGCG, the levels of phosphorylated STAT-1 Y701 were significantly reduced with EGCG pre-treatment. Pre-treatment with EGC also reduced the phosphorylation levels, surprisingly EC also showed this effect. ECG, however, showed a moderate attenuation in comparison to the other polyphenols. The levels of STAT-1 S727 showed a similar reduction when pre-treated with GTPs compared to the oxidative stress induced cells with H_2O_2 alone. The level of total STAT-1 remained constant under the various conditions, as did β-actin. Following exposure to H_2O_2 ERK-1/2 was activated as shown by the high levels of phosphorylated ERK-1/2 in comparison to control cells. The levels of active ERK-1/2 remained constant with all the GTPs except for EC which showed a decrease in the protein level. The levels of total ERK-1/2 remained constant.

These results suggest that the cardioprotective effects exhibited by EGCG, EGC and to a minor extent ECG may be via an inhibition of STAT-1 activation and not ERK phosphorylation. This further supports the theory that following an induction of oxidative stress ERK-1/2 pathway gets activated, but its downstream activation of STAT-1 is inhibited by GTPs. Conversely EC may in fact be inhibiting the activation of ERK-1/2 which in turn cannot activate STAT-1.

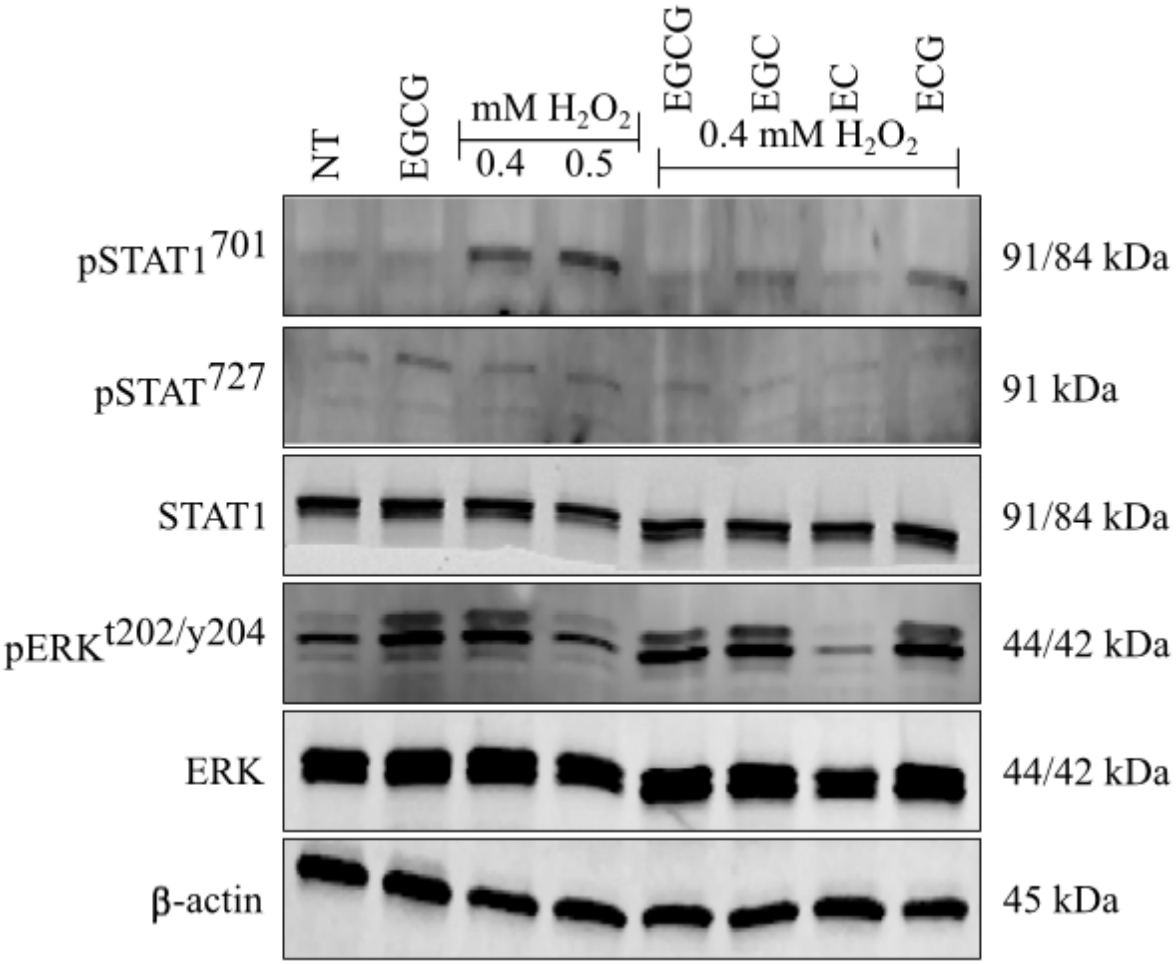

Figure 3.9 Cardioprotective effects of GTP on H9C2 cells following H_2O_2 exposure. Cells were incubated with indicated polyphenols for 1 h followed by a wash out before exposure to H_2O_2 for 1 h. Cells were harvested and assessed by immunoblotting using antibodies against phosphorylated STAT-1 Y701, phosphorylated STAT-1 S727, total STAT-1, phosphorylated ERK-1/2, total ERK and β-actin, which was used as the loading control. Levels of STAT-1 Y701 and S727 were shown to increase with exposure to H_2O_2 but were attenuated by pre-treatment with GTPs. Induction of H_2O_2 also resulted in the activation of phosphorylated ERK-1/2 but the phosphorylated protein levels were only reduced by EC pre-treatment. The levels of total ERK remained constant under the different conditions. Representative blot of three different experiments.

Quantitative assessment of viable cells was done by Trypan blue exclusion, where dead and dying cells took up the blue dye. Exposure to 400 and 500 μM for 1 h resulted in high toxicity, with 36% and 34.4% non-viable cells respectively (Figure 3.10). Pre-treatment with 100 μM GTPs for 1 h exhibited some protection resulting in an increased cell viability. Following exposure to 400 μM H_2O_2 EGCG showed the highest cell viability with 6.4% non-viable cells and EC the lowest with 15.43% non-viable cells. It was discovered that pre-treatment with EGC and exposure to a higher H_2O_2 concentration made it difficult for the cells to recover with an increase in non-viable cells to 19.6%. The other three GTPs showed roughly the same amount of non-viable cells despite the higher H_2O_2 concentration.

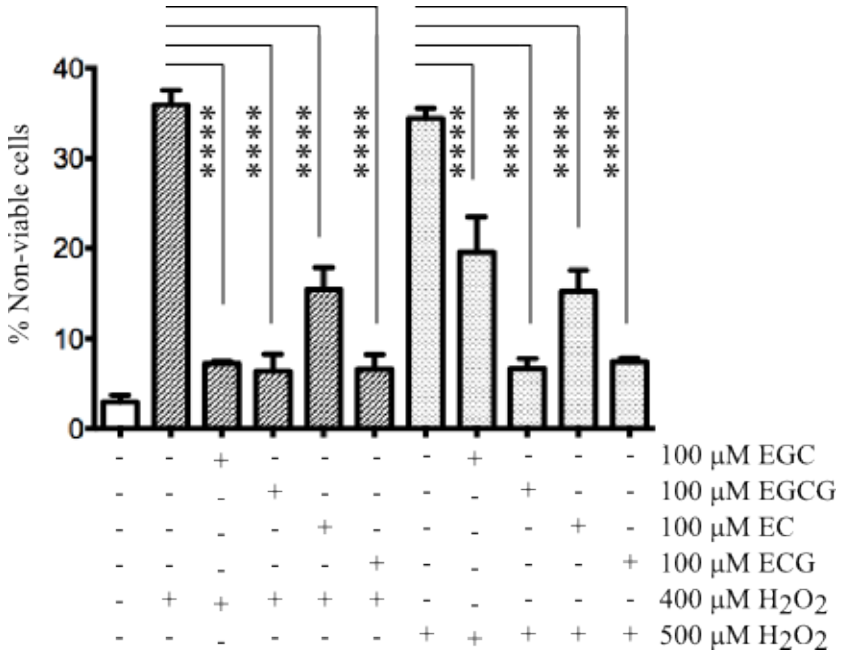

Figure 3.10 Quantitative assessment of H9C2 cells exposed to H_2O_2 following GTP pretreatment. Cells were pretreated with 100 μM of designated GTP for 1 h followed by 1 h incubation of 400 and 500 μM. Cell death was assessed using Trypan blue exclusion. Control non-treated cells showed the lowest about of non-viable cells with 3% and the highest non-viable cells exhibited by H_2O_2 exposure with more than 30% non-viable cells. All four polyphenols showed a reduction in non-viable cells, the lowest shown by EGCG with 6.4% and 6.6% after 400 and 500 μM exposure respectively. Data plotted is mean $\pm$ standard error. Statistical analysis was carried out using a one-way ANOVA using Graphpad Prism. Differences were considered statistically significant at values of $p < 0.001$. Representative graph of three different experiments.

Furthermore, exposure to H_2O_2 for longer timepoints showed the number of non-viable cells remained approximately the same for 500 μM with 32.7% non-viable cells after 3 h exposure. Phase-contrast assessment of cell morphology after 3 h treatment of 500 μM H_2O_2 showed cell shrinkage, which is a the typical characteristic of apoptotic cells. Exposure to 100 μM EGCG prior to cell death induction caused a reduction in shrunken cells and an attempted recovery of the cells resulting in a higher percentage of viable cells (Figure 3.11). Pre-treatment with EGCG however, only showed a reduction in non-viable cells by 11 and 15% after exposure to 200 and 500 μM H_2O_2 respectively after 3 h treatment (Figure 3.12).

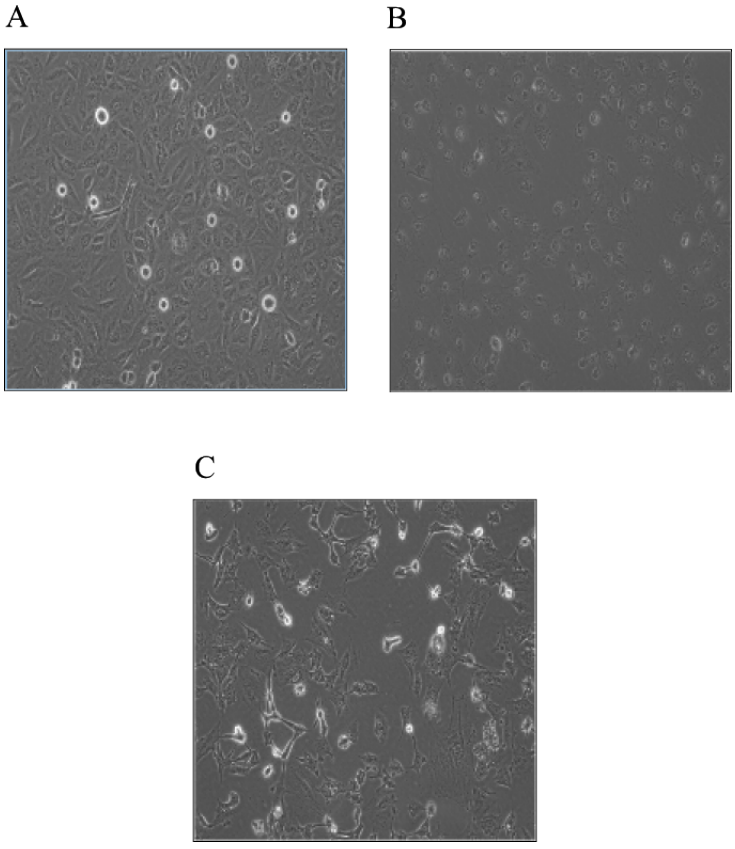

Figure 3.11 Cardioprotective effects of EGCG following cell death induction by H_2O_2 analysed by phase-contrast micrsoscopy. A) Control non-treated cells B) H9C2 cells exposed to 500 μM H_2O_2 for 3 h C) 1 h pretreatment of cells with 100 μM EGCG followed by treatment with 500 μM H_2O_2 for 3 h. Morphological assessment by phase-contrast microscopy showed cell death characteristics following exposure to 500 μM H_2O_2.

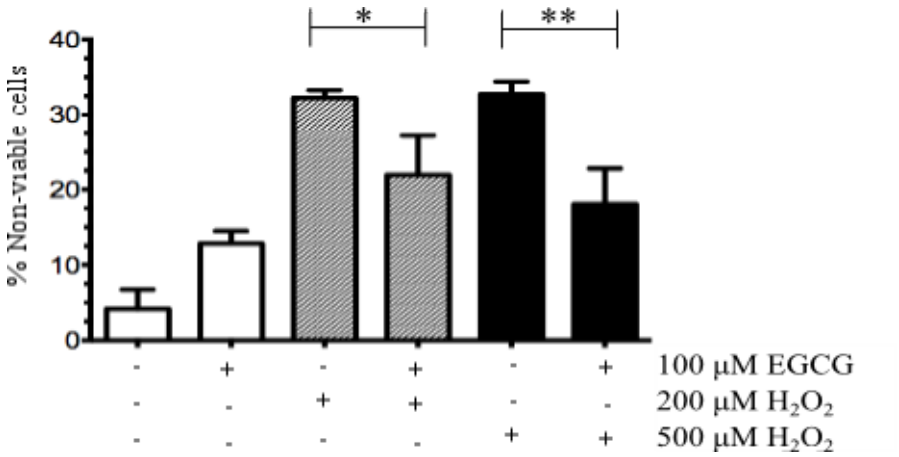

Figure 3.12 Cardioprotective effects of EGCG following cell death induction by H_2O_2 quantified by Trypan Blue exclusion. Trypan blue exclusion quantifying cardioprotective effects of EGCG following cell death induction with 500 μM H_2O_2 treatment for 3 h. Pre-incubation with EGCG showed cell recovery with more viable cells present. Quantitative assessment with trypan blue exclusion showed reduction in non-viable with EGCG pre-incubation by 11 and 15% after exposure to 200 and 500 μM H_2O_2 respectively. Data plotted is mean $\pm$ standard error. Representative images and graph of two different experiments. Statistical analysis was carried out using a one-way ANOVA using Graphpad Prism. Differences were considered statistically significant at values of $p < 0.05$.

3.2.4 Evaluating the cardioprotective effects of GTP during I/R injury

3.2.5 Induction of cell death by I/R injury in H9C2 cells

True I/R injury can only be experienced *in vivo*, therefore our *in vitro* methodology is a *simulated I/R injury* and this work will simply be referred to as I/R injury. The method used to simulate I/R injury in H9C2 was modified from a method developed by Esumi.[250] The ischaemic Esumi buffer was made up of 10 mM 2-deoxyglucose, which inhibited glycolysis, 12 mM KCl and 20 mM sodium lactate, both of which lead to membrane depolarisation via an increase in K^+ and Na^+ ion concentrations, an acidic pH of 6.2 and oxygen deprivation in an ischaemic chamber (5% CO_2/ 95% argon). Taken together, these conditions mimic that experienced by cardiomyocytes during ischaemia *in vivo*.

Control experiments were carried out using Esumi control buffer containing 3.8 mM NaCl and 10 mM glucose, instead of 2-deoxyglucose, and no sodium lactate, at a pH of 7.4. The cells were incubated under normoxic conditions in a humidified environment containing 20% O_2, 5% CO_2 with an N_2 balance for the duration of the ischaemia. Following ischaemia, the treated and control cells are washed with PBS to remove the Esumi buffer and replaced with normal growth media for the duration of reperfusion. Following reperfusion, H9C2 cells were either harvested and assessed by immunoblotting, or fixed with 4% paraformaldehyde to investigate changes in cell morphology following I/R injury as assessed by confocal microscopy.

In order to determine whether these I/R conditions induced cell death, cells were incubated in Esumi ischaemia buffer for 4 h followed by varying reperfusion times and control cells were incubated in Esumi control buffer. After 4 h ischaemia activation of STAT-1 Y701 and S727 phosphorylation were not detected by immunoblotting, corroborating previous studies that biological function is reduced with oxygen deprivation which occurs during I/R damage (Figure 3.13).

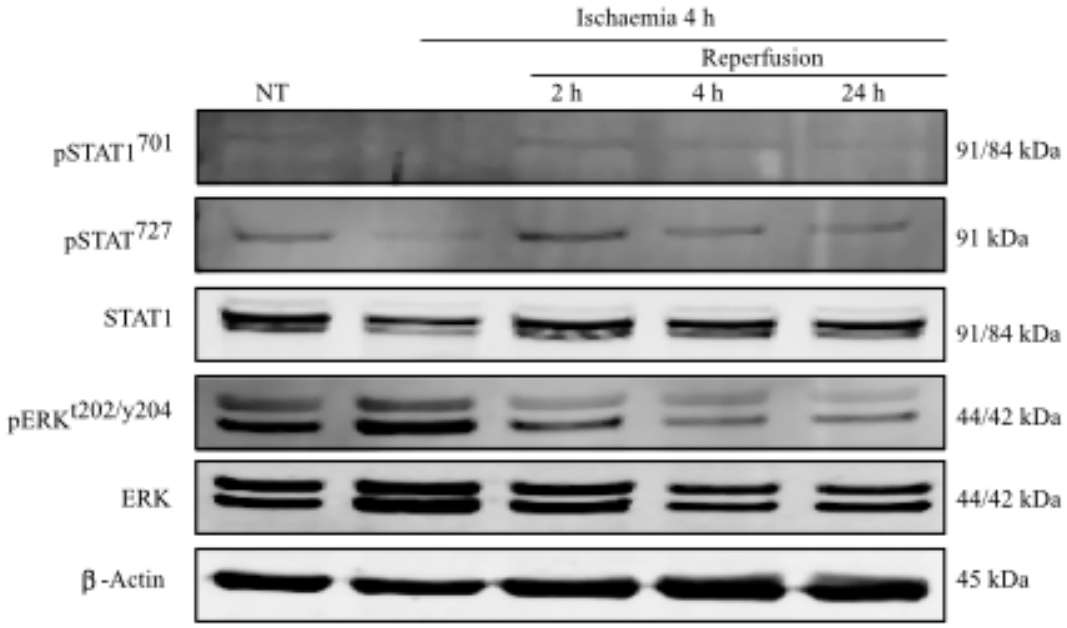

Figure 3.13 Induction of cell death following I/R injury on H9C2 cells. Control H9C2 cells were incubated with Esumi control buffer for 4 h ischaemia, washed with PBS and reperfused for 16 h in growth media. H9C2 cells were incubated with Esumi ischaemic buffer for 4 h ischaemia, washed in PBS and reperfused for indicated times in growth media.Cells were harvested and assessed immunoblotting using antibodies against STAT-1 Y701, STAT-1 S727, total STAT-1, phosphorylated ERK-1/2, total ERK and β-actin, which was used as the loading control. Levels of STAT-1 701 increased following 2 and 4 h reperfusion. Very low levels were observed after 24 h reperfusion. Levels of STAT-1 S727 were highest after 2 h reperfusion. Basal levels of phosphorylated ERK-1/2 was detected in the control cells. Elevated levels were detected after 4 h ischaemia and levels decreased with reperfusion. The levels of total STAT-1 and ERK-1/2 remained relatively constant. Representative blot of three different experiments.

During the reperfusion phase, elevated levels of STAT-1 Y701 and S727 were detected with the highest levels after 2 h reperfusion. In contrast, the highest phosphorylated ERK-1/2 were detected following ischaemia and the levels gradually reduced as the reperfusion phase progressed. The levels of total STAT-1 and ERK-1/2 remained relatively constant under the different conditions, as did β-actin, which was used as a loading control.

Morphological studies using confocal and phase-contrast microscopy confirmed the activation of phosphorylated STAT-1 Y701 and phosphorylated ERK-1/2 in Figure 3.14 and Figure 3.15. Confocal images showed that phosphorylation of STAT-1 at the Y701 residue and the phosphorylation of ERK-1/2 following 4 h ischaemia and reperfusion from 2 h to 24 h. It is noteworthy that although STAT-1 Y701 is activated, the nuclear translocation was only observed in some cells, specifically after 24 h reperfusion, and the majority of the staining remained in the cytoplasm.

Phase-contrast images show the negative effects of I/R damage on cell morphology; ischaemia damage resulted in cell shrinkage, detachment from the plates and death, with the more detrimental effects detected after 2 h reperfusion than at 4 h and 24 h reperfusion. There is some recovery observed after 24 h reperfusion as shown in Figure 3.13 and Figure 3.15. This is likely due to the H9C2 cells being an immortalised cell line, still capable of proliferation despite the harsh conditions they have been subjected to. Based on these results, further studies on the effects of GTPs on H9C2 cells were assessed using 4 h ischaemia and 2 h reperfusion.

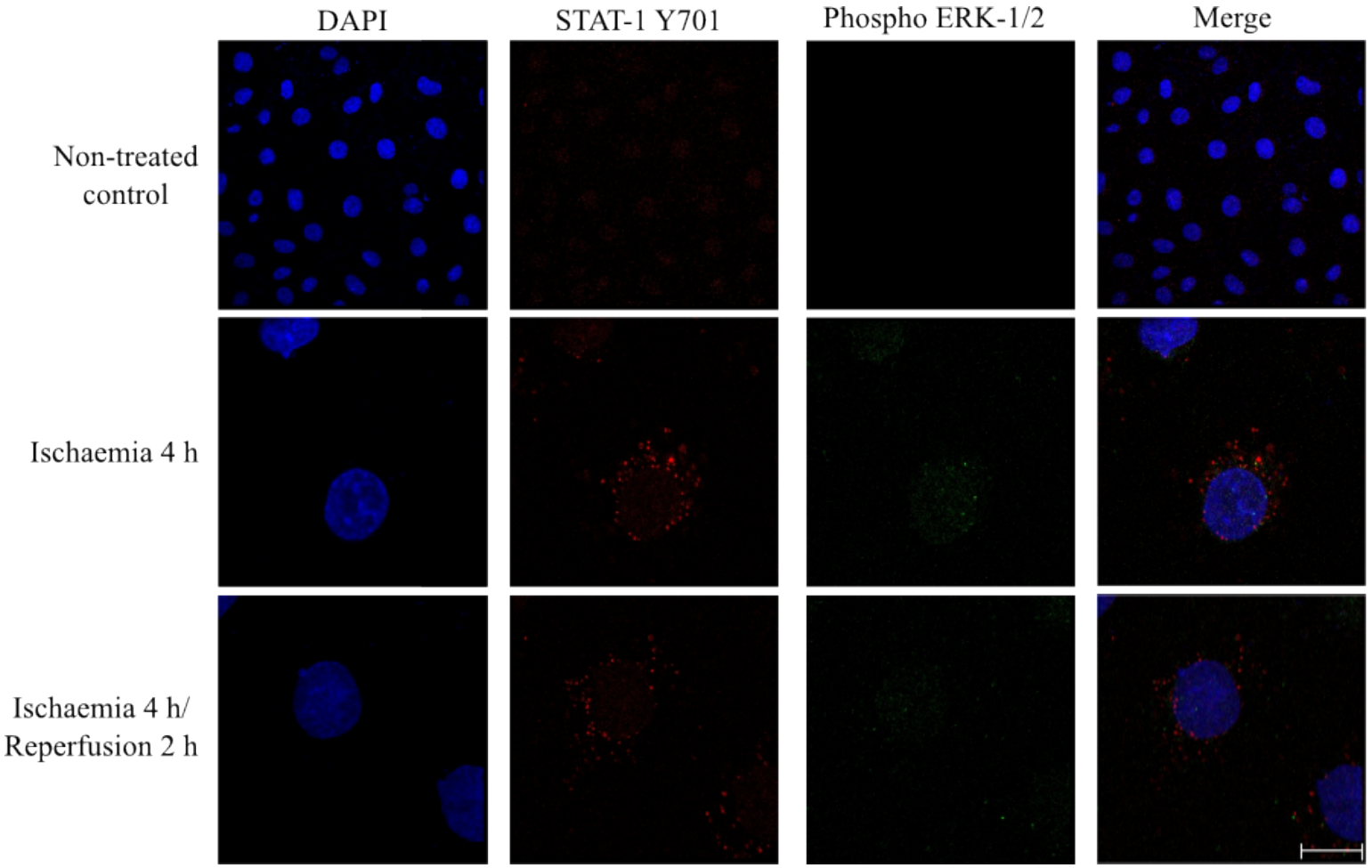

Figure 3.14 Induction of cell death of H9C2 cells following 4 h ischaemia and 2 - 24 h reperfusion injury. Cells were seeded on coverslips for 24 h before exposure to varying concentrations of H_2O_2 for 1 h. Cells were fixed in 4% paraformaldehyde and protein activation assessed by indirect immunoflorescent staining with flourescein-conjugated antibodies (STAT-1 Y701, red; and phosphorylated ERK-1/2, green). Cell nuclei was counterstained with DAPI. There was an increase in levels of phosphorylated STAT-1 Y701 and ERK-1/2 following an exposure to H_2O_2 for 1 h compared to the non-treated control cells. Representative images of three different experiments. Scale bar = 20 μM.

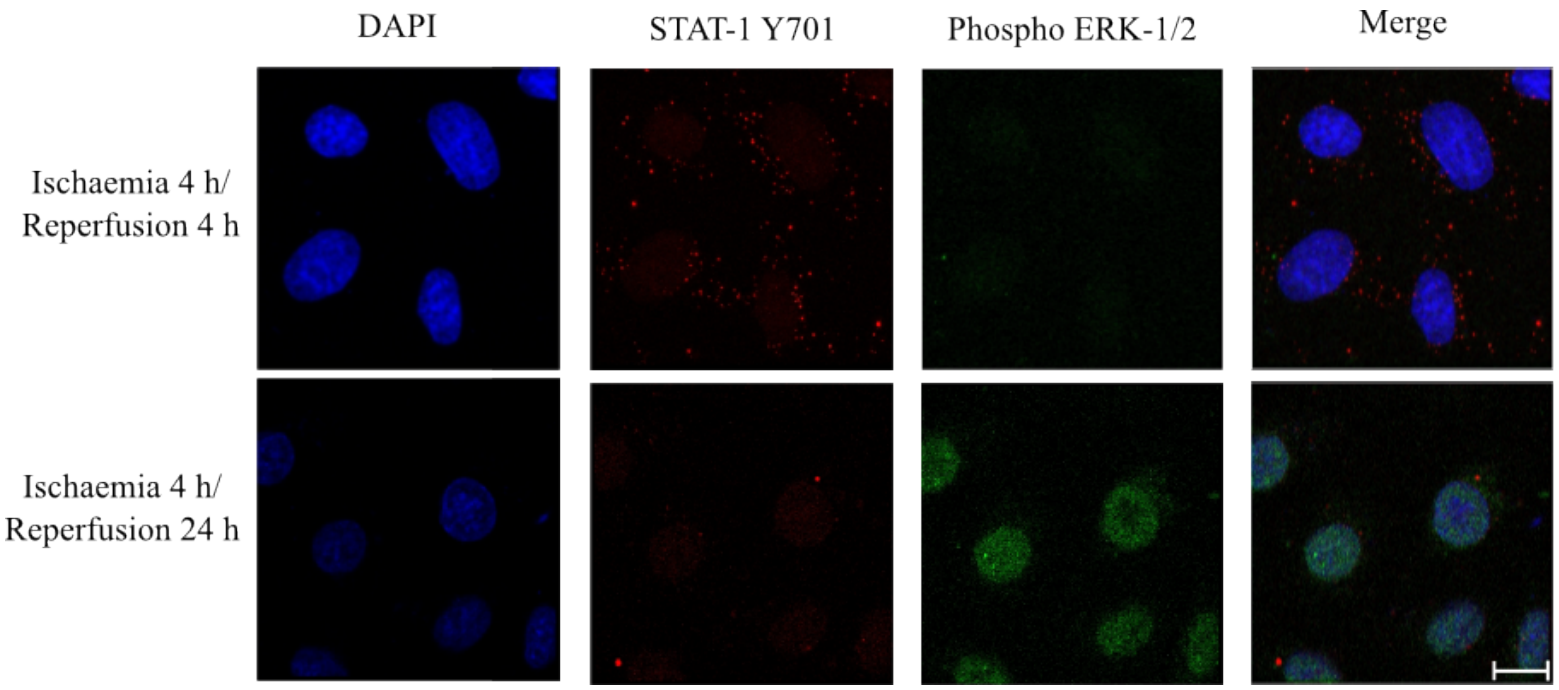

Figure 3.15 Induction of apoptotic cell death of H9C2 cells following an exposure to I/R injury. Cells were seeded on coverslips for 24 h before exposure to varying concentrations of H_2O_2 for 1 h. Cells were fixed in 4% paraformaldehyde and protein levels assessed by immunoflourescent staining with flourescein-conjugated antibodies (STAT-1 Y701, red; and STAT-1 S727, green) using confocal microscopy. Cell nuclei was counterstained with DAPI. Activated STAT-1 Y701 detected after 4 h ischaemia and 2 and 4 h reperfusion. Elevated levels of phosphorylated ERK-1/2 detected following 4 h ischaemia and 24 h reperfusion compared to the control cells. Phase contrast images of H9C2 cells following I/R injury. A) Control B) Ischaemia 4 h C) Ischaemia 4 h /Reperfusion 2 h D) Ischaemia 4 h /Reperfusion 4 h E) Ischaemia 4 h /Reperfusion 24 h. Cells exposed the I/R injury show cells shrinkage and detachment off the coverslip with largest changes detached after 2 h reperfusion. Some cell recovery can be observed following 24 h reperfusion. Scale bar = 20 μM.

3.2.5.1 Effects of GTP on H9C2 cells following I/R injury

The cardioprotective effects of GTP following I/R injury was initiated by pre-treating the H9C2 cells with 100 μM of GTPs for 1 h before subjecting the cells to I/R injury. The cells were washed with PBS before the addition of the Esumi ischaemia buffer and control cells were incubated with Esumi control buffer during the ischaemia phase. Both buffers were then replaced with normal growth media for the reperfusion phase.

Cells were exposed to 4 h of ischaemia before a wash out and the buffer was then replaced with normal growth media for 2 h reperfusion. Low levels of phosphorylated STAT-1 Y701 were detected with GTP pre-treatment but no significant changes were detected in comparison to control cells by immunoblotting (Figure 3.16). Pre-treatment with EGCG did not affect levels of phosphorylated STAT-1 Y701, which was not detectable in untreated H9C2 cells but only became detectable in the presence of 100 ng/mL IFN-γ, which was used as a positive control. Levels of phosphorylated STAT-1 S727 mirrored the effects seen with phosphorylated Y701 except that phosphorylated S727 levels were at a more readily detectable level. Total levels of STAT-1 remained at a level similar to the untreated cells under all treatment regiments. Treatment with IFN-γ did not have an effect on the phosphorylation of ERK-1/2 which remained at a similar level to untreated except in the case of EC pre-incubation where it increased.

Taken together, no significant changes in the levels of STAT-1 activation was detected following I/R injury. EC pre-treatment resulted in increased phosphorylation of ERK-1/2 suggesting that during I/R injury this polyphenol activated the ERK pathway. The total levels of STAT-1 and ERK-1/2 remained relatively constant under the conditions.

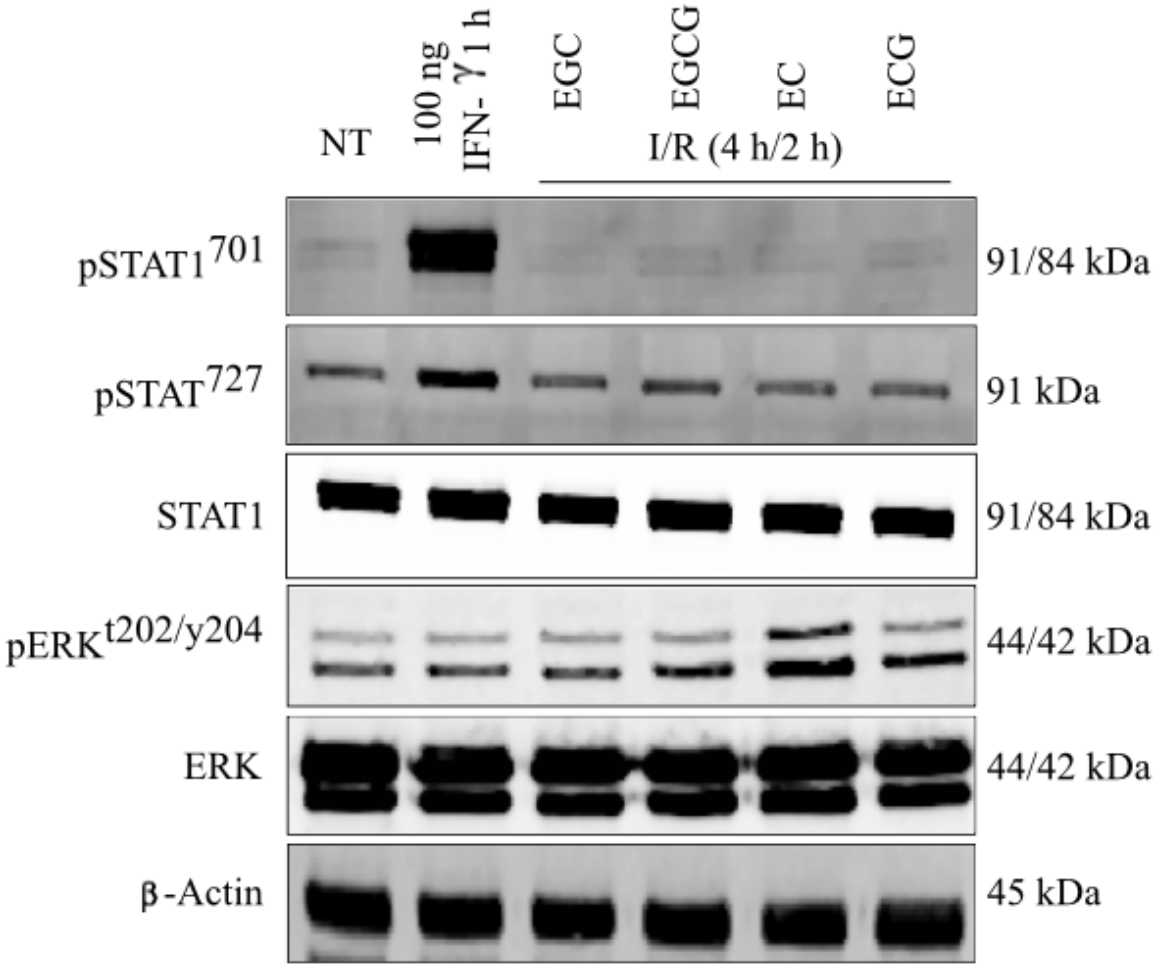

Figure 3.16 Cardioprotective effects of GTP on H9C2 cells following 4 h ischaemia and 2 h reperfusion injury. Control H9C2 cells were incubated with Esumi control buffer for 4 h ischaemia, washed with PBS and reperfused for 16 h in growth media. Positive cintrol cells were incubated with 100 ng/mL IFN-γ for 1 h. H9C2 cells pretreated with indicated 100 μM GTP 1 h and then incubated with Esumi ischaemic buffer for 4 h ischaemia, washed in PBS and reperfused 2 h in growth media.Cells were harvested and assessed immunoblotting using antibodies against STAT-1 Y701, STAT-1 S727, total STAT-1, phosphorylated ERK-1/2, total ERK and β-actin, which was used as the loading control. No significant changes were observed in the levels of STAT-1 Y701 and slightly higher levels of STAT-1 S727 was observed following EGCG pre-treatment. Higher phosphorylation levels of ERK-1/2 was detected with EC and ECG pre-treatment. Representative blot of three different experiments.

3.2.6 Effects of green tea analogues on H9C2 myoblast cells

In order to determine the EC_{50} values for the GTP analogues, cells were plated at a density of 5000 cells per well in a 96-well plate and allowed 24 h for attachment. Cells were incubated with compounds over a range of concentrations (0 - 1600 μM) for 24 h then cellular toxicity was determined by CyQUANT^{TM} assay and logistical dose-response curves were used to calculate EC_{50} values. The GTP analogue structures and EC_{50} values are displayed in Figure 3.17.

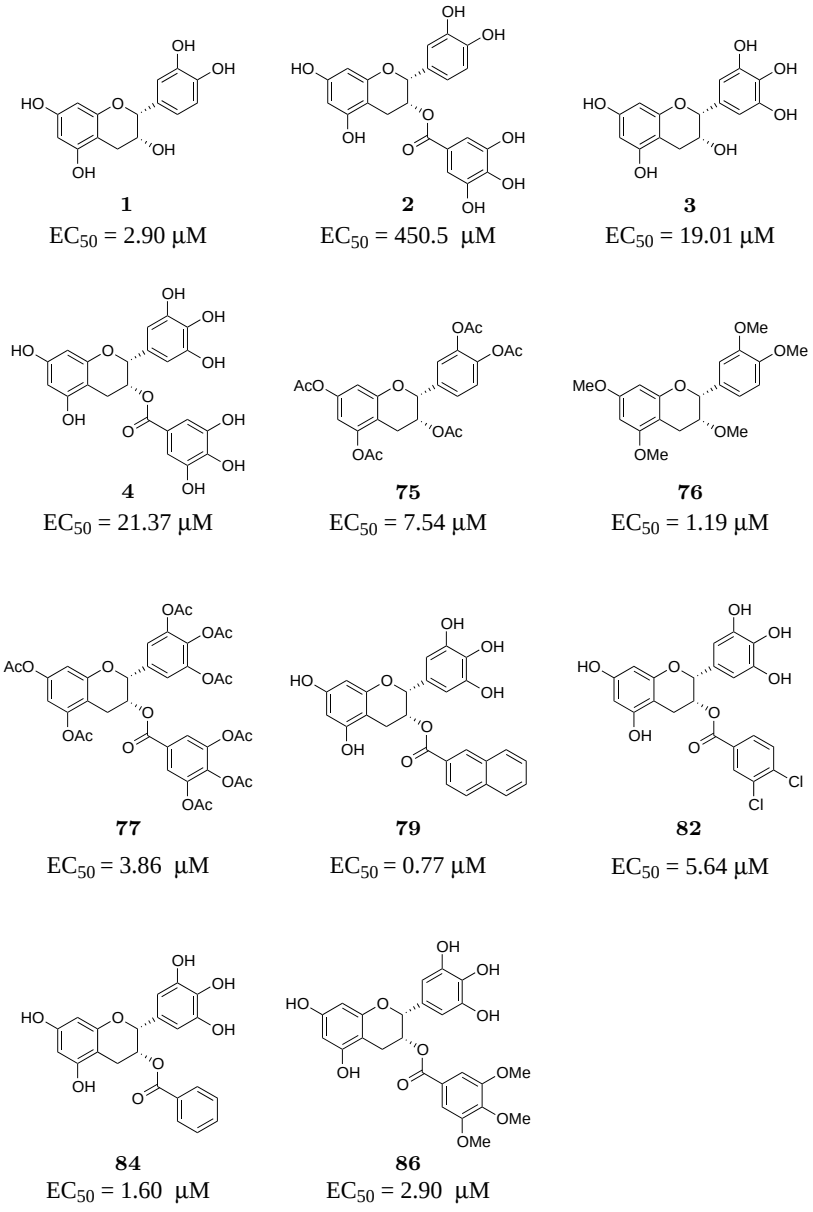

Figure 3.17 EC_{50} values of GTP and their analogues. Experiment performed in triplicate and values calculated using Graphpad Prism.

Analysis of the derivatives revealed some structural activity necessary for GTP activity. Substitution of the hydroxyl groups with acetyl groups on EC (**1**) had a negative effect on the activity by reducing the potency by nearly 2.5 fold. Conversely, acetyl substitution of EGCG (**4**) improved the potency by 5.5 fold. Substitution of the hydroxyl groups with methoxy groups in **76** improved the potency of EC by just over 2 fold. Substituting the Ring C significantly improved the potency of EGCG as observed with **79**, **82**, **84**, and **86**. Replacement of ring C with the di-chloro and tri-methoxy groups lowered the EC_{50} by 3- and 7-folds respectively. Substitution with benzoic and naphthoic groups greatly improved the activity by more than 13 fold with EC_{50} of 1.60 and 0.77 μM respectively.

Taken together, the analogues synthesised did improve the activity of the polyphenols as shown by the lower EC_{50} values. The acetyl groups improved the EC_{50} values of EGCG (**4**) but not as much for EC (**1**). Replacement of ring C on EGCG with benzoic (**84**) and naphthoic acid (**79**) groups greatly improved the activity compared with parent compound EGCG.

3.2.7 Evaluation of the cardioprotective effects of GTP and synthesised analogues during I/R injury in neonatal rat cardiomyocytes

3.2.7.1 Isolation of neonatal rat cardiomyocytes

Ventricular myocytes were isolated from the hearts of two day old rat neonatal Sprague Dawley rat neonatals using a method previously described by Simpson and Savion.[251] The interaction between cardiomyocytes and non-cardiomyocytes in the heart can alter the properties of cardiomyocytes and it is important to minimise this interaction in studies using primary rat heart cultures.This must be ensured because a lower cardiomyocyte content in culture results in slower beating rates and less negative membrane potential.[251]

In order to ensure that the cells isolated are healthy and the majority of isolated cells are cardiomyocytes, compared to non-cardiomyocytes, in particular fibroblasts. 5000 cells

were plated on gelatin-coated coverslips and incubated under normoxic conditions. Cells were fixed in 4% paraformaldehyde and stained with desmin and vimentin. Cells were analysed for desmin staining which is found near the Z line sarcomeres to identify cardiomyocytes. It is important in the maintenance of cell integrity and a known marker for cardiomyocytes.[252] Staining for vimentin was also carried out to identify fibroblasts. Fibroblasts are mesenchymal cells with many important functions including the synthesis on extracellular matrix in connective tissues. Fibroblasts are characterised by their spindle-shape morphology and their easy attachment to plastic culture vessels.They are also positively stained by the mesenchymal marker vimentin, a filament protein expressed in mesenchymal cells.[253]

Isolated NRCM assessed by confocal microscopy in Figure 3.18 show the distinct morphology of cardiomyocytes detected by the desmin filaments. The spindle shape of fibroblast is also shown by the vimentin mesenchymal marker. Cell count showed that >87% of total cells were cardiomyocytes after 48 h in culture.

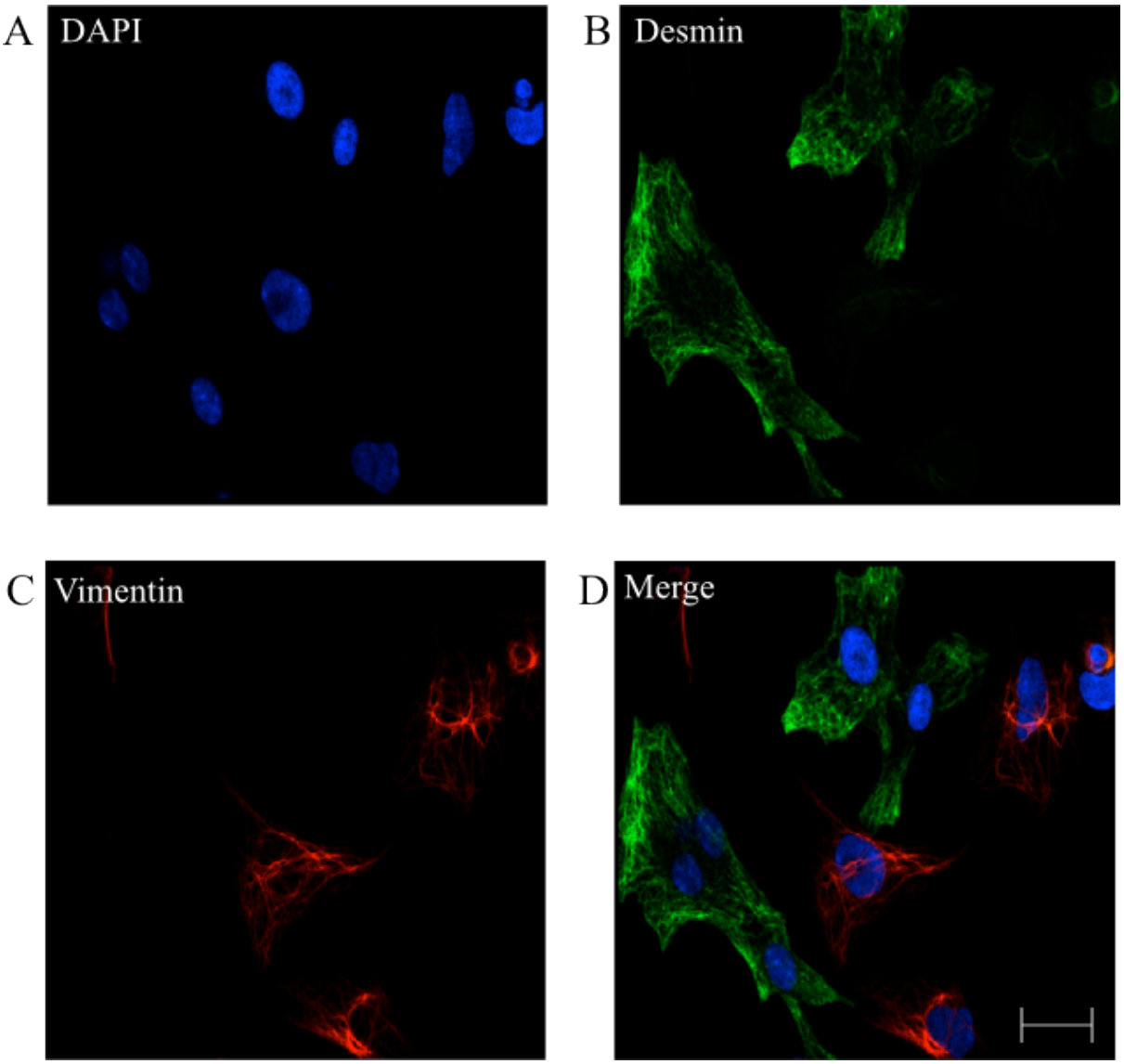

Figure 3.18 Confocal microscopy images of neonatal rat cardiac myocytes stained with desmin and vimentin. Cells were fixed in 4% paraformaldehyde and cell morphology assessed by fluorescent staining. Cells were stained with with DAPI (blue), Desmin (green) and Vimentin (red). Cardiomyocytes are detected by the desmin stain and fibroblasts are detected by the vimentin dye. Scale bar = 10 μm.

3.2.7.2 Establishing an *in vitro* model to induce cell death in NRCM

Cardiac myocytes were initially exposed to 4 h of ischaemia followed by 16 h reperfusion as these were the conditions developed by Townsend *et al.*[153] Following reperfusion, the cardiomyocytes were fixed with 4% paraformaldehyde in preparation for confocal microscopy in order to investigate changes in cell morphology following I/R injury. It is worth noting that a low level of cell death was expected in the control cells for a number of reasons, including that a number of cardiomyocytes die during the isolation procedure but can remain attached to the flask, resulting in false positives and as the myocytes are maintained in maintenance media (1% FBS in DMEM media) and cell death can occur over time. In spite of these limitations, there was still an increase in cell death following I/R injury over a period of time. Cells were stained with total STAT-1 as this is one of the proteins of interest, β-myosin heavy chain (β-MHC)was used as an NRCM marker because it is expressed in the ventricular myocardium of mammals and its expression is related to the contractile velocity of the heart muscle.[254]

Control cells were incubated for 4 h in Esumi control buffer then it was replaced with maintenance media for 16 h of reperfusion under normoxic conditions. Under normal conditions, inactive STAT-1 was localised predominantly in the cytoplasm, as shown by green fluorescent dye in Figure 3.19. The florescent staining of β-MHC allowed the long chains of branching sarcomeres (myofibrils), which make up the contractile unit of the cardiomyocytes to be observed.

Following exposure to I/R injury, there was a change in the cell morphology, losing their distinct oval shape as is observed in Figure 3.20 . Following I/R damage, the cardiac contractile function was significantly reduced as suggested by the disruption in the arrangement of the myofibrils as shown by β-MHC staining. The level of endogenous inactive STAT-1 was also drastically reduced based on the intensity, suggesting that some of the transcription factors may have been activated or an increase in proteosomal degradation.

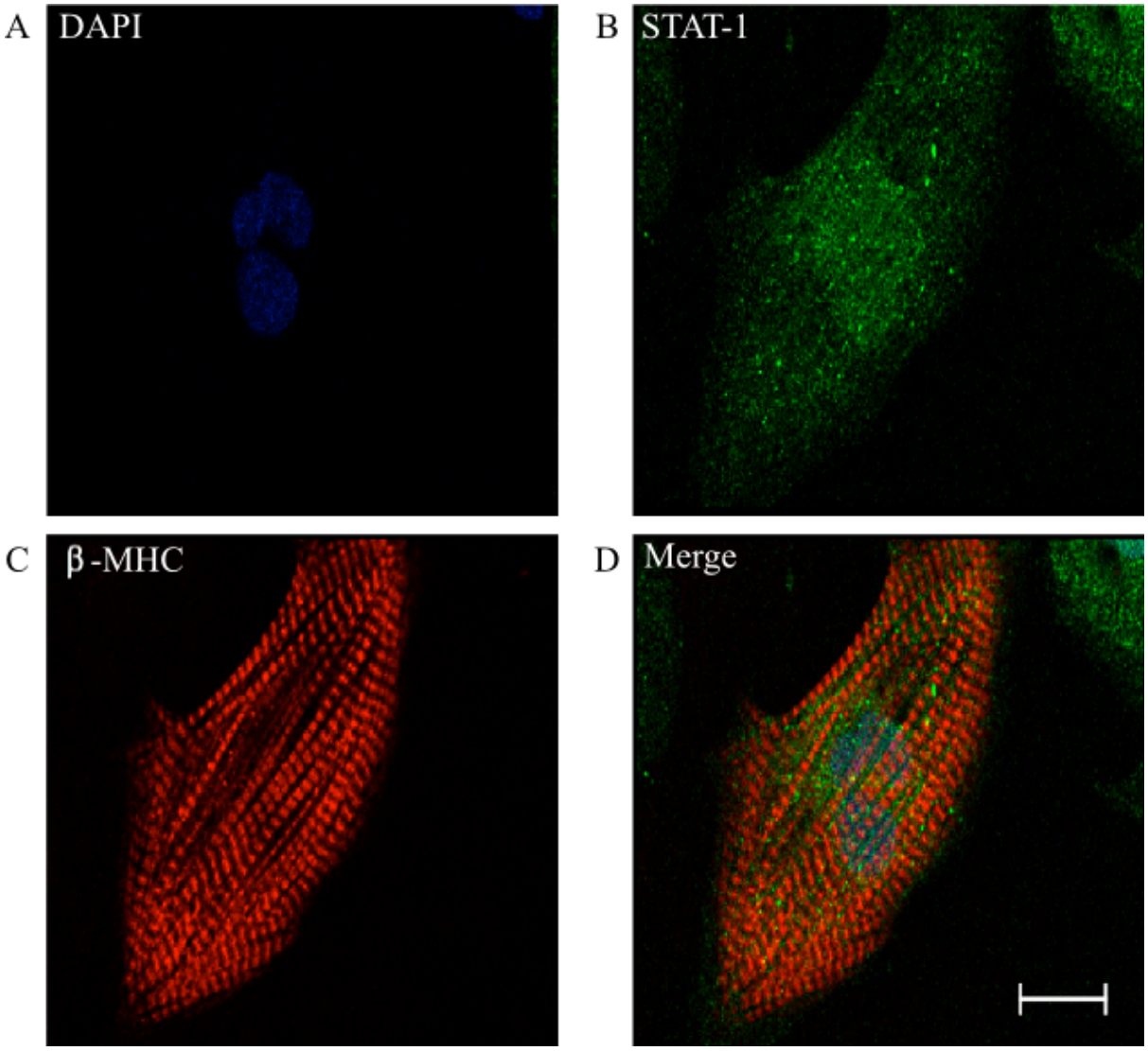

Figure 3.19 Confocal microscopy images of NRCM with inactive STAT-1 and β-MHC under normoxic conditions. Control cardiomyocytes were incubated with Esumi control buffer for 4 h ischaemia, washed in PBS and reperfused for 16 h in maintenance media. Cells were fixed in 4% paraformaldehyde and cell morphology assessed by fluorescent staining. Cells are stained with DAPI (A: blue), STAT-1 (B: green), β-MHC (C: red) and the merged image (D). DAPI was used to stain the nuclei, STAT-1 was used to detect endogenous levels of the protein and β-MHC was used to detect the muscle striations of the cardiomyocytes. The images shows a normal cell morphology observed in NRCM under normoxic conditions. Scale bar = 30 μm.

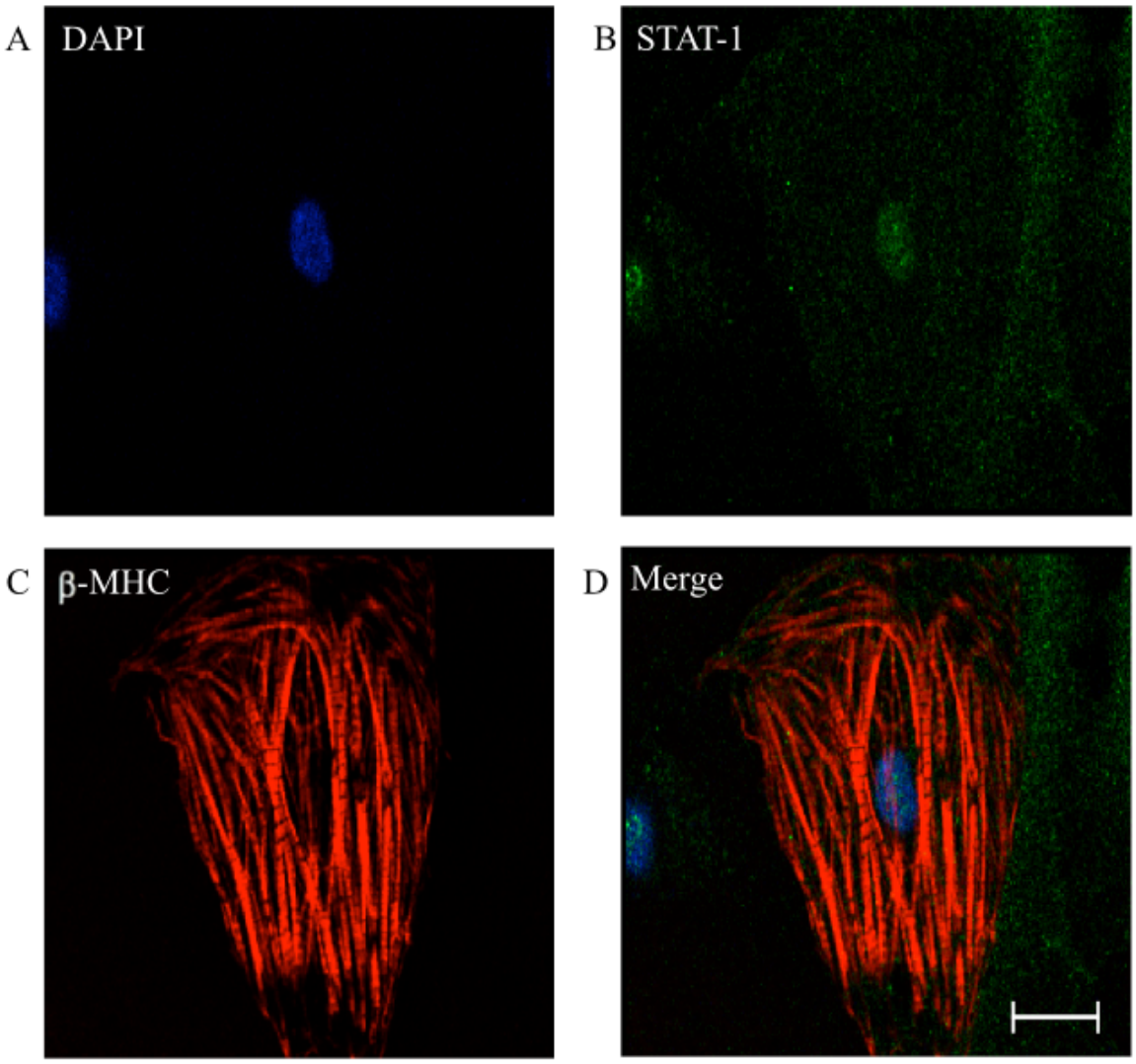

Figure 3.20 Confocal microscopy images of NRCM stained with inactive STAT-1 and β-MHC following 4 h ischaemia and 24 h reperfusion injury. Control cardiomyocytes were incubated with Esumi ischaemic buffer for 4 h ischaemia, washed in PBS and reperfused for 16 h in maintenance media. Cells were fixed in 4% paraformaldehyde and cell morphology assessed by fluorescent staining. Cells are stained with DAPI (A: blue), STAT-1 (B: green), β-MHC (C: red) and the merged image (D). DAPI was used to stain the nuclei, STAT-1 was used to detect endogenous levels of the protein and β-MHC was used to detect the muscle striations of the cardiomyocytes. Cells exposed to I/R damage show a disruption in the cell shape and muscle striations and well as a decreased in the levels of STAT-1 transcription factor compared to the control cardiomyocytes. Scale bar = 30 μm.

3.2.7.3 Investigating the cardioprotective effects of EGCG (4) and Ac-EGCG (77) on NRCM following I/R injury

The following experiments were used to investigate whether the GTP and the analogues protected NRCM from cell death. The cells were incubated with the GTP analogue acetylated EGCG **77** for 1 h then washed with PBS prior to the addition of Esumi ischaemia buffer. NRCMs were subjected to 4 h ischaemia followed by 16 h reperfusion, then cell death was assessed using Trypan Blue exclusion, which measures total cell death (apoptotic and necrotic), non-viable cells and total cells were counted by scoring 200 cells, three times per well, using a haemocytometer and the percentage was calculated.

As expected cells exposed to I/R injury had the highest percentage of non-viable cells with 24.49% ± 6.85% trypan blue positive cells. Cells pretreated with EGCG showed a reduction in non-viable cells with 19.66% ± 3.78% trypan blue positive. Interestingly, cells pretreated with acetylated EGCG at half the concentration of EGCG had the lowest percentage of non-viable cells of 16.34% ± 0.55% trypan blue positive (Figure 3.21).

Ester-based "pro-drugs" are a means of improving drug biovailability and curbing drug toxicity.[255] Examples of these include the acetylation of salicylic acid to form aspirin and the acetylation of morphine to obtain heroin.[255] This protecting group improves bioavailability by increasing hydrophobicity, reducing polar side chains and hydroxyl groups that would otherwise undergo biotransformation and/or degradation. Pro-drug Ac-EGCG **77** is converted to the polyphenol EGCG via a reaction with an esterase enzyme.[256] The peracetate ester of EGCG had been shown to be an improved proteasome inhibitor in Jurkat, human T cell leukaemia, over the naturally occurring EGCG.[257]

In conclusion, the preliminary data in this chapter suggests that the *in vitro* conditions established induced cell death in response to I/R injury. In addition, although EGCG and Ac-EGCG reduced the amount on non-viable cells following I/R injury, the acetylated EGCG analogue could be an improvement on the GTP EGCG and this compound would be worth investigating further.

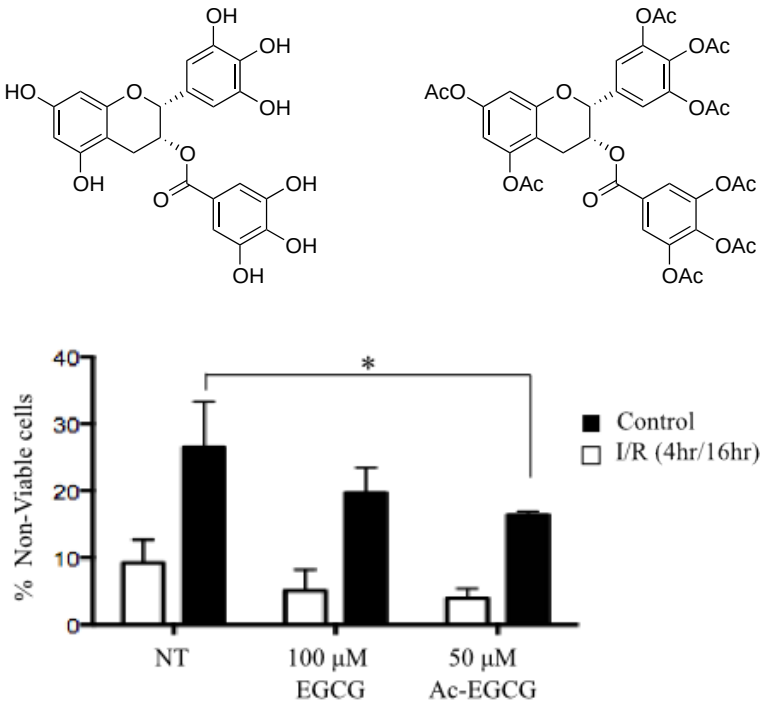

Figure 3.21 EGCG and acetylated EGCG analogue improve viable cell death following I/R injury. Cells are exposed to 4 h ischaemia followed by 16 h reperfusion. Cell death was assessed by Trypan Blue exclusion and the percentage of non-viable cells was calculated. Experiments repeated in triplicate. Statistical analysis was carried out using a one-way ANOVA using Graphpad Prism. Differences were considered statistically significant at values of $p < 0.05$.

3.3 Discussion

H9C2 cardiac myoblasts cell line have been used to investigate heart function in a number of studies[97, 258] because they possess morphological characteristics and signalling pathways similar to those detected in human adult cardiac cells. Established work in the group necessitated further study into the effects of oxidative stress and I/R injury-induced cell death that occurs during heart failure specifically in terms of the signalling pathways.

Initial experiments involved the determination of whether proteins of interest were expressed in H9C2 cell line. STAT-1 was activated by 100 ng of IFN-γ treatment leading to the induction of STAT-1 Y701 which was detected by immunoblotting in Figure 3.1. Although the levels of phosphorylated STAT-1 S727 remained relatively constant, the protein levels of phosphorylated ERK-1/2 reduced inversely, suggesting that ERK-1/2 may have contributed to the activation of STAT-1. An investigation into the cardioprotective effects of the four major GTPs on H9C2 cells gave EC_{50} values suggesting in order of potency that EGC>EGCG>EC>ECG (Figure 3.2) where the curves indicated EGC, EGCG and EC were stimulatory drugs and ECG with the highest EC_{50} value was more of an inhibitory drug. Further cell viability assessment corroborated the EC_{50} values with EGC and EGCG to have similar dose-response curves and the curves of EC and ECG showing them to be the least potent as the gradient over the active concentration was much less (Figure 3.3).

In this study, oxidative stress-induced cell death in H9C2 cells was caused by 1 h treatment of 400 and 500 μM H_2O_2 was assessed by immunoblotting in Figure 3.4 which showed an increase in the phosphorylation of STAT-1 Y701, S727 and ERK-1/2 compared to the non-treated cells. Indirect assessment by immunoflouresence also confirmed the activation the STAT-1 in Figure 3.6. Morphological changes observed were also consistent with cells undergoing apoptosis. GTP pretreatment, specifically with EGC, EGC and EGCG exhibited some protection by inhibiting STAT-1 activation but not ERK-1/2 phosphorylation. EC, on the other hand, inhibited the activation of ERK-1/2 preventing the activation of STAT-1 (Figure 3.4). A hypothetical model of regulation in Figure 3.22

shows how the GTP activate the ERK-1/2 and STAT-1 signalling pathway with EC inhibiting ERK-1/2 activation and ECG, EGC and EGCG inhibiting STAT-1 phosphorylation. Quantitative assessment in Figure 3.10 showed that following H_2O_2 exposure, EGCG pretreatment had the highest cell viability with 6.4% non-viable cells and the lowest cell viability observed with EC with 15.43% non-viable cells.

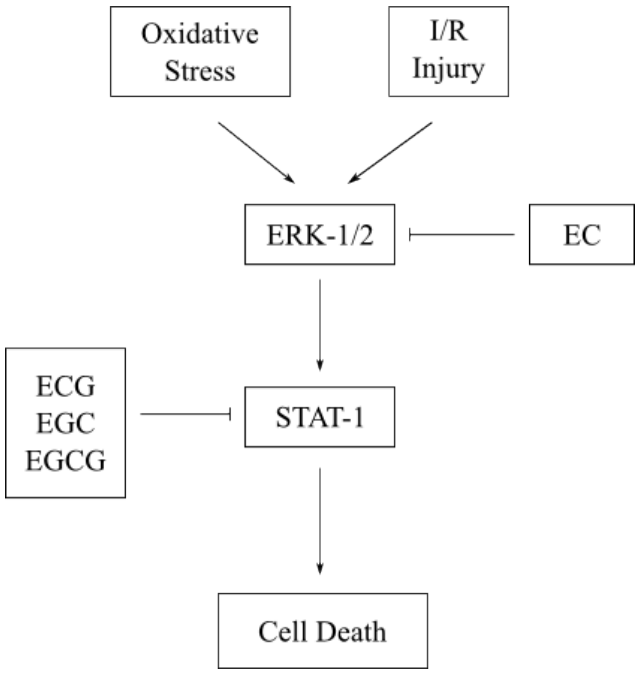

Figure 3.22 Hypothetical model of regulation of ERK-1/2 and STAT-1 in response to oxidative stress and I/R-induced cell death and cardioprotective function of GTP. The ERK-1/2 and STAT-1 pathways are activated by oxidative stress and I/R injury with the ERK-1/2 phosphorylation inhibited by EC which in turn inhibited the activation of STAT-1. ECG, EGC and EGCG where shown to inhibit the activation of STAT-1.

The effects of the synthesised analogues on H9C2 cells were also investigated and the EC_{50} values were calculated (Figure 3.17). The results showed that substitution of ring C with benzoic (**84**) and naphthoic (**79**) rings improved the potency by more than 13-fold compared to EGCG with EC_{50} values of 1.60 and 0.77 μM respectively. The structure-activity relationship described in Figure 3.23 suggest the importance of the ABD ring system and that ring C can be varied without detrimental effects on the GTP function. These results also suggest that further studies should be carried out on the acetylated EGCG (**77**) as well as the benzoic and naphthoic acid substituted analogues.

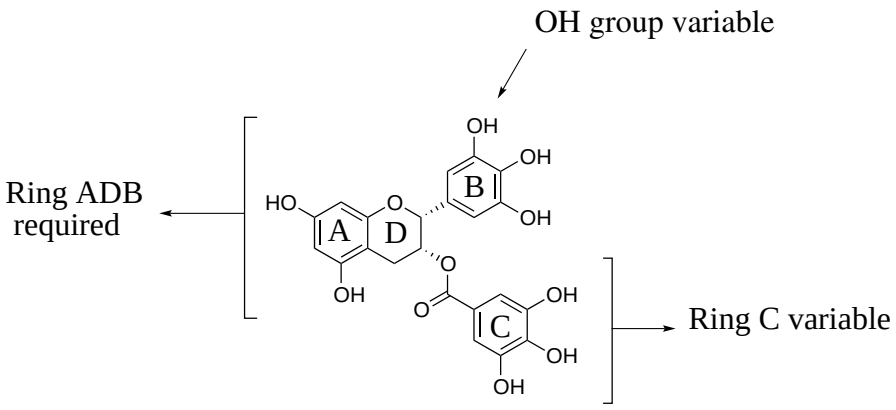

Figure 3.23 Structure-activity relationships of green tea polyphenol analogues. The SAR activity suggested that ABD ring system is required but the presence of the 3 OH group in ring might not be necessary and ring C can be modified in order to improve the potency and efficacy.

Upon evaluation of the protective effects of the GTPs against I/R injury on H9C2 cell death was induced using a modified Esumi ischaemia buffer in a modular incubator with 5% CO_2/95% Argon. Immunoblotting in Figure 3.13 following 4 h of ischaemia and then 2 h reperfusion showed an upregulation in STAT-1 Y701 and S727 phosphorylation as well as a reduction in the levels of activated ERK-1/2. Confocal microscopy images in Figure 3.14 and Figure 3.15 confirmed the activation and translocation of STAT-1 Y701 and moderate activation of ERK-1/2. Pretreatment with the four major GTPs resulted in decreased levels of phosphorylated STAT-1 S701 but no significant changes were observed with STAT-1 S727. EC pretreatment led to an upregulation of phosphorylated ERK-1/2, similar to results observed with H_2O_2 pretreatment.

These results led to a similar investigation using NRCM. Exposure to 4 h ischaemia followed by 16 h reperfusion resulted in changes in cell morphology with the NRCM taking on a more rounded shape as well as a disruption in the arrangements of the myofibrils, (Figure 3.19 and Figure 3.20) with a reduction in the levels of endogenous inactive STAT-1. Pretreatment with EGCG and Ac-EGCG (**77**) led to a decrease in non-viable cells compared to cells only exposed to I/R injury. Ac-EGCG (**77**) had the lowest number of non-viable cells at half the concentration of EGCG shown by Trypan Blue exclusion in Figure 3.21 suggesting that this analogue could be an improved form of EGCG.

3.4 Conclusion

This work demonstrated the IFN-γ-mediated phosphorylation of STAT-1 at Y701 and S727 where necessary for maximal activity.[259] They also showed that a crosstalk between ERK-1/2 and STAT-1 pathways particularly the phosphorylation at Y701 residue resulted in an induced expression of STAT-1 in the JAK-STAT pathway and this may represent an important pathway in cell survival/death in cardiomyocytes. Out of the four major GTPs, EGCG had the most cardioprotective activity under oxidative stress and I/R injury. Following I/R injury Ac-EGCG (**77**), resulted in a lower amount of non-viable cells compared to EGCG at half the treatment concentration indicating that a pro-drug might be the most efficient way of introducing the GTP into the target cells. Besides Ac-EGCG, analogues **79** and **84** had significantly lower EC_{50} values compared to EGCG but their cardioprotective activity would need to be investigated further.

Chapter 4

Materials And Methods

4.1 Materials

4.1.1 General Materials

Material	Company	Catalogue no.
15 mL Falcon® conical tubes	BD Bioscience	352096
50 mL Falcon® conical tubes	BD bioscience	352070
1.5 mL microcentrifuge tubes	Anachem	ABCT-1.5
0.5 mL microcentrifuge tubes	Anachem	ABCT-0.5
75 cm^2 culture flask (T75)	Corning	3290
175 cm^2 culture flask (T175)	Corning	3292
35 x 10 mm culture dish (10 cm)	Corning	3294
6 well plate	Corning	3335
12 well plate	Corning	3336
96 well plate (Flat-bottom; clear)	Corning	3300
96 well plate (Flat-bottom; clear)	Corning	3917
Microscope slide 76mm x 26mm	Fisher Scientific	11572203
12 mm round cover slips	Fisher Scientific	194310012

4.1.2 H9C2 Cell Culturing

4.1.2.1 Growth media

Components	Amount (mL)	Final concentration (%)	Company	Catalogue no.
Fetal bovine serum (FBS)	50	10	PAA	A15-101 lot # A10108-0190
Penicillin-streptomycin solution (10,000 Units / mL : 10,0000 μg / mL)	5	1	GIBCO	15140
DMEM-GlutaMAX™	445		GIBCO	32430

4.1.2.2 1X phosphate buffered saline (PBS)

Components	Amount	Company	Catalogue no.
PBS	1.5 g tablet	GIBCO	18912
H_2O	500 mL		
pH is 7.45			

4.1.3 Primary Culture of Neonatal Rat Cardiac Myocytes

4.1.3.1 Isolation buffer

Components	Mass	Final concentration (mM)	Company	Catalogue no.
NaCl	3.4 g	116	Sigma Aldrich	S7653
KCl	0.2 g	5.4	Sigma Aldrich	P9333
HEPES	2.38 g	20	Sigma Aldrich	H3375
NaH_2PO_4	0.06 g	0.77	Sigma Aldrich	S8282
D-(+)-Glucose	0.5 g	5.5	Sigma Aldrich	G8270
$MgSO_4$	0.05 g	0.4	Sigma Aldrich	M7506
dH_2O	500 mL			
Adjust to pH 7.35 oxygenate and filter sterilize				

4.1.3.2 Digestion buffer

Components	Amount	Final concentration (% w/v)	Company	Catalogue no.
Collagenase type 2	0.1 g	0.1	Worthington	CLS-2
Pancreatin	0.025 g	0.025	Sigma Aldrich	P3292
Isolation buffer	100 mL			
Filter sterilize				

4.1.3.3 Plating media

Components	Amount (mL)	Final concentration (% w/v)	Company	Catalogue no.
FBS	75	15	PAA	A15-101 lot # A10108-0190
Penicillin-streptomycin solution (10,000 Units / mL : 10,0000 μg / mL)	5	1	GIBCO	15140
DMEM-GlutaMAX™	420		GIBCO	32430

4.1.3.4 Maintenance media

Components	Amount (mL)	Final concentration (% w/v)	Company	Catalogue no.
Fetal bovine serum (FBS)	5	1	PAA	A15-101 lot # A10108-0190
Penicillin-streptomycin solution (10,000 Units / mL : 10,0000 μg / mL)	5	1	GIBCO	15140
DMEM-GlutaMAX™	490		GIBCO	32430

4.1.3.5 1% Gelatin

Components	Amount	Company	Catalogue no.
Gelatin	1 g	Sigma Aldrich	48723
1X	PBS 100 mL		
Boil and filter sterilize			

4.1.4 Cell Freezing

4.1.4.1 Freezing media

Components	Amount (mL)	Company	Catalogue no.
Fetal bovine serum (FBS)	8.5	PAA	A15-101 lot # A10108-0190
Dimethyl sulfoxide (DMSO)	1.5	Sigma Aldrich	D8418

4.1.5 Western Blot Analysis

4.1.5.1 5X Radioimmunoprecipitation assay (RIPA) buffer

Components	Stock	Volume (mL)	Final concentration (% w/v)	Company	Catalogue no.
NaCl	5 M	1.5	0.75 M	Sigma Aldrich	S7653
IgePal CA ^{530}	10 %	0.5	0.5 %	Sigma Aldrich	I3021
Sodium deoxycholate (DOC)	10 %	2.5	2.5 %	Sigma Aldrich	D6750
Sodium dodecyl sulfate (SDS)	10 %	0.5	0.5 %	Acros organics	230425000
Tris (pH = 8)	1 M	2.5	0.25	Fisher Scientific	BP152
dH_2O Up to 10 mL					

4.1.5.2 10X running buffer for SDS-PAGE Electrophoresis

Components	Amount	Final concentration (% w/v)	Company	Catalogue no.
Tris base	30.3 g	25 mM	Fisher Scientific	BP152
Glycine	144 g	192 mM	Fisher Scientific	BP381
SDS	10 g	0.01 %	Acros organics	230425000
dH_2O	1L			
pH is 8.3 and does not need to be adjusted				

4.1.5.3 1X running buffer

Components	Amount (mL)	Company	Catalogue no.
10X running buffer	100	Fisher Scientific	BP152
dH_2O	900		

4.1.5.4 1X transfer buffer

Components	Amount (mL)	Company	Catalogue no.
10X running buffer	100	Fisher Scientific	BP152
Methanol	200	Sigma Aldrich	34860
dH_2O	700		

4.1.5.5 10% SDS

Components	Amount	Company	Catalogue no.
SDS	100 g	Acros organics	230425000
dH_2O	1 L		

4.1.5.6 PBS-tween® (PBST)

Components	Amount	Final concentration	Company	Catalogue no.
PBS	2 5 g tablets		GIBCO	18912
Tween® 20	0.5 mL	0.05 % v/v	Sigma Aldrich	P1379
dH_2O	1 L			

4.1.5.7 Ponceau-S Red staining solution

Components	Amount	Final concentration (%)	Company	Catalogue no.
Ponceau-S	1 g	0.1 w/v	Sigma Aldrich	P3504
Glacial acetic acid	50 mL	5 v/v	Sigma Aldrich	320099
dH_2O	1 L			

4.1.5.8 5 % non-fat milk blocking buffer

Components	Amount	Final concentration	Company
Non-fat milk	2.5 g	5 % w/v	Marvel
PBST	50 mL		

4.1.5.9 5 % bovine serum albumin (BSA) blocking buffer

Components	Amount	Final concentration	Company	Catalogue no.
Bovine serum albumin (BSA)	2.5 g	5 % w/v	Fisher scientific	BP1600
PBST	50 mL			

4.1.6 Immunocytochemistry

4.1.6.1 4 % paraformaldehyde

Components	Amount	Final concentration	Company	Catalogue no.
Paraformaldehyde	40 g	4 % w/v	Sigma Aldrich	158127
1X PBS	1L			
pH is 8.3 and does not need to be adjusted				

800 mL of 1X PBS was added to a glass beaker on a stir plate in a ventilated hood. It was heated to approximately 60 °C and 40 g of paraformaldehyde powder was added forming a cloudy solution. The pH was slowly raised by drop-wise addition of 1 M NaOH until the solution cleared. Once the paraformaldehyde had dissolved, the solution was left to cool and the volume of the solution made up to 1 L by addition of 1X PBS. The pH was adjusted to 7.4 with small amounts of dilute HCl before being filtered, aliquoted and frozen or stored at 2-8 °C for up to one month.

4.1.6.2 Permeabilizing buffer

Components	Amount	Final concentration	Company	Catalogue no.
Sucrose	10.3 g	0.3 M	Sigma Aldrich	S7903
NaCl	0.292 g	50 mM	Sigma Aldrich	S7653
$MgCl_2 \cdot 6\,H_2O$	0.06 g	2.95 mM	Sigma Aldrich	M2670
Hepes	0.476 g	20 mM	Sigma Aldrich	H3375
1X PBS	100mL			
Adjust pH to 6.2				
Triton^{TM}X-100	0.5 mL	0.5 % v/v	Sigma Aldrich	T8787

4.1.6.3 Immunofluorescence blocking buffer

Components	Amount	Final concentration	Company	Catalogue no.
BSA	1 g	1 % w/v	Fisher scientific	BP1600
PBST	100 mL			

4.1.7 Induction of Cell Death

4.1.7.1 Esumi buffer

Components	Amount	Final concentration (mM)	Company	Catalogue no.
NaCl	0.8 g	137	Sigma Aldrich	S7653
KCl	0.09 g	12	Sigma Aldrich	P9333
$MgSO_4 \cdot 6\,H_2O$	0.01 g	0.49	Sigma Aldrich	M2670
$CaCl_2$	0.01 g	0.9	Sigma Aldrich	C1016
Hepes	0.095 g	4	Sigma Aldrich	H3375
2-deoxy-D-glucose	0.16 g	10	Sigma Aldrich	D6134
Sodium DL-lactate (60 %)	0.285 mL	20	Sigma Aldrich	L1375
dH_2O	100 mL			
Adjust pH 6.2 and autoclave before use				

4.1.7.2 Esumi control buffer

Components	Amount	Final concentration (mM)	Company	Catalogue no.
NaCl	0.8 g	137	Sigma Aldrich	S7653
KCl	0.03 g	3.8	Sigma Aldrich	P9333
$MgSO_4 \cdot 6\,H_2O$	0.01 g	0.49	Sigma Aldrich	M2670
$CaCl_2$	0.01 g	0.9	Sigma Aldrich	C1016
Hepes	0.095 g	4	Sigma Aldrich	H3375
Glucose	0.18 g	10	Sigma Aldrich	D6134
dH_2O	100 mL			
Adjust pH 7.4 and autoclave before use				

4.2 Methods

4.2.1 Cell Culturing

4.2.1.1 H9C2 Cells

H9C2 cells were a subclone of the original clonal cell line derived from embryonic BD1X rat embryonic ventricular myocardium. H9C2 cells, obtained from American Type Culture Collection (CRL-1446; Manassas, VA), were cultured in growth media (section 4.1.2.1) in a humidified atmosphere of 95% air-5% CO_2 at 37 °C. Prior to being detached from the bottom of the flask cells were washed with 10 mL PBS before incubating them in 5 mL trypsin at 37 °C for three minutes. Cells were resuspended in DMEM then gently pipetted up and down twice to ensure clumps of cells were disrupted, 1 mL of cell suspension was then added to a T75 flask containing 10 mL of supplemented media and returned to the incubator.

Twenty-four hours prior to treatment the cells are detached and split into 10 cm dishes at a density of $5x10^4$ cells/ mL per dish.

4.2.1.2 Preparation of Neonatal Rat Ventricular Cardiac Myocytes

Neonatal rat ventricular cardiac myocytes (NRCM) were isolated from the hearts of 1-3 day old Sprague Dawley rats. Hearts were removed and placed in filter-sterilized oxygenated Isolation buffer. After collecting all the tissue, the hearts were finely minced with iris scissors and enzymatically digested using 10 mL oxygenated digestion buffer for 10 minutes in a humidified incubator at 37 °C. The first supernatant containing digested cells was removed and discarded. Fresh digestion buffer was added to the tissue and incubated for a further ten minutes. The supernatant was removed and the digestion enzymes were neutralised with 100 % FBS. The cells were pelleted at 200 x g for five minutes at room temperature and resuspended in FBS before returning to the humidified

incubator at 37 °C. This digestion procedure was repeated a further nine times until the tissue was completely digested. After collecting the supernatants from each digestion step all the dissociated cells were pooled and pelleted by centrifugation at 200 x g for five minutes at room temperature in a Sorvall Legend RT centrifuge. The myocytes were resuspended in plating media and plated for 1hr at 37 °C to allow adherence of fibroblasts in a T175 culture flask. Myocytes were plated at a density of 1.0 x 10^6 cells /mL in plating media on six-well plates pre-coated for one hour with 1 % gelatine. Cells were allowed to attach overnight and the media was replaced with maintenance media. Typical cultures assessed by desmin staining yield >95% cardiac myocytes.

4.2.2 Cell Freezing

Cells were prepared for freezing in liquid nitrogen by washing a T75 flask with 10 mL PBS twice, then 5 mL trypsin-EDTA was added to the flask and incubated for five minutes at 37 °C. 10 mL of growth media was added to inactivate the trypsin when cells became detached from the bottom of the flask. The suspension was transferred to 15 mL falcon tube and cells were pelleted by centrifugation for five minutes at 260 x g, 4 °C in a Sorvall Legend RT centrifuge. The supernatant was removed and the pellet was resuspended in 10 mL freezing solution containing 8.5 mL FBS and 1.5 mL DMSO. This was then aliquoted into 2 mL Cryotubes and incubated at -80 °C for twenty four hours in a NalgeneTM Cryo 1 Freezing Container containing 250 mL Isopropanol, which chills the contents at a rate of 1 °C per minute, before being transferred to liquid nitrogen for storage.

4.2.3 Cell Counting

Cells were washed with PBS and detached as described above in section 4.2.2. 20 μL of resuspended cells were introduced to the counting chambers using a pipet and the area under the coverslip was allowed to fill by capillary action. The haemocytometer was placed under the 10X magnification lens of an Zeiss Axiovert 40C light microscope

and the number of cells localized in one large square (a cluster of 16 small squares) were counted, this was repeated four times in total and the average was calculated. The number of cells per mL was calculated using this equation:

Average number of cells per large square x $1x10^4$ = number of cells per mL

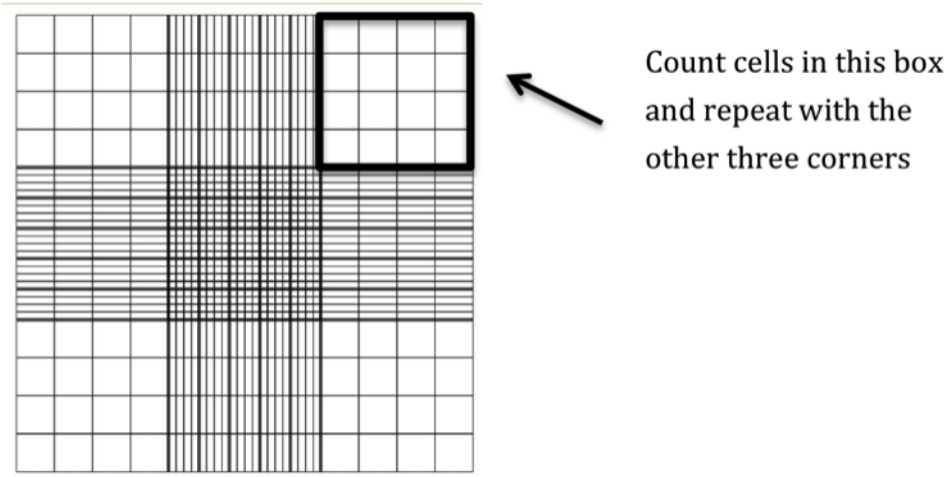

Figure 4.1 Diagram of a haemocytometer showing the grids. Cells localized in the four large squares are counted and the average is taken.

4.2.4 Western Blot Analysis

4.2.4.1 Harvesting and Lysing Cells

Total cell lysates were prepared by detaching cells from culture flasks or plates as described in section 4.2.1.1 and washed twice in 1 mL PBS then spun at 260 x g for five minutes at 4°C in a Sorvall Legend RT centrifuge. The PBS was removed and the cell pellet was incubated with an appropriate volume of RIPA lysis buffer (approximately 25 μl per $1x10^6$ cells) on ice for thirty minutes. To ensure complete lysis had occurred, cells samples were sonicated for ten seconds and cell debris was pelleted by centrifugation using an ALC® Multispeed refrigerated centrifuge (PK131R) at 16000 x g for five minutes at 4°C.

4.2.4.2 Protein Quantification

The protein concentration of cell lysates was determined using the Pierce® BCA (Bicinchoninic acid assay) Protein Assay kit according to the manufacturer's instructions. The absorbance of the lysate was determined at a wavelength of 562 nm using a Thermo Fisher Varioskan flash multimode plate reader. BSA was used to obtain a standard curve and the equation generated was a correlation between absorbance and concentration, where the relationship was linear. This equation was used to determine the total amount of protein in the cell lysates from the absorbance at 562 nm.

4.2.4.3 Protein Separation by SDS-Polyacrylamide Gel Electrophoresis

40 μg of protein from cell lysates was prepared by diluting with red loading buffer (7723S; Cell Signaling; 3X) and dithiothreitol (DTT) (B7709S; New England Biolabs; 30X). Samples were boiled at 95 °C for five minutes to ensure denaturation and reduction of the protein then spun for one minute at 16000 x g in a Sorvall Legend RT centrifuge to pellet any debris. Protein samples were separated by 8 % SDS-PAGE which was prepared as described in the table below:

Table 4.1 Solutions for preparing resolving and stacking gels for one gel mould of 8 % Tris-glycine SDS-polyacrylamide gel electrophoresis.

Resolving gel		**Stacking gel**	
Solution components	*Volume (mL)*	*Solution components*	*Volume (mL)*
dH_2O	4.6	dH_2O	1.4
30 % acrylamide mix	2.7	30 % acrylamide mix	0.33
1.5M Tris (pH 8.8)	2.5	1.0 M Tris (pH 6.8)	0.25
10 % SDS	0.1	10 % SDS	0.02
10 % ammonium persulfate	0.1	10 % ammonium persulfate	0.02
Tetramethylethylenediamine (TEMED)	0.006	TEMED	0.002

The resolving gel solution was poured between 1.5 mm glass plates with a pipette leaving about a 1/4 of free space for the stacking gel. The top was covered was isopropanol and

the gel was allowed to polymerise for approximately thirty minutes. The isopropanol was discarded and washed gently with distilled water. The stacking gel was poured carefully over the resolving gel carefully with a pipette minimising bubble formation and an appropriate-sized comb was inserted. The gel was allowed to polymerise and set for approximately thirty minutes. The comb was carefully removed and the gel was placed in a mini protean® 3 tetra system gel tank containing 1X running buffer (section 4.1.5.3). Protein samples were loaded alongside a protein marker and run for forty minutes at 200 volts. The gel was then removed from the plastic frame for western blotting.

4.2.4.4 Western Blotting

Proteins were separated by SDS-PAGE as described above and removed from the glass plates. Transfer was carried out to immobilise proteins on an Immobilon®-FL polyvinyl difluoride (PVDF) transfer membrane (IPFL 00010; Millipore) for immunodetection using a wet assembly method (i.e. completely submerged in transfer buffer). The PVDF membrane was cut to the appropriate size and activated by soaking in methanol for two minutes and then soaked in transfer buffer along with two pieces of mini trans-blot® filter paper (1703932; Bio-Rad) and two sponges for at least one minute. The cassette was placed in a container of transfer buffer to minimise air bubbles and assembled as described in figure Figure 4.2 below:

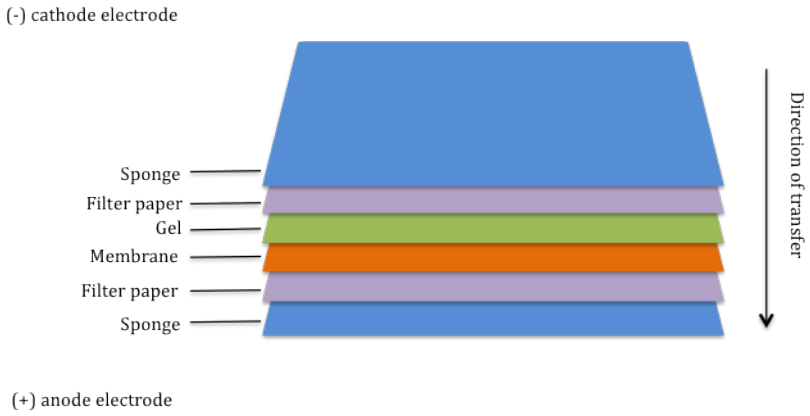

Figure 4.2 Transfer assembly for wet transfer in the transfer of proteins from SDS-PAGE gel onto a PVDF membrane.

The transfer was carried out in a Trans-Blot® Electrophoretic Transfer Cell (Bio-Rad) for ninety minutes at 75 volts with an ice block in the tank to prevent overheating. To check the success of the transfer, the membrane was incubated in Ponceau-S stain.

4.2.4.5 Ponceau-S Red Staining

The PVDF membrane was incubated in methanol for one minute followed by a one-minute incubation in Ponceau-S at room temperature with agitation. The membrane was then rinsed with deionized water to remove background staining but bands remained visible. The membrane was rinsed further with deionized water to remove the stain completely.

4.2.4.6 Immunodetection

The membrane was incubated in 20 mL BSA blocking buffer for one hour at room temperature with agitation to prevent any non-specific binding that may cause high background at the detection stage. Incubation with primary antibody was then carried out overnight at 4 °C with agitation for optimum detection of the protein. The dilutions at which primary antibodies were used in blocking buffer are listed in Table 4.2 below.

Anti-β actin antibody was used to show equal loading of the protein in the Western blot analyses.

Table 4.2 Primary antibodies and the dilutions used for immunodetection in western blot analysis.

Antibody	Species	Dilution	Company	Catalogue no.
β-Actin	Mouse	1:5000	Sigma Aldrich	A3854
STAT 1 p84/p91(E-23)	Rabbit	1:1000	Santa-Cruz	sc-346
Phospho-STAT 1 Y701	Mouse	1:1000	Invitrogen/Zymed	333400
Phospho-STAT 1 S727	Rabbit	1:1000	Millipore/Upstate	07-714
p44/42 MAP kinase	Rabbit	1:1000	Cell signaling	9101
phospho p44/42 MAP kinase	Rabbit	1:2000	Cell signaling	9102
NF-κB p65	Rabbit	1:2000	Cell signaling	4764
Phospho-NF-κB p65 (Ser536)	Rabbit	1:1000	Cell signaling	3033

Following overnight incubation with primary antibody the membrane was washed three times with PBST for five minutes each to remove traces of primary antibody and minimise background detection. Fluorescently-labeled secondary antibodies were selected against the animal in which the primary antibody was generated. The membrane was incubated with secondary antibody for one hour with agitation and protection from light at room temperature at the dilution shown in Table 4.3 :

Table 4.3 Secondary antibodies and the dilutions used for immunodetection in western blot analysis. All antibodies were made up in blocking buffer

Secondary antibody	Dilution	Licor® catalogue no.
IRDye 800CW Goat anti-Rabbit IgG (H + L)	1:25,000 (0.01% SDS)	926-32211
IRDye 680RD Goat anti-Rabbit IgG (H + L)	1:40,000 (0.02% SDS)	926-68071
IRDye 800CW Goat anti-Mouse IgG (H + L)	1:15,000 (0.01% SDS)	926-32210
IRDye 680RD Goat anti-Mouse IgG (H + L)	1:15,000 (0.01% SDS)	926-68070
IRDye 800CW Rabbit anti-HRP	1:5,000 (0.01% SDS)	926-32236

Following incubation with secondary antibody the membrane was washed another three times in PBS-tween for five minutes each and a final five minutes wash in PBS to remove

residual Tween® 20. After washing, the membrane was scanned using a Licor Odyssey® SA and the images analysed using Odyssey® Family of Imagers.

4.2.5 Immunocytochemistry

H9C2 cells and NRCMs were plated on cover slips coated in 1% gelatin in PBS. The media was removed, cover slips rinsed in PBS twice and fixed with 4 % paraformaldehyde for ten minutes at 4 °C. After incubation, 4 % paraformaldehyde was discarded and cover slips rinsed with PBS four times. The cells were covered with permeabilizing buffer for five minutes at room temperature. The cells were then washed with PBS once before being incubated with immunofluorescence blocking buffer for a further five minutes at room temperature. Cells were incubated and agitated with primary antibody overnight at 4°C using dilutions described in Table 4.4 below.

Table 4.4 Primary antibodies and the dilutions used for immunoflourescence. All antibodies were made up in immunofluorescence blocking buffer

Antibody	Species	Dilution	Company	Catalogue no.
STAT 1 p84/p91(E-23)	Rabbit	1:200	Santa-Cruz	sc-346
Anti-desmin	Rabbit	1:30	Abcam	ab8592
Monoclonal anti-vimentin conjugated directly to Cy3	Mouse	1:200	Sigma Aldrich	V6630
Anti-heavy chain cardiac myosin	Mouse	1:2500	Abcam	ab50967

After overnight incubation the primary antibody solution was removed and cells were rinsed with 2 mL PBST three times for five minutes each at 4°C with agitation. Secondary antibody was applied at dilutions in the table below for one hour at 4°C with agitation at dilutions shown in Table 4.5.

Table 4.5 Secondary antibodies and the dilutions used for immunoflourescence. All antibodies were made up in immunofluorescence blocking buffer

Antibody	Species	Dilution	Company	Catalogue no.
IgG-FITC	Rabbit	1:100	Sigma Aldrich	F9887
Alexa flour 594	Mouse	1:100	Invitrogen	A-11005

Secondary antibodies were removed and the cells were rinsed with 2 mL PBST three times at five minutes at 4 °C with agitation. Cells were mounted onto microscope slides with 20 μl VECTASHIELD® Mounting Medium containing DAPI (H-1200; Vector Lab), which stained the nucleus blue. Coverslips were permanently sealed around the perimeter with clear nail polish and left to dry for ten minutes. For co-localisation experiments, combinations of secondary antibodies with a low degree of spectral overlap were used. Cells were imaged using a Zeiss LSM 510 Meta confocal microscope.

4.2.6 Cell Treatment and Induction of Cell Death

4.2.6.1 H_2O_2 treatment

To induce oxidative stress conditions appropriate concentrations of H_2O_2 (216763; Sigma Aldrich) were freshly prepared in deionized water and added directly to the growth media for the indicated time periods. Control cells were left untreated or incubated with appropriate volumes of PBS. When drugs were used, they were prepared immediately before use and dissolved in PBS then added to the growth media at designated times prior to oxidative stress induction by H_2O_2. Cell death was measured using the methods described in the next section.

4.2.6.2 Simulated I/R injury

Simulated ischaemia was performed using a modular incubator chamber (MC-101; Billups-Rothenberg) supplied with 5% CO2, 95% argon and maintained at 37 °C. Cells were washed twice with PBS and incubated with 1 mL Esumi ischaemia buffer during ischaemia. Cells were removed from the chamber and washed twice with PBS. Reperfusion was simulated by replacing ischaemia buffer with maintenance media for nrcms or growth media for H9C2 cells and incubated in normoxic conditions (5 % CO_2, 95 % air in humidified chamber). Control cells were washed twice with PBS and incubated in control Esumi buffer in normal conditions. After ischaemia, the control buffer was removed and

replaced with maintenance media for nrcms or growth media for H9C2 cells and incubated in normoxic conditions. When drugs were used, they were prepared immediately before use then dissolved in PBS and added to the growth media at designated times prior to I/R injury.

4.2.7 Measurement of Cell Death

4.2.7.1 CellTiter-Glo® luminescent cell viability assay

The CellTiter-Glo® assay kit was performed according to the manufacturer's instructions. (G7570; Promega). Briefly, 5000 cells/well in 200 μL of growth media were seeded onto white flat bottom 96 well plates. After 24 h treatment with drugs the media was replaced with 100 μL of fresh growth media. The plates and its contents were allowed to equilibrate at room temperature for 30 minutes. Equal volume of CellTiter-Glo® reagent was added to each well and mixed on an orbital shaker for 2 minutes to induce cell lysis. The plate was incubated at room temperature for 10 minutes to stabilise luminescent signal and the luminescence was measured using a Thermo Fisher Varioskan flash multimode plate reader. Data analysis was done using Prism software to plot a dose-response curve and calculate the EC_{50} of each compounds.

4.2.7.2 CyQUANT® assay

The Cyqunat assay kit used CyQUANT® Cell proliferation assay (C-7026; Life Technologies). The assay was performed according to the manufacturer's instructions. Briefly, 5000 cells/well in 200 μL of growth media was seeded onto clear flat bottom 96 well plates. After 24 h treatment with drugs the media was removed by gently inverting onto tissue paper. The wells were washed once with PBS and blotted onto tissue paper to remove excess PBS. The cells were lysed by freezing the microplate overnight at - 80 °C. The plate was thawed out at room temperature before 200 μL of the CyQUANT® GR dye/cell-lysis buffer prepared in Table 4.6 was added. The plate was incubated for three

minutes at room temperature, protected from light and fluorescence was measured using a Thermo Fisher Varioskan flash multimode plate reader set at 480 nm excitation and 520nm emission. Data analysis was done using Prism software to plot a dose-response curve and calculate the EC_{50} of each compounds.

Table 4.6 Preparation 20 mL of CyQUANT® working solution enough for approximately 100 assays

Components	Volume
400X CyQUANT GR dye (Component A)	50 μL
20X Cell-lysis buffer (Component B)	1 mL
dH_2O	18.950 mL

4.2.7.3 Trypan Blue exclusion

Total cell death was determined by counting the number of cells unable to exclude Trypan blue. The cells were harvested as previously described in section 4.2.3 and resuspended in 1 mL PBS. 1 mL of cell suspension was combined with equal volume of 0.4 % Trypan Blue (T8154; Sigma Aldrich) and incubated for three minutes at room temperature. The number of non-viable (stained) cells were counted using a haemocytometer and expressed as a percentage of total cells counted. To obtain the total number of non-viable cells per mL of sample, the total number of non-viable cells was multiplied by 2 (the dilution factor for Trypan Blue) and the same was done to determine the total number of cells per mL of sample. The calculation of the percentage of non-viable cells is as follows:

$$\text{Non-viable cells (\%)} = \frac{\text{Total number of non-viable cells}}{\text{Total number of cells per mL of sample}} \times 100$$

Chapter 5

Experimental

5.1 General Procedure

NMR Spectra: Nuclear magnetic resonance spectra were recorded on Bruker AV300 FT-NMR spectrometer (at 300 and 75 MHz) or Bruker AV300 FT-NMR spectrometer (at 400 and 100 MHz) spectra at 298 K unless otherwise stated in $CDCl_3$ with chloroform (7.27 ppm ^{1}H, 77.0 ppm ^{13}C); $(CD_3)_2CO$ with acetone (2.09 ppm $_1$H; 30.6 and 206.7 ppm ^{13}C); $(CD_3)_2SO$ with DMSO (2.50 ppm ^{1}H, 39.5 ppm ^{13}C); or MeOD with methanol (3.30 and 4.78 ppm ^{1}H, 49.2 ppm ^{13}C) as an internal reference. Chemical shifts are quoted in parts per million downfield of tetramethylsilane with residual solvent as the internal standard. Assignments are made on the basis of chemical shifts, coupling constants, DEPT-135, and comparison with spectra of related compounds. Multiplets are indicated as *s* (singlet), *d* (doublet), *t* (triplet), *q* (quartet), *m* (multiplet), and *br* (broad); coupling constants, *J*, are reported as *Hz* and rounded to the nearest 0.1 Hz.

Infrared Spectra: Infrared spectra were recorded as a liquid or solid compression using ATR/golden gate method. Absorption maxima (ν_{max}) are described as s (strong), m (medium), w (weak) and br (broad) and are quoted in wavenumbers (cm^{-1}).

Mass Spectra: ESI spectra as recorded on a Single quadruple MS HP1050 mass spectrometer measuring mono-isotopic masses (mode: ESI^+ or ESI^-). m/z values were reported with their percentage abundance relative to the most intense signal and the relevant fragment ion in parenthesis. High resolution mass spectra were recorded by Dr. John Langley and Ms. Julie Herniman at the University of Southampton and are calculated to four decimal places from the molecular formula.

Chromatography Techniques: Thin-layer chromatography was carried out on Merck DC-Alufolien 60 F_{254} 0.2 mm aluminum-backed plates with a fluorescence indicator ($\lambda = 254$ nm). Visualization of TLC plates were carried out by UV light, then by either potassium permanganate (5% $KMnO_4$ in 5% aqueous NaOH) or cerium sulphate/ammonium molybdate stain with heat. Flash column chromatography was performed with 35-70 μm silica gel (Sigma Aldrich) with given solvent systems.

High-Performance Liquid Chromatography Purification: Analytical purification carried out with Waters 1525 binary HPLC pump using Atlantis T3 5 μm (6x10 mm) column (mobile phase A: 55% H_2O with 0.1% TFA; mobile phase B: 45% acetonitrile with 0.1% TFA, 1 mL/min over twenty minutes). Detection with a Waters 2998 photodiode array detector at 220 nm and 280 nm unless otherwise stated. Large-scale purification carried out using Atlantis T3 OBD 5 μm (19x100 mm) column (mobile phase A: 55% H2O with 0.1% TFA; mobile phase B: 45% acetonitrile with 0.1% TFA, 17 mL/min over twenty minutes; Detection at 220 nm and 280 nm) unless otherwise stated.

Chiral High-Performance Liquid Chromatography: Chiral HPLC was carried out using a Chiralpak^{TM} IA 5 μm (4.6x250 mm) using a Perkin Elmer Flexar LC pump, solvent manager and UV/VIS detector.

Solvents and Reagents: Commercially available reagents were purchased and used without further purification. THF was freshly distilled and dried over a purple solution of sodium and benzophenone immediately prior to use. Anhydrous *N*, *N*-Dimethylformamide (DMF) was dried over activated 4 Å molecular sieves. All reactions, which were air and/or moisture sensitive, were run under inert atmosphere of argon using oven-dried glassware.

5.1.1 Phloroglucinol triacetate (54)

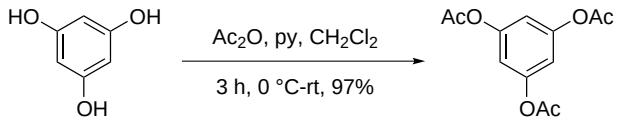

5

$C_6H_6O_3$
(126.03)

54

$C_{12}H_{12}O_6$
(252.06)

To a mixture of phloroglucinol **5** (11 g, 0.087 mol), pyridine (16 mL), and CH_2Cl_2 (160 mL), Ac_2O (28.86 mL, 0.305 mol) was added dropwise at 0 °C. The mixture was stirred for 30 min, allowed to warm up to room temperature and stirred for a further 3 h. The mixture was cooled to 0 °C and washed with 10% aqueous HCl (100 mL) and extracted with EtOAc (3 x 100 mL). The organic layers were combined and washed with brine (50 mL), and dried over anhydrous $MgSO_4$. The solvent was removed *in vacuo* to give **54** (21.4 g, 97%) as a white solid. These data are in accordance with those reported in the literature.[244]

^{1}H NMR	(300 MHz, $CDCl_3$) δ_H ppm 6.82 (s, 3H, ArH), 2.23 (s, 9H, COCH_3).
^{13}C NMR	(75 MHz, $CDCl_3$) δ_C ppm 168.34 (CO), 150.90 (C), 112.56 (CH), 20.75 (CH$_3$).
LRMS (m/z, ESI$^+$)	527.0 [2M+Na]$^+$(11.08%), 316.0 [M+Na+MeCN]$^+$(32.15%), 292.1 [M + k]$^+$ (100%).

5.1.2 1,3,5-*tris*-(benzyloxy)benzene (55)

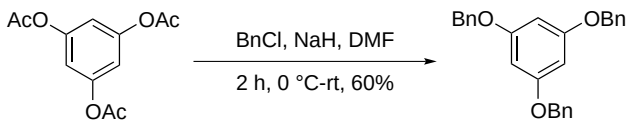

54

$C_{12}H_{12}O_6$
(252.06)

55

$C_{27}H_{24}O_3$
(396.17)

To a mixture of Phloroglucinol triacetate, **54** (25 g, 0.099 mol), benzyl chloride (41.06 mL, 0.357 mol), NaH (60% dispersed in mineral oil, 28.6 g, 0.714 mol) and 200 mL DMF, Water (5.36 mL, 0.297 mol) was added at 0 °C drop-wise over 30 min. After stirring at room temperature for 2 h, TLC showed no starting material. Reaction mixture was diluted with Et_2O and washed with water and brine. The organic layer was dried over anhydrous $MgSO_4$ and concentrated *in vacuo* to yield a yellow oil. Crystallization from MeOH yielded **55** (23.4 g, 60%) as a white solid. These data are in accordance with those reported in the literature.[260]

^{1}H NMR	(300 MHz, $CDCl_3$) δ_H ppm 7.46-7.28 (m, 15H, ArH), 6.30 (s, 3H, ArH), 5.08 (s, 6H, CH_3).
^{13}C NMR	(75 MHz, $CDCl_3$) δ_C ppm 160.7 (C), 136.8 (C), 128.6 (CH), 128.0 (CH), 127.59 (CH), 94.9 (CH), 70.1 (CH$_2$).
LRMS (m/z, ESI$^+$)	815.6 $[2M+Na]^+$ (8.17%), 419.2 $[M+Na]^+$ (100%).

5.1.3 3,5-*bis*-(benzyloxy)phenol (8b)

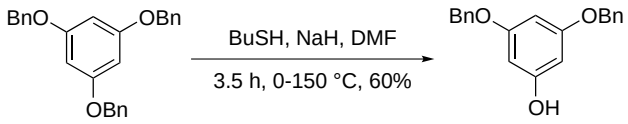

55 **8b**

$C_{27}H_{24}O_3$ (396.17) $C_{20}H_{18}O_3$ (306.13)

Under argon, butanethiol (9.75 mL, 0.091 mol) was added dropwise to a stirred suspension of sodium hydride (60% dispersion in mineral oil, 1.69 g, 0.042 mol) in dry DMF (120 mL) at 0 °C. After 1h, 1,3,5-*tris*-(benzyloxy)benzene, **55** (10 g, 0.025 mol) was added in 10 batches and the mixture was heated to 150 °C for 2.5 h. After the reaction was cooled, water (500 mL) was added and the mixture was extracted with EtOAc (4x80 mL). The combined organic layers were dried with anhydrous $MgSO_4$ and concentrated *in vacuo*. Purification by column chromatography (SiO_2, hexane/EtOAc, 100:0 to 90:10) gave the product **8b** (4.58 g, 60%) as white solid. These data are in accordance with those reported in the literature.[260]

^{1}H NMR	(300 MHz, $CDCl_3$) δ_H ppm 7.45-7.27 (m, 10H, Ar*H*), 6.26 (t, J=2.2 Hz, 1H, Ar*H*), 6.12 (d, J=2.2 Hz, 2H, Ar*H*), 5.01 (s, 4H, CH_2), 4.77 (s, 1H, O*H*).
^{13}C NMR	(75 MHz, $CDCl_3$) δ_C ppm 160.8 (*C*), 157.3 (*C*), 136.8 (*C*), 128.6 (*C*H), 128.0 (*C*H), 127.5 (*C*H), 95.4 (*C*H), 94.9 (*C*H), 70.1 (*C*H_2).
LRMS (m/z, ESI$^+$)	635.4 $[2M+Na]^+$ (100%), 370.2 $[M+Na+MeCN]^+$ (55.08%), 329.2 $[M+Na]^+$ (50.70%).

5.1.4 Methyl 3,4,5-*tris*-(benzyloxy)benzoate (47)

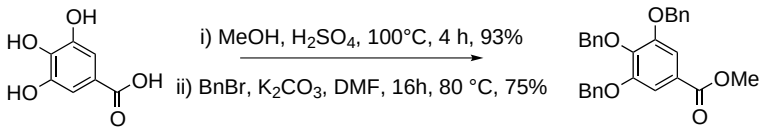

35 $C_7H_6O_5$ (170.02)

47 $C_{29}H_{26}O_5$ (454.18)

A mixture of 3,4,5-trihydroxybenzoic acid **35** (12.2 g, 0.0388 mol), MeOH (80 mL), H_2SO_4 (8 mL) was heated to reflux 100 °C for 4 h. After allowing to cool to room temperature, excess MeOH was removed by rotary evaporator. The resulting residue was dissolved in H_2O and the product extracted with EtOAc (3x100 mL). The organic layer was washed with brine and dried over anhydrous MgSO4. The solvent was removed *in vacuo* to give the ester as an off-white solid (13.4 g, 93%). The ester (13.4 g, 0.073 mol) was mixed with K_2CO_3 (60.4 g, 0.437 mol) in DMF (230 mL). 51.9 mL (0.437 mol) of BnBr was added dropwise and the reaction mixture was set to reflux at 80 °C overnight. After completion 230 mL of water was added and the product extracted with CH_2Cl_2 (3x100 mL). The organic layer was washed with brine, dried over anhydrous $MgSO_4$ and concentrated *in vacuo*. Purification by column chromatography (SiO_2, hexane/EtOAc 90:10) gave the product methyl 3,4,5-*tris*-(benzyloxy)benzoate, **47** (24.8 g, 75%) as a white fluffy solid. These data are in accordance with those reported in the literature.[232]

^{1}H NMR	(300 MHz, $CDCl_3$) δ_H ppm 7.49-7.25 (m, 17H, ArH), 5.16 (s, 4H, CH_2), 5.15 (s, 2H, CH_2), 3.91 (s, 3H,CH_3).
^{13}C NMR	(75 MHz, $CDCl_3$) δ_C ppm 166.6 (CO), 152.6 (C), 142.4 (C), 136.7 (C), 137.4 (C),128.5 (CH), 128.2 (CH), 128.0 (CH), 127.9 (CH), 127.5 (CH), 128.1 (CH), 125.2 (C), 109.1 (CH), 75.1 (CH_2), 71.2(CH_2), 52.2 (CH$_3$).
LRMS (m/z, ESI$^+$)	477.2 [M+Na]$^+$ (100%), 472.3 [M+K]$^+$ (24.75%).

5.1.5 Methyl 3,4-*bis*-(benzyloxy)benzoate (71)

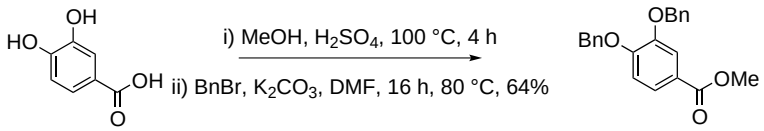

69
$C_7H_6O_4$
(154.03)

71
$C_{22}H_{20}O_4$
(348.14)

Following the procedure for the preparation of **47**, but with 3,4,-trihydroxybenzoic acid **69** (20 g, 0.1298 mol) as starting material, **71** was obtained as a white solid with a 64% yield. These data are in accordance with those reported in the literature.[244261]

^{1}H NMR (300 MHz, $CDCl_3$) δ_H ppm 7.64-7.47 (m, 2H, ArH), 7.41-7.17 (m, 10H, ArH), 6.85 (d, J=8.1 Hz, 1H, ArH), 5.13 (s, 2H, CH_2), 5.11 (s, 2H, CH_2), 3.79 (s, 3H, CH_3).

^{13}C NMR (75 MHz, $CDCl_3$) δ_C ppm 166.8 (CO), 152.9 (C), 148.3 (C), 136.8 (C), 136.6 (C), 128.6 (CH), 128.5 (CH), 128.0 (CH), 127.9 (CH), 127.4 (CH), 127.1 (CH), 124.0 (CH), 123.1 (C), 115.5 (CH), 113.2 (CH), 71.2 (CH_2), 70.8(CH_2), 52.0 (CH$_3$).

LRMS (m/z, ESI$^+$) 371.2 [M+Na]$^+$ (15.50%).

5.1.6 3,4,5-*tris*-(benzyloxy)benzaldehyde (35)

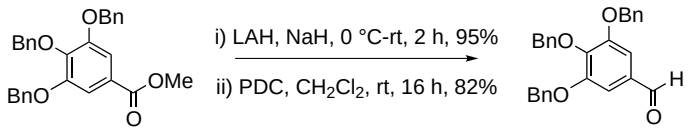

47
$C_{29}H_{26}O_5$
(454.18)

35
$C_{28}H_{24}O_4$
(424.17)

Methyl 3,4,5-*tris*-(benzyloxy)benzoate, **47** (19.3 g, 0.425 mol) was dissolved in THF (140

mL) under argon atmosphere and cooled to 0 °C. $LiAlH_4$ (3.22 g, 0.849 mol) was added in batches to the reaction mixture and stirred for 2 h at room temperature until completion. 140 mL of hexane was added followed by dropwise addition of a saturated solution of NH_4HF_2 (7 mL) and stirred at room temperature for 1 h. The mixture was filtered and washed with EtOAc, dried over $MgSO_4$ and concentrated *in vacuo* to give the benzyl alcohol (17.2 g, 95%). Under argon, the benzyl alcohol was stirred with 4 Å molecular sieves in CH_2Cl_2 at room temperature. PDC (30.36 g, 0.807 mol) was added and the reaction mixture was stirred at room temperature overnight. When TLC showed no starting material present, the reaction was quenched with Et_2O and filtered through a layer of silica gel. The solid was thoroughly washed with Et_2O (200 mL) and the solvent was evaporated to yield the 3,4,5-*tris*-(benzyloxy)benzaldehyde, **35** (14 g, 82%) as a white solid. These data are in accordance with those reported in the literature.[262]

^{1}H NMR	(300 MHz, $CDCl_3$) δ_H ppm 9.73 (s, 1H, COH), 7.40-7.15 (m, 15H, ArH), 7.11 (s, 2H, ArH), 5.09 (s, 4H, CH_2), 5.04 (s, 2H, CH_2).
^{13}C NMR	(75 MHz, $CDCl_3$) δ_C ppm 191.0 (CHO), 153.2 (C), 137.2 (C), 136.4 (C), 131.8 (C), 128.6 (CH), 128.5 (CH), 128.2 (CH), 128.1 (CH), 127.5 (CH), 108.9 (CH), 106.4 (CH), 75.2 (CH_2), 71.3(CH_3).
LRMS (m/z, ESI$^+$)	875.5 $[2M+Na]^+$ (11.25%), 449.2 $[M+Na]^+$ (100%).

5.1.7 3,4-*tris*-(benzyloxy)benzaldehyde (72)

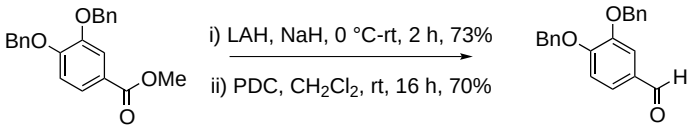

71

$C_{22}H_{20}O_4$
(348.14)

72

$C_{21}H_{18}O_3$
(318.13)

Following the procedure for the preparation of **35**, but with **71** (20 g, 0.057 mol) as starting material, **72** was obtained with a 70% yield as a yellow oil. The proton NMR is in accordance with those reported in the literature.[236]

^{1}H NMR (300 MHz, $CDCl_3$) δ_H ppm 9.82 (s, 1H, COH), 7.51-7.27 (m, 12H, ArH), 7.04 (d, J=8.3 Hz, 1H, ArH), 5.27 (s, 2H, CH_2), 5.23 (s, 2H, CH_2).

^{13}C NMR (75 MHz, $CDCl_3$) δ_C ppm 192.1(CHO), 160.8 (C), 159.3 (C), 137.8 (C), 136.3 (C), 130.1 (C), 128.7 (CH), 128.5 (CH), 128.4 (CH), 128.2 (CH), 127.6 (CH), 127.0 (CH), 123.7 (CH), 122.2 (CH), 113.3 (CH), 70.2 (CH$_2$).

LRMS (m/z, ESI$^+$) 319.2 $[M+H]^+$ (62.12%), 341.2 $[M+Na]^+$ (11.32%).

5.1.8 (*E*)-ethyl 3-(3,4,5-*tris*-(benzyloxy)phenyl)acrylate (65)

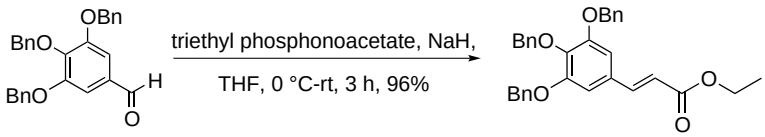

35

$C_{28}H_{24}O_4$
(424.17)

65

$C_{32}H_{30}O_5$
(494.21)

3,4,5-*tris*-(benzyloxy)benzaldehyde, **35** (14 g, 0.033 mol) was dissolved in THF (120 mL)

and triethyl phoshphonoactate (13.1 mL, 0.66 mol) was added. The reaction mixture was cooled to 0 °C and NaH (60% dispersion in mineral oil, 1.98 g, 0.50 mol) was added in batches. The reaction was allowed to warm up to room temprature and stirred for 3 h after which 50 mL saturated $NaHCO_3$. The organic layer was separated and the aqueous layer was extracted with EtOAc (4x60 mL). The organic layers were combined, dried with anhydrous $MgSO_4$, filtered and concentrated *in vacuo* to afford a solid. The solid was thoroughly washed with hexane to remove any excess mineral oil and triethyl phoshphonoactate to give title compound, **65** (15.6 g, 96%). These data are in accordance with those reported in the literature.[232]

^{1}H NMR	(300 MHz, $CDCl_3$) δ_H ppm 7.48 (d, J=15.7 Hz, 1H, COCH=CH), 7.38-7.18 (m, 15H, ArH), 6.76 (s, 2H, ArH), 6.21 (d, J=15.7 Hz, 1H, COCH=CH), 5.06 (s, 4H, CH_2), 5.04 (s, 2H, CH_2), 4.20 (q, J=7.3 Hz, 2H, COOCH_2), 1.27 (t, J=7.1 Hz, 3H, CH_2CH_3).
^{13}C NMR	(75 MHz, $CDCl_3$) δ_C ppm 167.0 (C), 153.0 (C), 144.5 (CH), 137.6 (C), 136.7 (C), 130.0 (CH), 128.6 (CH), 128.2 (CH), 128.0 (CH), 127.9 (CH), 127.4 (C), 117.5 (CH), 107.8 (CH), 75.3 (CH_2) 71.3 (CH_2), 60.5 (CH_2), 14.3 (CH_3).
LRMS (m/z, ESI$^+$)	1011.7 $[2M+Na]^+$ (24.75%), 517.3 $[M+Na]^+$ (100%), 495.3 $[M+H]^+$ (88.52%).

5.1.9 (*E*)-ethyl 3-(3,4-*tris*-(benzyloxy)phenyl)acrylate (73)

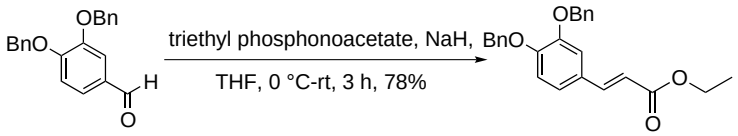

72

$C_{21}H_{18}O_3$
(318.13)

73

$C_{25}H_{24}O_4$
(388.17)

Following the procedure for the preparation of **65** but with **72** (7.2 g, 0.023 mol) as starting material, **73** was obtained with a 78% yield as an orange residue. These data are in accordance with those reported in the literature.[263]

^{1}H NMR (300 MHz, $CDCl_3$) δ_H ppm 7.59 (d, J=16.1 Hz, 1H, C*H*), 7.49-7.38 (m, 10H, Ar*H*), 7.16-7.12 (m, 1H, Ar*H*), 7.11-7.05 (m, 1H, Ar*H*), 6.93 (d, J = 8.4 Hz, 1H, Ar*H*), 6.26 (d, J =16.1 Hz, 1H, COCH=C*H*), 5.20 (s, 2H, CH_2), 5.19 (s, 2H, CH_3CH_2, 4.32-4.13 (m, 2H, CH_2CH_3), 1.46-1.13 (m, 3H, CH_2CH_3).

^{13}C NMR (100 MHz, $CDCl_3$) δ_C ppm 167.2 (*C*O), 151.0 (**C**), 148.9 (*C*), 144.3 (*C*), 136.9 (*C*), 136.8 (*C*), 128.6 (*C*H), 127.9 (*C*H), 127.3 (*C*H), 127.2 (*C*H), 122.8 (*C*H), 116.2(*C*H), 114.3 (*C*H), 113.7 (*C*H), 71.3 (CH_2), 70.9(CH_2), 62.8 (CH_2), 62.7 (CH_2), 62.6 (CH_2), 60.4 (CH_2), 14.3 (CH_3), 14.1 (CH_3).

LRMS (m/z, ESI$^+$) 799.5 $[2M+Na]^+$ (1.50%), 411.2 $[M+Na]^+$ (2.97%).

5.1.10 (*E*)-3-(3,4,5-*tris*-(benzyloxy)phenyl)prop-2-en-1-ol (9b)

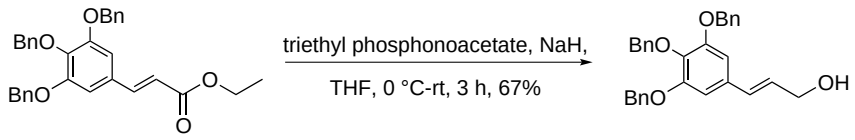

65

$C_{32}H_{30}O_5$
(494.21)

9b

$C_{30}H_{28}O_4$
(452.20)

To a solution of **65** (9.16 g, 0.019 mol) in dry THF (100 mL) at -78 °C under argon, DIBAL (1M in toluene, 55.56 mL, 0.056 mol) was added dropwise. The mixture was stirred at -78 °C for 16 h. The reaction was quenched at -20 °C with methanol warmed to 0 °C and saturated aqueous Rochelle salt solution was added and stirred at room temperature for 1 h. The reaction mixture was extracted with EtOAc (3x75 mL), washed with brine, dried over anhydrous $MgSO_4$ and concentrated *in vacuo* to give the title compound, **9b** (5.9 g, 67%). These data are in accordance with those reported in the literature.[232]

^{1}H NMR	(300 MHz, $CDCl_3$) δ_H ppm 7.40-7.19 (m, 15H, Ar*H*), 6.63 (s, 2H, Ar*H*), 6.43 (d, J=16.2 Hz, 1H, C*H*), 6.15 (dt, J=16.5, 5.9 Hz, 1H, C*H*, 5.06 (s, 4H, CH_2), 5.01 (s, 2H, CH_2), 4.24 (dd, J=5.3, 1.1 Hz, 2H, CH_2OH).
^{13}C NMR	(75 MHz, $CDCl_3$) δ_C ppm 153.0 (*C*), 138.4 (*C*), 137.8 (*C*H), 137.1 (*C*), 132.4 (*C*), 131.0 (*C*H), 128.6 (*C*H), 128.0 (*C*H), 106.3 (*C*H), 75.3 (*C*H_2), 71.3 (*C*H_2), 63.6 (*C*H_2).
LRMS (m/z, ESI$^+$)	927.9 $[2M+Na]^+$ (5.4%), 475.3 $[M+Na]^+$ (29.54%), 470.3 $[M+NH_4]^+$ (8.98%).

5.1.11 (*E*)-3-(3,4-*tris*-(benzyloxy)phenyl)prop-2-en-1-ol (74)

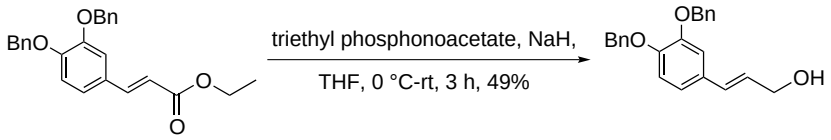

73

$C_{25}H_{24}O_4$
(388.17)

74

$C_{23}H_{22}O_3$
(346.16)

Following the procedure for the preparation of **9b**, but with **73** (11.5 g, 0.023 mol) as starting material, **74** was obtained as a pale yellow solid with a 49% yield. These data are in accordance with those reported in the literature.[236]

^{1}H NMR (300 MHz, $CDCl_3$) δ_H ppm 7.52-7.27 (m, 10H, Ar*H*), 7.04 (s, 1H, Ar*H*), 6.98-6.86 (m, 2H, Ar*H*), 6.50 (d, J = 15.8 Hz, 1 H, C*H*), 6.19 (dt, J=15.8, 5.8 Hz, 1H, CHC*H*), 5.27-5.13 (m, 4H, CH_2), 4.28 (dd, J = 5.8, 1.3 Hz, 2H, CH_2OH).

^{13}C NMR (75 MHz, $CDCl_3$) δ_C ppm 149.0 (*C*), 148.8 (*C*), 137.3 (*C*), 130.8 (*C*), 130.5 (*C*H), 128.5 (*C*H), 127.9 (*C*H), 127.4 (*C*H), 127.3 (*C*H), 126.9 (*C*H), 120.3 (*C*H), 115.0 (*C*H), 113.0 (*C*H), 71.4 (CH_2), 71.3(CH_2), 63.7 (*C*H_2).

LRMS (m/z, ESI$^+$) 715.6 $[2M+Na]^+$ (57.98%), 369.3 $[M+Na]^+$ (100%).

5.1.12 (*E*)-(3,5-*bis*-(benzyloxy)-2-(3-(3,4,5-*tris*-(benzyloxy)phenyl)-allyl)phenoxy)(tert-butyl)dimethylsilane (66)

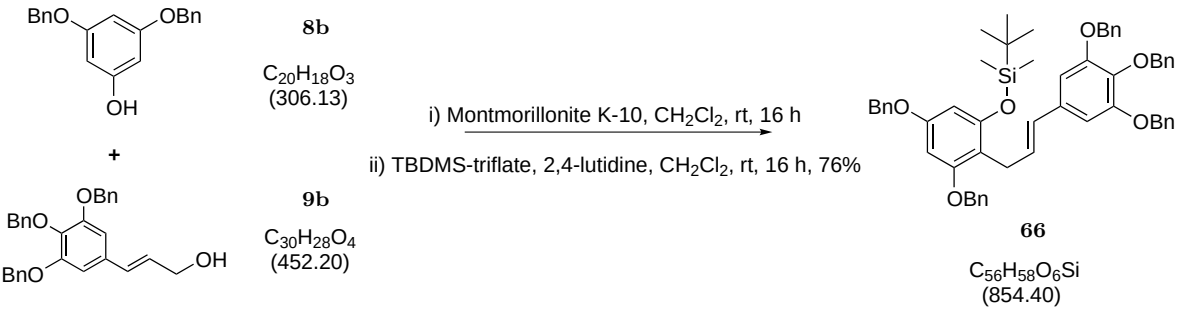

To a well- stirred mixture of 3,5-*bis*-(benzyloxy)phenol **8b** (3.83 g, 12.5 mmol) in anhydrous CH_2Cl_2 (156 mL) under argon, Montmorillonite K-10 (3.83 g) was added at room temperature. After 10 min, a solution of (*E*)-3,4-*bis*-(benzyloxy)cinn-amyl alcohol **9b** (1.89 g, 4.17 mmol) in CH_2Cl_2 (83.4.4 mL) was added dropwise over 45 min. The resulting purple mixture was stirred at room temperature overnight and then filtered through a layer of Celite, and rinsed with EtOAc (4x15 mL). After evaporation, the residue was purified by column chromatography (SiO_2 hexane/EtOAc, 100:0 to 60:40) to afford crude mixture of the desired allyl phenol and 3,5-*bis*-(benzyloxy)phenol. This mixture was diluted with anhydrous CH_2Cl_2 (20 mL) under argon and cooled to -78 °C then 2, 6-lutidine (1.07 mL, 9.19 mmol) and TBDMS-triflate (2.11 mL, 9.19 mmol) were successively added drop-wise and the reaction mixture was stirred -78 °C for 30 min to 1h. The reaction was quenched with MeOH and allowed to warm to room temperature and stirred for 15 min. The mixture diluted with CH_2Cl_2, washed with H_2O, brine, dried and concentrated *in vacuo* and then purified by column chromatography (SiO_2, hexane/CH_2Cl_2, 100:0 to 40:60) to afford titled compound, **66** (2.72 g, 76%) as a colorless oil. These data are in accordance with those reported in the literature.[232]

^{1}H NMR (300 MHz, $CDCl_3$) δ_H ppm 7.28-7.00 (m, 25H, Ar*H*), 6.38 (s, 2H, Ar*H*), 6.15-5.89 (m, 4H, Ar*H*, C*H*, C*H*), 4.86 (s, 4H, ArCH_2), 4.83 (s, 4H, ArCH_2), 4.81 (s, 2H, ArCH_2), 3.30 (d, J = 4.4 Hz, 2H, C$_1H_2$), 0.81 (s, 9H, C(CH_3)), 0.00 (s, 6H, SiCH_2).

^{13}C NMR (75 MHz, $CDCl_3$) δ_C ppm 158.3 (*C*), 158.1 (*C*), 154.7 (*C*), 152.8 (*C*), 138.0 (*C*), 137.5 (*C*), 137.3 (*C*), 137.1 (*C*), 134.0 (*C*), 129.3 (*C*H), 129.0 (*C*H), 128.6 (*C*H), 128.6 (*C*H), 128.5 (*C*H), 128.1 (*C*H), 128.0 (*C*H), 127.8 (*C*H), 127.4 (*C*H), 112.1 (*C*), 105.8 (*C*H), 98.4 (*C*H), 93.9 (*C*H), 75.2 (*C*H$_2$), 71.2 (*C*H$_2$), 70.2 (*C*H$_2$), 26.8 (*C*), 25.8 (*C*H$_3$), 18.3 (*C*H$_3$), -4.1 (*C*H$_3$).

LRMS (m/z, ESI$^+$) 1733.7 [2M+Na]$^+$ (44.28%), 877.7 [M+Na]$^+$ (100%).

5.1.13 (*E*)-(3,5-*bis*-(benzyloxy)-2-(3-(3,4-*tris*-(benzyloxy)phe-nyl)-allyl)phenoxy)(tert-butyl)dimethylsilane (75)

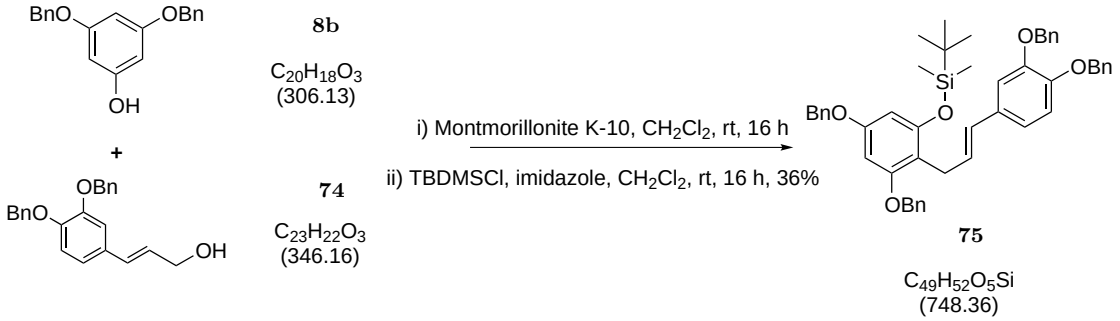

Following the procedure for the preparation of **66**, but with **8b** (5.29 g, 17.27 mmol) and **74** (2 g, 5.76 mmol) as starting materials, **75** was obtained with a 36% yield (two steps) as a colourless oil. These data are in accordance with those reported in the literature.[242]

^{1}H NMR (300 MHz, $CDCl_3$) δ_H ppm 7.25-6.99 (m, 20H, Ar*H*), 6.77-6.58 (m, 3H, Ar*H*x2, C*H*), 6.13-5.91 (m, 4H, Ar*H*, Ar*H*, C_3H), 4.95 (d, J = 5.9 Hz, 4H, CH_2), 4.91-4.78 (m, 4H, CH_2x2), 3.40 (d, J=5.9Hz,1H, C_1H), 3.31 (d, J = 5.9Hz,1H, C_1H), 0.89-0.64 (m, 9H, C(CH_3)).

^{13}C NMR (75 MHz, $CDCl_3$) δ_C ppm 175.7 (*C*), 158.0 (*C*), 154.7 (*C*), 149.0 (*C*), 147.9 (*C*), 146.3 (*C*), 140.2(*C*), 137.4(*C*), 137.1(*C*), 132.3 (*C*), 129.0 (*C*), 128.6 (*C*H), 128.4 (*C*H), 128.0 (*C*H), 127.7 (*C*H), 127.4 (*C*H),127.3 (*C*H), 127.1 (*C*H) 119.5(*C*H), 115.2(*C*H), 112.5 (*C*), 112.3 (*C*H), 98.4 (*C*H), 98.2 (*C*H), 93.8 (*C*H), 71.4 (CH_2), 71.3 (CH_2), 70.2 (CH_2), 26.8 (CH_2), 26.5 (*C*, 25.8 (CH_3), 25.7 (CH_2), -4.1 (CH_3), -4.4 (CH_3).

LRMS (m/z, ESI$^+$) 1521.1 $[2M+Na]^+$ (37.14%), 771.8 $[M+Na]^+$ (100%), 749.7 $[M+H]^+$ (24.45%).

5.1.14 (*1S,2S*)-3-(2,4-*bis*-(benzyloxy)-6-hydroxyphenyl)-1-(3,4,5-*tris*-(benzyloxy)phenyl)propane-1,2-diol (11b)

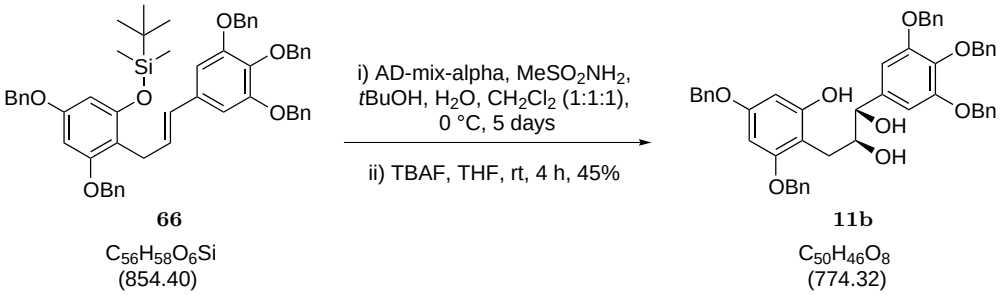

66
$C_{56}H_{58}O_6Si$
(854.40)

11b
$C_{50}H_{46}O_8$
(774.32)

AD-mix-α (5.64 g) and methanesulfonamide (0.38 g) were dissolved in a solvent mixture of *t*BuOH (25 mL) and water (25 mL). The resulting mixture was stirred at room temperature for 5 minutes, until two clear solutions are observed. The reaction was cooled to 0 °C and a solution of (*E*)-(3,5-*bis*-(benzyloxy)-2-(3-(3,4,5-*tris*-(benzyloxy)phenyl)allyl)phenoxy) (tert-butyl)dimethylsilane, **66** (1.72 g, 2.01 mmol) in CH_2Cl_2 (25 mL) was added all at once. After stirring overnight at 0 °C, a total of four batches of AD-mix-α (2.82 g) and methanesulfonamide (0.19 g) were added at 24h intervals. After stirring for another 24 h at 0 °C, TLC showed reaction had gone to completion.

A 10% $Na_2S_2O_3$ aqueous solution (25 mL) was added to quench the reaction. After stirring for 15 min at room temperature, the mixture was filtered through a pad of Celite, and was rinsed with EtOAc (4x20 mL). The phases were separated and the aqueous layer was further extracted with EtOAc (4x30 mL). The organic phases were combined, dried over anhydrous $MgSO_4$ and concentrated *in vacuo*. The crude residue was used in the next step without further purification.The desired fractions were concentrated to dryness (2.72 g, 3.6 mmol) then dissolved in anhydrous THF (60 mL) and TBAF (1.45 g, 4.58 mmol) was added. The resulting mixture was stirred at room temperature for 4h, after which time TLC analysis showed complete deprotection of the material. Saturated aqueous $NaHCO_3$ solution (10 mL) was added and the mixture was extracted with EtOAc (3x15mL). The organic layers were combined, dried over anhydrous $MgSO_4$ and the solvents evaporated. The residue was purified by column chromatography (SiO_2, $CHCl_3$/EtOAc 100:0 to 60:40) to give the titled compound, **11b** (0.7 g, 45%) as a white solid. These data are in accordance with those reported in the literature.[232]

^{1}H NMR (300 MHz, $CDCl_3$) δ_H ppm 7.46-7.17 (m, 25H, Ar*H*), 6.63 (s, 2H, Ar*H*), 6.23 (d, J=2.2 Hz, 1H, Ar*H*), 6.29 (d, J=2.2 Hz, 1H, Ar*H*), 5.05-4.95 (m, 8H, CH_2x4), 4.91 (s, 2H, CH_2), 4.45 (d, J = 5.9Hz, 1H, CHO*H*), 3.98-3.90 (m, 1H, CHO*H*), 2.98-2.84 (m, 1H, C*H*H), 2.84-2.73 (m, 1H, CH*H*).

^{13}C NMR	(75 MHz, $CDCl_3$) δ_C ppm 159.1 (*C*), 157.8 (*C*), 157.2 (*C*), 152.7 (*C*), 138.1 (*C*), 137.8 (*C*), 136.8 (*C*) 136.8 (*C*), 136.1 (*C*), 128.5 (*C*H), 128.4 (*C*H), 128.1 (*C*H), 127.9 (*C*H), 127.8 (*C*H), 127.6 (*C*H), 127.4 (*C*H), 126.6 (*C*H), 106.3 (*C*H), 106.1 (*C*), 95.9 (*C*H), 93.5 (*C*H), 75.1 (*CH*2), 71.1 (CH_2), 70.1 (CH_2), 26.7 (CH_2).
LRMS (m/z, ESI$^+$)	1572.1 $[2M+Na]^+$ (21.77%), 797.6 $[M+Na]^+$ (100%).
$\boldsymbol{\alpha}_D$	+ 8.4 (c = 0.5, $CHCl_3$).

5.1.15 (*1S,2S*)-3-(2,4-*bis*-(benzyloxy)-6-hydroxyphenyl)-1-(3,4-*tris*-(benzyloxy)phenyl)propane-1,2-diol (77)

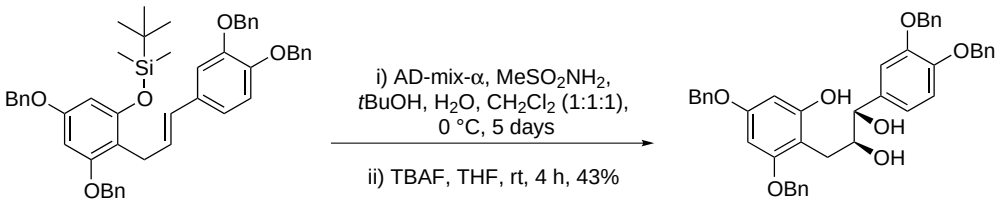

75
$C_{49}H_{52}O_5Si$
(748.36)

77
$C_{43}H_{40}O_7$
(668.28)

Following the procedure for the preparation of **11b**, but with **75** (2.49 g, 3.33 mmol) as starting material, **77** was obtained as a white solid with a 43% yield. These data are in accordance with those reported in the literature.[242]

^{1}H NMR	(300 MHz, DMSO) δ_H ppm 7.49-7.26 (m, 20H, Ar*H*), 7.05 (s, 1H, Ar*H*), 6.95 (d, J = 8.1 Hz, 1H, Ar*H*), 6.81 (d, J = 8.1 Hz, 1H, Ar*H*), 6.25-6.20 (m, 1H, Ar*H*), 6.12 (s, 1H, Ar*H*), 4.90-5.17 (m, 8H, CH_2x4), 4.30 (d, J = 4.4 Hz,1H, CHO*H*), 3.82-3.72 (m, 1H, CHO*H*), 2.69 (dd, J = 13.5, 3.7 Hz, 1H, C*H*H), 2.60-2.53 (m, 1H, CH*H*).
^{13}C NMR	(75 MHz, DMSO) δ_C ppm 157.7 (*C*), 147.7(*C*), 147.1(*C*), 137.4 (*C*), 137.3 (*C*), 137.2 (*C*), 136.4 (*C*), 128.3 (*C*H), 128.3 (*C*H), 127.6 (*C*H), 127.6 (*C*H), 127.5 (*C*H), 127.4 (*C*H), 126.8 (*C*H), 119.7 (*C*H, 113.8 (*C*H), 113.5 (*C*H), 107.0 (*C*H), 95.2 (*C*H), 91.7 (*C*H), 75.7 (*C*H), 74.9 (*C*H), 70.2 (*C*H_2), 69.2 (*C*H_2), 69.1 (*C*H_2), 26.9 (*C*H_2).
LRMS (m/z, ESI$^+$)	1359.3 $[2M+Na]^+$ (74.79%), 691.4 $[M+Na]^+$ (100%).
$\boldsymbol{\alpha}_D$	+ 6.4 (c = 1.38, DMSO).

5.1.16 (*2R,3S*)-5,7-*bis*-(benzyloxy)-2-(3,4,5-*tris*-(benzyloxy)-phenyl)-chroman-3-ol

(13b)

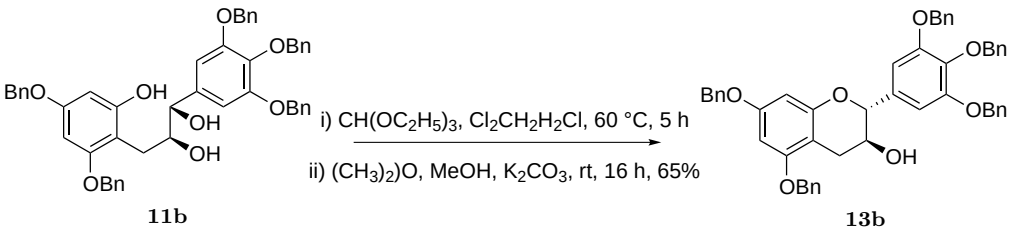

11b
$C_{50}H_{46}O_8$
(774.32)

13b
$C_{50}H_{44}O_7$
(756.31)

Triethyl orthoformate (2.37 mL) was added to a suspension of diol **11b** (2.57 g, 0.33 mmol) in 1,2-dichloroethane (6.5 mL) was added, followed by pyridinium *p*-toluenesulfonate

(0.5 g, 0.097 mmol). The mixture was stirred at room temperature for 20 min and the solid had dissolved. The mixture was heated to 60 °C for 5h until TLC showed the reaction was complete. After evaporation of the solvent, the residue was redissolved in DME (35 mL) and MeOH (35 mL), 0.46 g (0.033 mmol) K_2CO_3 was added, and the mixture was stirred at room temperature overnight. The solvent was evaporated, and the residue was purified by column chromatography (SiO_2, hexane/EtOAc, 100:0 to 75:25) to afford the titled compound, **13b** as white solid (1.62 g, 65%). These data are in accordance with those reported in the literature.[232]

^{1}H NMR	(300 MHz, $CDCl_3$) δ_H ppm 7.41-7.16 (m, 25H, Ar*H*), 6.66 (s, 2H, Ar*H*), 6.21 (d, J = 2.2 Hz, 1H, Ar*H*), 6.15 (d, J = 2.2 Hz, 1H, Ar*H*), 5.09-5.01 (m, 4H, CH_2x2), 4.98 (s, 2H, CH_2), 4.96 (s, 2H, CH_2), 4.93 (s, 2H, CH_2), 4.53 (d, J = 8.1 Hz, 1H, CHO*H*), 3.89 (ddd, J = 8.8, 8.1, 5.9 Hz, 1H, CHO*H*), 3.03 (dd, J = 16.5, 5.9 Hz, 1H, C*H*H), 2.57 (dd, J = 16.5, 8.8 Hz, 1H, CH*H*), 2.09 (s, 1H, O*H*).
^{13}C NMR	(75 MHz, $CDCl_3$) δ_C ppm 158.9 (*C*), 157.8 (*C*), 155.2 (*C*), 153.0(*C*), 138.8 (*C*), 137.8 (*C*), 136.8 (*C*), 133.2 (*C*), 128.5 (*C*H), 128.0 (*C*H) 127.6 (*C*H), 106.8 (*C*H), 102.3 (*C*), 94.4(*C*H), 93.9 (*C*H), 81.8 (*C*H), 75.2 *C*H_2), 71.2 (*C*H_2), 70.1 (*CH*2), 68.3 (*C*H_2), 27.6 (*C*H_2).
LRMS (m/z, ESI$^+$)	779.4 $[M+Na]^+$ (68.80%), 757.4 $[M+H]^+$ (100%).
$\boldsymbol{\alpha}_D$	- 8.1 (c = 1.38, $CHCl_3$).

5.1.17 (*2R,3S*)-5,7-*bis*-(benzyloxy)-2-(3,4,5-*tris*-(benzyloxy)-phenyl)-chroman-3-ol

(78)

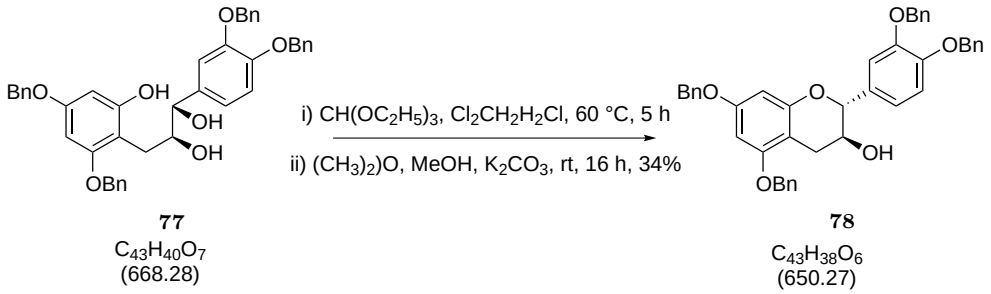

77
$C_{43}H_{40}O_7$
(668.28)

78
$C_{43}H_{38}O_6$
(650.27)

Following the procedure for the preparation of **13b**, but with **77** (0.49 g, 0.731 mmol) as starting material, **78** was obtained with a 34% yield. These data are in accordance with those reported in the literature.[264]

^{1}H NMR (300 MHz, $CDCl_3$) δ_H ppm 7.48-7.27 (m, 20H, Ar*H*), 7.00-6.95 (m, 3H, Ar*H*x3), 6.29 (d, J = 2.2 Hz, 1H, Ar*H*), 6.23 (d, J = 2.2 Hz, 1H, Ar*H*), 5.31 (s, 2H, CH_2), 5.24-5.13 (s, 2H, CH_2), 5.03 (s, J = 10.2 Hz, 4 H, CH_2), 4.64 (d, J = 8.1 Hz, 1H, C*H*), 4.05-3.96 (m, 1H, C*H*OH), 3.12 (dd, J = 16.3, 5.7 Hz, 1H, C*H*H), 2.66 (dd, J = 16.5, 8.8 Hz, 1H, CH*H*), 1.63-1.54 (m, 1H, O*H*).

^{13}C NMR (75 MHz, $CDCl_3$) δ_C ppm 158.8 (*C*), 157.8 (*C*), 155.3 (*C*), 149.4 (*C*), 149.1(*C*), 137.2 (*C*), 137.0 (*C*), 136.9 (*C*), 130.9 (*C*), 128.6 (*C*H), 128.5 (*C*H), 128.0 (*C*H), 127.9 (*C*H), 127.5 (*C*H), 127.5 (*C*H), 127.2 (*C*H), 127.1 (*C*H), 120.6 (*C*H), 115.0 (*C*H), 113.9 (*C*H), 102.3 (*C*), 94.4 (*C*H), 93.8 (*C*H), 81.6 (*C*H), 71.3 (*C*H_2), 71.2 (*C*H_2), 70.1 (*C*H_2), 69.9 (*C*H_2), 68.2 (*C*H_2), 27.6 (*C*H_2).

LRMS (m/z, ESI$^+$) 1324.0 $[2M+Na]^+$ (91.65%), 673.4 $[M+Na]^+$ (67.07%).

$\boldsymbol{\alpha}_D$ - 11.57 (c = 1.15, $CHCl_3$)

5.1.18 (*2S,3S*)-5,7-*bis*-(benzyloxy)-2-(3,4,5-*tris*- (benzyloxy)-phenyl)-chroman-3-ol

(15a)

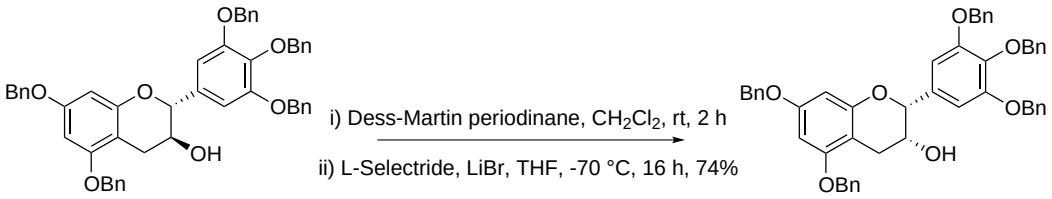

13b
$C_{50}H_{44}O_7$
(756.31)

15a
$C_{50}H_{44}O_7$
(756.31)

Dess-Martin Periodinane (0.57 g, 1.33 mmol) was added in one batch to a stirred solution of (*2R,3S*)-5,7-*bis*-(benzyloxy)-2-(3,4,5-*tris*-(benzyloxy)phenyl)chroman-3-ol, (0.46 g 0.603 mmol) in anhydrous CH_2Cl_2 (16 mL) under argon. The mixture was stirred at room temperature for about 2 h until completion. Subsequently, saturated aqueous $NaHCO_3$ solution (16 mL) and 10% aqueous $Na_2S_2O_3$ solution (16 mL) were added to quench the reaction. The organic layer was separated, and the aqueous layer was extracted with CH_2Cl_2 (3x15 mL). The combined organic phases were dried over $MgSO_4$ and the solvents evaporated. The ketone residue was a yellow oil used without further purification. Under nitrogen, the ketone (0.31 g, 0.409 mmol) was dissolved in dry THF (5 mL), and the solution was cooled to - 78 °C. Then, L-Selectride® (0.65 mL, 1.0 M solution in THF, 0.65 mmol) was added dropwise. The resulting solution was stirred at - 78 °C overnight. When TLC showed the reaction was complete, saturated $NaHCO_3$ aqueous solution (5 mL) was added to quench the reaction. The organic layer was separated and the aqueous layer was extracted with EtOAc (3x10 mL). The combined organic phases were dried over anhydrous $MgSO_4$ and the solvents evaporated. The residue was purified by column chromatography (SiO_2 hexane/ EtOAc 100:0 to 80:20) to give the titled compound, **15a**

with 74% yield. These data are in accordance with those reported in the literature.[265]

^{1}H NMR	(300 MHz, $CDCl_3$) δ_H ppm 7.42-7.14 (m, 25H, Ar*H*), 6.73 (s, 2H, Ar*H*), 6.21 (s, 2H, Ar*H* x 2), 5.05 (s, 4H, *C*H_2), 4.98 (s, 2H, *C*H_2, 4.94 (s, 4H,*C*H_2x2), 4.81 (s, 1H, C*H*), 4.15-4.09 (m, 1H, C*H*OH), 2.93 (dd, J = 17.6, 2.2 Hz, 1H, C*H*H), 2.84 (dd, J = 17.1, 4.4 Hz, 1H, CH*H*).
^{13}C NMR	(75 MHz, $CDCl_3$) δ_C ppm 158.9 (*C*), 158.8 (*C*), 158.3 (*C*), 155.1 (*C*), 153.1 (*C*), 138.4 (*C*) 137.8 (*C*), 137.0 (*C*), 136.9 (*C*), 133.8 (*C*), 128.5 (*C*), 128.2 (**CH**), 128.0 (*C*H), 127.9 (*C*H), 127.8 (*C*H), 127.6 (*C*H), 127.2 (*C*H), 106.2 (*C*H), 101.0 (*C*), 94.7 (*C*H), 94.2 (*C*H), 78.6 (*C*H), 75.3 (*C*H), 71.4 (*C*H_2), 70.2 (*C*H_2), 66.4 (*C*H), 28.1 (*C*H_2).
LRMS (m/z, ESI$^+$)	1537.4 $[2M+Na]^+$ (33.50%), 779.6 $[M+Na]^+$ (91.38%), 757.6 $[M+H]^+$ (100%).
$\boldsymbol{\alpha}_D$	- 24.6 (c = 1.79, $CHCl_3$).

5.1.19 (*2S,3S*)-5,7-*bis*-(benzyloxy)-2-(3,4-*tris*-(benzyloxy)phe-nyl)-chroman-3-ol

(80)

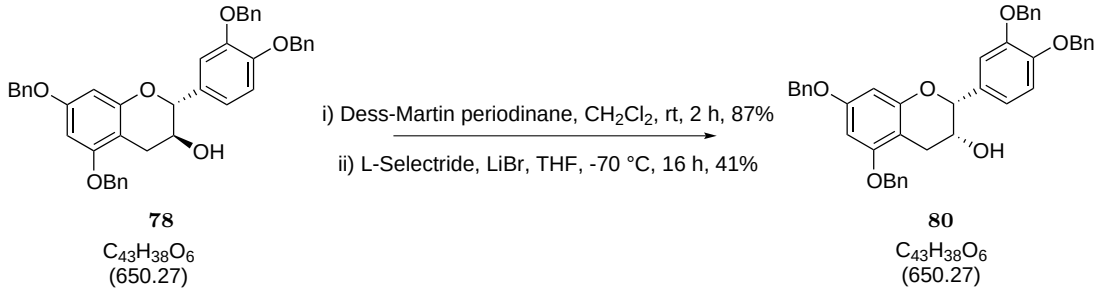

78
$C_{43}H_{38}O_6$
(650.27)

80
$C_{43}H_{38}O_6$
(650.27)

Following the procedure for the preparation of **15a**, but with **78** (0.30 g, 0.467 mmol) as starting material, **80** was obtained as an orange solid with a 40% yield. These data are in accordance with those reported in the literature.[264]

^{1}H NMR	(300 MHz, $CDCl_3$) δ_H ppm 7.41-7.16 (m, 20H, Ar*H*), 7.07 (s, 1H, Ar*H*), 6.95-6.86 (m, 2H, Ar*H*x2), 6.19 (s, 2H, Ar*H*x2), 5.11 (s, 2H, CH_2), 5.09 (s, 2H, CH_2), 4.94 (s, 2H, CH_2), 4.93 (s, 2H, CH_2), 4.83 (s, 1H, C*H*), 4.17-4.06 (m, 1H, C*H*H), 2.96-2.80 (m, 2H, CH*H*).
^{13}C NMR	(75 MHz, $CDCl_3$) δ_C ppm 158.8 (*C*), 158.3 (*C*), 155.3 (*C*), 149.1(*C*), 148.9 (*C*), 137.3 (*C*), 137.2 (*C*), 137.0 (*C*), 136.9 (*C*), 131.5 (*C*), 128.6 (*C*H), 128.5 (*C*H), 128.0 (*C*H), 127.9 (*C*H), 127.5 (*C*H) 127.3 (*C*H), 127.2 (*C*H), 119.5 (*C*H), 115.1(*C*H), 113.5 (*C*H), 94.7 (*C*H), 94.1 (*C*H), 78.4 (*C*H), 71.4 (*C*H_2), 71.3 (*C*H_2), 70.2 (*C*H_2), 70.0 (*C*H_2), 66.4 (*C*H_2), 28.2 (*C*H_2).
LRMS (m/z, ESI$^+$)	1325.3 $[2M+Na]^+$ (37.84%), 673.5 $[M+Na]^+$ (67.07%).
$\boldsymbol{\alpha}_D$	- 21.9 (c = 2.33, $CHCl_3$).

5.1.20 (–)-Epigallocatechin (3)

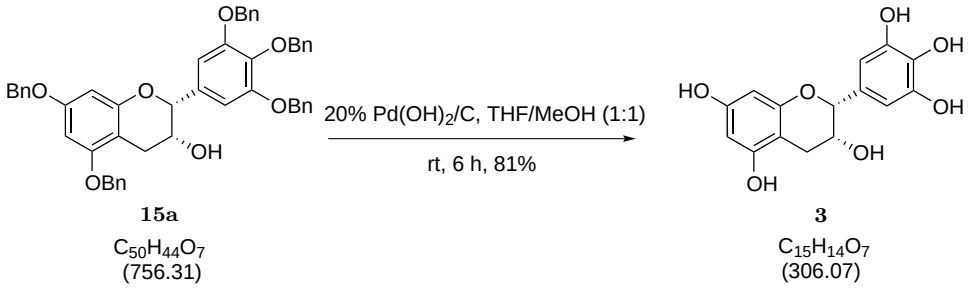

15a
$C_{50}H_{44}O_7$
(756.31)

3
$C_{15}H_{14}O_7$
(306.07)

Under an H_2 atmosphere, 20% $Pd(OH)_2/C$ (0.024 g) was added to a solution of **15a** (0.0251 g, 0.24 mmol) in a solvent mixture of THF/MeOH (1:1 v/v, 15 mL). The resulting reaction mixture was stirred at room temperature under H_2 for 6 h, TLC showed that the reaction was completed. The reaction mixture was filtered through Celite and washed with THF/MeOH (3x10 mL). The filtrate was evaporated, and the residue was rapidly purified by HPLC and freeze-dried affording **3** (0.0079 g, 81%) as a white solid. These data are in accordance with those reported in the literature.[266]

^{1}H NMR	(300 MHz, MeOD) δ_H ppm 9.08 (s, 1H, *O*H), 8.88 (s, 1H, *O*H), 8.69 (s, 1H, *O*H), 7.93 (s, 1H, *O*H), 6.38 (s, 2H, Ar*H*x2), 5.89 (d, J = 2.2Hz, 1H, Ar*H*), 5.71 (d, J = 2.2Hz, 1H, Ar*H*), 4.66 (s, 1H), 4.60 (d, J = 4.4Hz, 1H, C*H*), 3.91 - 4.06 (m,1H, C*H*), 2.70 (d, J = 4.4Hz, 1H, C*H*), 2.65 (d, J = 4.4Hz,1H, C*H*), 2.44 (d, J = 3.3Hz,1H).
FT-IR	3749.86 (w), 3444.98 (w), 3253.45 (w), 2248.98 (s), 2123.79 (w), 1739.29 (s), 1620.11 (w), 1367.15 (w), 1216.53 (w), 1052.49 (s), 1024.83 (s), 1006.27 (s).
LRMS (m/z, ESI$^-$)	305.2 $[M-H]^-$ (59.89%).
HRMS (m/z, ESI$^-$)	$C_{15}H_{15}O_7[M+H]^+$ requires 307.0809; found 307.0812.
$\boldsymbol{\alpha}_D$	- 98.4 (c = 1.69, MeOH).

5.1.21 (–)-Epicatechin (1)

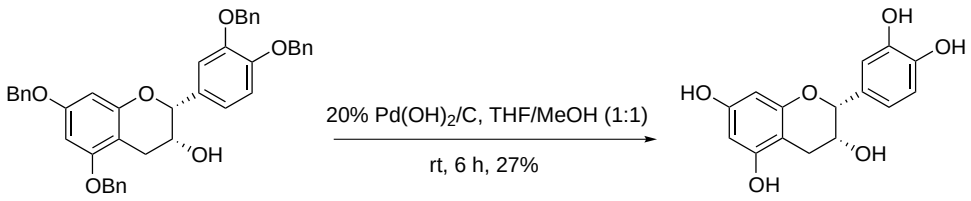

80
$C_{43}H_{38}O_6$
(650.27)

1
$C_{15}H_{14}O_6$
(290.08)

Following the procedure for the preparation of **3**, but with **80** as starting material, **1** was obtained as a white solid (5.6 mg, 27% yield). These data are in accordance with those reported in the literature.[266]

^{1}H NMR	(300 MHz, DMSO−d_6) δ_H ppm 9.10 (s, 1H, Ar*H*), 8.89 (s, 1H, Ar*H*), 8.79 (s, 1H, Ar*H*), 8.71 (s, 1H, Ar*H*), 6.89 (s, 1H), 6.73-6.62 (m, 2H, Ar*H*x2), 5.89 (d, J = 2.2 Hz, 1H, C*H*), 5.71 (d, J = 2.2 Hz, 1H), 4.73 (s, 1H), 4.65 (d, J = 4.4 Hz, 1H, C*H*), 4.00 (d, J = 4.0 Hz, 1H, C*H*), 3.35 (s, 1H, *O*H), 2.68 (dd, J = 1.0 Hz, 1H, C*H*).
^{13}C NMR	(75 MHz, DMSO−d_6) δ_C ppm 156.5 (*C*), 156.2 (*C*), 155.7 (*C*), 144.5 (*C*), 144.4 (*C*), 130.6 (*C*), 117.9 (*C*H), 114.8 (*C*H), 114.7 (*C*H), 98.4 (*C*H), 95.0 (*C*H), 94.0 (*C*H), 78.0 (*C*H), 64.9 (*C*H), 28.2 (CH_2).
FT-IR	2930.38 (br), 1619.61 (s), 1519.37 (s), 1467.98 (s), 1439.11 (s), 1387.27 (w),1286.02 (w), 1258.03 (w), 1223.41 (s), 1180.67 (s), 1092.25 (s), 1014.29 (s).
LRMS (m/z, ESI$^+$)	289.1 $[M-H]^-$ (100%).
HRMS (m/z, ESI$^-$)	$C_{15}H_{14}O_6[M+H]^+$ requires 291.0862; found 291.0863.
$\boldsymbol{\alpha}_D$	- 69.3 (c = 0.19, MeOH).

5.1.22 3,4,5-*tris*-(benzyloxy)benzoic acid (68)

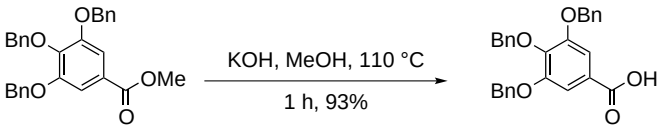

47
$C_{29}H_{26}O_5$
(454.18)

68
$C_{28}H_{24}O_5$
(440.16)

47 (1 g, 2.2 mmol) was combined with potassium hydroxide (1.23 g, 22 mmol) in MeOH: Dioxane (25 mL, 1:1 v/v) and set to reflux at 120 °C for 16 h. The reaction mixture was cooled and the solvents were removed under vacuum to give a white suspension. The resulting mixture was diluted in water and extracted with EtOAc (3x100 mL). The organic phases were combined and washed with 10% aqueous HCl and brine before drying with anhydrous $MgSO_4$ and the solvents evaporated to give the titled compound as a white solid with a 93% yield. These data are in accordance with those reported in the literature.[267]

^{1}H NMR	(300 MHz, DMSO−d_6) δ_H ppm 12.96 (br. s., 1H, O*H*), 7.52-7.24 (m, 17H, Ar*H*), 5.19 (s, 4H, CH_2), 5.05 (s, 2H, CH_2).
^{13}C NMR	(75 MHz, DMSO−d_6) δ_C ppm 166.8 *C*O, 152.0 (*C*), 140.9 (*C*), 137.3 (*C*), 136.8 (*C*), 128.4 (*C*H), 128.1 (*C*H), 128.0 (*C*H), 127.9(*C*H), 127.5 (*C*H), 126.0 (*C*H), 108.2 (*C*H), 74.2 (*C*H$_2$), 70.2 (*C*H$_2$).
LRMS (m/z, ESI$^+$)	903.6 [2M+Na]$^+$ (15.94%), 497.2 [M+k]$^+$ (11.59%), 463.2 [M+k]$^+$ (25.64%), 458.3 [M+NH_4]$^+$ (52.23%).

5.1.23 (*2R,3R*)-5,7-*bis*-(benzyloxy)-2-(3,4,5-*tris*-(benzyloxy)phenyl)chroman-3-yl 3,4,5-*tris*-(benzyloxy)benzoate (16)

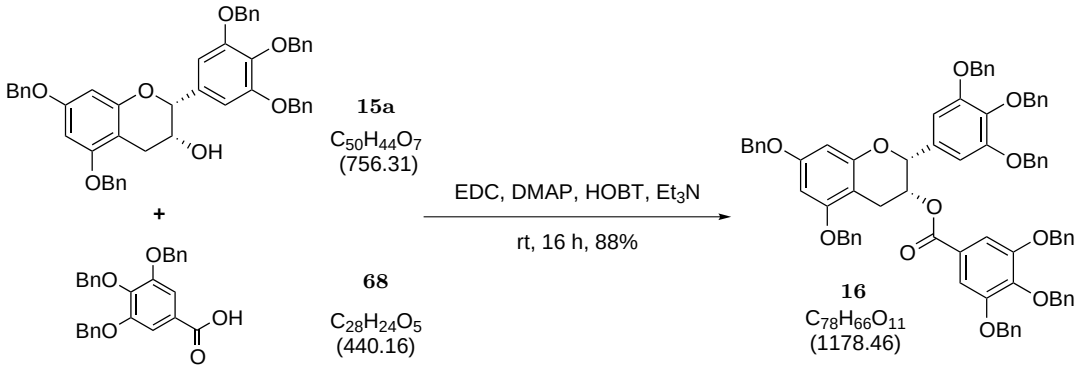

To a stirred solution of **15a** (0.057 g, 0.075 mmol) and 3,4,5-*tris*-(benzyloxy)benzoic acid **68** (0.067 g, 0.150 mmol) in CH_2Cl_2 (3 mL) under argon, 1-Ethyl-3-(3-dimethylaminopropyl)carbodiimide (0.11 g, 0.579 mmol), 4-(Dimethylamino)pyridine (0.0083 g, 0.391 mmol), 1-hydoxybenzotriazole (0.0091 g, 0.068 mmol) and triethylamine (0.074 mL, 0.534 mmol) were added at room temperature and stirred overnight until all the alcohol had been consumed. The mixture was poured into 2 M HCl solution and extracted with EtOAc (3x10 mL), dried over $MgSO_4$ and concentrated *in vacuo*. The crude was purified by column chromatography (SiO_2, hexane/EtOAc 80:20) to afford the desired product **16** (0.078 g, 88%). These data are in accordance with those reported in the literature.[232]

^{1}H NMR (300 MHz, $CDCl_3$) δ_H ppm 7.52-7.41 (m, 2H, Ar*H*), 7.38-7.11 (m, 40H, Ar*H*), 6.65 (s, 2H, Ar$_C$*H*), 6.31 (s, 1H, Ar*H*), 6.27 (s, 1H, Ar*H*), 5.61-5.56 (m, 1H, C*H*), 5.20-5.00 (m, 1H, C*H*), 5.00-4.81 (m, 13H, CH_2),4.72 (d, J = 11.3 Hz, 2H, CH_2), 4.59 (d, J = 11.3 Hz, 2H, CH_2), 3.07-2.97 (m, 2H, CH_2).

^{13}C NMR	(75MHz, $CDCl_3$) δ_C ppm 166.3 (CO), 161.1(C), 155.5 (C), 152.9 (C), 143.4 (C), 142.9 (C), 137.8 (C), 137.0 (C), 136.5 (C), 135.6 (C), 129.0 (CH), 128.9 (CH), 128.7 (CH), 128.6 (CH), 128.5 (CH), 128.4 (CH), 128.3 (CH), 127.9 (CH), 125.5 (C), 109.6 (CH), 105.2 (C), 75.5 (CH_2), 71.6 (CH_2), 70.1 (CH_2), 67.1 (CH_2), 66.1 (CH), 25.5 (CH_2).
FT-IR	3355.42 (br.), 2942.16 (s), 2865.41 (s), 1711.36, (w), 1462.85 (s), 1384.46 (w), 1247.44 (w), 1105.25 (s, 1063.06 (s), 1013.47 (s).
LRMS (m/z, ESI$^+$)	1196.8 $[M+NH_4]^+$ (31.45%), 1179.5 $[M+H]^+$ (8.10%).
$\boldsymbol{\alpha_D}$	- 18.7 (c = 1.07, $CHCl_3$).

5.1.24 (*2R,3R*)-5,7-*bis*-(benzyloxy)-2-(3,4-*tris*-(benzyloxy)phe-nyl)-chroman-3-yl 3,4,5-*tris*-(benzyloxy)benzoate (82)

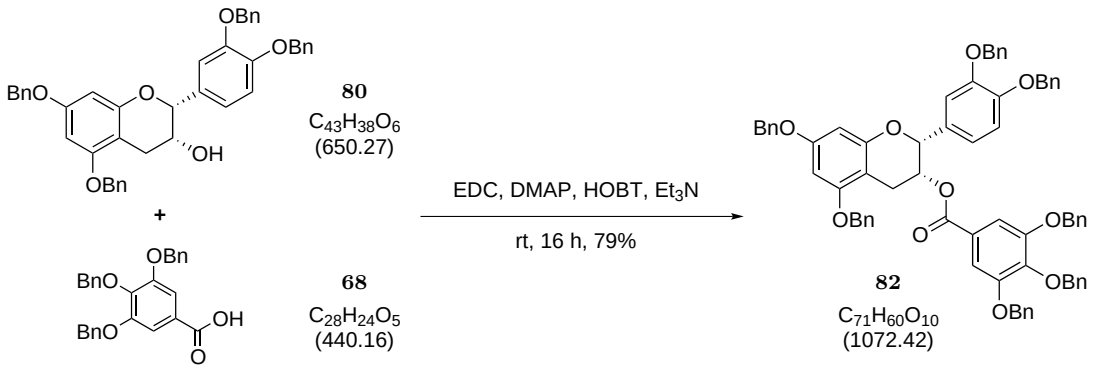

Following the procedure for the preparation of **16**, but with **80** (0.42 g, 0.64 mmol) and 3,4-*tris*-(benzyloxy)benzoic acid **42** (0.62 g, 1.41mmol) as starting materials, **82** was obtained in a 79%. These data are in accordance with those reported in the literature.[266]

^{1}H NMR	(300 MHz, $CDCl_3$) δ_H ppm 7.46-7.18 (m, 35H, ArH), 6.78 (s, 2H, Ar$_C H$), 6.25 (s, 2H, ArH), 5.14-4.91 (m, 14H, CH_2), 4.85 (s, 2H, ArH), 4.17 (br. s., 1H, CH), 3.01-2.84 (m, 2H, CH_2), 1.19 (t, J=7.0 Hz, 1H).
^{13}C NMR	(75 MHz, $CDCl_3$) δ_C ppm 159.2 (CH), 158.7 (CH), 155.5 (CH), 153.4 (CH), 138.8 (CH), 138.2 (CH), 137.4 (CH), 134.1 (CH), 129.0 (CH), 128.9 (CH), 128.9 (CH), 128.6 (CH), 128.4 (CH), 128.3 (CH), 128.2 (CH), 128.0 (CH), 127.6 (CH), 106.5 (CH), 101.4 (C), 100.7 (C), 95.1(CH) , 94.5 (CH), 78.9 (CH$_2$), 77.8 (CH$_2$), 77.4 (CH$_2$), 75.6 (CH$_2$), 71.7 (CH$_2$), 70.5 (CH$_2$), 70.3 (CH$_2$), 66.8 (CH), 28.5 (CH$_2$).
FT-IR	3019.83 (w), 2359.61 (w), 2110.24 (w), 1710.55 (w), 1426.88 (w), 1214.21 (s), 1150.30 (w), 1021.74 (w).
LRMS (m/z, ESI$^+$)	1095.9 [M+Na]$^+$ (69.19%).
$\boldsymbol{\alpha}_D$	- 140.1 (c = 1.22, $CHCl_3$).

5.1.25 (*2R,3R*)-5,7-dihydroxy-2-(3,4,5-trihydroxyphenyl)-chroman-3-yl benzoate (91)

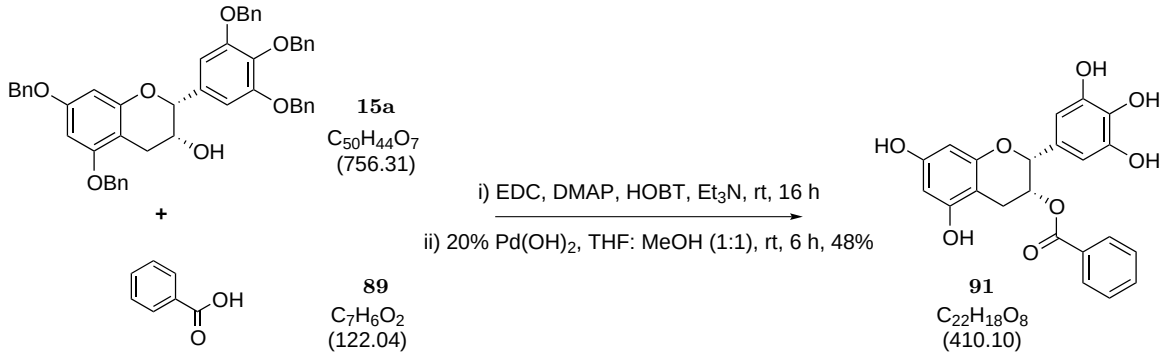

Following the procedure for the preparation of **16**, but with **15a** (0.095 g, 0.126 mmol) and benzoic acid **90** (0.034 g, 0.276 mmol) as starting materials, benzylated **91** was prepared and the crude was submitted to debenzylation under an H_2 atmosphere, 20% $Pd(OH)_2/C$ in a solvent mixture of THF/MeOH (1:1 v/v, 9 mL). The reaction mixture was filtered through celite and washed with MeOH (3x10 mL). The filtrate was evaporated, and the residue was rapidly purified by HPLC with desired product **91** as a white solid (48% two steps yield).

^{1}H NMR	(300 MHz, MeOH) δ_H ppm 6.24-6.18 (m, 1H, Ar$_C$*H*), 5.77 (d, J = 7.2 Hz, 1H, Ar$_C$*H*), 5.70-5.62 (m, 1 H, Ar$_C$*H*), 3.10 (s, 6 H, Ar*H*, Ar*H*), 1.53-1.46 (m, 4H, C*H*x2, C*H*, C*H*).
FT-IR	3324.21 (br), 2984.17 (w), 2945.20 (w), 2833.77 (w), 2477.00 (s), 2213.86 (w), 2070.65 (s), 1908.63 (w), 1416.36 (w), 1120.37 (s), 1027.45 (s).
LRMS (m/z, ESI$^+$)	542.0 $[M+TFA+NH_4]^+$ (55.79%).
$\boldsymbol{\alpha}_D$	- 9.4 (c = 0.18, MeOH).

5.1.26 (*2R,3R*)-5,7-dihydroxy-2-(3,4,5-trihydroxyphenyl)chr-oman-3-yl 3,4-dichlorobenzoate (89)

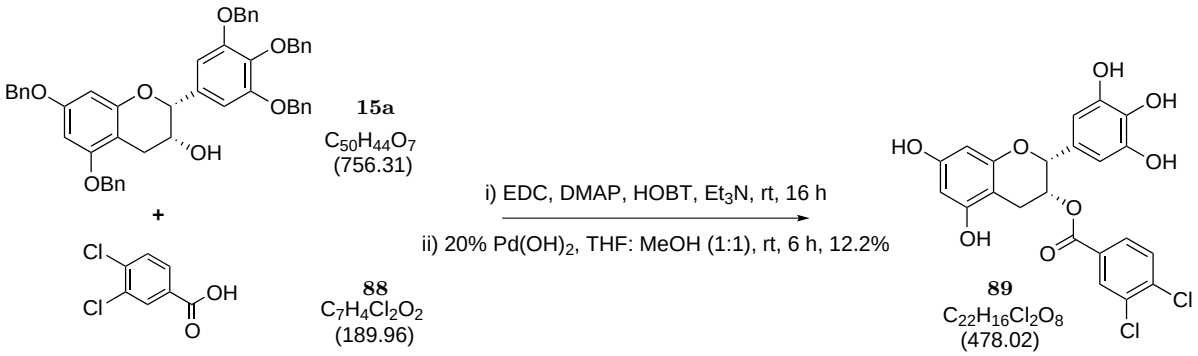

Following the procedure for the preparation of **41**, but with **14b** and 3,4-dichlorobenzoic acid **87** as starting materials, benzylated 19.4 was prepared and the crude was submitted to debenzylation under an H_2 atmosphere, 20% $Pd(OH)_2/C$ in a solvent mixture of THF/MeOH (1:1 v/v, 9 mL). The reaction mixture was filtered through celite and washed with MeOH (3x10 mL). The filtrate was evaporated, and the residue was rapidly purified by HPLC with desired product **88** in a 12.2% yield.

^{1}H NMR	(400 MHz, ACETONE−*d-6*) δ_H ppm 7.99-7.75 (m, 1H, Ar$_C$*H*), 7.36-7.15 (m, 1H, Ar$_C$*H*), 6.52 (s, 1H, Ar$_C$*H*), 5.94-5.90 (m, 2H, Ar*H*), 5.48 (ddd, J = 4.4, 2.7, 1.5 Hz, 1H, C*H*), 5.00 (s, 1H, O*H*), 2.89-2.79 (m, 1H, C*H*), 2.79-2.71 (m, 1H, C*H*).
FT-IR	3446.03 (br), 2995.25 (s), 2912.22 (s), 2333.72 (w), 2116.86 (w), 1697.12 (w), 1435.40 (s), 1407.66 (s), 1309.85 (s), 1041.55 (s), 652.12 (s), 696.90 (s), 666.95 (s).
LRMS (m/z, ESI$^+$)	496.1 $[M+NH_4]^+$ (8.62%).
α_D	- 4.45 (c = 0.78, MeOH).

5.1.27 ((*2R*,*3R*)-5,7-dihydroxy-2-(3,4,5-trihydroxyphenyl)chroman-3-yl 2-naphthoate (87)

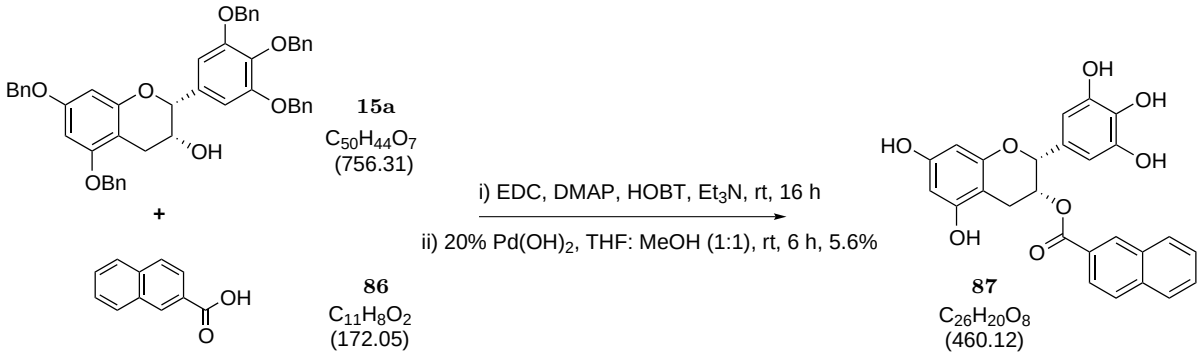

Following the procedure for the preparation of **16**, but with **15a** (0.095 g, 0.126 mmol) and 2-naphthanoic acid **85** (0.048 g, 0.276 mmol) as starting materials, benzylated **87** was prepared and the crude was submitted to debenzylation under an H_2 atmosphere, 20% $Pd(OH)_2$ /C in a solvent mixture of THF/MeOH (1:1 v/v, 9 mL). The reaction mixture was filtered through celite and washed with MeOH (10 mL). The filtrate was evaporated, and the residue was rapidly purified by HPLC with desired product **87** as an off-white solid (5.6% two-step yield).

^{1}H NMR	(300 MHz, MeOH) δ_H ppm 8.61 (s, 1H, Ar$_C$*H*), 8.06-7.90 (m, 3H, Ar$_C$*H*), 7.65-7.53 (m, 3H, Ar$_C$*H*), 4.91 (s, 6H, Ar*H*, Ar*H*), 3.35-3.26 (m, 2H, C*H*x2).
FT-IR	3327.74 (br), 2944.97 (w), 2833.66 (w), 2477.79 (s), 2212.15 (w), 2070.76 (s), 1897.19 (w), 1415.42 (s), 1344.31 (w), 1120.30 (s), 1088.81 (w).
LRMS (m/z, ESI$^+$)	524.1 [M+MeCN+Na]$^+$ (5.28%).
$\boldsymbol{\alpha}_D$	- 3.5 (c = 0.45, MeOH).

5.1.28 (*2R,3R*)-5,7-dihydroxy-2-(3,4,5-trihydroxyphenyl)chr-oman-3-yl 3,4,5-trimethoxybenzoate (91)

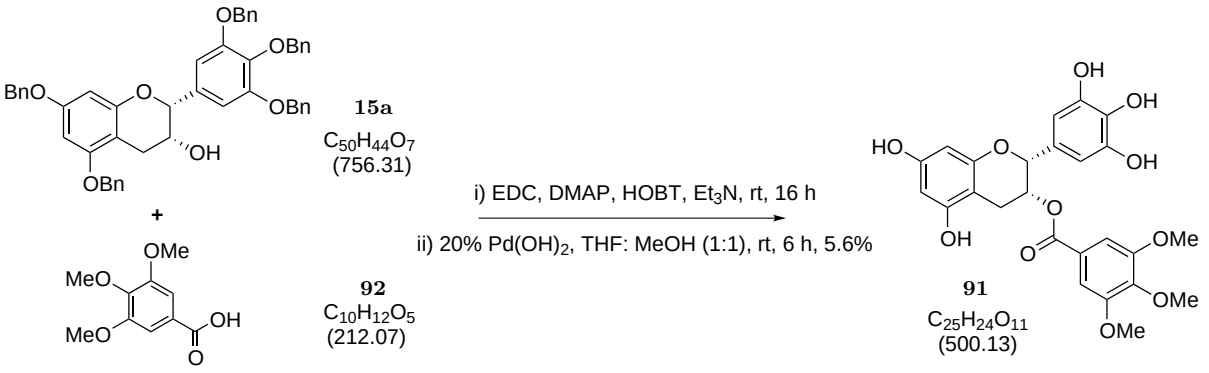

Following the procedure for the preparation of **16**, but with **15a** (0.095 g, 0.126 mmol) and 3,4,5-trimethoxybenzoic acid **92** (0.059 g, 0.276 mmol) as starting materials, benzylated **93** was prepared and the crude was submitted to debenzylation under an H_2 atmosphere, 20% $Pd(OH)_2/C$ in a solvent mixture of THF/MeOH (1:1 v/v, 9 mL). The reaction mixture was filtered through celite and washed with MeOH (3x10 mL). The filtrate was evaporated, and the residue was rapidly purified by HPLC with desired product **93** as a white solid (5.6% two-step yield). These data are in accordance with those reported in the literature.[268]

^{1}H NMR	(400 MHz, ACETONE−*d-6*) δ_H ppm 7.16 (s, 2H, Ar$_C$*H*), 6.67 (s, 2H, Ar*H*), 6.07-6.01 (m, 2H, Ar*H*), 5.51-5.47 (m, 1H, C*H*), 5.17-5.13 (m, 1H, C*H*), 3.89-3.78 (m, 6H, OCH_3), 3.75 (s, 3H, OCH_3), 3.13-3.04 (m, 1H, C*H*), 3.03 (d, J = 3.0 Hz, 1H, C*H*).
FT-IR	332.7.85 (br), 2983.76 (w), 2945.10 (w), 2833.72 (w), 2480.28 (w), 2212.45 (w), 2070.88 (s), 1416.36 (w), 1173.28 (w), 1026.96 (s), 975.90 (s).
LRMS (m/z, ESI$^+$)	523.1 [M+Na]$^+$ (96.21%), 1023.3 [2M+Na]$^+$ (100%).
$\boldsymbol{\alpha}_D$	- 40.0 (c = 0.15, Acetone).

5.1.29 (−)-Epigallocatechin gallate (4)

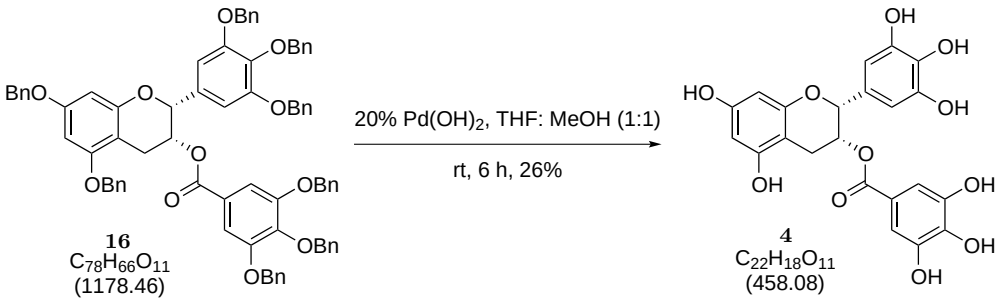

16
$C_{78}H_{66}O_{11}$
(1178.46)

4
$C_{22}H_{18}O_{11}$
(458.08)

Under an H_2 atmosphere, 20% $Pd(OH)_2$ /C (68.4 mg) was added to a solution of **16** (80 mg, 0.068 mmol) in a solvent mixture of THF/MeOH (1:1 v/v, 9 mL). The resulting reaction mixture was stirred at room temperature under H_2 for 6 h, TLC showed that the reaction was completed. The reaction mixture was filtered through celite and washed with MeOH (3x10 mL). The filtrate was evaporated, and the residue was rapidly purified by HPLC with desired product as a white solid (8 mg, 26%). These data are in accordance with those reported in the literature.[232]

^{1}H NMR	(400 MHz, ACETONE−*d6*) δ_H ppm 7.01 (s, 2H, ArCH), 6.61 (s, 2H, ArH), 6.05 (d, J = 1.0 Hz, 1H, ArH), 6.02 (d, J = 2.0 Hz, 1H, ArH), 5.61-5.49 (m, 1H, CH), 5.06 (s, 8H), 3.03 (dd, J = 1.0 Hz, 1H, CH), 2.89 (dd, J = 17.7, 2.0 Hz, 1H, CH), 2.89-2.77 (m, 1H, CH)
^{13}C NMR	(75 MHz, ACETONE−*d6*) δ_C ppm 165.9 (CO), 157.6 (C), 157.3 (C), 156.9 (C), 146.1 (C), 145.7 (C), 138.6 (C), 133.0 (C), 130.6 (C), 121.7 (C), 109.8 (CH), 106.6 (C), 98.9 (CH), 96.3 (CH), 95.7 (CH), 77.9 (CH), 69.1 (CH), 26.5 (CH$_2$).
FT-IR	3352.63 (b), 2942.99 (s), 2866.19 (s), 2115.74 (w), 1699.55 (s), 1610.53 (w), 1534.40 (w), 1464.03. (w), 1330.94 (w), 1245.20 (s), 1145.16 (w), 1104.25 (s), 1032.55 (s).
LRMS (m/z, ESI$^-$)	457.1[M-H]$^-$ (100%), 915.4 [2M-H]$^-$ (26.11%).

HRMS (m/z, ESI$^-$) $C_{22}H_{18}O_{11}[M+Na]^+$ requires 481.0743; found 481.074.

$\boldsymbol{\alpha}_D$ - 199.0 (c = 0.54, Acetone).

5.1.30 5-((((*2R,3R*)-5,7-diacetoxy-2-(3,4,5-triacetoxyphenyl)chr-oman-3-yl)oxy)carbonyl)benzene-1,2,3-triyl triacetate (85)

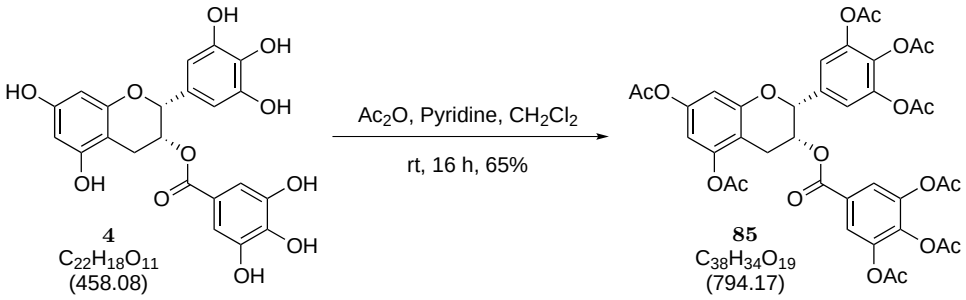

4 was combined with 1 mL Ac_2O and 2 mL pyridine and stirred at room temperature overnight. This reaction mixture was concentrated *in vacuo* and redissolved in CH_2Cl_2. The mixture was washed with H_2O and brine and concentrated *in vacuo*. The crude was purified via HPLC to yield 65% of **85** as a pale pink solid. These data are in accordance with those reported in the literature.[255]

^{1}H NMR (400 MHz, ACETONE−*d-6*) δ_H ppm 7.40 (s, 2H, Ar$_C$*H*), 7.18 (s, 2H, Ar*H*), 6.51 (d, J = 2.5 Hz, 1H, Ar*H*), 6.38 (d, J = 2.0 Hz, 1H, Ar*H*), 5.56-5.52 (m, 1H, C*H*), 5.33-5.29 (m, 1H, C*H*), 2.97 (d, J = 4.5 Hz, 1H, C*H*), 3.07-2.79 (m, 1H, C*H*), 2.59 (s, 24H, C=OCH_3).

^{13}C NMR	(75 MHz, $CDCl_3$) δ_C ppm 176.6 (*C*O), 169.5 (*C*O), 169.2 (*C*), 168.1 (*C*), 150.1 (*C*), 144.3 (*C*), 143.7 (*C*), 142.8 (*C*), 139.7 (*C*), 135.5 (*C*), 127.6 (*C*H), 126.8 (*C*H), 122.6 (*C*), 119.2 (*C*H), 116.1 (*C*H), 110.0 (*C*), 109.9 (*C*), 109.4 (*C*H), 108.5 (*C*H), 68.0 (*C*H), 60.8 (*C*H), 31.2 (CH_2), 21.4 (CH_3), 21.1 (CH_3), 20.9 (CH_3), 20.7 (CH_3), 20.5 (CH_3), 14.5 (CH_3).
FT-IR	3019.92 (w), 2357.66 (w), 2183.12 (w), 2160.41 (w), 1739.80 (w), 1428.33 (w), 1368.88 (w), 1214.14 (s), 1021.79 (w).
LRMS (m/z, ESI$^+$)	817.1 $[M+Na]^+$ (100%)
$\boldsymbol{\alpha}_D$	- 75.3 (c = 0.25, MeOH).

5.1.31 (−)-Epicatechin gallate (2)

Following the procedure for the preparation of **4**, but with **82** as starting material, **2** was obtained with a 43% yield. These data are in accordance with those reported in the literature.[261]

^{1}H NMR	(400 MHz, ACETONE−*d-6*) δ_H ppm 8.25-8.13 (m, 3H, Ar_CH, Ar*H*), 8.07-7.71 (m, 2H, Ar*H*), 7.07-7.00 (m, 2H, Ar*H*x2), 6.04 (dd, J = 11.1, 2.5 Hz, 1H, C*H*), 5.58-5.50 (m, 1H, C*H*), 3.10- 3.00 (m, 1H, C*H*), 2.96-2.88 (m, 1H, C*H*).
FT-IR	3325.09 (br), 2985.47 (w), 2945.08 (w), 2479.25 (s), 2211.66 (w), 2070.78 (s), 1717.48 (w), 1148.55 (s), 1120.10 (s), 1027.21 (s).
LRMS (m/z, ESI$^-$)	441.1$[M-H]^-$ (50.15%).

HRMS (m/z, ESI$^-$)	$C_{22}H_{19}O_{10}[M+H]^+$ requires 443.0972; found 443.0973.
$\boldsymbol{\alpha}_D$	- 131.3 (c = 0.15, MeOH).

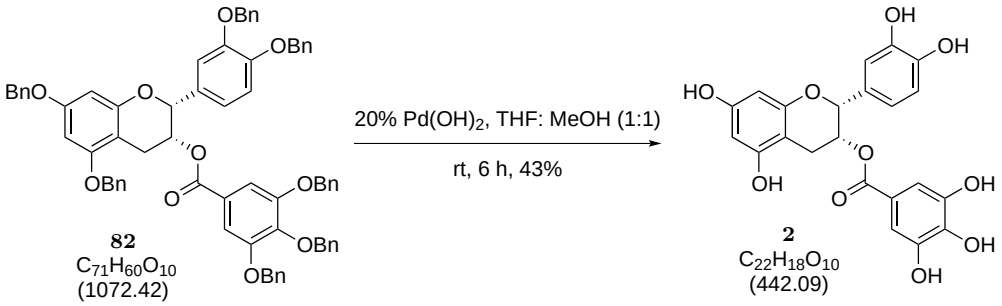

82
$C_{71}H_{60}O_{10}$
(1072.42)

2
$C_{22}H_{18}O_{10}$
(442.09)

5.1.32 (*2R,3R*)-2-(3,4-diacetoxyphenyl)chroman-3,5,7-triyl triacetate (84)

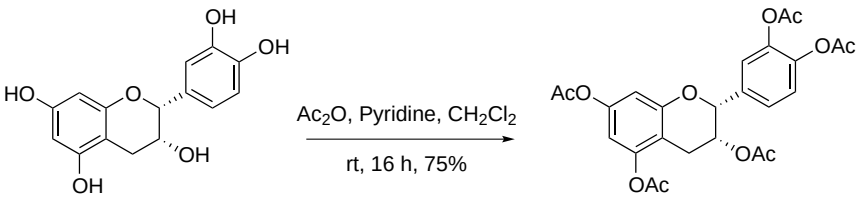

1
$C_{15}H_{14}O_6$
(290.08)

84
$C_{25}H_{24}O_{11}$
(500.13)

Epicatechin **1** (0.050 g, 0.172 mmol) was combined with 1 mL Ac_2O and 2 mL pyridine and stirred at room temperature overnight. The reaction mixture was stirred until competition and quenched with 10% aqueous HCl and stirred for 30 min. The organic layer was separated and the aqueous layer was extracted with EtOAc (3x3 mL). The organic layers were combined, dried over anhydrous $MgSO_4$ and the solvents evaporated. The residue was purified by HPLC to give the titled compound as a white solid in a 62%.

^{1}H NMR (300 MHz, ACETONE−*d-6*) δ_H ppm 7.45-7.35 (m, 2H, Ar*H*), 7.33-7.14 (m, 1H, Ar*H*), 6.68 (d, J = 2.3 Hz, 1H, Ar*H*), 6.60 (d, J = 2.3 Hz, 1H, Ar*H*), 5.53-5.45 (m, 1H, C*H*), 5.43-5.33 (m, 1H, C*H*), 3.13-2.94 (m, 1H, C*H*), 2.93-2.76 (m, 1H, C*H*), 2.31-2.17 (m, 15H, C=OCH_3), 1.84 (s, 3H,C=OCH_3).

^{13}C NMR (75 MHz, ACETONE−*d-6*) δ_H ppm 170.2 (*C*O), 169.4 (*C*O), 168.0 (*C*O), 168.8 (*C*O), 168.6 (*C*O), 156.0 (*C*), 151.1 (*C*), 150.9 (*C*), 143.2 (*C*), 143.1 (*C*), 137.3 (*C*), 125.4 (*C*H), 124.1 (*C*H), 123.0 (*C*H), 111.1 (*C*H), 109.8 (*C*H), 108.6 (*C*H), 77.5 (*C*H), 67.4 (*C*H), 26.6 (CH_2), 20.9 (CH_3), 20.3 (CH_3), 20.5 (CH_3).

FT-IR 3859.55 (s), 3675.28 (s), 3491.27 (s), 3308.10 (s), 3124.53 (s), 2939.76 (s), 2757.21 (s), 2387.59 (s), 2202.57 (s), 2017.40 (s), 1838.96 (s), 1652.80 (s), 1262.74 (w), 1214.41 (w), 1124.64 (w).

LRMS (m/z, ESI$^+$) 1023.1 [2M+Na]$^+$ (1.87%), 539.0 [M+k]$^+$ (11.84%), 523.0 [M+Na]$^+$ (100%).

HRMS (m/z, ESI$^+$) $C_{25}H_{24}O_{11}$[M+H]$^+$ requires 501.1394; found 501.1391.

$\boldsymbol{\alpha}_D$ - 18.7 (c = 1.49, Acetone).

5.1.33 (*2R,3R*)-2-(3,4-dimethoxyphenyl)-3,5,7-trimethoxychroman (85)

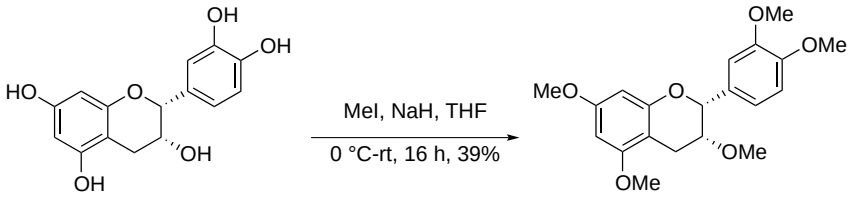

1
$C_{15}H_{14}O_6$
(290.08)

85
$C_{20}H_{24}O_6$
(360.16)

Epicatechin **1** (0.051 g, 0.176 mmol) was stirred in THF (1 mL) at 0 °C. NaH (0.105 g, 2.64 mmol) and MeI (0.17 mL, 2.64 mmol) were added and stirred for 15 minutes and allowed to warm up. The reaction mixture was stirred until competition and quenched with aqueous NH_4Cl solution. The organic layer was separated and the aqueous layer was extracted with EtOAc (3x3 mL). The organic layers were combined, dried over anhydrous $MgSO_4$ and the solvents evaporated. The residue was purified by HPLC to give the titled compound as a white solid in a 39%.

^{1}H NMR (300 MHz, MeOH) δ_H ppm . 7.05-6.90 (m, 2H, Ar*H*x2), 4.91 (s, 13H, Ar*H*, *C*H_3), 4.24-4.16 (m, 1H, C*H*), 3.84 (d, J = 4.5 Hz, 3H, Ar*H*, Ar*H*), 3.35-3.25 (m, 4H, *C*H_3, C*H*), 2.96-2.85 (m, 1H, C*H*), 2.80-2.67 ppm (m, 1H, C*H*).

^{13}C NMR	(75 MHz, ACETONE−*d-6*) δ_H ppm 159.1 (*C*), 157.7 (*C*), 157.2 (*C*), 150.0 (*C*), 120.1 (*C*), 112.2 (*C*H), 100.7 (*C*), 96.0 (*C*H), 96.1 (*C*H), 79.5 (*C*H), 68.1 (*C*H), 67.0 (*C*H), 56.2 (CH_3), 37.9 (CH_3), 32.7 (CH_3), 30.7, 30.4, 30.2, 29.7, 29.4, 29.1, 23.4(CH_2), 14.4 (CH_2).
FT-IR	2977.30 (w), 2866.45 (w), 2256.23 (w), 2115.34 (w), 1700.64 (s), 1515.12 (w), 1445.64 (w), 1382.50 (w), 1243.95 (s), 1117.87 (s), 1031.53 (s).
$\boldsymbol{\alpha}_D$	- 50.2 (c = 0.2 , MeOH).

References

1 C. Cabrera, R. Artacho, and Giménez R. Beneficial effects of green tea–a review. *Journal of the American Chemical Society*, 25(2):77–99, 2006.

2 NHS. Coronary heart disease, June 2013.

3 M. C. Fishbein. The vulnerable and unstable atherosclerotic plaque. *Cardiovascular pathology*, 19(1):6–11, 2010.

4 Pasterkamp C. and Falk E. Atherosclerotic plaque rupture: an overview. *Journal of Clinical and Basic Cardiology*, 3(2):81–86, 2000.

5 M. A. Afzal, S. A Saeed, and B. H. Shah. Atherosclerosis and plaque rupture: An update. *Journal of Pakistan Medical Association*, (37-43), 1999.

6 P. D. Richardson, M. J. Davies, and G. V. Born. Influence of plaque configuration and stress distribution on fissuring of coronary atherosclerotic plaques. *Lancet*, 2(8669):941–4, 1989.

7 V. Kumar. Robbins basic pathology: Dystrophic calcification, September 2013.

8 D. Yellon. Myocardial reperfusion injury. *New England Journal of Medicine*, 357(11):1121–35, 2007.

9 R. B. Jennings, H. M. Sommers, G. A. Smyth, H. A. Flack, and H. Linn. Myocardial necrosis induced by temporary occlusion of a coronary artery in the dog. *Archives of Pathology*, 70:68–78, 1960.

10 G. R. Heyndrickx, R. W. Millard, R. J. McRitchie, P. R. Maroko, and S. F. Vatner. Regional myocardial functional and electrophysiological alterations after brief coronary artery occlusion in conscious dogs. *Journal of Clinical Investigation*, 56(4):978–85, 1975.

11 F. Prunier, Y. Kawase, D. Gianni, C. Scapin, S. B. Danik, P. T. Ellinor, R. J. Hajjar, and F. Del Monte. Prevention of ventricular arrhythmias with sarcoplasmic reticulum Ca^{2+} ATPase pump overexpression in a porcine model of ischemia reperfusion. *Circulation*, 118(6):614–24, 2008.

12 S. H. Rezkalla and R. A. Kloner. No-reflow phenomenon. *Circulation*, 105:656–662, 2002.

13 J. Flores, D. R. DiBona, C. H. Beck, and A. Leaf. The role of cell swelling in ischemic renal damage and the protective effect of hypertonic solute. *Journal of clinical investigation*, 51(1):118–26, 1972.

14 P. G. Anderson, S. P. Bishop, and S. B. Digerness. Transmural progression of morphologic changes during ischemic contracture and reperfusion in the normal and hypertrophied rat heart. *American Journal of Pathology*, 129(1):152–67, 1987.

15 R. A. Kloner. Does reperfusion injury exist in humans? *Journal of the American College of Cardiology*, 21(2):537–45, 1993.

16 G. J. Gross and J. A. Auchampach. Reperfusion injury: does it exist? *Journal of molecular and cellular cardiology*, 42(1):12–8, 2007.

17 H. M. Piper, D. García-Dorado, and M. Ovize. A fresh look at reperfusion injury. *Cardiovascular Research*, 38(2):291–300, 1998.

18 L. M. Buja. Myocardial ischemia and reperfusion injury. *Cardiovascular pathology : the official journal of the Society for Cardiovascular Pathology*, 14(4):170–5, 2005.

19 P. Krijnen, R. Nijmeijer, and C. Meijer. Apoptosis in myocardial ischaemia and infarction. *Journal of clinical Pathology*, 55(11):801–11, 2002.

20 R. Gottlieb, K. Burleson, and R. Kloner. Reperfusion injury induces apoptosis in rabbit cardiomyocytes. *Journal of Clinical Investigation*, 94(4):1621–28, 1994.

21 F. Reggiori and D. J. Klionsky. Autophagosomes: biogenesis from scratch? *Current Opinion in Cell Biology*, 17(4):415–22, 2005.

22 A. Haunstetter and S. Izumo. Apoptosis: basic mechanisms and implications for cardiovascular disease. *Circulation Research*, 82(11):1111–29, 1998.

23 A. B. Gustafsson and R. A. Gottlieb. Recycle or die: the role of autophagy in cardioprotection. *Journal of molecular and cellular cardiology*, 44(4):654–61, 2008.

24 A. B. Gustafsson and R. A. Gottlieb. Autophagy in ischemic heart disease. *Circulation Research*, 104(2):150–8, 2009.

25 K. Nishida, S. Kyoi, O. Yamaguchi, J. Sadoshima, and K. Otsu. The role of autophagy in the heart. *Cell Death and Differentiation*, 16(1):31–8, 2009.

26 Å. Gustafsson. Mechanisms of apoptosis in the heart. *Journal of clinical immunology*, 23(6):447–459, 2003.

27 G. D. Dispersyn, L. Mesotten, B. Meuris, A. Maes, L. Mortelmans, W. Flameng, F. Ramaekers, and M. Borgers. Dissociation of cardiomyocyte apoptosis and dedifferentiation in infarct border zones. *European Heart Journal*, 23(11):849–57, 2002.

28 V. P. M. Van Empel, A. T. A. Bertrand, L. Hofstra, H. J. Crijns, P. A. Doevendans, and L. J. De Windt. Myocyte apoptosis in heart failure. *Cardiovascular Research*, 67(1):21–9, 2005.

29 W. R. MacLellan and M. D. Schneider. Death by design. programmed cell death in cardiovascular biology and disease. *Circulation Research*, 81(2):137–44, 1997.

30 D. Wencker, M. Chandra, K. Nguyen, W. Miao, S. Garantziotis, S. M. Factor, J. Shirani, R. C. Armstrong, and R. N. Kitsis. A mechanistic role for cardiac myocyte apoptosis in heart failure. *Journal of Clinical Investigation*, 111(10):1497–504, 2003.

31 S. Nagata. Apoptosis by death factor. *Cell*, 88(3):355–65, 1997.

32 P. M. Kang and S. Izumo. Apoptosis and heart failure: A critical review of the literature. *Circulation Research*, 86(11):1107–13, 2000.

33 Y Lee. Role of apoptosis in cardiovascular disease. *Apoptosis*, 14(4):536–48, 2009.

34 B. P. Giroir, J. H. Johnson, T. Brown, G. L. Allen, and B. Beutler. The tissue distribution of tumor necrosis factor biosynthesis during endotoxemia. *Journal of Clinical Investigation*, 90(3):693–8, 1992.

35 R. J. Youle and A. Strasser. The bcl-2 protein family: opposing activities that mediate cell death. *Nature Reviews. Molecular Cell Biology*, 9(1):47–59, 2008.

36 N. Bahi, J. Zhang, M. Llovera, M. Ballester, J. X. Comella, and D. Sanchis. Switch from caspase-dependent to caspase-independent death during heart development: essential role of endonuclease g in ischemia-induced dna processing of differentiated cardiomyocytes. *Journal of Biological Chemistry*, 281(32):22943–52, 2006.

37 P. Li, D. Nijhawan, I. Budihardjo, S. M. Srinivasula, M. Ahmad, E. S. Alnemri, and X. Wang. Cytochrome c and dATP-dependent formation of Apaf-1/caspase-9 complex initiates an apoptotic protease cascade. *Cell*, 91(4):479–89, 1997.

38 L. Virág and C. Szabó. The therapeutic potential of poly(ADP-ribose) polymerase inhibitors. *Pharmacological Reviews*, 54(3):375–429, 2002.

39 E. Daugas, S. A. Susin, N. Zamzami, K. F. Ferri, T. Irinopoulou, N. Larochette, M. C. Prévost, B. Leber, D. Andrews, J. Penninger, and G. Kroemer. Mitochondrio-nuclear translocation of aif in apoptosis and necrosis. *FASEB journal : official publication of the Federation of American Societies for Experimental Biology*, 14(5):729–39, 2000.

40 A. Gross, J. M. McDonnell, and S. J. Korsmeyer. Bcl-2 family members and the mitochondria in apoptosis. *Genes & development*, 13(15):1899–911, 1999.

41 M. S. Ola, M. Nawaz, and H. Ahsan. Role of bcl-2 family proteins and caspases in the regulation of apoptosis. *Molecular and Cellular Biochemistry*, 351(1-2):41–58, 2011.

42 C. L. Murriel, E. Churchill, K. Inagaki, L. I. Szweda, and D. Mochly-Rosen. Protein kinase Cdelta activation induces apoptosis in response to cardiac ischemia and reperfusion damage: a mechanism involving bad and the mitochondria. *Journal of Biological Chemistry*, 279(46):47985–91, 2004.

43 A. B. Gustafsson, J. G. Tsai, S. E. Logue, M. T. Crow, and R. A. Gottlieb. Apoptosis repressor with caspase recruitment domain protects against cell death by interfering with bax activation. *Journal of Biological Chemistry*, 279(20):21233–8, 2004.

44 D. A. Kubli, J. E. Ycaza, and Asa B. Gustafsson. Bnip3 mediates mitochondrial dysfunction and cell death through Bax and Bak. *Biochemical Journal*, 405(3):407–15, 2007.

45 L. A. Kirshenbaum and D. De Moissac. The bcl-2 gene product prevents programmed cell death of ventricular myocytes. *Circulation*, 96(5):1580–5, 1997.

46 A. B. Gustafsson and R. A. Gottlieb. Bcl-2 family members and apoptosis, taken to heart. *American journal of physiology. Cell physiology*, 292(1):C45–51, 2007.

47 Q. L. Deveraux, N. Roy, H. R. Stennicke, T. Van Arsdale, Q. Zhou, S. M. Srinivasula, E. S. Alnemri, G. S. Salvesen, and J. C. Reed. IAPs block apoptotic events induced by caspase-8 and cytochrome c by direct inhibition of distinct caspases. *The EMBO journal*, 17(8):2215–23, 1998.

48 G. Wu, J. Chai, T. L. Suber, J. W. Wu, C. Du, X. Wang, and Y. Shi. Structural basis of IAP recognition by Smac/DIABLO. *Nature*, 408(6815):1008–12, 2000.

49 S. Bhuiyan and K. Fukunaga. Inhibition of HtrA2/Omi ameliorates heart dysfunction following ischemia/reperfusion injury in rat heart in vivo. *European journal of pharmacology*, 557(2-3):168–77, 2007.

50 T. Koseki, N. Inohara, S. Chen, and G. Núñez. ARC, an inhibitor of apoptosis expressed in skeletal muscle and heart that interacts selectively with caspases. *Proceedings of the National Academy of Sciences of the United States of America*, 95(9):5156–60, 1998.

51 Y-J. Nam, K. Mani, A. W. Ashton, C-F. Peng, B. Krishnamurthy, Y. Hayakawa, P. Lee, S. J. Korsmeyer, and R. N. Kitsis. Inhibition of both the extrinsic and intrinsic death pathways through nonhomotypic death-fold interactions. *Molecular Cell*, 15(6):901–12, 2004.

52 M. Irmler, M. Thome, M. Hahne, P. Schneider, K. Hofmann, V. Steiner, J. L. Bodmer, M. Schröter, K. Burns, C. Mattmann, D. Rimoldi, L. E. French, and J. Tschopp. Inhibition of death receptor signals by cellular FLIP. *Nature*, 388(6638):190–5, 1997.

53 R. Ferrari, C. Ceconi, S. Curello, A. Cargnoni, E. Pasini, F. De Giuli, and A. Albertini. Role of oxygen free radicals in ischemic and reperfused myocardium. *The American Journal of Clinical Nutrition*, 53(1):215S–222S, 1991.

54 N. R. Madamanchi and M. S. Runge. Mitochondrial dysfunction in atherosclerosis. *Circulation Research*, 100(4):460–73, 2007.

55 M. K. Misra, M. Sarwat, P. Bhakuni, R. Tuteja, and N. Tuteja. Oxidative stress and ischemic myocardial syndromes. *Medical Science Monitor*, 15:RA209–RA219, 2009.

56 D. B. Zorov, C. R. Filburn, L. O. Klotz, J. L. Zweier, and S. J. Sollott. Reactive oxygen species (ROS)-induced ROS release: a new phenomenon accompanying induction of the mitochondrial permeability transition in cardiac myocytes. *Journal of Experimental Medicine*, 192(7):1001–14, 2000.

57 J. L. Zweier, J. T. Flaherty, and M. L. Weisfeldt. Direct measurement of free radical generation following reperfusion of ischemic myocardium. *Proceedings of the National Academy of Sciences of the United States of America*, 84(5):1404–7, 1987.

58 R. Bolli, M. O. Jeroudi, B. S. Patel, C. M. DuBose, E. K. Lai, R. Roberts, and P. B. McCay. Direct evidence that oxygen-derived free radicals contribute to postischemic myocardial dysfunction in the intact dog. *Proceedings of the National Academy of Sciences of the United States of America*, 86(12):4695–9, 1989.

59 G. Ambrosio, J. L. Zweier, W. E. Jacobus, M. L. Weisfeldt, and J. T. Flaherty. Improvement of postischemic myocardial function and metabolism induced by administration of deferoxamine at the time of reflow: the role of iron in the pathogenesis of reperfusion injury. *Circulation*, 76(4):906–15, 1987.

60 R. E. Williams, J. L. Zweier, and J. T. Flaherty. Treatment with deferoxamine during ischemia improves functional and metabolic recovery and reduces reperfusion-induced oxygen radical generation in rabbit hearts. *Circulation*, 83(3):1006–14, 1991.

61 G. Solaini and D. A. Harris. Biochemical dysfunction in heart mitochondria exposed to ischaemia and reperfusion. *Biochemical Journal*, 390(Pt 2):377–94, 2005.

62 G. Loor, J. Kondapalli, H. Iwase, N. S. Chandel, G. B. Waypa, R. D. Guzy, T. L. Vanden Hoek, and P. T. Schumacker. Mitochondrial oxidant stress triggers cell death in simulated ischemia-reperfusion. *Biochimica et Biophysica Acta*, 1813(7):1382–94, 2011.

63 T. L. Vanden Hoek, Y. Qin, K. Wojcik, C-Q. Li, Z-H. Shao, T. Anderson, L. B. Becker, and K. J. Hamann. Reperfusion, not simulated ischemia, initiates intrinsic apoptosis injury in chick cardiomyocytes. *American Journal of Physiology. Heart and Circulatory Physiology*, 284(1):H141–50, 2003.

64 H. J. Oskarsson, L. Coppey, R. M. Weiss, and W. G. Li. Antioxidants attenuate myocyte apoptosis in the remote non-infarcted myocardium following large myocardial infarction. *Cardiovascular Research*, 45(3):679–87, 2000.

65 J. T. Flaherty, B. Pitt, J. W. Gruber, R. R. Heuser, D. A. Rothbaum, L. R. Burwell, B. S. George, D. J. Kereiakes, D. Deitchman, and N. Gustafson. Recombinant human superoxide dismutase (h-SOD) fails to improve recovery of ventricular function in patients undergoing coronary angioplasty for acute myocardial infarction. *Circulation*, 89(5):1982–91, 1994.

66 W. Siems, O. Sommerburg, L. Schild, W. Augustin, C-D. Langhans, and I. Wiswedel. Beta-carotene cleavage products induce oxidative stress in vitro by impairing mitochondrial respiration. *FASEB Journal*, 16(10):1289–91, 2002.

67 G. L. Johnson and R. Lapadat. Mitogen-activated protein kinase pathways mediated by ERK, JNK, and p38 protein kinases. *Science*, 298(5600):1911–2, 2002.

68 B. A. Rose, T. Force, and Y. Wang. Mitogen-activated protein kinase signaling in the heart: angels versus demons in a heart-breaking tale. *Physiological Reviews*, 90(4):1507–46, 2010.

69 G. Pearson, F. Robinson, T. Beers Gibson, B. E. Xu, M. Karandikar, K. Berman, and M. H. Cobb. Mitogen-activated protein (MAP) kinase pathways: regulation and physiological functions. *Endocrine Reviews*, 22(2):153–83, 2001.

70 M. Raman, W. Chen, and M. H. Cobb. Differential regulation and properties of MAPKS. *Oncogene*, 26(22):3100–12, 2007.

71 H. Martín, M. Flández, C. Nombela, and M. Molina. Protein phosphatases in mapk signalling: we keep learning from yeast. *Molecular Microbiology*, 58(1):6–16, 2005.

72 D. M. Owens and S. M. Keyse. Differential regulation of MAP kinase signalling by dual-specificity protein phosphatases. *Oncogene*, 26(22):3203–13, 2007.

73 J. M. Kyriakis and J. Avruch. Mammalian MAPK signal transduction pathways activated by stress and inflammation: a 10-year update. *Physiological Reviews*, 92(2):689–737, 2012.

74 J. C. Lee, J. T. Laydon, P. C. McDonnell, T. F. Gallagher, S. Kumar, D. Green, D. McNulty, M. J. Blumenthal, J. R. Heys, and S. W. Landvatter. A protein kinase involved in the regulation of inflammatory cytokine biosynthesis. *Nature*, 372(6508):739–46, 1994.

75 M. A. Bogoyevitch, J. Gillespie-Brown, A. J. Ketterman, S. J. Fuller, R. Ben-Levy, A. Ashworth, C. J. Marshall, and P. H. Sugden. Stimulation of the stress-activated mitogen-activated protein kinase subfamilies in perfused heart. p38/RK mitogen-activated protein kinases and c-Jun N-terminal kinases are activated by ischemia/reperfusion. *Circulation Research*, 79(2):162–73, 1996.

76 Y. Wang, S. Huang, V. P. Sah, J. Ross, Jr, J. H. Brown, J. Han, and K. R. Chien. Cardiac muscle cell hypertrophy and apoptosis induced by distinct members of the p38 mitogen-activated protein kinase family. *Journal of Biological Chemistry*, 273(4):2161–8, 1998.

77 A. T. Saurin, J. L. Martin, R. J. Heads, C. Foley, J. W. Mockridge, M. J. Wright, Y. Wang, and M. S. Marber. The role of differential activation of p38-mitogen-activated protein kinase in preconditioned ventricular myocytes. *FASEB Journal*, 14(14):2237–46, 2000.

78 E. Marais, S. Genade, B. Huisamen, J. G. Strijdom, J. A. Moolman, and A. Lochner. Activation of p38 MAPK induced by a multi-cycle ischaemic preconditioning protocol is associated with attenuated p38 MAPK activity during sustained ischaemia and reperfusion. *Journal of Molecular and Cellular Cardiologyolecular and cellular cardiology*, 33(4):769–78, 2001.

79 S. Schneider, W. Chen, J. Hou, C. Steenbergen, and E. Murphy. Inhibition of p38 mapk alpha/beta reduces ischemic injury and does not block protective effects of preconditioning. *American Journal of Physiology. Heart and Circulatory Physiology*, 280(2):H499–508, 2001.

80 S. Dhingra, A. K. Sharma, D. K. Singla, and P. K. Singal. p38 and ERK1/2 MAPKs mediate the interplay of TNF-alpha and IL-10 in regulating oxidative stress and cardiac myocyte apoptosis. *American journal of physiology. Heart and circulatory physiology*, 293(6):H3524–31, 2007.

81 R. Sucher, P. Gehwolf, T. Kaier, M. Hermann, M. Maglione, R. Oberhuber, T. Ratschiller, A. V. Kuznetsov, F. Bösch, A. V. Kozlov, M. I. Ashraf, S. Schneeberger, G. Brandacher, R. Ollinger, R. Margreiter, and J. Troppmair. Intracellular signaling pathways control mitochondrial events associated with the development of ischemia/ reperfusion-associated damage. *Transplant International*, 22(9):922–30, 2009.

82 J. S. Jaswal, M. Gandhi, B. A. Finegan, J. R. B. Dyck, and A. S. Clanachan. Inhibition of p38 MAPK and AMPK restores adenosine-induced cardioprotection in hearts stressed by antecedent ischemia by altering glucose utilization. *American Journal of Physiology. Heart and Circulatory Physiology*, 293(2):H1107–14, 2007.

83 W-J. Fan, S. Genade, A. Genis, B. Huisamen, and A. Lochner. Dexamethasone-induced cardioprotection: a role for the phosphatase MKP-1? *Life Sciences*, 84(23-24):838–46, 2009.

84 R. J. Davis. Signal transduction by the JNK group of MAP kinases. *Cell*, 103(2):239–52, 2000.

85 R. M. Fryer, H. H. Patel, A. K. Hsu, and G. J. Gross. Stress-activated protein kinase phosphorylation during cardioprotection in the ischemic myocardium. *American journal of physiology. Heart and circulatory physiology*, 281(3):H1184–92, 2001.

86 P. Ping, J. Zhang, S. Huang, X. Cao, X. L. Tang, R. C. Li, Y. T. Zheng, Y. Qiu, A. Clerk, P. Sugden, J. Han, and R. Bolli. PKC-dependent activation of p46/p54 JNKs during ischemic preconditioning in conscious rabbits. *American Journal of Physiology*, 277(5):H1771–85, 1999.

87 D. Hreniuk, M. Garay, W. Gaarde, B. P. Monia, R. A. McKay, and C. L. Cioffi. Inhibition of c-Jun N-terminal kinase 1, but not c-Jun N-terminal kinase 2, suppresses apoptosis induced by ischemia/reoxygenation in rat cardiac myocytes. *Molecular Pharmacology*, 59(4):867–74, 2001.

88 P. Xie, S. Guo, Y. Fan, H. Zhang, D. Gu, and H. Li. Atrogin-1/MAFbx enhances simulated ischemia/reperfusion-induced apoptosis in cardiomyocytes through degradation of MAPK phosphatase-1 and sustained JNK activation. *Journal of Biological Chemistry*, 284(9):5488–96, 2009.

89 Z-F. Song, X-P. Ji, X-X. Li, S-J. Wang, S-H. Wang, and Y. Zhang. Inhibition of the activity of poly (ADP-ribose) polymerase reduces heart ischaemia/reperfusion injury via suppressing JNK-mediated AIF translocation. *Journal of Cellular and Molecular Medicine*, 12(4):1220–8, 2008.

90 C. Ferrandi, R. Ballerio, P. Gaillard, C. Giachetti, S. Carboni, P-A. Vitte, J-P. Gotteland, and R. Cirillo. Inhibition of c-Jun N-terminal kinase decreases cardiomyocyte apoptosis and infarct size after myocardial ischemia and reperfusion in anaesthetized rats. *British Journal of Pharmacology*, 142(6):953–60, 2004.

91 P. Andreka, J. Zang, C. Dougherty, T. I. Slepak, K. A. Webster, and N. H. Bishopric. Cytoprotection by Jun kinase during nitric oxide-induced cardiac myocyte apoptosis. *Circulation Research*, 88(3):305–12, 2001.

92 T. H. Tran, P. Andreka, C. O. Rodrigues, K. A. Webster, and N. H. Bishopric. Jun kinase delays caspase-9 activation by interaction with the apoptosome. *Journal of Biological Chemistry*, 282(28):20340–50, 2007.

93 Z. Shao, K. Bhattacharya, E. Hsich, L. Park, B. Walters, U. Germann, Y-M. Wang, J. Kyriakis, R. Mohanlal, K. Kuida, M. Namchuk, F. Salituro, Y-M. Yao, W-M Hou, X. Chen, M. Aronovitz, P. N. Tsichlis, S. Bhattacharya, T. Force, and H. Kilter. c-Jun N-terminal kinases mediate reactivation of Akt and cardiomyocyte survival after hypoxic injury in vitro and in vivo. *Circulation Research*, 98(1):111–8, 2006.

94 N. Hatano, Y. Mori, M. Oh-hora, A. Kosugi, T. Fujikawa, N. Nakai, H. Niwa, J-I. Miyazaki, T. Hamaoka, and M. Ogata. Essential role for ERK2 mitogen-activated protein kinase in placental development. *Genes to cells : devoted to molecular & cellular mechanisms*, 8(11):847–56, 2003.

95 M. K. Saba-El-Leil, F. D. J. Vella, B. Vernay, L. Voisin, L. Chen, N. Labrecque, S-L. Ang, and S. Meloche. An essential function of the mitogen-activated protein kinase ERK2 in mouse trophoblast development. *EMBO Reports*, 4(10):964–8, 2003.

96 N. R. Bhat and P. Zhang. Hydrogen peroxide activation of multiple mitogen-activated protein kinases in an oligodendrocyte cell line: role of extracellular signal-regulated kinase in hydrogen peroxide-induced cell death. *Journal of Neurochemistry*, 72(1):112–9, 1999.

97 J. Liu, W. Mao, B. Ding, and C-S. Liang. ERKs/p53 signal transduction pathway is involved in doxorubicin-induced apoptosis in H9c2 cells and cardiomyocytes. *American Journal of Physiology. Heart and Circulatory Physiologyournal of physiology. Heart and circulatory physiology*, 295(5):H1956–65, 2008.

98 J. Dong, S. Ramachandiran, K. Tikoo, Z. Jia, S. S. Lau, and T. J. Monks. EGFR-independent activation of p38 MAPK and EGFR-dependent activation of ERK1/2 are required for ROS-induced renal cell death. *American journal of physiology. Renal physiology*, 287(5):F1049–58, 2004.

99 D. J. Lips, O. F. Bueno, B. J. Wilkins, N. H. Purcell, R. A. Kaiser, J. N. Lorenz, L. Voisin, M. K. Saba-El-Leil, S. Meloche, J. Pouysségur, G. Pagès, L. J. De Windt, P. A. Doevendans, and J. D. Molkentin. MEK1-ERK2 signaling pathway protects myocardium from ischemic injury in vivo. *Circulation*, 109(16):1938–41, 2004.

100 A. Bonni, A. Brunet, A. E. West, S. R. Datta, M. A. Takasu, and M. E. Greenberg. Cell survival promoted by the ras-mapk signaling pathway by transcription-dependent and -independent mechanisms. *Science*, 286(5443):1358–62, 1999.

101 S. Dhingra, A. K. Sharma, R. C. Arora, J. Slezak, and P. K. Singal. IL-10 attenuates TNF-alpha-induced nf-kappab pathway activation and cardiomyocyte apoptosis. *Cardiovascular Research*, 82(1):59–66, 2009.

102 A. Aries, P. Paradis, C. Lefebvre, R. J. Schwartz, and M. Nemer. Essential role of GATA-4 in cell survival and drug-induced cardiotoxicity. *Proceedings of the National Academy of Sciences of the United States of America*, 101(18):6975–80, 2004.

103 R. Aikawa, I. Komuro, T. Yamazaki, Y. Zou, S. Kudoh, M. Tanaka, I. Shiojima, Y. Hiroi, and Y. Yazaki. Oxidative stress activates extracellular signal-regulated kinases through Src and Ras in cultured cardiac myocytes of neonatal rats. *Journal of Clinical Investigation*, 100(7):1813–21, 1997.

104 D. S. Aaronson. A road map for those who don't know JAK-STAT. *Science*, 296(5573):1653–1655, 2002.

105 L. Klampfer. Signal transducers and activators of transcription (STATs): Novel targets of chemopreventive and chemotherapeutic drugs. *Current Cancer Drug Targets*, 6:107–121, 2006.

106 A. Stephanou. Activated STAT-1 pathway in the myocardium as a novel therapeutic target in ischaemia/reperfusion injury. *European cytokine network*, 13(4):401–3, 2002.

107 H. S. Kim and M-S. Lee. STAT1 as a key modulator of cell death. *Cellular Signalling*, 19(3):454–65, 2007.

108 X. Chen, U. Vinkemeier, Y. Zhao, D. Jeruzalmi, J. E. Darnell, Jr, and J. Kuriyan. Crystal structure of a tyrosine phosphorylated STAT-1 dimer bound to DNA. *Cell*, 93(5):827–39, 1998.

109 K. Imada and W. J. Leonard. The JAK-STAT pathway. *Molecular Immunology*, 37(1-2):1–11, 2000.

110 J. M. Cavaillon. Cytokines and macrophages. *Biomed Pharmacother*, 48(10):445–53, 1994.

111 M. A. Meraz, J. M. White, K. C. F. Sheehan, E. A. Bach, S. J. Rodig, A. S. Dighe, D. H. Kaplan, J. K. Riley, A. C. Greenlund, D. Campbell, K. CarverMoore, R. N. DuBois, R. Clark, M. Aguet, and R. D. Schreiber. Targeted disruption of the STAT1 gene in mice reveals unexpected physiologic specificity in the JAK-STAT signaling pathway. *Cell*, 84:431–442, 1996.

112 P. Kovarik, D. Stoiber, P. A. Eyers, R. Menghini, A. Neininger, M. Gaestel, P. Cohen, and T. Decker. Stress-induced phosphorylation of STAT1 at Ser727 requires p38 mitogen-activated protein kinase whereas IFN-gamma uses a different signaling pathway. *Proceedings of the National Academy of Sciences of the United States of America*, 96:13956–13961, 1999.

113 A. Stephanou and D.S. Latchman. StatâĂŘ1: a novel regulator of apoptosis. *International Journal of Experimental Pathology*, 84(6):239–244, 2003.

114 T. Sekimoto, K. Nakajima, T. Tachibana, T. Hirano, and Y. Yoneda. Interferon-gamma-dependent nuclear import of stat1 is mediated by the gtpase activity of ran/tc4. *Journal of Biological Chemistry*, 271(49):31017–20, 1996.

115 K. Melen, R. Fagerlund, J. Franke, M. Kohler, L. Kinnunen, and I. Julkunen. Importin alpha nuclear localization signal binding sites for STAT1, STAT2, and influenza A virus nucleoprotein. *Journal of Biological Chemistry*, 278(30):28193–200, 2003.

116 T. Meyer and U. Vinkemeier. Nucleocytoplasmic shuttling of STAT transcription factors. *European Journal of Biochemistry*, 271(23-24):4606–12, 2004.

117 K. Shuai and B. Liu. Regulation of JAK-STAT signalling in the immune system. *Nature reviews. Immunology*, 3(11):900–11, 2003. Shuai, Ke Liu, Bin England Nat Rev Immunol. 2003 Nov;3(11):900-11.

118 T. Meyer, A. Marg, P. Lemke, B. Wiesner, and U. Vinkemeier. DNA binding controls inactivation and nuclear accumulation of the transcription factor STAT1. *Genes & development*, 17(16):1992–2005, 2003.

119 K. M. McBride, C. McDonald, and N. C. Reich. Nuclear export signal located within the DNA-binding domain of the STAT1 transcription factor. *EMBO Journal*, 19:6196–6206, 2000.

120 K. M. McBride, G. Banninger, C. McDonald, and N. C. Reich. Regulated nuclear import of the STAT1 transcription factor by direct binding of importin-alpha. *EMBO Journal*, 21:1754–1763, 2002.

121 L. Klampfer. Signal transducers and activators of transcription (STATs): Novel targets of chemopreventive and chemotherapeutic drugs. *Current Cancer Drug Targets*, 6:107–121, 2006.

122 K. Boengler, D. Hilfiker-Kleiner, H. Drexler, G. Heusch, and R. Schulz. The myocardial JAK/STAT pathway: From protection to failure. *Pharmacology & Therapeutics*, 120:172–185, 2008.

123 Haspel R. L., Salditt-Georgieff M., and Darnell J.E. The rapid inactivation of nuclear tyrosine phosphorylated STAT1 depends upon a protein tyrosine phosphatase. *Embo Journal*, 15(22):6262–6268, 1996.

124 W. S. Alexander, R. Starr, J. E. Fenner, C. L. Scott, E. Handman, N. S. Sprigg, J. E. Corbin, A. L. Cornish, R. Darwiche, C. M. Owczarek, T. W. Kay, N. A. Nicola, P. J. Hertzog, D. Metcalf, and D. J. Hilton. SOCS1 is a critical inhibitor of interferon gamma signaling and prevents the potentially fatal neonatal actions of this cytokine. *Cell*, 98(5):597–608, 1999.

125 J. C. Marine, C. McKay, D. Wang, D. J. Topham, E. Parganas, H. Nakajima, H. Pendeville, H. Yasukawa, A. Sasaki, A. Yoshimura, and J. N. Ihle. SOCS3 is essential in the regulation of fetal liver erythropoiesis. *Cell*, 98(5):617–27, 1999.

126 L. Larsen and C. Röpke. Suppressors of cytokine signalling: SOCS. *APMIS : acta pathologica, microbiologica, et immunologica Scandinavica*, 110(12):833–44, 2002.

127 T. Kamura, S. Sato, D. Haque, L. Liu, W. G. Kaelin, Jr, R. C. Conaway, and J. W. Conaway. The elongin bc complex interacts with the conserved socs-box motif present in members of the socs, ras, wd-40 repeat, and ankyrin repeat families. *Genes & Development*, 12(24):3872–81, 1998.

128 J. S. Rawlings. The JAK/STAT signaling pathway. *Journal of Cell Science*, 117(8):1281–1283, 2004.

129 A. Sasaki, H. Yasukawa, A. Suzuki, S. Kamizono, T. Syoda, I. Kinjyo, M. Sasaki, J. A. Johnston, and A. Yoshimura. Cytokine-inducible SH2 protein-3 (CIS3/SOCS3) inhibits janus tyrosine kinase by binding through the N-terminal kinase inhibitory region as well as SH2 domain. *Genes to Cells*, 4(6):339–51, 1999.

130 D. Xu and C.K. Qu. Protein tyrosine phosphatases in the jak/stat pathway. *Frontiers in bioscience: a journal and virtual library*, 13:4925, 2008.

131 C. J. Greenhalgh and D. J. Hilton. Negative regulation of cytokine signaling. *Journal of Leukocyte Biology*, 70:348–356, 2001.

132 T. Yi, J. Zhang, O. Miura, and J. Ihle. Hematopoietic-cell phosphatase associates with erythropoietin (EPO) receptor after EPO-induced receptor tyrosine phosphorylation - identification of potential binding-sites. *Blood*, 85:87–95, 1995.

133 K. Shuai. Modulation of STAT signaling by STAT-interacting proteins. *Oncogene*, 19(21):2638–44, 2000.

134 C. D. Chung, J. Liao, B. Liu, X. Rao, P. Jay, P. Berta, and K. Shuai. Specific inhibition of STAT3 signal transduction by PIAS3. *Science*, 278(5344):1803–5, 1997.

135 B. Liu, J. Liao, X. Rao, S. A. Kushner, C. D. Chung, D. D. Chang, and K. Shuai. Inhibition of STAT1-mediated gene activation by PIAS1. *Proceedings of the National Academy of Sciences of the United States of America*, 95(18):10626–31, 1998.

136 R. Ananthakrishnan, K. Hallam, Q. Li, and R. Ramasamy. JAK-STAT pathway in cardiac ischemic stress. *Vascular Pharmacology*, 43(5):353–356, 2005.

137 J. Pan, K. Fukuda, H. Kodama, and S. Makino. Role of angiotensin II in activation of the JAK/STAT pathway induced by acute pressure overload in the rat heart. *Circulation Research*, 81(4):611–7, 1997.

138 D. C. H. Ng, N. W. Court, C. G. Dos Remedios, and M. A. Bogoyevitch. Activation of signal transducer and activator of transcription (STAT) pathways in failing human hearts. *Cardiovascular Research*, 57(2):333–46, 2003.

139 A. Stephanou, T. M. Scarabelli, B. K. Brar, Y. Nakanishi, M. Matsumura, R. A. Knight, and D. S. Latchman. Induction of apoptosis and Fas receptor/Fas ligand expression by ischemia/reperfusion in cardiac myocytes requires serine 727 of the STAT-1 transcription factor but not tyrosine 701. *Journal of Biological Chemistry*, 276(30):28340–7, 2001.

140 A. Stephanou, B. K. Brar, T. M. Scarabelli, A. K. Jonassen, D. M. Yellon, M. S. Marber, R. A. Knight, and D. S. Latchman. Ischemia-induced STAT-1 expression and activation play a critical role in cardiomyocyte apoptosis. *Journal of Biological Chemistry*, 275(14):10002–8, 2000.

141 H. El-Adawi, L. Deng, A. Tramontano, S. Smith, E. Mascareno, K. Ganguly, R. Castillo, and N. El-Sherif. The functional role of the JAK-STAT pathway in post-infarction remodeling. *Cardiovascular Research*, 57(1):129–38, 2003.

142 E. Mascareno, M. El-Shafei, N. Maulik, M. Sato, Y. Guo, D. K. Das, and M. A. Siddiqui. JAK/STAT signaling is associated with cardiac dysfunction during ischemia and reperfusion. *Circulation*, 104(3):325–9, 2001.

143 R. Bolli and B. Dawn. Role of the JAK-STAT pathway in protection against myocardial ischemia/reperfusion injury. *Trends in Cardiovascular Medicine*, 13(2):72–9, 2003.

144 A. Stephanou, B. Brar, R. Heads, R. D. Knight, M. S. Marber, D. Pennica, and D. S. Latchman. Cardiotrophin-1 induces heat shock protein accumulation in cultured cardiac cells and protects them from stressful stimuli. *Journal of Molecular and Cellular Cardiology*, 30(4):849–855, 1998.

145 W. J. Lee, J. Y. Shim, and B. T. Zhu. Mechanisms for the inhibition of DNA methyltransferases by tea catechins and bioflavonoids. *Molecular Pharmacology*, 68(4):1018–30, 2005.

146 O. Krämer, D. Baus, and S. Knauer. Acetylation of STAT1 modulates nf-κb activity. *Genes & Development*, 20(4):473–85, 2006.

147 A. Stephanou, B. Brar, and Z. Liao. Distinct initiator caspases are required for the induction of apoptosis in cardiac myocytes during ischaemia versus reperfusion injury. *Cell Death and Differentiation*, 8(4):434–4, 2001.

148 Townsend P. A., Scarabelli T. M., Davidson S. M., Knight R. A., Latchman D. S., and Stephanou A. STAT-1 interacts with p53 to enhance DNA damage-induced apoptosis. *Journal of Biological Chemistry*, 279(7):5811–5820, 2003.

149 A. Stephanou and D. S. Latchman. Opposing actions of STAT-1 and STAT-3. *Growth Factors*, 23(3):177–82, 2005.

150 K. Ramsauer, I. Sadzak, A. Porras, A. Pilz, A. R. Nebreda, T. Decker, and P. Kovarik. p38 MAPK enhances STAT1-dependent transcription independently of Ser-727 phosphorylation. *Proceedings of the National Academy of Sciences of the United States of America*, 99(20):12859–64, 2002.

151 J. McCormick, S. P. Barry, A. Sivarajah, G. Stefanutti, P. A. Townsend, K. M. Lawrence, S. Eaton, R. A. Knight, C. Thiemermann, D. S. Latchman, and A. Stephanou. Free radical scavenging inhibits STAT phosphorylation following in vivo ischemia/reperfusion injury. *FASEB J*, 20(12):2115–7, 2006.

152 R. Bolli, B. Dawn, and Y.T. Xuan. Role of the JAK-STAT pathway in protection against myocardial ischemia/reperfusion injury. *Trends in Cardiovascular Medicine*, 13(2):72–79, 2003.

153 P.A. Townsend, T.M. Scarabelli, E. Pasini, G. Gitti, M. Menegazzi, H. Suzuki, R. A. Knight, D. S. Latchman, and A. Stephanou. Epigallocatechin-3-gallate inhibits STAT-1 activation and protects cardiac myocytes from ischemia/reperfusion-induced apoptosis. *FASEB Journal*, 18(13):1621–3, 2004.

154 N. Ahmad and H. Mukhtar. Green tea polyphenols and cancer: biological mechanisms and practical implications. *Nutrition reviews*, 57(3):78–83, 1999.

155 J. Lambert and S. Sang. Antioxidative and anti-carcinogenic activities of tea polyphenols. *Archives of toxicology*, 83(1):11–21, 2009.

156 J. B. Harborne and C. A. Williams. Advances in flavonoid research since 1992. *Phytochemistry*, 55(6):481–504, 2000.

157 A. Crozier, I. B. Jaganath, and M. N. Clifford. Dietary phenolics: chemistry, bioavailability and effects on health. *Natural Product Reports*, 26(8):1001–43, 2009.

158 V. P. Androutsopoulos, A. Papakyriakou, D. Vourloumis, A. M. Tsatsakis, and D. A. Spandidos. Dietary flavonoids in cancer therapy and prevention: substrates and inhibitors of cytochrome P450 CYP1 enzymes. *Pharmacology Therapeutics*, 126(1):9–20, 2010.

159 Y. Zuo, H. Chen, and Y. Deng. Simultaneous determination of catechins, caffeine and gallic acids in green, oolong, black and pu-erh teas using HPLC with a photodiode array detector. *Talanta*, 57(2):307–16, 2002.

160 I. C. Arts, B. Van De Putte, and P. C. Hollman. Catechin contents of foods commonly consumed in the Netherlands. 2. tea, wine, fruit juices, and chocolate milk. *Journal of Agricultural and Food Chemistry*, 48(5):1752–7, 2000.

161 C. D. Wu and G. X. Wei. Tea as a functional food for oral health. *Nutrition*, 18:443–444, 2002.

162 I. A. Hakim, R. B. Harris, and U. M. Weisgerber. Tea intake and squamous cell carcinoma of the skin: Influence of type of tea beverages. *Cancer Epidemiology Biomarkers & Prevention*, 9:727–731, 2000.

163 I. C. Arts, B. Van De Putte, and P. C. Hollman. Catechin contents of foods commonly consumed in The Netherlands. 2. tea, wine, fruit juices, and chocolate milk. *Journal of Agricultural and Food Chemistry*, 48(5):1752–1757, 2000.

164 S. Bhagwat, D. B. Haytowitz, , and J. M. Holden. USDA database for the flavonoid content of selected foods, June 2013.

165 P. L. Fernandez, F. Pablos, M. J. Martin, and A. G. Gonzalez. Study of catechin and xanthine tea profiles as geographical tracers. *Journal of Agricultural and Food Chemistry*, 50:1833–1839, 2002.

166 C. Cabrera, R. Gimenez, and M. C. Lopez. Determination of tea components with antioxidant activity. *Journal of Agricultural and Food Chemistry*, 51:4427–4435, 2003.

167 P. D. Collier and R. Mallows. Estimation of flavanols in tea by gas chromatography of their trimethylsilyl derivatives. *Journal of Chromatography A*, 57:29–45, 1971.

168 H. Horie, T. Mukai, and K. Kohata. Simultaneous determination of qualitatively important components in green tea infusions using capillary electrophoresis. *Journal of Chromatography A*, 758:332–335, 1997.

169 F. Yayabe, H. Kinugasa, and T. Takeo. A simple preparative chromatographic-separation of green tea catechins. *Nippon Nogeikagaku Kaishi-Journal of the Japan Society For Bioscience Biotechnology and Agrochemistry*, 63:845–847, 1989.

170 T. Goto, Y. Yoshida, M. Kiso, and H. Nagashima. Simultaneous analysis of individual catechins and caffeine in green tea. *Journal of Chromatography A*, 749:295–299, 1996.

171 W. E. Bronner and G. R. Beecher. Method for determining the content of catechins in tea infusions by high-performance liquid chromatography. *Journal of Chromatography A*, 805(1-2):137–142, 1998.

172 J. J. Dalluge, B. C. Nelson, J. B. Thomas, and L. C. Sander. Selection of column and gradient elution system for the separation of catechins in green tea using high-performance liquid chromatography. *Journal of Chromatography A*, 793:265–274, 1998.

173 W. Pongsuwan, T. Bamba, K. Harada, T. Yonetani, A. Kobayashi, and E. Fukusaki. High-throughput technique for comprehensive analysis of japanese green tea quality assessment using ultra-performance liquid chromatography with time-of-flight mass spectrometry (UPLC/TOF MS). *Journal of Agricultural and Food Chemistry*, 56:10705–10708, 2008.

174 G. K. Poon. Analysis of catechins in tea extracts by liquid chromatography electrospray ionization mass spectrometry. *Journal of Chromatography A*, 794:63–74, 1998.

175 N. Sueoka, M. Suganuma, E. Sueoka, S. Okabe, S. Matsuyama, K. Imai, K. Nakachi, and H. Fujiki. A new function of green tea: prevention of lifestyle-related diseases. *Annals of the New York Academy of Sciences*, 928:274–280, 2001.

176 M. G. L. Hertog, E. J. M. Feskens, and D. Kromhout. Antioxidant flavonols and coronary heart disease risk. *Lancet*, 349:699–699, 1997.

177 W. Kim, M. H. Jeong, S. H. Cho, J. H. Yun, H. J. Chae, Y. K. Ahn, M. C. Lee, X. Cheng, T. Kondo, T. Murohara, and J. C. Kang. Effect of green tea consumption on endothelial function and circulating endothelial progenitor cells in chronic smokers. *Circulation Journal*, 70:1052–1057, 2006.

178 S. Sasazuki, H. Kodama, K. Yoshimasu, Y. Liu, M. Washio, K. Tanaka, S. Tokunaga, S. Kono, H. Arai, Y. Doi, T. Kawano, O. Nakagaki, K. Takada, S. Koyanagi, K. Hiyamuta, T. Nii, K. Shirai, M. Ideishi, K. Arakawa, M. Mohri, and A. Takeshita. Relation between green tea consumption and the severity of coronary atherosclerosis among japanese men and women. *Annals of Epidemiology*, 10:401–408, 2000.

179 R. Hirano, Y. Momiyama, R. Takahashi, H. Taniguchi, K. Kondo, H. Nakamura, and F. Ohsuzu. Comparison of green tea intake in japanese patients with and without angiographic coronary artery disease. *American Journal of Cardiology*, 90:1150–3, 2002.

180 Y. C. Yang, F. H. Lu, J. S. Wu, C. H. Wu, and C. J. Chang. The protective effect of habitual tea consumption on hypertension. *Archives of Internal Medicine*, 164:1534–1540, 2004.

181 K. Y. Chyu, S. M. Babbidge, X. N. Zhao, R. Dandillaya, A. G. Rietveld, J. Yano, P. Dimayuga, B. Cercek, and P. K. Shah. Differential effects of green tea-derived catechin on developing versus established atherosclerosis in apolipoprotein e-null mice. *Circulation*, 109(20):2448–2453, 2004.

182 D. G. Raederstorff, M. F. Schlachter, V. Elste, and P. Weber. Effect of EGCG on lipid absorption and plasma lipid levels in rats. *Journal of Nutritional Biochemistry*, 14:326–332, 2003.

183 P. V. A. Babu, K. E. Sabitha, and C. S. Shyamaladevi. Therapeutic effect of green tea extract on oxidative stress in aorta and heart of streptozotocin diabetic rats. *Chemico-Biological Interactions*, 162(2):114–20, 2006.

184 E. B. Rimm, M. B. Katan, A. Ascherio, M. J. Stampfer, and W. C. Willett. Relation between intake of flavonoids and risk for coronary heart disease in male health professionals. *Annals of Internal Medicine*, 125:384–389, 1996.

185 M. G. L. Hertog, P. M. Sweetman, A. M. Fehily, P. C. Elwood, and D. Kromhout. Antioxidant flavonols and ischemic heart disease in a welsh population of men: The caerphilly study. *American Journal of Clinical Nutrition*, 65:1489–1494, 1997.

186 K. H. Van Het Hof, S. A. Wiseman, C. S. Yang, and L. B. M. Tuburg. Plasma and lipoprotein levels of tea catechins following repeated tea consumption. *Proceedings of the Society For Experimental Biology and Medicine*, 220:203–209, 1999.

187 V. Stangl, H. Dreger, K. Stangl, and M. Lorenz. Molecular targets of tea polyphenols in the cardiovascular system. *Cardiovascular Research*, 73(2):348, 2007.

188 N. S. Dhalla, R. M. Temsah, and T. Netticadan. Role of oxidative stress in cardiovascular diseases. *Journal of Hypertension*, 18(6):655–73, 2000.

189 P. Libby. Inflammation in atherosclerosis. *Nature*, 420:868–874, 2002.

190 Z. M. Ruggeri. Platelets in atherothrombosis. *Nature Medicine*, 8(11):1227–34, 2002.

191 C. Borza, D. Muntean, C. Dehelean, G. Săvoiu, C. Şerban, G. Simu, M. Andoni, M. Butur, and S. Drăgan. *Lipid Metabolism.* http://www.intechopen.com/books/export/citation/BibTex/lipid-metabolism/oxidative-stress-and-lipid-peroxidation-a-lipid-metabolism-dysfunction, January 2013.

192 M. Akhlaghi and B. Bandy. Mechanisms of flavonoid protection against myocardial ischemia–reperfusion injury. *Journal of Molecular and Cellular Cardiology*, 46(3):309–317, 2009.

193 M. Kashima. Effects of catechins on superoxide and hydroxyl radical. *Chemical & Pharmaceutical Bulletin*, 47:279–283, 1999.

194 F. Nanjo, M. Mori, K. Goto, and Y. Hara. Radical scavenging activity of tea catechins and their related compounds. *Bioscience Biotechnology and Biochemistry*, 63:1621–1623, 1999.

195 Q. N. Guo, B. L. Zhao, M. F. Li, S. R. Shen, and W. J. Xin. Studies on protective mechanisms of four components of green tea polyphenols against lipid peroxidation in synaptosomes. *Biochimica Et Biophysica Acta-Lipids and Lipid Metabolism*, 1304:210–222, 1996.

196 A. N. Pham, G. Xing, C. J. Miller, and T. D. Waite. Fenton-like copper redox chemistry revisited: Hydrogen peroxide and superoxide mediation of copper-catalyzed oxidant production. *Journal of Catalysis*, 301:54–64, 2013.

197 I. Morel, G. Lescoat, P. Cogrel, O. Sergent, N. Pasdeloup, P. Brissot, P. Cillard, and J. Cillard. Antioxidant and iron-chelating activities of the flavonoids catechin, quercetin and diosmetin on iron-loaded rat hepatocyte cultures. *Biochemical Pharmacology*, 45:13–19, 1993.

198 E. Graf, J. R. Mahoney, R. G. Bryant, and J. W. Eaton. Iron-catalyzed hydroxyl radical formation. stringent requirement for free iron coordination site. *Journal of Biological Chemistry*, 259:3620–3624, 1984.

199 M. Melidou, K. Riganakos, and D. Galaris. Protection against nuclear DNA damage offered by flavonoids in cells exposed to hydrogen peroxide: The role of iron chelation. *Free Radical Biology and Medicine*, 39:1591–1600, 2005.

200 V. A. Kostyuk, A. I. Potapovich, E. N. Strigunova, T. V. Kostyuk, and I. B. Afanas'ev. Experimental evidence that flavonoid metal complexes may act as mimics of superoxide dismutase. *Archives of Biochemistry and Biophysics*, 428:204–208, 2004.

201 R.F. Anderson, L.J. Fisher, Y. Hara, T. Harris, W. B. Mak, L. D. Melton, and J. E. Packer. Green tea catechins partially protect DNA from (.)OH radical-induced strand breaks and base damage through fast chemical repair of DNA radicals. *Carcinogenesis*, 22:1189–1193, 2001.

202 N. Q. Zhu, T. C. Huang, Y. N. Yu, E. J. LaVoie, C. S. Yang, and C. T. Ho. Identification of oxidation products of (-)-epigallocatechin gallate and (-)-epigallocatechin with H_2O_2. *Journal of Agricultural and Food Chemistry*, 48:979–981, 2000.

203 N. Caturla, E. Vera-Samper, J. Villalain, C. R. Mateo, and V. Micol. The relationship between the antioxidant and the antibacterial properties of galloylated catechins and the structure of phospholipid model membranes. *Free Radical Biology and Medicine*, 34:648–662, 2003.

204 C. A. Rice-Evans, N. J. Miller, and G. Paganga. Structure-antioxidant activity relationships of flavonoids and phenolic acids. *Free Radical Biology and Medicine*, 20(7):933–56, 1996.

205 E. Skrzydlewska, J. Ostrowska, R. Farbiszewski, and K. Michalak. Protective effect of green tea against lipid peroxidation in the rat liver, blood serum and the brain. *Phytomedicine*, 9:232–238, 2002.

206 S. Azam, N. Hadi, N. U. Khan, and S. M. Hadi. Prooxidant property of green tea polyphenols epicatechin and epigallocatechin-3-gallate: implications for anticancer properties. *Toxicology in vitro : an international journal published in association with BIBRA*, 18(5):555–61, 2004.

207 A. Ludwig, M. Lorenz, N. Grimbo, F. Steinle, S. Meiners, C. Bartsch, K. Stangl, G. Baumann, and V. Stangl. The tea flavonoid epigallocatechin-3-gallate reduces cytokine-induced VCAM-1 expression and monocyte adhesion to endothelial cells. *Biochemical and Biophysical Research Communications*, 316:659–665, 2004.

208 R. Hofbauer, M. Frass, B. Gmeiner, S. Handler, W. Speiser, and S. Kapiotis. The green tea extract epigallocatechin gallate is able to reduce neutrophil transmigration through monolayers of endothelial cells. *Wiener Klinische Wochenschrift*, 111:278–282, 1999.

209 K. Takano, K. Nakaima, M. Nitta, F. Shibata, and H. Nakagawa. Inhibitory effect of (-)-epigallocatechin 3-gallate, a polyphenol of green tea, on neutrophil chemotaxis in vitro and in vivo. *Journal of Agricultural and Food Chemistry*, 52:4571–4576, 2004.

210 K. Kawai, N. H. Tsuno, J. Kitayama, Y. Okaji, K. Yazawa, M. Asakage, S. Sasaki, T. Watanabe, K. Takahashi, and H. Nagawa. Epigallocatechin gallate induces apoptosis of monocytes. *Journal of Allergy and Clinical Immunology*, 115:186–191, 2005.

211 E. Darra, K. Shoji, S. Mariotto, and H. Suzuki. Protective effect of epigallocatechin-3-gallate on ischemia/reperfusion-induced injuries in the heart: STAT1 silencing flavonoid. *Genes & Nutrition*, 2(3):307–310, 2007.

212 Y. Wang. Mitogen-activated protein kinases in heart development and diseases. *Circulation*, 116:1413–1423, 2007.

213 S-M. Won, Y-H. Park, H-J. Kim, K-M. Park, and W-J. Lee. Catechins inhibit angiotensin II-induced vascular smooth muscle cell proliferation via mitogen-activated protein kinase pathway. *Experimental and Molecular Medicine*, 38:525–534, 2006.

214 T. S. Blackwell and J. W. Christman. The role of nuclear factor-kappab in cytokine gene regulation. *American Journal of Respiratory Cell and Molecular Biology*, 17(1):3–9, 1997.

215 R. Aneja, P. W. Hake, T. J. Burroughs, A. G. Denenberg, H. R. Wong, and B. Zingarelli. Epigallocatechin, a green tea polyphenol, attenuates myocardial ischemia reperfusion injury in rats. *Molecular Medicine*, 10(1-6):55–62, 2004.

216 S. Nam, D. M. Smith, and Q. P. Dou. Ester bond-containing tea polyphenols potently inhibit proteasome activity in vitro and in vivo. *Journal of Biological Chemistry*, 276:13322–13330, 2001.

217 M. Nomura, W. Ma, N. Chen, A. M. Bode, and Z. Dong. Inhibition of 12-o-tetradecanoylphorbol-13-acetate-induced NF-kappaB activation by tea polyphenols, (-)-epigallocatechin gallate and theaflavins. *Carcinogenesis*, 21(10):1885–90, 2000.

218 S. B. Kim, M. J. Lee, J. I. Hong, C. Li, T. J. Smith, G. Y. Yang, D. N. Seril, and C. S. Yang. Plasma and tissue levels of tea catechins in rats and mice during chronic consumption of green tea polyphenols. *Nutrition and Cancer-An International Journal*, 37:41–48, 2000.

219 C. A. Lipinski, F. Lombardo, B. W. Dominy, and P. J. Feeney. Experimental and computational approaches to estimate solubility and permeability in drug discovery and development settings. *Advanced Drug Delivery Reviews*, 46(1-3):3–26, 2012.

220 J. Kanwar, M. Taskeen, I. Mohammad, C. Huo, T.H. Chan, and Q. P. Dou. Recent advances on tea polyphenols. *Frontiers in bioscience (Elite edition)*, 4:111–31, 2012.

221 H. Lu, X. F. Meng, M. J. Lee, C. Li, P. Maliakal, and C. S. Yang. Bioavailability and biological activity of tea polyphenols. *Food Factors In Health Promotion and Disease Prevention*, 851:9–15, 2003.

222 J. D. Lambert and C. S. Yang. Cancer chemopreventive activity and bioavailability of tea and tea polyphenols. *Mutation Research*, 523-524:201–8, 2003.

223 J. Lambert and S. Sang. Biotransformation of green tea polyphenols and the biological activities of those metabolites. *Molecular Pharmaceutics*, 4(6):819–25, 2007.

224 N. Khan and H. Mukhtar. Tea polyphenols for health promotion. *Life Sciences*, 81(7):519–33, 2007.

225 C. Yang, S. Sang, and J. Lambert. Bioavailability issues in studying the health effects of plant polyphenolic compounds. *Molecular Nutrition & Food Research*, 52(Suppl 1):S139–51, 2008.

226 R. J. Moore, K. G. Jackson, and A. M. Minihane. Green tea (camellia sinensis) catechins and vascular function. *British Journal of Nutrition*, 102(12):1790–802, 2009.

227 J. B. Vaidyanathan and T. Walle. Glucuronidation and sulfation of the tea flavonoid (-)-epicatechin by the human and rat enzymes. *Drug Metabolism and Disposition*, 30:897–903, 2002.

228 C. Li, M. J. Lee, S. Q. Sheng, X. F. Meng, S. Prabhu, B. Winnik, B. M. Huang, J. Y. Chung, S. Q. Yan, C. T. Ho, and C. S. Yang. Structural identification of two metabolites of catechins and their kinetics in human urine and blood after tea ingestion. *Chemical Research In Toxicology*, 13:177–184, 2000.

229 W. Y. Feng. Metabolism of green tea catechins: an overview. *Current Drug Metabolism*, 7(7):755–809, 2006.

230 H. Lu, X. Meng, C. Li, S. Sang, C. Patten, S. Sheng, J. Hong, N. Bai, B. Winnik, C-T. Ho, and C. S. Yang. Glucuronides of tea catechins: enzymology of biosynthesis and biological activities. *Drug Metabolism and Disposition: the biological fate of chemicals*, 31(4):452–61, 2003.

231 J. D. Lambert, J. E. Rice, J. Hong, Z. Hou, and C. S. Yang. Synthesis and biological activity of the tea catechin metabolites, M4 and M6 and their methoxy-derivatives. *Bioorganic & Medicinal Chemistry Letters*, 15(4):873–6, 2005.

232 L. Li and T. H. Chan. Enantioselective synthesis of epigallocatechin-3-gallate (EGCG), the active polyphenol component from green tea. *Organic Letters*, 3(5):739–41, 2001.

233 J. C. Anderson, C. Headley, P. D. Stapleton, and P. W. Taylor. Asymmetric total synthesis of b-ring modified (–)-epicatechin gallate analogues and their modulation of [beta]-lactam resistance in staphylococcus aureus. *Tetrahedron*, 61(32):7703–7711, 2005.

234 N. T. Zaveri. Synthesis of a 3, 4, 5-trimethoxybenzoyl ester analogue of epigallocatechin-3-gallate (EGCG): a potential route to the natural product green tea catechin, egcg. *Organic Letters*, 3(6):843–6, 2001.

235 J. W. Clark-Lewis and D. C. Skingle. Flavan derivatives. XVIII. synthesis of hemiketals containing the peltogynol ring system: 3(3')-hydroxyisochromano (4', 3': 2, 3) chromans. conversion of 2'-hydroxychalcones into flav-3-enes and its biosynthetic implications. *Australian Journal of Chemistry*, 20(10):2169–90, 1967.

236 K. Ohmori, T. Yano, and K. Suzuki. General synthesis of epi-series catechins and their 3-gallates: reverse polarity strategy. *Organic & Biomolecular Chemistry*, 8(12):2693–6, 2010.

237 T. Higuchi, K. Ohmori, and K. Suzuki. General and convenient approach to flavan-3-ols: Stereoselective synthesis of (–)-gallocatechin. *Chemistry Letters*, 35(9):1006–1007, 2006.

238 J.C. Anderson, C. Headley, P.D. Stapleton, and P.W. Taylor. Synthesis and antibacterial activity of hydrolytically stable (-)-epicatechin gallate analogues for the modulation of [beta]-lactam resistance in staphylococcus aureus. *Bioorganic and Medicinal Chemistry Letters*, 15(10):2633–2635, 2005.

239 B. Nay, V. Arnaudinaud, and J. Vercauteren. Gram-scale production and applications of optically pure ^{13}C-labelled (+)-catechin and (-)-epicatechin. *European Journal of Organic Chemistry*, 2001(12):2379–2384, 2001.

240 N. Vaiana, L. Rizzi, M. G. Pezzano, R. Restelli, F. Rota, S. Stefanini, S. Vicentini, and S. Romeo. Synthesis of gallocatechin-3-gallate analogues. *Letter in Organic Chemistry*, 4(4):288–291, 2007.

241 K. Krohn, I. Ahmed, and M. John. Enantioselective synthesis of flavan-3-ols using a mitsunobu cyclization. *Synthesis*, (5):779–786, 2009.

242 P. K. Sharma, M. He, L. J. Romanczyk Jr, and H. Schroeter. Synthesis of [2-13C, 4-13C]-(2R,3S)-catechin and [2-13C, 4-13C]-(2R,3R)-epicatechin. *Journal of Labelled Compounds and Radiopharmaceuticals*, 53(10):605–612, 2010.

243 H. Kawamoto, F. Nakatsubo, and K. Murakami. O-benzylation of phloroglucinol via phloroglucinol triacetate. *Synthetic Communications*, 26(3):531–534, 1996.

244 S.B. Wan, K. R. Landis-Piwowar, D. J. Kuhn, D. Chen, Q. P. Dou, and T. H. Chan. Structure-activity study of epi-gallocatechin gallate (EGCG) analogs as proteasome inhibitors. *Bioorganic & Medicinal Chemistry*, (6):2177–2185, 2005.

245 T. Watanabe, N. Miyaura, and A. Suzuki. Synthesis of sterically hindered biaryls via the palladium-catalyzed cross-coupling reaction of arylboronic acids or their esters with haloarenes. *Synlett*, 1992(3):207–210, 1992.

246 K. S. Reddy, O-H. Ko, D. Ho, P. E. Persons, and J. M. Cassady. A novel enantioselective cyclization of a chiral epoxide to a benzofuran system. *Tetrahedron Letters*, 28(27):3075–3078, 1987.

247 T. Ding and X. Wang. A fast assembly of (-)-Epigallocatechin-3-gallate [(-)-EGCG] via intra-and inter-molecular mitsunobu reaction. *Chinese Journal of Chemistry*, 24(11):1618–1624, 2006.

248 D. B. Dess and J. C. Martin. A useful 12-I-5 triacetoxyperiodinane (the dess-martin periodinane) for the selective oxidation of primary or secondary alcohols and a variety of related 12-I-5 species. *Journal of the American Chemical Society*, 113(19):7277–87, 1991.

249 A. P. Kozikowski, W. Tückmantel, G. Böttcher, and L. J. Romanczyk. Studies in polyphenol chemistry and bioactivity. 4.(1) synthesis of trimeric, tetrameric, pentameric, and higher oligomeric epicatechin-derived procyanidins having all-4beta,8-interflavan connectivity and their inhibition of cancer cell growth through cell cycle arrest. *The Journal of Organic Chemistry*, 68(5):1641–58, 2003.

250 K. Esumi, M. Nishida, D. Shaw, T. W. Smith, and J. D. Marsh. NADH measurements in adult rat myocytes during simulated ischemia. *American Journal of Physiology*, 260(6 Pt 2):H1743–52, 1991.

251 P. Simpson and S. Savion. Differentiation of rat myocytes in single cell cultures with and without proliferating nonmyocardial cells. cross-striations, ultrastructure, and chronotropic response to isoproterenol. *Circulation Research*, 50(1):101–16, 1982.

252 N. Weisleder, G. E. Taffet, and Y. Capetanaki. Bcl-2 overexpression corrects mitochondrial defects and ameliorates inherited desmin null cardiomyopathy. *Proceedings of the National Academy of Sciences of the United States of America*, 101(3):769–74, 2004.

253 T. Goodpaster, A. Legesse-Miller, M. R. Hameed, S. C. Aisner, J. Randolph-Habecker, and H. A. Coller. An immunohistochemical method for identifying fibroblasts in formalin-fixed, paraffin-embedded tissue. *Journal of Histochemistry and Cytochemistry*, 56(4):347–58, Apr 2008.

254 J. E. López, B. E. Myagmar, P. M. Swigart, M. D. Montgomery, S. Haynam, M. Bigos, M. C. Rodrigo, and P. C. Simpson. β-myosin heavy chain is induced by pressure overload in a minor subpopulation of smaller mouse cardiac myocytes. *Circulation Research*, 109(6):629–38, 2011.

255 J. D. Lambert, S. Sang, J. Hong, S-J. Kwon, M-J. Lee, C-T. Ho, and C. S. Yang. Peracetylation as a means of enhancing in vitro bioactivity and bioavailability of epigallocatechin-3-gallate. *Drug Metabolism and Disposition*, 34(12):2111–2116, 2006.

256 Q. Ping Dou. Molecular mechanisms of green tea polyphenols. *Nutrition and Cancer*, 61(6):827–35, 2009.

257 W. H. Lam, A. Kazi, D. J. Kuhn, L. M. C. Chow, A. S. C. Chan, Q. P. Dou, and T. H. Chan. A potential prodrug for a green tea polyphenol proteasome inhibitor: evaluation of the peracetate ester of (-)-epigallocatechin gallate [(-)-EGCG]. *Bioorganic & Medicinal Chemistry*, 12(21):5587–93, 2004.

258 T. Zhang, D. Yang, Y. Fan, P. Xie, and H. Li. Epigallocatechin-3-gallate enhances ischemia/reperfusion-induced apoptosis in human umbilical vein endothelial cells via AKT and MAPK pathways. *Apoptosis*, 14(10):1245–54, 2009.

259 Y. Zhang, Y-Y. Cho, B. L. Petersen, F. Zhu, and Z. Dong. Evidence of STAT1 phosphorylation modulated by MAPKs, MEK1 and MSK1. *Carcinogenesis*, 25(7):1165–75, 2004.

260 H. Chow and Z. Wang. An accelerated, improved synthetic route for the preparation of polyether-based dendritic fragments. *Tetrahedron*, 54(45):13818–24, 1998.

261 S. B. Wan, D. Chen, Q. Ping Dou, and T. Hang Chan. Study of the green tea polyphenols catechin-3-gallate (CG) and epicatechin-3-gallate (ECG) as proteasome inhibitors. *Bioorganic & Medicinal Chemistry*, 12(13):3521–3527, 2004.

262 M. A. Zhuravel, N. E. Davis, S. T. Nguyen, and I. Koltover. Dendronized protein polymers: synthesis and self-assembly of monodisperse cylindrical macromolecules. *Journal of the American Chemical Society*, 126(32):9882–3, 2004.

263 A. Gissot, A. Wagnera, and C. Mioskowskia. Buffer-induced, selective mono-c-alkylation of phloroglucinol: application to the synthesis of an advanced intermediate of catechin. *Tetrahedron*, 60:6807–6812, 2004.

264 I. Tarascou, K. Barathieu, Y. André, I. Pianet, E. J. Dufourc, and E. Fouquet. An improved synthesis of procyanidin dimers: Regio- and stereocontrol of the interflavan bond. *European Journal of Organic Chemistry*, 23:5367–5377, 2006.

265 K. Krohn, I. Ahmed, Markus J., M. C. Letzel, and D. Kuck. Stereoselective synthesis of benzylated prodelphinidins and their diastereomers with use of the mitsunobu reaction in the preparation of their gallocatechin precursors. *European Journal of Organic Chemistry*, 13:2544–2554, 2010.

266 S.B. Wan, D. Chen, Q. Ping Dou, and T. Hang Chan. Study of the green tea polyphenols catechin-3-gallate (CG) and epicatechin-3-gallate (ECG) as proteasome inhibitors. *Bioorganic & Medicinal Chemistry*, 12(13):3521–3527, 2004.

267 M. Thapa, Y. Kim, J. Desper, K-O. Chang, and D. H. Hua. Synthesis and antiviral activity of substituted quercetins. *Bioorganic & Medicinal Chemistry Letters*, 22(1):353–6, 2012.

268 N.T Zaveri. Synthesis of a 3, 4, 5-trimethoxybenzoyl ester analogue of epigallocatechin-3-gallate (EGCG): a potential route to the natural product green tea catechin, egcg. *Organic Letters*, 3(6):843–846, 2001.